THE ROLE OF CHOLESTEROL ESTERIFICATION IN ADIPOCYTE EXPANDABILITY AND ITS ASSOCIATED METABOLIC DISORDERS

QING LIU

PhD

THE HONG KONG POLYTECHNIC UNIVERSITY

2023

THE HONG KONG POLYTECHNIC UNIVERSITY

Department of Applied Biology and Chemical Technology

THE ROLE OF CHOLESTEROL ESTERIFICATION IN ADIPOCYTE EXPANDABILITY AND ITS ASSOCIATED METABOLIC DISORDERS

QING LIU

A thesis submitted in partial fulfilment of the requirements for the degree of Doctor of Philosophy

August 2023

CERTIFICATE OF ORIGINALITY

I hereby declare that this thesis is my own work and that, to the best of my knowledge and belief, it reproduces no material previously published or written, nor material that has been accepted for the award of any other degree or diploma, except where due acknowledgement has been made in the text.

(Signed)

Qing LIU (Name of Student)

Abstract

Obesity is characterized by the excessive expansion of adipose tissue, while cholesterol homeostasis is important for maintaining adipose tissue function. Among the regulators of cholesterol homeostasis, SOAT1 is the key enzyme responsible for converting free cholesterol into cholesteryl ester in adipocytes. However, the role of cholesterol esterification in regulating adipocyte expandability remains unclear. Here, we investigated the role of SOAT1 in regulating adipogenesis and cholesterol homeostasis within adipocytes, as well as the physiological function of SOAT1 in mature adipocytes. A positive correlation between the expression pattern of SOAT1 in adipose tissue and adiposity in both murine and human was observed, suggesting a potential role of SOAT1 in adipose tissue expansion. Supportively, SOAT1 was found to be essential for adipogenesis, but not for adipocyte hypertrophy in vitro. We found SOAT1 deficiency alters cholesterol trafficking and distribution within adipocytes, leading to impaired maturation of SREBP2. Notably, the adipogenic capacity of SOAT1-deficient preadipocytes could be restored by enhancing the transcription of PPARγ or SREBP1, as well as through the addition of specific nutritional factors, like oleic acid and high cholesterol. These results demonstrated an important role of SOAT1 in maintaining cholesterol homeostasis and adipogenesis in adipocytes.

To examine the physiological functions of SOAT1 in mature adipocytes, we generated adipocyte-specific SOAT1-knockout (AKO) mice by crossing Adiponecin-Cre mice with SOAT1 $^{flox/flox}$ mice. SOAT1 $^{flox/flox}$ mice were used as control (CTRL) ones.

To investigate the importance of SOAT1 in adipocytes in response to excessive exogenous cholesterol overload, we employed a high cholesterol diet treatment for those mice. We found the AKO mice displayed elevated energy expenditure and browning in the iWAT even under normal room temperature conditions compared to CTRL. Furthermore, the ATGL protein level were enhanced in iWAT of AKO mice. Consistently, we knockout SOAT1 in vitro also exhibited a similar phenotype. These findings suggest that SOAT1 may play a crucial role in promoting WAT beiging through ATGL-mediated enhanced lipolysis.

To investigate the adipocyte-SOAT1 function during obesity development, we

employed a high fat high cholesterol diet with normal diet as control. Under HFHC feeding, AKO mice exhibited little impact on BW and fat mass, however it demonstrated a decreased non-alcoholic fatty liver disease (NAFLD) severity phenotype. Furthermore, echocardiography revealed a significant decrease in heart function parameters and an increase of heart mass in AKO mice. These findings suggested the participation of adipocyte-SOAT1 in the crosstalk between adipose tissue and distant organs. Under ND feeding, AKO mice exhibited increased fat mass as well as adipocyte size compared with CTRL. This pro-adiposity effect of SOAT1 deficiency was observed as early as 8-week old. These findings indicate the adipocyte-SOAT1 may engage in the adipose tissue development at early stage.

In summary, our study has elucidated the important role of SOAT1 as a regulator in maintaining cholesterol distribution and adipogenesis in vitro, as well as activating WAT thermogenesis in vivo under HCD feeding. The process of cholesterol esterification plays a critical role in adipose tissue expansion and overall metabolic health.

(491 words)

Acknowledgements

I would like to express my sincerest gratitude and appreciation to all those who have supported and guided me throughout my PhD journey.

To Dr. Yuyan ZHU, my PhD supervisor, for proposing the idea of this project and guiding me throughout the research journey. She is an exceptional scientist with numerous ideas and insightful comments regarding our study. She dedicates a significant amount of time to training and inspiring me through meetings and discussions. I am profoundly grateful for her patient guidance and unwavering support.

To my teammates at the YYZ lab, Xiaohan Pan, Xiaolin Wu, and Xiaohan Cao, who have shared numerous wonderful ideas and provided encouragement during challenging times.

To Ms. Shiu Ho Ting, for her generous advice and assistance in my project.

To Dr. Kekao Long, for his continuous support in providing materials and sharing valuable experimental skills and experiences.

To Dr. Alan Leung, who has provided technical help in metabolic cage experiments and confocal microscopy.

To Ms. Yangyang and Mr. Kwok Tsun Ka, for their collaboration, discussions, and shared experiences, which have played a crucial role in broadening my understanding and refining my ideas.

To Vicki, Iris, and Tracy, undergraduate students who have provided valuable help in my research.

To Dr. Wenxuan Yu, for providing useful information and laboratory materials that have assisted me in my research.

To Dr. Miao Zhang, for her encouragement and sharing of inspiring research ideas.

To Xiaoqing Kuang, for her expertise in histological skills and wonderful ideas.

To Shuqing SUN, for her help in my reseach and always encourage me.

Finally, to my mother and father, for their unconditional love and encouragement throughout my entire journey. I wish them eternal happiness and all the best.

Publications

1. Xia X#, **Liu Q#,** Zhu Y, et al. Recent advances of triboelectric nanogenerator based applications in biomedical systems[J]. EcoMat, 2020, 2(4): e12049. (#co-first authors)
2. **Liu Q**, Zhu Y. SOAT1 deficiency impairs cholesterol metabolism and adipogenesis in adipocytes. 2023. (in preparation)
3. **Liu, Q**. Zhu Y. Adipocyte SOAT1 deficiency enhance adipose tissue inflammation and promote iWAT beige in high cholesterol fed mice. 2023. (in preparation)
4. Zhu, Y., Kim, S. Q., Zhang, Y., **Liu, Q**., & Kim, K. H. (2021). Pharmacological inhibition of acyl-coenzyme A: Cholesterol acyltransferase alleviates obesity and insulin resistance in diet-induced obese mice by regulating food intake. *Metabolism*, *123*, 154861.

Conference Presentations and Awards

Awards: Best Early Career Researcher Poster Award (International Congress of Obesity 2022)

Conference Presentations (selected):

1. **Liu Q**, Zhu Y. The role of SOAT1 in regulating intracellular cholesterol redistribution during adipogenesis. International Congress of Obesity 2022- Melbourne, Australia.
2. **LIU Q,** Zhu Y. Adipocyte-specific SOAT1 deficiency decreased diet induced hepatic steatosis and promoted heart hypertrophy. Symposium of Metabolic Biology Branch of Chinese Biophysical Society 2023- Henan, China.

Other PolyU on campus presentations:

1. **LIU Q,** Zhu Y. SOAT1 regulates adipocyte cholesterol homeostasis and promotes lipid droplet during adipogenesis. The 2ed ABCT Research Postgraduate Symposium in the Biology Discipline 2021- PolyU, HK
2. **LIU Q,** Zhu Y. Adipocyte-specific SOAT1 deficiency decreased diet induced hepatic steatosis and promoted heart hypertrophy. The 4th ABCT Research Postgraduate Symposium in the Biology Discipline 2023- PolyU, HK

Table of Contents

List of Figures

List of Tables

List of Abbreviations

ABCA1	ATP-Binding Cassette Transporter A1
ABCG1	ATP-binding cassette sub-family G member 1
ACC	Acetyl-CoA carboxylase
ACLY	ATP citrate lyase
ACTB	Actin Beta
AgRP	Agouti Related Neuropeptide
AKO	Adipocyte-specific knockout
AKT	Alpha serine/threonine-protein kinase
AMPK	AMP-activated protein kinase
ANP	Atrial natriuretic peptide
AT	Adipose tissue
ATGL	Adipose triglyceride lipase
AVA	Avasimibe
BAT	Brown adipose tissue
BMI	Body mass index
BW	Body weight
CAF	Centralized Animal Facilities
cAMP	Cyclic adenosine monophosphate
CE	Cholesterol ester
CETP	Cholesterol ester transfer protein
ChREBP	Carbohydrate-responsive element-binding protein
CL	Cardiolipin
CM	Chylomicrons
COX7a1	C oxidase subunit 7A1
COX8b	Cytochrome c oxidase subunit 8B
CTRL	Control
DAGs	Diacylglycerols
DEGs	Differentially expressed genes

DGAT	Diacylglycerol acyltransferase
DGE	Digital gene expression
DIO	Diet induced obese
DNL	De novo lipogenesis
EE	Energy expenditure
EF	Ejection fraction
ER	Endoplasmic reticulum
eWAT	Epididymal white adipose tissue
FC	Free cholesterol
FFA	Free fatty acid
FS	Fraction shortening
GAPDH	Glyceraldehyde-3-phosphate dehydrogenase
GBM	Glioblastoma
GLUT4	Glucose transporter type 4
GTT	Glucose tolerance test
HCD	High cholesterol diet
HDL-c	High-density lipoprotein
HFD	High fat diet
HFHC	High fat high cholesterol diet
HOMA-IR	Homeostatic model assessment
HSL	Hormone-sensitive lipase
IBMX	3-isobutyl-1-methylxanthine
IHC	Immunohistochemistry
IR	Insulin resistance
ITT	Insulin tolerance test
iWAT	Inguinal White Adipose Tissue
KD	Knockdown
KEGG	Kyoto Encyclopedia of Genes and Genomes
KO	Knockout

KRPH	Krebs Hepes Buffer
LD	Lipid droplet
LDLR	Low density lipoprotein receptor
LV	Left ventricular
LXR	Liver X receptor
MA	Mature adipocyte
MAM	Mitochondria-associated membrane
MHO	Metabolic healthy obese
MUO	Metabolic unhealthy obese
NAFLD	Nonalcoholic fatty liver disease
ND	Normal diet
NEFA	Non-esterified fatty acids
OA	Oleic acid
OE	Overexpression
ORO	Oil red O
PM	Plasma membrane
PTT	Pyruvate tolerance test
RER	Respiratory exchange ratio
Retro-WAT	Retroperitoneal white adipose tissue
RIPA	Radioimmunoprecipitation assay
RT	Room temperature
SCAP	SREBP cleavage-activating protein
SCD1	Stearoyl-CoA Desaturase-1
SFA	Saturated fatty acid
SGBS	Simpson-Golabi-Behmel syndrome
SOAT	Sterol O-acyltransferase
SVF	Stromal vascular fraction
sWAT	Subcutaneous white adipose tissue
TG	Triglyceride

CHAPTER 1. LITERATURE REVIEW

1.1 Obesity

Obesity is a pressing public health concern as it involves the excessive accumulation of calories in the body due to an imbalance between energy intake and expenditure. This results in weight gain and various health complications. According to the latest report from The Lancet [1], the key factors that influence obesity are systematic power, environmental factors, and personal lifestyle. Individuals experiencing poverty often face restricted access to nutritious food choices, resulting in a dependence on affordable, high-calorie foods. This reliance on calorie-dense options can contribute to weight gain. Consuming a diet that is high in calories, sugar, and saturated fat can also contribute to weight gain, as can a sedentary lifestyle with limited opportunities for physical activity. Obesity has become a global problem and requires a multifaceted approach to prevention and treatment.

1.1.1 The occurrence of obesity and related diseases

According to a report from the WHO in 2017, the global development of obesity continues to rise, affecting approximately 650 million adults, 340 million adolescents, and 39 million children. These data indicate a concerning trend of increasing obesity rates worldwide [2]. The prevalence of obesity is significant in China, with more than one in seven individuals meeting the criteria for overall obesity, and one in three individuals meeting the criteria for abdominal obesity [3]. In Hong Kong, around 30% of the adult population is obese [4]. The WHO estimates that one out of five adults worldwide will be obese by 2025 [5].

Obesity is associated with an increased risk of developing various diseases, including type 2 diabetes (T2D). In obesity, adipocytes are less responsive to insulin, which impedes the capacity of insulin to stimulate cells to uptake glucose. resulting in high blood glucose levels. Adipocyte hypertrophy also triggers the secretion of

inflammatory molecules, including TNF-alpha and MCP-1, which can promote inflammation and further impair the insulin signal pathway [6]. Obesity promotes high insulin levels in the blood, which further promotes lipogenesis and inhibits lipolysis in the liver, causing NAFLD happened [7]. The development of NAFLD in obese individuals can also be influenced by specific genetic factors. For example, the PNPLA3 and TM6SF2 genes have been identified as potential contributors to the elevated risk of NAFLD in obese individuals [8].

A high insulin level in the bloodstream also contributes to atherosclerosis, or the buildup of plaques in the arteries, which can result in heart attack and stroke, increasing the risk of CVD. Obesity is closely link to inflammation, which causes DNA damage, and high insulin levels in the blood promote cancer cell growth. Some hormones, such as IGF-1, promote certain types of cancer and are secreted more by obesity [9].

In summary, obesity is associated with an increased risk of type 2 diabetes, CVD, respiratory problems, and musculoskeletal disorders [10]. Developing effective anti-obesity drugs is crucial for improving health outcomes, reducing the economic burden of obesity, and offering additional treatment options for individuals facing challenges associated with obesity.

1.1.2 Treatment for obesity

The pharmaceutical industry has made significant progress in combating obesity due to the rapid advancement of scientific technology. Anti-obesity strategies including calorie restriction, lifestyle management, drug therapy, and weight-loss surgery have been suggested, such as bariatric surgery, but these interventions are inadequate to meet the worldwide medical demands [11]. Recently, numerous studies focusing on reducing appetite or increasing satiety pathways have been proposed [12], and Liraglutide (a GLP-1 agonist) is one of the most promising drugs for anti-obesity treatment. GLP-1 is a gut-derived hormone that can be stimulated by the presence of nutrients in the blood and then released by intestine L-cells. The circulating GLP-1 levels elevate after a meal. GLP-1 exerts its functions through its receptor - GLP-1Rs, which have broad

expression in pancreas, liver, and brain. Activate GLP-1 receptors inhibits the release of hunger hormone neuropeptide Y (NPY) and appetite-stimulating hormone ghrelin, which reduces appetite and increases satiety. In the pancreas, GLP-1 stimulates the release of insulin through the cAMP signal pathway to elevate blood glucose levels, and also inhibits the release of glucagon, which aids in the reduction of blood glucose levels. In the liver, GLP-1 reduces glucose production and promotes the storage of glucose as glycogen. The demonstrated effects of GLP-1 indicate its potential as an attractive candidate for treating T2D and various metabolic conditions [13]. In a clinical study, obese patients were treated with Beinaglutide, a GLP-1 agonist, for a period of three months. The results showed significant reductions in fasting blood glucose levels, body mass index (BMI), as well as decreased levels of leptin and tumor necrosis factor [14].

Other anti-obesity drugs include Orlistat, which works by blocking the absorption of dietary fat into smaller components in the intestines by inhibiting the lipase enzyme, leading to weight loss. Phentermine, a sympathomimetic amine, works by activating the release of norepinephrine, a neurotransmitter that helps to reduce appetite and increase energy expenditure, leading to reduced calorie intake and weight loss. Bupropion is a combination medication that is a prescription medication that works by reducing appetite and cravings, leading to reduced calorie intake and weight loss. Figure 1-1 lists the weight-loss drugs in clinical development during 2015-2019. However, these drugs still have some limitations, such as causing gastrointestinal side effects (such as diarrhea, abdominal pain, and flatulence), dry mouth, constipation, insomnia, etc. [15].

Figure 1-1 [16] Weight-loss medications that have been under clinical development since 2015

Table 1. Weight-loss drugs in clinical development after 2015

Agent type	Agent	Indication	Manufacturer	Trials	ClinicalTrials.gov ID/ref.
Energy intake					
MC4R agonist	PL-8905	Obesity	Palatin Technologies	Announced	Not Recorded
NPY5R antagonist	S-237648	Obesity	Shionogi & Co.	In-house	See R&D Pipeline
Triple reuptake inhibitor/ SNDRI	Tesofensine/NS-2330	Obesity	NeuroSearch A/S	Phase 2	NCT00394667
Peripheral CB1 receptor blocker	GFB-024 (inverse agonist)	Kidney diseases	Goldfinch Bio	Phase 1	NCT04880291
	AM-6545 (antagonist)	Obesity	MAKScientific	Preclinical	See R&D Pipeline
GLP-1R agonist	Beinaglutide/Benaglutide	Obesity	Shanghai Benemae	Phase 3	NCT03986008
	Dulaglutide	T2D	Eli Lilly and Company	Phase 3	NCT03015220
				Phase 2	NCT02973100
				Phase 4	NCT02750410
	LY3502970	Obesity, T2D	Eli Lilly and Company	Phase 1	NCT05086445
				Phase 2	NCT05051579
				Phase 2	NCT05048719
	Efpeglenatide/^{LAPS}Exd4 Analog	T2D	Hanmi Pharmaceutical	Phase 3	NCT03353350
	Exenatide	HO	AstraZeneca	Phase 3	NCT02860923
	PB-119	T2D	PegBio Co.	Phase 3	NCT04504396
				Phase 3	NCT04504370
	Danuglipron/PF-06882961	Obesity, T2D	Pfizer	Phase 2	NCT04707313
				Phase 2	NCT04617275
				Phase 2	NCT03985293
	PF-07081532	Obesity, T2D	Pfizer	Phase 1	NCT04305587
	RGT001-075	T2D	Regor Therapeutics	Phase 2	NCT05297045
	Noiiglutide/SHR20004	Obesity	Hansoh Pharma	Phase 2	NCT04799327
	TG103	Obesity	CSPC Pharmaceutical	Phase 2	NCT05299697
	TTP273	T2D	vTv Therapeutics	Phase 2	NCT02653599
	XW003	Obesity	Sciwind Biosciences	Phase 2	NCT05111912
	XW004	Obesity, T2D	Sciwind Biosciences	Phase 1	NCT05184322
GCGR agonist	HM15136/^{LAPS}Glucagon Analog	Obesity, T2D	Hanmi Pharmaceutical	Phase 1	NCT04167553
	NN9030/NNC9204-0530	Obesity	Novo Nordisk	Phase 1	NCT02835235
GIPR agonist	ZP 6590	Obesity	Zealand Pharma	Preclinical	See R&D Pipeline
GLP-1R/GCGR dual agonist	Pemvidutide/ALT-801	Obesity	Altimmune	Phase 2	NCT05295875
	BI 456906	Obesity	Boehringer Ingelheim	Phase 2	NCT04667377
	CT-388	T2D	Carmot Therapeutics	Phase 1	NCT04838405
	CT-868	Obesity, T2D	Carmot Therapeutics	Phase 2	NCT05110846
	DD01	Obesity, T2D	D&D Pharmatech	Phase 1	NCT04812262
	JNJ-64565111	Obesity, T2D	Johnson & Johnson	Phase 2	NCT03586830
				Phase 2	NCT03486392
	NN9277/NNC9204-1177	Obesity	Novo Nordisk	Phase 1	NCT02941042
	Efinopegdutide/^{LAPS}GLP/GCG	NASH	Hanmi Pharmaceutical	Phase 2	NCT03486392
	SAR425899	T2D	Sanofi	Phase 1	NCT03376802
	OXM analog—Cotadutide/MEDI0382	T2D	AstraZeneca	Phase 1	NCT02548585
				Phase 1	NCT04208620
	OXM analog—G3215	Obesity, T2D	Imperial College London	Phase 1	NCT02692040
	OXM analog—IBI362/LY3305677	Obesity, T2D	Eli Lilly and Company	Phase 2	NCT04904913
				Phase 1	NCT04440345
	OXM analog—MOD-6031	Obesity, T2D	OPKO Health	Phase 1	NCT02692781
	OXM analog—OPK-88003/LY2944876	Obesity, T2D	OPKO Health	Phase 2	NCT03406377
GLP-1R/GIPR dual agonist	HS-20094	T2D	Hansoh Pharma	Phase 1	NCT05116410
	Tirzepatide/LY3298176	Obesity, T2D	Eli Lilly and Company	Phase 3	NCT05024032
				Phase 3	NCT04844918
				Phase 3	NCT04657016
				Phase 3	NCT04660643
				Phase 3	NCT04657003
				Phase 3	NCT04184622

Table 1. continued

Agent type	Agent	Indication	Manufacturer	Trials	ClinicalTrials.gov ID/ref.
GLP-1R/GIPR/GCGR triple agonist	HM15211/^{LAPS}Triple Agonist	NASH	Hanmi Pharmaceutical	Phase 2	NCT04505436
	LY3437943	Obesity, T2D	Eli Lilly and Company	Phase 1	NCT04823208
				Phase 2	NCT04881760
				Phase 2	NCT04867785
	NN9423/NNC9204-1706	Obesity	Novo Nordisk	Phase 1	NCT03095807
	NNC0480-0389				
	SAR441255	Obesity	Sanofi	Phase 1	NCT04521738
GLP-1R agonist and GIPR antagonist	AMG133	Obesity	Amgen	Phase 1	NCT04478708
	GMA106	Obesity	Gmax Biopharm	Phase 1	NCT05054530
DPP-4 inhibitor	HSK7653	T2D	Haisco Pharmaceutical	Phase 3	NCT04556851
	Sitagliptin	T2D, NAFLD	Merck & Co.	Phase 4	NCT05195944
				Phase 3	NCT02849080
	Yogliptin	Obesity, T2D	Easton Biopharmaceuticals	Phase 3	NCT05318326
AMYR agonist	Cagrilintide/NN9838/AM833/NNC0174-0833	Obesity, T2D	Novo Nordisk	Phase 1	NCT04940078
				Phase 1	NCT05254158
				Phase 2	NCT03856047
	ZP8396	Obesity	Zealand Pharma	Phase 1	NCT05096598
AMYR/CTR dual agonist	KBP-042	T2D	Nordic Bioscience	Phase 2	NCT03230786
	KBP-089	T2D	Nordic Bioscience	Phase 1	NCT03907202
TAS2R agonist	ARD-101	Obesity	Aardvark Therapeutics	Phase 2	NCT05121441
PYY/Y2R signaling	NNC0165-1562	Obesity	Novo Nordisk	Phase 1	NCT03574584
	PYY1875/NNC0165-1875	Obesity	Novo Nordisk	Phase 1	NCT03707990
	NN9748/NN9747	Obesity, T2D	Novo Nordisk	Phase 1	NCT03574584
Ghrelin signaling	NOX-B11	Obesity	NOXXON Pharma	Preclinical	Not Recorded
	GLWL-01	PWS	GLWL Research	Phase 2	NCT03274856
	RM-853/T-3525770	PWS	Rhythm Pharmaceuticals	Preclinical	See R&D Pipeline
	TZP-301	Obesity	Ocera Therapeutics	Preclinical	Not Recorded
	EX-1350	Obesity, T2D	Elixir Pharmaceuticals	Preclinical	Not Recorded
Leptin analog	Metreleptin	Lipodystrophy	AstraZeneca	Phase 3	NCT05164341
Leptin sensitizer	Celastrol	Obesity, T2D	Research Use Only	Preclinical	PMID: 26000480[420]
	Withaferin A	Obesity, T2D	Research Use Only	Phase 1	PMID: 30904387[421]
	ERX1000	Obesity	ERX Pharmaceuticals	Phase 1	NCT04890873
GDF15 agonist	LA-GDF15	Obesity	Novo Nordisk	Phase 1	See R&D Pipeline
	LY3463251	Obesity	Eli Lilly and Company	Phase 1	NCT03764774
α7-nAChR agonist	GTS-21/DMXB-A	Obesity	Otsuka Pharmaceutical	Phase 1	NCT02458313
Energy absorption					
Strain product	WST01	Obesity, T2D	SJTUSM	Phase 2	NCT04797442
	Xla1	Obesity	YSOPIA Bioscience	Phase 1	NCT04663139
Orlistat and acarbose	EMP16-02	Obesity	Empros Pharma AB	Phase 1	NCT04521751
Energy storage					
MGAT2 inhibitor	BMS-963272	Obesity	Bristol Myers Squibb	Phase 1	NCT04116632
	S-309309	Obesity	Shionogi & Co.	In-house	See R&D Pipeline
DGAT2 inhibitor	Ervogastat/PF-06865571	NASH, NAFLD	Pfizer	Phase 1	NCT03513588
Sirt1/AMPK/eNOS signaling	NS-0200/Leucine-Metformin-Sildenafil	Obesity	NuSirt Biopharma	Phase 2	NCT03364335
Labisia pumila extract	SKF7	Obesity	Medika Natura	Phase 2	NCT04557267
Stimulating IDE synthesis	Cyclo-Z (cyclo(his-pro) plus zinc)	T2D	NovMetaPharma	Phase 2	NCT03560271
					NCT02784275
αGI inhibitor	Sugardown/BTI320	Prediabetes	Boston Therapeutics	Phase 2	NCT02358668
CCR2/CCR5 dual agonist	Cenicriviroc	T2D, NAFLD	AbbVie	Phase 2	NCT02330549
Energy expenditure					
SGLT2 inhibitor	Ipragliflozin/ASP1941	T2D	Astellas Pharma	Phase 3	NCT02452632
	Bexagliflozin/EGT1442	T2D	Theracos	Phase 3	NCT02836873
				Phase 3	NCT02715258
				Phase 3	NCT02558296

Table 1. continued

Agent type	Agent	Indication	Manufacturer	Trials	ClinicalTrials.gov ID/ref.
	Remogliflozin etabonate	T2D	Avolynt	Phase 2	NCT02537470
	Canagliflozin	Obesity, T2D	Johnson & Johnson	Phase 4	NCT02360774
	Dapagliflozin	T2D, HF, CKD	AstraZeneca	Phase 2	NCT05179668
				Phase 4	NCT04249778
				Phase 2	NCT03968224
				Phase 3	NCT02413398
	Empagliflozin	T1D, T2D	Boehringer Ingelheim	Phase 3	NCT04233801
				Phase 2	NCT03132181
				Phase 4	NCT03157414
				Phase 3	NCT02863328
				Phase 3	NCT02580591
				Phase 3	NCT02414958
	Ertugliflozin	T2D, HF	Merck & Co.	Phase 3	NCT03717194
SGLT1/2 inhibitor	Licogliflozin/LIK066	Obesity	Novartis	Phase 2	NCT03320941
				Phase 2	NCT03100058
	Sotagliflozin	T1D, T2D, CKD	Lexicon Pharmaceuticals	Phase 3	NCT03242252
				Phase 3	NCT03242018
				Phase 3	NCT02531035
				Phase 3	NCT02384941
MetAP2 inhibitor	Beloranib/ZGN-440/ZGN-433	Obesity	Larimar Therapeutics	Phase 2	NCT01666691
	ZGN-1061	Obesity, T2D	Larimar Therapeutics	Phase 2	NCT03254368
FGF21/FGFR1c/β-Klotho signaling	LLF580	Obesity	Novartis Pharmaceuticals	Phase 1	NCT03466203
	NN9499/NNC0194-0499	Obesity	Novo Nordisk	Phase 1	NCT03479892
	MK-3655/NGM313	Obesity, NASH	Merck & Co.	Phase 1	NCT02708576
					NCT04583423
	BFKB8488A	NAFLD	Genentech	Phase 1	NCT02593331
FGFR4 inhibitor	IONIS-FGFR4Rx	Obesity	Ionis Pharmaceuticals	Phase 2	NCT02476019
FXR agonist	ASC42	Obesity, NASH	Gannex Pharma	Phase 1	See R&D Pipeline
THR-β agonist	ASC41	Obesity, NAFLD	Gannex Pharma	Phase 1	NCT04686994
sGC stimulator	Praliciguat/IW-1973	T2D	Cyclerion Therapeutics	Phase 2	NCT02906579
Neutrophil elastase inhibitor	PHP-303	Obesity	pH Pharma	Phase 1	NCT03775278
PDE4/5 inhibitor	Roflumilast	Obesity	Altana Pharma	Phase 3	NCT04800172
	Tadalafil	Obesity	Eli Lilly and Company	Phase 2	NCT02819440
Glabridin analog	HSG4112	Obesity	Glaceum	Phase 1	NCT05310032
				Phase 2	NCT05197556
				Phase 1	NCT04703764
ActRII inhibition	Bimagrumab/BYM338	T2D	Novartis	Phase 2	NCT03005288

1.2 Adipose tissue

Adipose tissue was first identified as a connective tissue filled with lipid droplets in the late 1940s [17], and it was originally thought of as an organ that only served as an energy storage warehouse to store calories after feeding. Later, more and more studies found multiple functions (energy storage, thermoregulation, endocrine organ) of adipose tissue [17].

1.2.1 Adipose tissue function

Adipocytes accumulate lipids through two main processes. One is the uptake of circulating FFAs liberated from TAGs by lipoprotein lipase (LPL). LPL hydrolyzes

TAGs in lipoproteins such as VLDL and chylomicrons (CM) produced by the liver and small intestine, respectively. Glucose uptake by adipocytes is accompanied by its conversion into glycerol, which serves as the foundation for TG synthesis. Free fatty acids are esterified by the enzyme diacylglycerol acyltransferase (DGAT) and synthesized into TAGs. DGATs are key enzymes in maintaining adipocyte lipid metabolism. Mice lacking either DGAT1 or DGAT2 in adipocytes do not show a significant metabolic phenotype in ND feeding. However, adipocyte-specific KO of DGAT1 result in an reduction of WAT mass and LDs accumulating in the liver in HFD feeding, suggesting the importance of DGAT1 [18]. Another process is de novo lipogenesis (DNL), which encompasses the synthesis and esterification of fatty acids. After a meal, particularly a high-carbohydrate diet, adipocytes take up excess glucose through insulin-dependent (GLUT4) or insulin-independent (GLUT1) pathways, through glycolysis and the TCA cycle, fatty acid precursors undergo a series of metabolic transformations to produce citrate. ACLY and ACC1 then generate acetyl-coenzyme A (acetyl-CoA), which serves as the substrate for fatty acid synthase (FASN) to synthesize palmitic acid.The palmitic acid is further elongated and desaturated to synthesize fatty acids. The main transcriptional regulators in the DNL process involved in ChREBP and SREBP1 in adipose tissue. Adipose tissue-specific knockout of ChREBP in mice decreased DNL ability and led to insulin resistance [19]. Nevertheless, global KO SREBP1 in mice did not yield any significant effects on adipose tissue [20].

1.2.1.1 Lipid storage

The equilibrium of TAG homeostasis is upheld through the interplay between lipogenesis and lipolysis. Lipolysis of stored TAGs is activated in all tissues during fasting, exercise, or exposure to cold stimuli. ATGL, MGL and HSL regulate the lipolysis process by breaking down TAGs into diacylglycerols (DAGs) and monoacylglycerols (MAGs), which are then converted into FFAs and glycerol. FFAs can either be re-esterified within the adipocyte to participate in the process of

lipogenesis or be released into the bloodstream for utilization by the liver in gluconeogenesis or by the muscles in oxidative phosphorylation [21].

1.2.1.2 Secretory functions

Adipose tissue, in addition, functions as an endocrine organ, releasing a diverse range of mediators, including lipids, miRNAs, proteins, and peptide hormones (Figure 1-2). Leptin, adiponectin, and resistin are well-documented adipokines that are secreted by adipose tissue and have important regulatory effects. However, some pro-inflammatory and insulin-antagonist mediators like IL-8, IL-6, and RBP4 are secreted under hypertrophy and obesity physiology, which can also attenuate adiponectin secretion [22].

Figure 1-2 Summary of adipocyte- secreted mediators

Mediator	Functions in adipocytes	Reference
BMPs	Activate transcription factors and signal pathway to promote the process of preadipocytes differentiation into mature adipocytes. BMP4 has been linked to elevated adiposity and insulin resistance in both human and rodent. BMP4 activates nuclear entry of the pparγ transcriptional activator ZFP423 to promote adipose tissue adipogenesis.	[23]
RBP4	A protein produced by liver and adipose tissue, inhibit insulin signal pathway in adipocytes and lead to insulin resistance. Promote lipolysis in adipocytes and increase circulating FFAs.	[24]
PAI-1	Inhibit insulin signal pathway in adipocytes lead to insulin resistance. Increase lipogenesis and decrease lipolysis in adipocytes.	[25]
Omentin	A hormone produced by adipose tissue improves insulin sensitivity by enhancing the insulin signal in adipocytes, increasing glucose uptake and utilization. Increases lipolysis, which helps to reduce adipocyte size and number, preventing obesity.	[26]
FGF21	A hormone mainly produced by liver and adipose tissue, directly to brown adipocytes to improve insulin sensitivity. Increase lipolysis.	[27]

Apelin	A peptide produced by adipose tissue, improve insulin sensitivity.	[28]
Visfatin	An adipokine, enhancing adipocytes insulin signal	[29]
miRNAs	Regulate adipogenesis process, like miR-33a and miR-122 have shown to modulate target genes involved in both fatty acid synthesis and oxidation. miR-155 have shown to promote the pro-inflammatory cytokines in adipose tissue.	[30]
Lipocalins	Stimulates lipolysis in adipocytes and exhibits anti-inflammatory effects by inhibiting pro-inflammatory cytokines and chemokines. lipocalin-2 has been shown to regulate glucose uptake and utilization in adipocytes.	[31]
Vaspin	An adipokine predominantly expressed in adipose tissue. Improve insulin sensitivity and increase lipolysis. Individuals with obesity often exhibit reduced levels of vaspin, which plays a significant role in the development of insulin resistance and various metabolic disorders.	[32]
Adipsin	A protein produced by adipose tissue, promote triglycerides synthesis and regulate inflammation in WAT.	[33]

Leptin, the first hormone derived from adipocytes [34]. It is positively related to fat mass in both humans and mice, and its main function is to inhibit food intake by regulating appetite through leptin-melanocortin pathway. Due to its function as an appetite suppressant, leptin has been developed as an anti-obesity drug. However, in mice that are obese or have been fed HFD for a long time, leptin resistance can develop, which makes them unable to respond to leptin.

Adiponectin has many beneficial functions, including anti-hyperglycemic and anti-inflammatory effects, these characteristics make it a promising target for obesity treatment. The level of adiponectin in human plasma is 2-20 μg/ml, which is significantly higher than most other secreted factors such as resistin, insulin and leptin [35]. In contrast to leptin, adiponectin levels exhibit a negative correlation with fat mass and obesity. Adiponectin manifests in three forms: HMW, MMW, and LMW trimers, representing the oligomers of varying molecular sizes. HMW is the beneficial form of

adiponectin, which can lower plasma glucose levels and improve insulin sensitivity. Adiponectin also has many beneficial effects in other organs, such as inhibiting hepatic glucose uptake, promoting glucose uptake in muscles, as well as enhances fatty acid oxidation and insulin sensitivity. Administration of adiponectin into adiponectin-knockout mice ameliorates insulin resistance and improves insulin sensitivity [36].

Resistin is an adipokine hormone secreted by adipose tissue, with regulatory roles in metabolism. Encoded by the RETN gene, it is primarily produced by adipocytes but also found in other tissues like the liver and skeletal muscle. Resistin can hinder insulin signaling in the liver and skeletal muscle, leading to reduced glucose uptake and increased glucose production. It has been associated with inflammation and the immune system, potentially in obesity and metabolic disorders [37]. Additional investigation is necessary to elucidate the specific functions of resistin, its potential protective effects against inflammation require further investigation [38].

1.2.2 Adipogenesis

1.2.2.1 Adipogenesis process

Adipogenesis is the process through which preadipocytes undergo differentiation to become fully mature adipocytes, specialized cells responsible for storing and releasing lipids based on metabolic requirements. Adipogenesis occurs primarily in adipose tissue, but also occurs to some extent in other tissues like muscle and bone marrow. Adipogenesis encompasses multiple stages, beginning with the commitment of preadipocytes to the adipocyte lineage. This commitment is controlled by TFs such as early EBF1, KLF4, and C/EBPδ. Following the commitment of preadipocytes, the subsequent stages of adipogenesis involve the proliferation and differentiation. The process is regulated by growth factors such as FGF1 and PDGF, which support the expansion of the preadipocyte population. The differentiation process is further controlled by key TFs, including PPARγ, C/EBPα, and SREBP1c. These factors facilitate the gene expression related with lipid metabolism and storage. The process of

adipogenesis is characterized by the maturation of mature adipocytes, which includes the formation of lipid droplets—specialized organelles responsible for storing triglycerides and other lipids [39]. The regulation of adipogenesis involves a complex interplay of TFs and signaling pathways that are essential for controlling the expression of genes related to adipocyte differentiation and function (Figure 1-3).

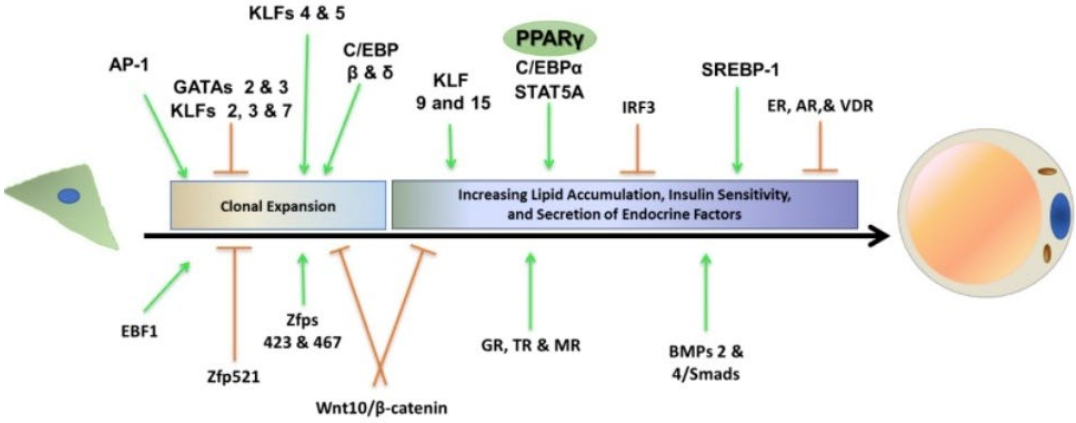

Figure 1-3 [40] Transcription regulators involved in adipogenesis.

GATAs: GATA-binding factor; KLFs: Krüppel-like factors; EBF-1: Early B-cell factor; ZFPs: Zinc Finger Protein; BMPs: Bone morphogenetic proteins; C/EBPs: CCAAT-enhancer-binding proteins.

1.2.2.2 activator of adipogenesis

PPARγ is the principal transcription factor that promotes adipogenesis. It is expressed in preadipocytes and upregulated during the differentiation process. PPARγ directly controls the expression of genes which are critical for adipocyte differentiation and function, including adipose protein 2 (aP2), LPL, and FASN. These genes participate in crucial functions such as the uptake, synthesis, and storage of lipid molecules within adipocytes. Adipocyte-specific PPARγ KO mice exhibited decreased fat mass and insulin resistance [41]. Human mutations in PPARγ lead to severe insulin resistance and lipodystrophy [42]. Thiazolidinediones (TZDs) are a type of drugs that bind to and activate PPARγ, and they are used clinically to treat type 2 diabetes by improving insulin sensitivity.

During early adipogenesis, C/EBPβ and C/EBPδ work together to promote adipocytes differentiation by inducing gene expression for adipogenic TFs C/EBPα and PPARγ

[43]. C/EBPα promotes the gene expression related with lipid metabolism and storage, like ap2 and LPL. The expression pattern and activity of C/EBP family members are positively regulated by several hormonal and metabolic factors, such as insulin, glucocorticoids, and dietary factors.

The Signal Transducer and Activator of Transcription (STAT) family of TFs exert crucial function in regulating adipocyte metabolism and function. Except for their involvement in adipogenesis, STATs also contribute to lipid metabolism and glucose regulation, as well as the secretion of adipokines like leptin and adiponectin. Activation of STAT3 in adipocytes leads to increased mRNA level of genes related with lipid metabolism and storage, such as FASN, ACC, and perilipin. STAT3 also influences genes related to insulin sensitivity, such as GLUT4 and IRS1. On the other hand, STAT1 and STAT4 are linked with the regulation of inflammation and immune function within adipose tissue. Activation of STAT1 and STAT4 in adipocytes lead to the down-regulation of genes connected with lipid metabolism and insulin sensitivity, facilitating the occurrence of metabolic dysfunction like insulin resistance and T2D [44].

1.2.2.3 Inhibitors of adipogenesis

Wingless-related integration site (Wnt) signaling is a complex pathway that exerts decisive function in the regulation of adipogenesis. During early adipogenesis, Wnt signaling pathway impedes the differentiation of adipocytes by suppressing the activity of TFs involved in adipogenesis. The inhibition of adipogenic gene expression is mediated through the foster the canonical Wnt pathway, which triggers the β-catenin stability. This stabilization then leads to the suppression of adipogenic gene expression. However, during late adipogenesis, Wnt signaling promotes adipocyte differentiation and function by inducing the genes connected with lipid metabolism and storage, such as LPL, FASN, and adiponectin. The activation of the non-canonical Wnt pathway, which includes the activation of Wnt receptors, mediates the promotion of gene expression involved in lipid metabolism and storage, such as FZD5 and RORα, and downstream effectors, such as JNK and PKC [45].

GATA transcription factors are named based on their DNA binding specificity in the

GATA sequence. The GATA family includes six members (GATA1-6). GATA2 and GATA3 are transcription factors that are expressed in preadipocytes and are upregulated during the differentiation process, which could promote adipocyte differentiation. GATA4 and GATA6 are late transcription factors that are expressed in mature adipocytes and are essential for the continuation of adipocyte function. GATA1 and GATA5 are transcription factors that play distinct roles in adipose tissue biology. GATA1 promotes the gene expression connected to erythropoiesis and angiogenesis, contributing to adipose tissue expansion. Additionally, GATA5 regulates the genes inculpated to lipid metabolism and storage, including FASN and ADRP (adipose differentiation-related protein) [46].

Generally, pro-inflammatory cytokines inhibit adipogenesis. Pro-inflammatory cytokines inhibit adipocyte differentiation by suppressing the adipogenic TFs, like PPARγ and C/EBPα. TNF-α, IL-6 and IL-1β competent to activate intracellular signaling pathways, which lead to decreased gene expression of adipogenic. Furthermore, foster adipocyte apoptosis and inflammation by pro-inflammatory cytokines contribute to the onset of metabolic disorders [47].

1.2.3 Adipose tissue remodeling during obesity

1.2.3.1 Adipose tissue hypertrophy and hyperplastic

WAT expands through two ways: hypertrophy and hyperplasia. Adipose tissue hypertrophy occurs when the size of existing adipocytes increases due to an accumulation of triglycerides, while hyperplasia refers to an increasement of adipocytes number through preadipocytes differentiation. The presence of hypertrophic adipocytes is linked to the development of metabolic dysfunction, including insulin resistance, T2D, and CVDs. This occurs because hypertrophic adipocytes display reduced insulin sensitivity and release higher amounts of pro-inflammatory cytokines and adipokines. These factors can lead to the emergence of metabolic dysfunction. Adipose tissue hyperplasia occurs when preadipocytes differentiate into mature adipocytes. This

process can occur in response to positive energy balance, physical activity, and certain hormonal and metabolic factors. Compared to hypertrophic adipose tissue, hyperplastic adipose tissue is associated with enhanced insulin sensitivity as well as the reduction risk of metabolic disorders [48].

1.2.3.2 Signaling modulators in obesity

1.2.3.2.1 PI3K/AKT pathway

The PI3K/Akt pathway have an important role in participating adipocyte differentiation, glucose uptake, and lipid metabolism. It influences the activity of PPARγ by promoting its phosphorylation and activation [49]. Insulin, a key component of this pathway, triggers its activation by engage with its cell surface receptor. Insulin stimulates the downstream activation of PI3K, which then activates Akt. Akt, in turn, modulates the function of various downstream targets, including GLUT4 and FoxO1. Upon the PI3K/Akt pathway activation, the phosphorylation and inhibition of glycogen synthase kinase 3 (GSK3) occur, leading to the re-translocate GLUT4 from cytoplasm to PM and facilitating glucose uptake. Additionally, the PI3K/Akt pathway promotes the degradation of Sort1, a crucial component for GLUT4 translocation [50].

PI3k/AKT pathway regulate appetite through CNS system and FoxO1. Akt signaling has been shown to promote the activity of POMC neurons by inhibiting the activity of the FoxO1 transcription factor, which normally functions to suppress POMC gene expression. Akt also promotes the processing of POMC into α-MSH, which is released to suppress appetite. In addition to its effects on POMC neurons, Akt signaling has also been shown to inhibit the activity of AgRP neurons by promoting the degradation of the neuropeptide Y (NPY) receptor, which is required for AgRP signaling. Inhibit PI3K pathway abolish leptin effect on suppressed appetite [51].

The mTOR pathway is modulated by the PI3K/AKT pathway, which is activated when growth factors such as insulin bind to their respective cell surface receptors. This activation triggers PI3K, which subsequently activates Akt. Akt, in turn, activates mTOR by inhibiting the TSC1/TSC2 complex, which typically suppresses mTOR

signaling. In the hypothalamus, mTOR pathway activation exhibited decreased appetite and improve age-related obesity in animal studies. This effect is mediated through the activation of POMC neurons, which are stimulated by mTOR signaling to release α-MSH to suppresses appetite [52, 53].

1.2.3.2.2 MAPK signal pathway

MAPK (mitogen-activated protein kinase) pathway activation has been shown to promote adipogenesis and increase adipocyte size and number, leading to increased adiposity and the development of obesity. Dysregulation of the MAPK pathway has been linked with IR and impaired glucose uptake, as it involved in controlling thermogenesis, appetite, glucose metabolism, and insulin sensitivity. The ERK (extracellular signal-regulated kinase) branch of the MAPK pathway exert a critical role in maintaining proper metabolic equilibrium. Activation of the ERK pathway stimulates POMC activation and suppresses AgRP activity. In mice lacking JNK1, a component of this pathway, reduced appetite and increased EE are observed [54].

ERK pathway activation promotes adipogenesis by stimulating PPARγ and C/EBPα expression. Whole-body ERK KO mice exhibited resistance to obesity under HFD treatment, and SVF differentiated adipocytes show impaired adipogenesis [55]. p38 MAPK pathway activation is pivotal for the differentiation of preadipocytes into mature adipocytes, as observed in 3T3-L1 cells. When p38 MAPK is inhibited, adipocyte differentiation is suppressed, resulting in reduced lipid accumulation and a reduction in the expression of adipocyte markers like PPARγ and adiponectin [56]. In human adipocytes, p38 MAPK pathway activation stimulates the secretion of pro-inflammatory cytokines, containing IL-6 and TNF-α, which bring about the onset of insulin resistance and metabolic dysfunction in adipocytes [57].

The activation of the ERK pathway has negative impact on insulin signaling and diminish insulin sensitivity in multiple cell types, including adipocytes and hepatocytes. ERK activation has been shown to phosphorylate IRS-1 leading to its degradation and impaired insulin signaling. JNK1 and JNK2 activation phosphorylate IRS-1, inducing insulin resistance in obese individuals, while JNK3 activation improves insulin

sensitivity [58]. The MAPK pathway also regulates thermogenesis through IL-27 and irisin secretion to enhance thermogenesis regulated gene expression. Overexpression of MEK6 (MAPK/ERK kinase 6)- upstream of p38, decreased UCP1 and HSL expression in adipocytes [59].

1.3 The role of cholesterol homeostasis in Adipose tissue

Cholesterol, an essential fat naturally occurring in the body, serves a critical role in numerous cellular functions. These include the synthesis of hormones, production of vitamin D, and formation of bile acids. Adipose tissue is the largest free cholesterol pool inside our body, which has a paramount role in regulating cholesterol metabolism. While WAT retains the highest amount of free cholesterol in the entire body, the biosynthesis activity of cholesterol in adipocytes is relatively low. Therefore, the main resource of cholesterol in adipocyte is from circulating lipoprotein [60].

1.3.1 Cholesterol homeostasis in adipocyte

1.3.1.1 Unique role of adipocyte in cholesterol storage

WAT is a crucial part in the storage of fat within the body, produce hormone and thermogenesis, its metabolism deeply influence the whole body metabolism [61]. Almost all cholesterol reside in adipose tissue are located in adipocytes with its unesterified form, and 88% of them reside in the lipid droplet surface while the other part rest in plasma membrane [62]. It is worth note that adipocyte has unique position among other type of cells since peripheral cells contain few FC and most of the FC locate in plasma membrane. Adipocyte also quite different from adrenal cell (steroid-hormone production) as well as foam cell (cholesterol laden in atherosclerotic), which are able to produce excess cholesterol ester (CE) and store it [63]. The excess FC has detrimental effect on cells. The uptake of exogenous cholesterol by cells results in the suppression of endogenous cholesterol biosynthesis and decreased LDLR expression. These cells have developed other mechanism to consume the excess cholesterol [64] (figure 1-4), one mechanism is cholesterol esterification by the SOATs. There are two

isoforms of SOAT- SOAT1 and SOAT2. While SOAT1 is widely expressed in different cell types, SOAT2 is specifically found in intestinal epithelial cells and hepatocytes [65]. The other mechanism is cholesterol efflux to prevent FC accumulation, we will discuss it later. Within peripheral cells, FC undergoes a transformation into CE in the ER and is subsequently stored in droplets. The CE stored in droplet will go through hydrolysis process and become cholesterol consistently, and the if the body does not need cholesterol, the excess cholesterol will be returned to ER to undergo re-esterification process and re-sediment in droplet. In adipocytes, most cholesterol exist as the FC form because SOAT activity is low in adipocytes [66]. The large amount of FC reside in a stable status in adipocyte due to its solubility of FC in TG and it can efflux into circulating lipoprotein [67].

Cholesterol ester transfer protein (CETP) exert key function in regulating CE and TG transportation in plasma lipoprotein, which has the potential function to transfer the CE from ER to lipid droplet (LD) [68]. Except for its rich expression in hepatic, it can also be synthesized by adipose tissue, tissue macrophage and adrenal. Growing evidence show that it has the intracellular functions in mediate CE uptake form HDL into adipocyte in mouse hepatocytes [69]. CETP plays a crucial role in facilitating the reverse cholesterol transport (RCT) process by enhancing the upregulation of LDL receptors. A deficiency in CETP function may increase the susceptibility to atherosclerosis. Liver X receptor (LXR) and etoposide is the activator of CETP, which is a strong nuclear factor and a topoisomerase II inhibitor to induce CETP gene expression, respectively [70]. CETP expression is tightly associated with cholesterol homeostasis, they have observed that CETP deficiency led to cellular CE increased 2-3 fold in SW872 adipocytes, as well as disturb the capacity of efflux cholesterol to receptor of these cells [71]. Thus, the ectopic cholesterol deposition cause influence on error sense of sterol status and break cholesterol homeostasis finally [72].

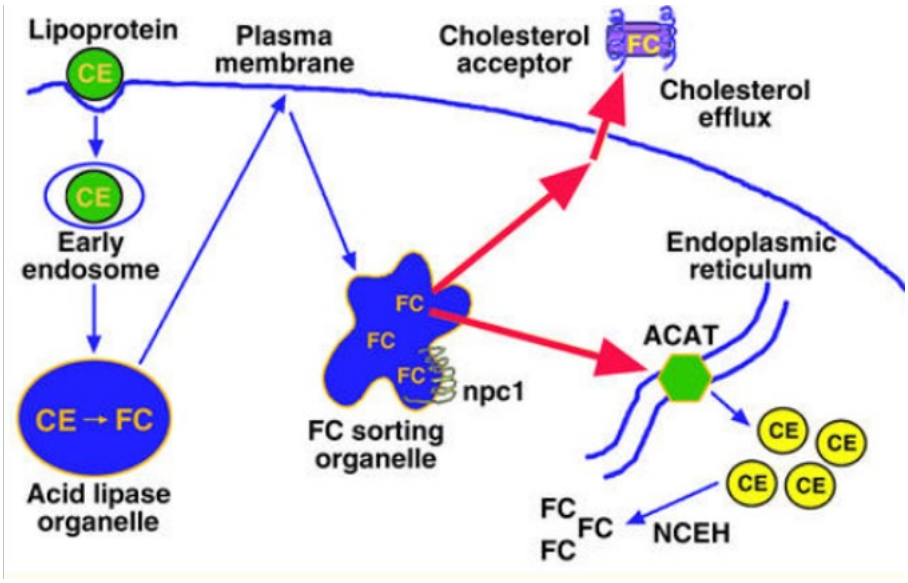

Figure 1-4 The mechanism of excess FC transportation.

FC uptake from lipoprotein and transport to ER become CE by SOAT, npc1 will influence cholesterol transportation. The other part of FC will remove from intracellular to extracellular when cholesterol acceptor present.

1.3.1.2 Cholesterol efflux pathway in adipocytes

ABCA1 and ABCG1, both members of the ATP-binding cassette transporters family, have a crucial function in facilitating the transport of cholesterol to HDL particles and apoA1. This process was essential for the formation of nascent HDL particles [73, 74]. HDL transport cholesterol has high rate in adipocyte, while there are few studies have reported the associated metabolic disease. Several researches have introduced the important role of ABCA1 in control intracellular cholesterol level. For example, Hayden et al [75] revealed that mice AT specific KO ABCA1 impaired glucose homeostasis through GTT and ITT test, along with decreased insulin secretion when subjected to HFD feeding. ABCA1 deficiency in brain would alert motor activity and sensorimotor function, reduce the insulin release if lack in β cells. The cholesterol efflux in gonadal adipose tissue (GAT) reduced upon ABCA1 knockdown with the increased cholesterol storage [76, 77]. ABCA1 is regulated by multiple mechanism, such as LXR and RXR. LXR belongs to the nuclear receptor superfamily of protein and

serves as the primary cholesterol sensor in cells. LXR is capable of activating ABCA1 expression, which in turn promotes cholesterol efflux [78]. Although LXR deficiency mice exhibit lean phenotype as well as prevent diet-induced obesity compared with their little mate, the mechanism is still under debate. This maybe explain as LXR deficiency mice led to less fat depot, increase lipid oxidation and reduce cholesterol efflux. LXR agonist will reduce cholesterol accumulation of cells and prevent the lesion of atherosclerosis [79]. Recent research has indicated that the OE ABCA1 has a positive impact on the progression of atherosclerosis in apoE knockout transgenic mice [80]. Furthermore, LXRs are implicated in regulate cholesterol efflux transporters ABCA1 and ABCG1 transcriptional, ABCA1 deficiency has close relationship with body weight loss while ABCG1 deficiency prevent diet-induced obesity. In the LXR deficiency mice they also observe fatty acid oxidation regulation, especially increased activity of uncoupling protein1 (UCP1), which caused the adipose tissue browning. ABCG1 promote cholesterol move from ER to plasma membrane (PM), thus, easily to release sterol to exocellular lipoprotein acceptors [81, 82].

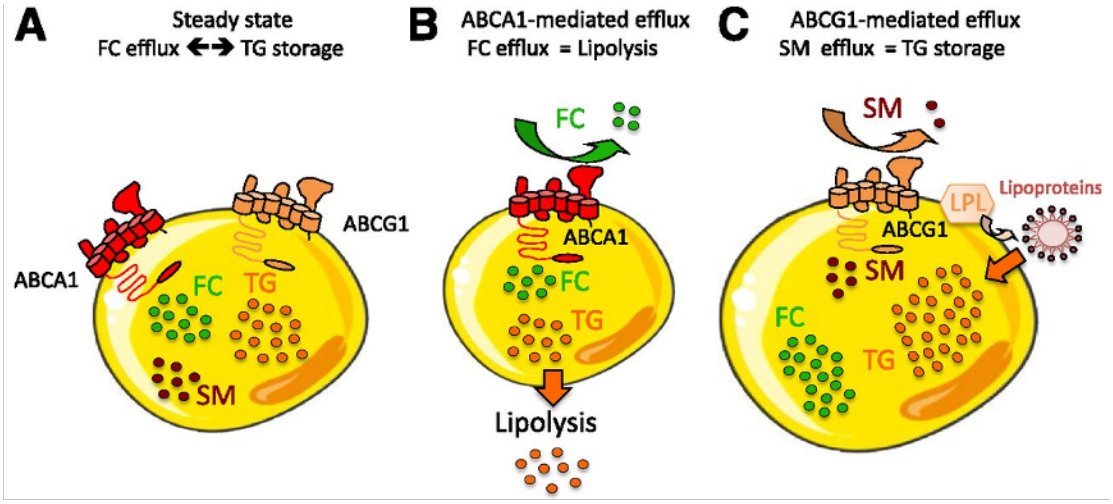

Figure 1-5 [83] Model of ABCA1 and ABCG1 regulate adipose fat storage.

Under stable condition, 95% cholesterol storage in adipose tissue as free cholesterol form and balance with TG. The relationship between FC, TG and SM content is unknown. The adipocyte maintains the FC and TG content in a relative stable level mainly through the ABCA1 mediated cholesterol efflux

function to led to lipolysis process, while the mechanism is not clear. The efflux of SM mediated by ABCG1 is linked to a reduction in the amount of SM present in the plasma membrane.

1.3.1.3 Uptake of cholesterol

Although adipose tissue functions as the primary reservoir of free cholesterol in the body, its capacity for synthesizing cholesterol is relatively limited, accounting for only 4% of that of the liver. Thus, the main source of cholesterol for adipocyte is from circulating lipoproteins, such as from ox-LDL and HDL [84]. CD36, alongside SR-BI, belongs to the family of cell surface glycoproteins known as type B scavenger receptors. CD36 is ubiquitous express in various cell type, such as adipocyte, cardiac myocytes, macrophages, and microglia. It has two transmembrane domains; two very short intracellular domain and its extracellular domain contain binding sites. CD36 plays vital function in lipid metabolism sensing and dietary lipid content regulation [85]. CD36 in taste cell recognize FA in dietary and induce cytosolic calcium upraise, led to neurotransmitter release and central fat sensing. CD36 also mediate the proportion of FA and cholesterol in CM (chylomicron), it removes the dietary lipid from intestine to blood. The particle size of CM in CD36 deficiency mice is smaller than WT mice, what is more, CD36 deficiency will damage the process of CM remove from bold, which cause hyperlipidemia in postprandial and fasting states. There is also evidence show that high level of CM residual with postprandial hyperlipidemia in CD36 deficiency patients. CD36 is the main FA transporter and support energy for beta-oxidation in cells. CD36 is the marker of progenitors in human adipocytes, the cells contain higher CD36 have the potential to form fat and TG storage capacity. CD36 silence reduce the fat accumulation in adipocyte in both vivo and vitro condition. The level and transportation of CD36 is also consistent with lipolysis and FA re-esterification. CD36 deficiency interact with SRC and ERK signal pathway to increase cAMP level, result in TG hydrolysis and free FA increased in blood [86-88]. Thus, CD36 is necessary to maintain lipid homeostasis.

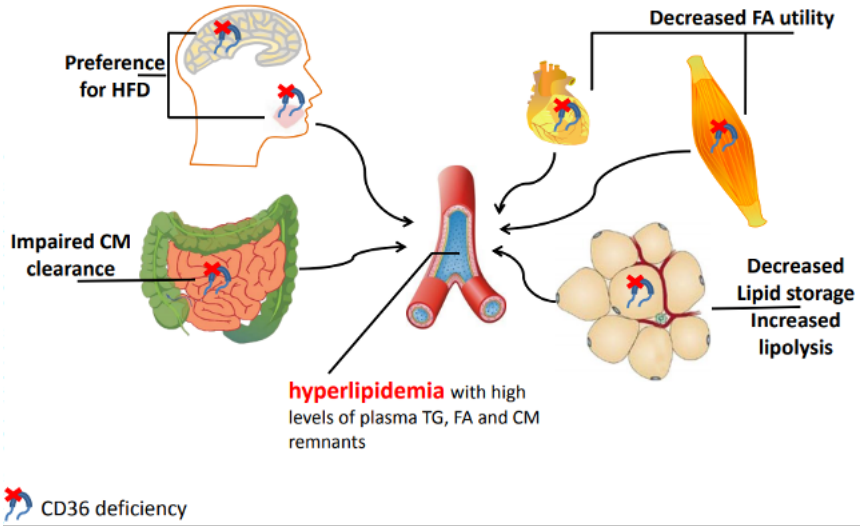

Figure 1-6 [89] The mechanism of hyperlipidemia in CD36 deficiency patients.

Loss of CD36 cause preference to HFD. Damage to CM clearance process, lipid metabolism, reduced fat storage and lipolysis effect increased further cause hyperlipidemia happened.

OLR1 is a scavenger receptor that is responsible for binding, endocytosing, and hydrolyzing oxidized LDL. OLR1 is expressed at minimal levels in mature adipocytes, its expression is significantly increased following treatment with thiazolidinedione (TZD), a ligand for the PPARg receptor. TZD treatment or adenvirus delivery will upregulate OLR1 expression, which led to increased ox-LDL in adipocyte uptake process. And it will also raise cholesterol content in adipocyte and reduce ox-LDL level in serum. The interaction between CD36 and OLR1 is crucial for adipocytes to maintain proper cholesterol levels, particularly in the presence of oxidized LDL. ox-LDL is considered as booster for early lesion to plaque rupture in atherosclerosis [90, 91]. Thus, adipose tissue is serve as the antidote for ox-LDL efflux, inhibit the formation of foam cell and atherosclerosis disease.

Scavenger receptor type-BI (SR-BI) is localize in PM cholesterol-enriched microdomains caveolae, participate selective uptake CE from liver and sterol formation tissue of HDL. There is abundant express of SR-BI in adipocytes, but its function and regulation is still unclear. The uptake of CE and SR-BI occurs specifically in a subset of caveolae that are abundant in cholesterol. Within these caveolae, CE can be hydrolyzed into free cholesterol [92, 93].

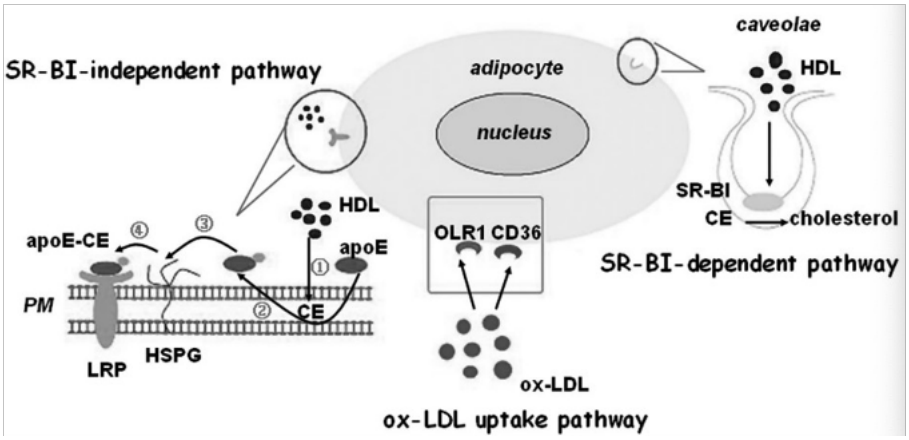

Figure 1-7 [94] Cholesterol uptake pathway in adipocyte,

The pathway is regulated by ox-LDL, SR-BI independent and dependent pathway.

1.3.2 Experiment model of hypercholesterolemia

Adipocytes can uptake cholesterol from plasma, and the concentration of PM cholesterol directly affects the cholesterol levels present in adipocytes., which is then stored. Several studies have shown that the cholesterol concentration in adipocytes can increase with an enahnced circulating cholesterol levels. African Green monkeys fed HCD exhibited elevated levels of FC and increased adipocyte sizes specifically in the visceral fat region. In addition to the cholesterol levels, the pro-inflammatory genes and macrophage recruitment, as well as the FC efflux protein levels, were also increased, while the cholesterol biosynthesis and lipoprotein uptake were decreased in visceral fat [95]. After adding dietary cholesterol to the diet of LDLR −/− mice for 24 weeks, resulted in the manifestation of increased insulin resistance, adipocyte hypertrophy, macrophage accumulation, and local inflammation to be more severe in the intraabdominal adipose tissue compared to other diets [96]. Rats that were exposed to a HFHC diet exhibited evident signs of steatosis and inflammation. Additionally, hepatocyte ballooning and fibrosis were observed in their liver tissues., in comparison to rats fed a HFD diet after 18 weeks of treatment [97].

In conclusion, exposure to cholesterol through dietary intake or genetic factors that induce hypercholesterolemia results in the aggregation of cholesterol in WAT, generate

the development of IR. This phenotype varies in different animal models.

1.3.3 Cholesterol imbalance in adipocytes

In the context of obesity, the accumulation of free cholesterol can result in an approximate 50% increase in the total body free cholesterol levels. Thus, the unstable cholesterol level in adipocyte is regarded as an omen of obese. Strong evidence show that adipocyte dysfunction has close relationship with cholesterol metabolism, including cholesterol overload re-attribution and efflux. When adipocytes are larger in size, they tend to contain more cholesterol. This suggests that cholesterol may be overloaded in larger adipocytes [95, 98]. In addition, the triglyceride accumulation is also increased proportionally to the cholesterol content, although few research shows they are not always following the same pattern [99, 100]. Although cholesterol will accumulate within the lipid droplet with the adipocyte growth, however, the plasma membrane cholesterol content decreased in hypertrophied adipocyte [101], which imply that adipocyte hypertrophy will alter cholesterol distribution. The cholesterol balance will be interrupted in enlarged adipocyte and associate with whole body metabolic complication occur. In individuals with obesity, dyslipidemia manifests as elevated levels of LDL cholesterol, commonly known as the "bad" cholesterol, and reduced levels of HDL cholesterol, referred to as the "good" cholesterol. Elevated LDL cholesterol can lead to the development of cholesterol plaques in arteries, increasing the likelihood of atherosclerosis and heart disease. Conversely, higher amounts of HDL cholesterol are connected with a decreased occurance of heart disease.

1.4 SOAT enzymes

1.4.1 SOATs introduction

Sterol O-acyltransferase (SOAT), also referred to as cholesterol acyltransferase 1 (ACAT), including SOAT1 and SOAT2, were the primary enzyme located in the ER responsible for esterifying free cholesterol into cholesteryl esters. While SOAT1 is

present in various tissues, SOAT2 is primarily expressed in the liver and intestines. The cDNA sequence for SOAT1 was first identified in TY-Chuang's lab [102]. The majority of human SOAT1 mRNA is transcribed from exon 1-16, which can translate into a 50 kDa protein. Less mRNA from exon Xa translates into a 56 kDa size protein that has less SOAT enzyme activity. Human SOAT2 is located on chromosome 12 and translates into a 46 kDa protein [65]. In mice, SOAT1 mRNA is transcribed from exon 1-17, which can translate into a 48 kDa size protein [103]. SOAT1 is a protein located in the ER and contains nine transmembrane segments. The active-site residue of SOAT1 is His460, and its structure is a dimer of a dimer [104]. SOAT2 mRNA levels are relatively low compared to SOAT1 in adult liver, liver cell line L02 and hepatocytes. However, in several tumor cells, such as HCC, SOAT2 mRNA is significantly upregulated compared to normal cells [105]. This suggests that SOAT2 expression is inducible while SOAT1 is more constant. The expression pattern of SOAT1/SOAT2 in mice and monkeys closely resembles that of humans, with the exception that SOAT2 exhibits high expression levels in the liver under normal conditions. For example, the SOAT2 activity is four-fold higher in African monkeys compared to human liver [106]. SOAT2 is the primary isoform in mouse hepatocytes and plays an essential role in the storage and packaging of CE into lipoproteins that contain apoB within the liver. Notably, the highest expression levels of SOAT2 are observed in the proximal small intestine of mice. Moreover, SOAT2 is likely involved in the control of various cholesterol metabolism gene expression in the small intestine, including NPC1L1, accountable for the uptake of dietary cholesterol.

1.4.2 SOATs in various study

Meiner et al. first generated global knockout mice for SOAT1 [103] and SOAT2 [107]. SOAT1 deficiency in mice decreased CE levels in fibroblasts, adrenal membrane, and peritoneal macrophages, but not in the liver, suggesting tissue-specific regulation of SOAT1. Global KO of SOAT1 in mice did not affect their viability but resulted in a shortened lifespan compared to the control group. Additionally, these KO mice

exhibited an accumulation of free cholesterol (FC) in the skin and brain tissues. [108] and larger atherosclerotic lesion areas [109]. Myeloid-specific SOAT1 KO mice exhibited resistance to HFD-induced obesity and decreased inflammation in WAT. In both chow and HFD feeding, adipocyte size decreased and insulin sensitivity was upregulated in KO mice [110]. Myeloid-specific KO of SOAT1 in ApoE-/- mice models for early lesions significantly decreased macrophages in the lesion area and suppressed atherosclerosis progress. In advanced lesion stages, mice lacking myeloid SOAT1 also reduced lesion cholesterol crystal content and reduced lesion size [111].

The study conducted on SOAT2 deficiency mice revealed resistance to hypercholesterolemia induced by diet and the formation of cholesterol gallstones. Additionally, these mice exhibited reduced accumulation of hepatic LDs [107]. This was due to the intestine lacking CE synthesis ability and reduced cholesterol absorption ability. These findings suggest the significant engagement of SOAT2 in the body's response to dietary cholesterol, suggesting that inhibiting SOAT2 could be a valuable approach for treating hypercholesterolemia [112]. Mice with either liver or intestinal-specific KO of SOAT2, when fed with HCD, demonstrated reduced cholesterol absorption and lower accumulation of CE. Furthermore, these mice exhibited decreased levels of biliary cholesterol. [113]. SOAT2 KO exhibited a beneficial effect in several kinds of disease models. The absence of functional LDL receptors in LDLR KO mice hinders the effective clearance of LDL particles from the bloodstream. As a consequence, these mice experience elevated levels of LDL cholesterol, which contributes to the development of atherosclerosis. However, cross SOAT2 $^{-/-}$ mice with LDLR $^{-/-}$ mice; their offspring exhibited a 19% decrease in total plasma cholesterol levels, and atherosclerosis was 88% lower [106]. ApoE$^{-/-}$ mice were susceptible to atherosclerosis; however, when SOAT2 $^{-/-}$ mice are crossed with ApoE$^{-/-}$ mice, their offspring no longer had significant atherosclerosis, and the apoB-containing lipoprotein contained TGs instead of CE. The deficiency of SOAT2 in the ApoE-/- background resulted in a compensatory effect, leading to increased activity of lecithin-cholesterol acyltransferase. This, in turn, further enhanced the promotion of CE accumulation in HDL particles in the plasma. [112].

The majority of SOAT inhibitors are hydrophobic, and this characteristic enables them to penetrate the lipid bilayer of the membrane and interact with residues that are essential for substrate binding. The SOAT1-specific inhibitor-K604, which is being investigated by Kowa [114], has shown efficacy in reducing atherosclerotic lesions in atherosclerosis mice, improving liver steatosis and inflammation in NAFLD model, and inhibiting tumor growth in mouse models of lung cancer and liver cancer. The administration of SOAT inhibitors, such as CI-1011, F-1394, and K604, result in decreased CE levels within atherosclerotic lesions, leading to the regression of plaques without significant alteration of overall serum cholesterol levels. However, in human patients, CI-1011 did not demonstrate enhanced efficacy when combined with statins in reducing the development of coronary atherosclerosis. Notably, the administration of CI-976, an SOAT inhibitor that targets both intestinal and hepatic, rabbits on a hypercholesterolemic diet resulted in a decrease in aortic foam cell area [115].

SOAT1 also serves as a target for many cancer treatments. In both human pancreatic cancer and pancreatic cancer cell lines, there is a notable accumulation of SOAT1. The inhibition of SOAT1 using shRNA or targeted inhibitors has demonstrated significant potential in suppressing tumor growth and inhibiting metastasis, as evidenced by studies conducted in an orthotopic mouse model. Furthermore, SOAT1 inhibition led to an increase in intracellular FC levels, which are closely linked to ER stress and apoptosis [116]. Inhibiting SOAT1 decreased LDs formation in GBM, suppressing the lipogenesis process in GBM and prolonging xenograft mouse survival [117]. SOAT1 promotes lipid synthesis in gastric cancer. Knockdown or inhibition of SOAT1 suppresses GC cell proliferation and CE synthesis [118]. The depletion of SOAT1 in cancer cells results in a reorganization of cellular cholesterol distribution, leading to a significant reduction in the proliferation and migration of hepatocellular carcinoma [119]. In a rat study, an increase in SOAT1 methylation levels improved rat heart failure [120]. KD SOAT1 or using avasimibe increased PM cholesterol levels of CD8+ T cells, further enhancing their proliferation [121].

1.4.3 SOATs relationship with obesity

Inhibition of SOAT1 effectively reduces CE synthesis and LD formation in human podocytes [122]. In pig intramuscular differentiation, OE SOAT2 inhibits differentiation and LD formation, which is rescued by avasimibe [123]. OE SOAT2 in 3T3-L1 pre-adipocytes inhibits adipocyte differentiation and promotes lipolysis [100]. Honoki can inhibit adipogenesis and promote WAT browning to alleviate obesity in mice, and the mechanism is mainly through SOAT1 [124].

Under physiological conditions, treatment of DIO mice with the SOAT1 inhibitor avasimibe markedly reduces body weight, fat mass, appetite, with increasing EE. The administration of avasimibe has been found to significantly decrease blood glucose and insulin levels of obese mice. Additionally, it has demonstrated ameliorated glucose tolerance in these mice [125]. Huang et al. (2019) shown that myeloid-specific KO of SOAT1 in mice fed with HFD decreases adipocyte size and increases insulin sensitivity, making them resistant to obesity. SOAT1-deficient mice also demonstrate decreased infiltrating macrophages in WAT [126]. Additionally, myeloid-specific KO of SOAT1 decreases the presence of macrophages within atherosclerotic lesions and effectively inhibits the progression of atherosclerosis. However, in another study of global KO of SOAT1 in mice fed with HFD, body weight is significantly increased compared to WT mice [127]. Thus, the mechanism of how SOAT1 regulates fat mass development is still unclear.

1.5 Hypothesis and aims of the study

SOAT1 was studied as a treatment target for arteriosclerosis for a long time, however, its study in adipocytes and role in obesity development is limited known. We hypothesize that cholesterol esterification by SOAT1 is critical for LD expandability in adipocytes and adipocyte-SOAT1 deficiency may lead to systemic metabolic disorder. In this study, we will reveal how SOATs mediate adipocyte-LD expandability, as well as demonstrate a link between adipose tissue expansion and metabolic disorders,

providing essential insights for further developing pharmaceutical strategies to ameliorate obesity associated metabolic syndrome by targeting adipose tissue expandability.

In summary, the specific aims are as follows:

1. Functional characterization of SOAT in lipid droplet (LD) development during LD initiation
2. Elucidation of the molecular mechanism by which SOAT functionally contribute to LD initiation
3. Evaluation of the physiological significance of adipocyte-SOAT1 in systemic metabolism in vivo

1.6 Acknowledgement

The authors for “Signaling pathways in obesity: mechanisms and therapeutic interventions” ,“ Adipose Tissue: Physiology to Metabolic Dysfunction”, “Adipose Modulation of ABCG1 Uncovers an Intimate Link Between Sphingomyelin and Triglyceride Storage”, “CD36 and lipid metabolism in the evolution of atherosclerosis” and “Cholesterol imbalance in adipocytes: a possible mechanism of adipocytes dysfunction in obesity” are fully acknowledged for allowing me to use figure 1-1- 1-7.

CHAPTER2. SOAT1 DEFICIENCY IMPAIRS CHOLESTEROL METABOLISM AND ADIPOGENESIS IN ADIPOCYTES

2.1 Abstract

Cholesterol homeostasis is critical to maintain adipocyte function during obesity progression. However, the role of cholesterol esterification in adipocytes remains elusive. Sterol O-acyltransferase 1 (SOAT1) is the dominant enzyme to synthesize cholesteryl ester from free cholesterol in adipocytes. Our previous study has revealed that either SOAT1 or SOAT2 knockdown inhibited adipogenesis, while the mechanism remains unclear. In this study, we found a higher level of SOAT1 mRNA in adipose tissue from obese human than that from lean subjects. Knocking down SOAT1 in either human preadipocytes or primary murine preadipocytes attenuated adipogenesis as indicated by ~70% reduction in lipid content. Notably, the inhibition of adipogenesis caused by SOAT1 could be rescued by facilitating the transcription of PPARγ or SREBP1. Paradoxically, the free cholesterol levels decreased upon SOAT1 knockdown, accompanied by disturbed cholesterol trafficking and distribution within adipocytes. Additionally, the maturation of sterol regulatory element-binding protein-2 (SREBP-2) and the expression of its downstream genes involved in cholesterol uptake were down-regulated in response to SOAT1 deficiency. Moreover, the adipogenic ability of SOAT1-deficient preadipocytes could be restored by nutritional factors such as oleic acid or high cholesterol conditions. In summary, our results reveal that SOAT1 is essential for adipogenesis and maintaining cholesterol homeostasis within adipocytes. These findings highlight the potential role of cholesterol esterification in adipose tissue expansion and overall adipocyte function.

2.2 Introduction

Obesity is a globally emerging disease, and the use of GLP-1R agonists has shown promise as an anti-obesity drug for treating obese patients [14]. However, these drugs have been associated with side effects such as nausea, vomiting, and abdominal discomfort. Clinical research has also demonstrated an increased risk of medullary thyroid cancer (MTC) with the use of GLP-1R agonists, leading the FDA to prohibit their application in patients with a personal or family history of MTC [128].Certain anti-obesity drugs and lipodystrophy treatments have been found to have side effects on the cardiovascular system. Previous studies have reported that Orlistat, while reducing BW, also lowers serum sterols, including FC, and oxidized sterols in obese patients [129]. Many anti-Asian obesity lack of white adipose tissue (WAT) expandability but high cholesterol in plasma [130]. Besides the potential direct effect of the anti-obesity drugs on the cardiovascular system/hypercholesterolemia [131], the function of WAT in storing surplus energy and regulate metabolism systemically as an endocrine organ may be disrupted by these anti-obesity strategies and led to the unfavorable health concerns. Thus, a deeper understanding about the role of WAT expansion is needed to help develop safer anti-obesity strategies to combat different obesity segments.

WAT overexpansion is a hallmark of obesity development. There are significant changes during WAT expansion upon a continuous demand of energy storage, including hypertrophy and hyperplasia [132]. However, the increment of cholesterol in WAT during fat mass expansion is often overlooked. About four decades ago, Kovanen PT and Miettinen TA research teams have found WAT as a major cholesterol reservoir, with nearly 50% of body cholesterol in obese people [133]. Meanwhile, during WAT expansion, cholesterol is proportionally increased with TG in WAT [99]. Further studies by Hartman reported that cholesterol level in WAT increased dramatically when plasma cholesterol level was high, especially on subcutaneous WAT [134], suggesting that WAT may help to clean up excessive cholesterol in the plasma by accumulating cholesterol in WAT. Given that

intracellular cholesterol homeostasis is critical for maintaining the plasma membrane fluidity, signalling transduction and hormonal production [135], it is important to investigate the role of cholesterol homeostasis in adipocytes, including the key players responsible for cholesterol homeostasis in WAT, and the effect of surplus cholesterol to WAT.

Plasma membrane (PM) and lipid droplet (LD) membrane in adipocytes are the major sites where cholesterol located in WAT [136]. Thus, the connections between cholesterol homeostasis and adipocyte function have also been preliminarily explored. During adipocyte hypertrophy stage, the plasma membrane cholesterol decreased in hypertrophied adipocytes [137], suggesting a potential role of cholesterol distribution in WAT expansion. Additionally, β-cyclodextrin or apoA-I could facilitate cholesterol trafficking between the PM and LD and subsequently effluxing cholesterol from PM [136]. Meanwhile, SR-BI and ABCA1 in adipocytes could also promote cholesterol transfer to HDL particles in vivo [138]. Parks et. al. demonstrated that in adipocyte-specific ABCA1 knockout mice, the level of HDL cholesterol in plasma decreased by 30% [139]. These findings suggested a homeostatic situation of cholesterol between adipocytes and plasma. In addition to cholesterol itself, perturbing cholesterol homeostasis has an enormous impact on metabolism in adipocytes. The metabolic pathways of fatty acids and cholesterol are tightly regulated by a group of nuclear receptors that are sensitive to the intracellular lipid type and amount [140]. In the context of this regulation, it has been observed that the ability of fatty acid uptake was significantly diminished in 3T3-L1 adipocytes as a consequence of sterol depletion [141]. Moreover, cholesterol efflux gene-ABCA1 deficiency in adipocytes could result in cholesterol accumulation within adipocytes, accompanied with the reduction in the TG content [139]. However, the key players regulating cholesterol homeostasis during adipocyte expansion has not been fully elucidated.

The cholesterol homeostasis is determined by uptake, transport, esterification, *de novo* synthesis, and efflux [142]. Among these key players, SOAT [as known as acyl-CoA: cholesterol acyltransferase (ACAT)] esterifies cholesteryl ester (CE)

from free cholesterol and fatty acids with the help of ATP and coenzyme A [143]. SOAT enzymes play a vital role in converting FC and long-chain fatty acids into CE. Two isoforms, SOAT1 and SOAT2, have been identified, with SOAT1 expressed widely and SOAT2 expressed in predominantly in the liver and small intestine [144, 145]. The enzyme activity of SOATs is primarily regulated by the presence of substrates, while the protein level of SOATs itself is not subject to regulation [146]. The SOAT1 protein consists of nine transmembrane domains and is primarily located in the ER [147]. Additionally, it is also found in the MAM (mitochondria-associated membrane), which serves as the connection between the ER and mitochondria [148]. SOAT1 is emerging as a potential target for pancreatic cancer [149], gastric cancer [118], hepatocellular carcinoma [119], heart failure [120] and Alzhemier's disease [144]. However, to our knowledge, there are only a handful studies reported the SOATs function in adipocytes or obesity. Previously, we found that either SOAT1 or SOAT2 deficiency attenuated adipogenesis in murine 3T3-L1 preadipocytes [150]. Interestingly, overexpressing SOAT1 in murine 3T3-L1 adipocytes reduced LD size and led to adipocyte dysfunction *in vitro* [151]. These data suggested that SOAT1 may be regulated precisely in adipocytes. Up to now, the role of SOAT1 in adipocytes is still ambiguous and the mechanism remain unclear.

In the present study, we found that SOAT1 level increased during WAT expansion both in mice and human, furthermore, SOAT1 level increased during adipogenesis both in mice and human preadipocytes. Consistently, knocking down SOAT1 in murine 3T3-L1 preadipocytes or human SGBS preadipocytes suppressed cholesterol uptake, de novo lipogenesis and LD development during adipogenesis. However, SOAT1 deficiency showed little effect on LD size in mature adipocytes in vitro. Mechanistically, SOAT1-deficiency altered the transcription levels of genes for cholesterol trafficking at the early stage of adipogenesis, accompanied with the increased intracellular-FC level and reduced PM-FC content. Subsequently, the increased intracellular-FC suppressed SREBP2 maturation and reduced SRE binding activity, and thus reduced its downstream genes involved in

cholesterol uptake. As expected, overexpressing SOAT1 or replenishing PM cholesterol restored the expression of genes involved in cholesterol uptake and adipogenesis in SOAT1-deficient adipocytes. Surprisingly, either agonists for adipogenic transcriptional factors, PPARr and LXR, or nutritional factors, oleic acid, could rescue the impaired adipogenesis in SOAT1-deficient preadipocytes in vitro. Collectively, our results demonstrated that SOAT1 is an important positive regulator for adipogenesis in vitro via manipulating cholesterol trafficking and distribution, but SOAT1's positive role in adipogenesis could be replaced by either adipogenic transcriptional factors or nutritional interventions.

2.3 Methods and materials

2.3.1 Animal model and treatment

All animal experiments were conducted at The Hong Kong Polytechnic University and were approved by the Centralized Animal Facilities (CAF). The mice used in this study were of C57BL/6J background and were housed at room temperature with a 12-hour light/dark cycle. They were fed a standard chow diet (PicoLab Rodent Diet 20) and given sterile water ad libitum. SOAT1flox/flox mice were generated by inserting two Loxp sites covering SOAT1 exon 14 (provided by Dr. Ta-Yuan Chang [126]). Adipocyte-specific SOAT1 knockout mice (Adipoq-SOAT1) were generated by crossing SOAT1flox/flox mice with adiponectin-Cre (Adipoq-Cre, provided by Dr. CHENG, King Yip [152]). Male SOAT1flox/flox mice aged 4-6 weeks were used in this study for stromal vascular fraction isolation

2.3.2 Cell culture and treatment

3T3-L1 mouse preadipocytes (ATCC #CL-173) were acquired and maintained in DMEM/F12 medium (Gibco) supplemented with 10% FBS and 100 IU/ml penicillin/streptomycin.

For the isolation and culture of mouse pre-adipocytes, inguinal fat pads were surgically

extracted from male SOAT1 $^{flox/flox}$ mice aged 4-6 weeks (kindly provided by Dr. Ta-Yuan Chang [126]) and were minced in 3-cm dishes. To prepare the digestion solution, collagenase type II (17101015, Thermo) at a concentration of 1mg/ml and Dispase II (D4693, Sigma-Aldrich) at a concentration of 2.4 IU/ml were added to Dulbecco's PBS buffer. The inguinal fat pads were minced and then subjected to digestion using 2 ml of the prepared digestion solution in a shaking water bath at 37°C for 30-60 minutes. Following digestion, the suspensions were filtered through a 100 μm cell strainer (Falcon) and supplemented with 10 ml of pre-warmed PBS buffer. After centrifugation at 1000 g for 5 minutes, the cell pellets at the bottom of the tube were collected and cultured with DMEM. SGBS cells, provided by Prof. Martin Wabitsch, were cultured using a previously described protocol [153]. The cells were maintained in a controlled incubation environment at 37°C with 5% CO2, providing optimal conditions for their growth and viability.

Adipocyte differentiation**:** For 3T3-L1 and iWAT-isolated SVFs, adipocyte differentiation protocol was slightly modified from a previous study [154]. In short, the day when the cells reached 100% confluence was designated as day -2. On day 0, which was two days post-confluence, the cells were treated with 10 μg/ml insulin (I6634, Sigma-Aldrich), 0.5 mM 1-methyl-3-isobutylxanthine (IBMX) (I7018, Sigma-Aldrich), 1 μM dexamethasone (D4902, Sigma-Aldrich), and 0.1 μM rosiglitazone (R2408, Sigma-Aldrich). The cells were then incubated with these compounds for 2 days, referred to as day 2. Then cells were incubated with 10 μg/ml insulin until harvest day. Nuclear DNA and lipid droplets were stained with Hoechst 33342 (H1399, Thermo) and Oil Red O (O1391, Sigma-Aldrich), respectively, and were visualized with the help of optical microscopy (Olympus CKX41, Tokyo, Japan).

2.3.3 Plasmids

SRE-luciferase plasmids were generated by inserting four copies of the sterol regulatory element (SRE, ATCACGTG) from the pGMSREBP (Yeasen) into a pNL2.1-Nluc (Promega) luciferase vector.

RFP labeled Domain 4 plasmid were generously provided by Dr. Deng Yongqiang and sequence were listed in Table 2-1.

2.3.4 Luciferase assay

To perform reporter assays, the same protocol as described in a previous study [155] was followed. In short, 3T3-L1 cells were transfected with pGL4.2-SRE-Luc2, which is an expression plasmid containing Firefly luciferase (Promega). Following a 3-day differentiation period, the Dual-Luciferase™ reporter system (Promega E1910) was utilized to measure luciferase activity. The plates were allowed to cool for 10 minutes, and then 30 µl of each assay reagent was added. Subsequently, the plates were shaken for 10 minutes using a multi-plate shaker. Luminescence readings were obtained using an EnVision plate reader (Perkin Elmer) with a 100 msec integration time.

2.3.5 Virus transduction

To achieve KD SOAT1 in 3T3-L1 pre-adipocytes, we applied the lentivirus-mediated shRNA interference technique. The shRNA sequence for SOAT1 was 5'-GCAAGAGTTCTCACCCATTGA-3', the sequence for scramble was 5'-TTCTCCGAACGTGTCACGTTTCAAGAGAACGTGACACGTTCGGAGAATTTTTT- 3', the KD virus was Lent-U6-GFP-shSOAT1-Puro ($3x10^8$ particles/mL, WZ Biosciences, Inc. Jinan, China), the control virus was Lent-U6-GFP-shCTRL-Puro ($5x10^8$ particles/mL, WZ Biosciences, Inc. Jinan, China). $1x10^6$ 3T3-L1 cells were seeded in a 6-well plate and infected with a mixture of 10 µg/ml Polybrene and 1 µL lentivirus. We further performed puromycin selection at 2 µg/ml for 3 days and differentiated to adipocytes for various analyses.

For the generation of SOAT1 KO in SVF-derived pre-adipocytes, the cells were seeded at $1x10^6$/well and infected with 100 MOI Adenovirus. Adenoviruses carrying the Cre gene (Ad5-CMV-Cre-mCMV -copGFP, $2x10^{10}$ particles/mL) and empty adenovirus (Ad5-CMV-copGFP, $2x10^{10}$ particles/mL) were constructed by WZ Biosciences, Inc. Jinan, China.

For the generation of SOAT1 OE in 3T3-L1 pre-adipocytes, the cells were seeded at $1x10^6$/well and infected with 100 MOI Adenovirus. Adenoviruses expressing SOAT1 (pADM-CMV-SOAT1-mCherry, $2x10^{10}$ particles/mL) and control (pADM-CMV-mCherry, $2x10^{10}$ particles/mL) were purchased from WZ Biosciences, Inc. Jinan, China).

2.3.6 Gene expression analysis

To analyze gene expression, total RNA was extracted using Trizol Reagent and converted into cDNA with a First-Strand cDNA Synthesis Kit. Real-time PCR using SYBR Green was employed to quantify the PCR products, and the mRNA levels were normalized to β-actin or GAPDH using the delta-delta Ct method. The primer sequences for qPCR can be found in the supplementary table (S2)..

2.3.7 Western blotting

Protein samples were extracted using RIPA lysis buffer (P0013B, Beyotime) supplemented with a protease inhibitor cocktail (HY-K0021, MedChem Express). The protein concentrations were determined using the BCA Protein Assay Kit (23225, Thermo Fisher Scientific). Equal amounts of protein were loaded onto 12% SDS-PAGE gels, followed by transfer onto PVDF membranes (Millipore). The subsequent steps were carried out according to the previously described procedure [156]. The primary antibodies against SOAT1, Glut4, SREBP2 were purchased from Abcam, and the primary antibodies against PI3K, P-PI3K, P-AKT (Ser-473), P-AKT (Ser-308) from Cell Signaling Technology. The primary antibodies against GAPDH, Cav-1 were purchased from Thermo Fisher Scientific. Primary antibodies were all diluted by 1:1000 in dilution buffer. Secondary antibodies of horseradish peroxidase-conjugated anti-mouse (1:10000) or anti-rabbit (1:10000) were purchased from Thermo Fisher Scientific. The membranes were processed by ECL (32106, Thermo Fisher Scientific) and delivered to ChemiDoc Imaging System (Bio-Rad) to capture picture and further were analyzed with ImageJ software.

2.3.8 Immunofluorescence staining

Cells cultured on glass coverslips in 6-well dishes were fixed with 10% (v/v) formalin in PBS for 20 minutes at room temperature. After two rinses with PBS, the coverslips were permeabilized with 0.1% (v/v) Triton X-100 in PBS for 5 minutes at 4°C. Following two additional rinses with PBS, the coverslips were incubated overnight at 4°C with a primary antibody diluted in PBS (1:100). Subsequently, the cells were washed three times with 1 ml of PBS and incubated with a secondary antibody for 1 hour at room temperature in the dark. After four additional washes with 1 ml of PBS, the coverslips were mounted on slides using ProLong Diamond antifade mountant (#S36936, Thermo). Confocal microscopy was performed using a Leica TCS SPE Confocal Microscope (Leica, Germany), with a 63X/1.4 oil immersion objective used for imaging, unless otherwise specified for specific requirements.

2.3.9 Cholesterol and cholesteryl ester measurement

To begin, cholesterol was extracted from adipocytes or adipose tissue by combining hexane (Ajax FineChem) and isopropanol (Ajax FineChem) in a ratio of 3:2. The mixture was allowed to incubate for 30 minutes in the fume hood. The solvent was then transferred to 2-ml glass vials. The dried samples were subsequently diluted in an appropriate volume of 1x reaction buffer, and the levels of free cholesterol (FC) and cholesterol esters (CE) were determined using the Amplex Red cholesterol assay kit (A12216, Thermo) following the manufacturer's instructions. The reaction mixtures were incubated for 30 minutes at 37°C, shielded from light, and the fluorescence was measured using a microplate reader (Thermo Scientific Varioskan LUX). After drying the dish, the cells were lysed with 0.1M NaOH for 15 minutes at room temperature. Protein concentrations were determined using a BCA Kit, and the cholesterol contents were normalized to the protein level.

To measure the plasma membrane (PM) and intracellular cholesterol content, a cholesterol oxidation-based method previously described [121] was employed. In brief,

cells were fixed with 0.1% glutaraldehyde and then treated with 2Uml−1 cholesterol oxidase for 15 minutes to oxidize the plasma membrane cholesterol. The cholesterol was subsequently extracted using hexane/isopropanol (vol/vol, 3:2), and the non-oxidized cholesterol was quantified using the Amplex Red cholesterol assay kit. By subtracting the intracellular cholesterol from the total cellular cholesterol, the value of the plasma membrane cholesterol was obtained.

2.3.10 Modulation of the plasma membrane cholesterol level by MβCD and MβCD-coated cholesterol

We depleted the lipid in serum by adding fumed silica (Sigma, S5130, 20g/L) to FBS followed by incubation overnight, centrifugation and filtering [157]. To remove cholesterol from the plasma membrane, adipocytes were exposed to 5 mM MβCD for 15 minutes at 37 °C, followed by three washes with PBS. For cholesterol replenishment, adipocytes were incubated with culture medium containing 20 μg/ml of MβCD-coated cholesterol for 15 minutes at 37 °C.

2.3.11 Glucose uptake

Glucose uptake was induced by the addition of 1 mM 2-deoxyglucose for 20 minutes, followed by cell lysis. Intracellular glucose levels were determined using the Glucose Uptake Colorimetric Assay Kit (#K676, BioVision) according to the manufacturer's instructions. Initially, the cells were starved by incubating them with KRPH buffer for 40 minutes on the day of sample collection. Subsequently, the cells were treated with or without 1 μM insulin for 20 minutes. Following insulin treatment, 10 mM 2-DG was added to each well to measure glucose uptake, and the OD was measured at 412 nm wavelength.

2.3.12 Statistical analysis

The data are presented as means ± S.D. or means ± S.E.M., as specified in the figure legends. Statistical significance for comparisons between control and treatment groups was assessed using GraphPad Prism software with a two-tailed student's t-test or one-

way ANOVA. Statistical significance is reported for comparisons with a p-value < 0.05, as indicated in the figure legends.

2.4 Results

2.4.1 The expression of SOAT1 in adipocytes was associated with WAT expansion

To identify the association of SOAT1 expression in WAT and fat mass expansion, we re-analyzed the RNA-seq data of subcutaneous white adipose tissue (sWAT) and found that the mRNA level of SOAT1 in sWAT from lean people was significantly lower than that from either metabolic healthy obese (MHO) or metabolic unhealthy obese (MUO) ones (Figures 2-1A [158], S2-1A [159], S2-1B [160]). In contrast, the mRNA level of SOAT2 in sWAT was extremely low based on the RNA-seq data [158]. Therefore, the expression of SOAT1, instead of SOAT2, in human sWAT seems associated with the fat mass expansion, but it is unknown whether the increased SOAT1 level during fat mass expansion is attributed to adipocytes or non-adipocytes who are resident in WAT. To identify the potential role of adipocyte-SOAT1 during fat mass expansion, we further isolated mature adipocytes from WAT in lean and obese mice, respectively. Accordingly, the mRNA levels of SOAT1 was higher in mature adipocytes from obese mice than that from lean ones in either epiWAT or ingWAT (Figure 2-1B). Interestingly, SOAT2 was also expressed (although much lower than SOAT1) in murine adipocytes and its mRNA level was positively associated with adiposity in epiWAT, but not in ingWAT in mice (Figure S2-1C). Considering the potential mRNA degradation during mature adipocyte isolation, we also isolated RNA from bulk WAT and found that mRNA levels of both SOAT1 and 2 in epiWAT from DIO mice were higher than those from lean ones, respectively (Figure S2-1D), without altering CD146 [161], a marker for macrophage foam cells which express SOAT1 significantly [162]. At the protein level, the SOAT1 protein expression was also higher in Epi-WAT of DIO and *ob/ob* mice than that of lean ones (Figure 2-1C). In contrast, the SOAT2 protein level was undetectable in epiWAT (Figure S2-1E). Furthermore, FC, CE and CE:FC were higher

in epiWAT (Figures 2-1 D-F) and ingWAT (Figure S2-1 H-J) from obese mice than that from lean ones, indicating an increased SOAT activity during fat mass expansion. Collectively, these data illustrated a positive association between adipocyte-SOAT1 and fat mass expansion.

Adipogenesis, together with adipocyte hypertrophy, is a major contributor to fat mass expansion when extra calories need to be stored. To study the role of SOAT1 in adipogenesis, we employed cell models from both murine and human sources. As expected, SOAT1's mRNA level was upregulated upon adipogenic stimulation in human SGBS preadipocytes without SOAT2 inducement (Figure 2-1G). Consistently, SOAT1 was induced at both mRNA and protein levels during adipogenesis in murine cell models: mature adipocytes differentiated from mouse adipose stromal vascular fraction (SVF) (Figures S2-1 F-G) and 3T3-L1 cell line (Figure 2-1 H-J). Furthermore, the level of CE and CE:FC were also gradually upregulated during adipogenesis in the murine 3T3-L1 model (Figure 2-1 K-M). Thus, these results demonstrated a positive association between SOAT1 and adipogenesis both in murine and human.

2.4.2 SOAT1 was important for adipogenesis, but not necessary for adipocyte hypertrophy in vitro

Previously, we have demonstrated that inhibiting SOAT1 or knocking down SOAT1 would attenuate adipogenesis in murine 3T3-L1 cells [163]. Interestingly, overexpressing SOAT1 by 1500 fold could also inhibit adipogenesis in murine 3T3-L1 cells [100]. This "controversy" suggested that the role of SOAT1 in adipogenesis may require precise regulation. To further confirm the role of SOAT1 in adipogenesis, we employed different cell models and gene manipulation methods. Firstly, we generated lentivirus-mediated shSOAT1 to knockdown SOAT1 in 3T3-L1 preadipocytes, achieving ~60% KD efficiency without significant compensatory increasement of SOAT2 at the mRNA level (Figure S2-2A). Additionally, the SOAT1 enzyme activity was determined by the fluorescent intensity of 22-(N-(7-nitrobenz-2-oxa-1,3-diazol-4-yl)amino)-23,24-bisnor-5-cholen-3β-ol (22-NBD cholesterol) [145]. As expected, the

fluorescence intensity was significantly lower in shSOAT1 cells than shCTRL ones (Figure S2-2B). After six days of differentiation, SOAT1-KD adipocytes significantly decreased LD formation as reflected by Nile red and Oil Red O staining, compared with sh CTRL adipocytes (Figure 2-2A, S2-2 C-D). Consistently, upon six days' adipogenic inducement, the mRNA levels of genes for TG synthesis (PPARγ, DGAT2, SCD1) and lipid formation (GPAT3, AGPAT2) were significantly lower in shSOAT1 adipocytes than shCTRL ones (Figure 2-2B). To examine the potential off-target effect of shSOAT1, adenovirus-mediated overexpression of SOAT1 with a 200-250 fold of increasement at the mRNA level was used (Figure S2-2E). As expected, overexpressing SOAT1 rescued the attenuated adipogenesis in shSOAT1 cells, as indicated by the rescued intracellular lipid level (Figures 2-2 C-D) with increased mRNA levels of genes involved in adipogenesis (PPARγ) and lipid synthesis (DGAT2, GLUT4, CD36, SCD1) (Figure 2-2E). In contrast, overexpressing the catalytic dead mutant (SOAT1-H460A) had no effect on adipogenesis (Figure S2-2F). Secondly, we isolated SVF from ingWAT of $SOAT1^{fl/fl}$ mice and induced adipogenesis in vitro. We knocked out SOAT1 with cre-expressing adenovirus at the preadipocyte stage (Figure 2-2F), with the knockout efficiency of 70% at the protein level (Figure S2-2G). In agree with our previous findings, knock out SOAT1 significantly attenuated adipogenesis, as determined by ORO and adipogenic-related gene expression (PPARγ, FAS, ACC, SCD1) (Figures 2-2 G-I). Finally, the importance of SOAT1 during adipogenesis was also confirmed in human SGBS preadipocytes (Figures 2-2 J-K, S2-2L), without SOAT2 compensation.

Glucose can be converted into glycerol-3-phosphate, which serves as a backbone for TG synthesis within adipocytes [164]. Therefore, we hypothesize that SOAT deficiency impairs glucose uptake during adipogenesis. Adipocytes differentiated at D4 of KD or OE SOAT1 were treated with or without 100 nM insulin to measure the glucose uptake ability. At the basal level, SOAT1 deficiency did not alter glucose uptake much, however, overexpressing SOAT1 was able to increase glucose uptake (Figure 2-2L). Under the insulin stimulation condition, knocking down SOAT1 suppressed the glucose uptake by 50% (figure 2-2M). On contrast, OE SOAT1 increased the glucose uptake

ability by 3 folds as to response to insulin stimulation, and fully rescued glucose uptake ability in shSOAT1 adipocytes (Figure 2-2M). These data suggested that SOAT1 is important for insulin mediated glucose uptake.

To overlooking the transcriptional changes caused by SOAT1 deficiency during adipogenesis, we generated shCTRL and shSOAT1 preadipocytes in murine 3T3-L1 cells with lentivirus-mediated shRNA-based interference system, and performed RNA sequencing (RNA-seq) analysis on shCTRL and shSOAT1 cells at day 0, day 3 and day 6 post adipogenic stimulation, respectively (Figure S2-3B). The biological process analysis revealed that SOAT1-deficiency attenuated the transcriptional inducement in genes involved in fatty acid, lipid regulation, coenzyme and sterol metabolic process pathway during adipogenesis (Figures 2-3A). The attenuation was even greater after 6 days of induction compared to day 3 (Figure S2-3A). The deficiency of SOAT1 attenuated adipogenesis in the early stage of adipogenesis, as characterized by the lower transcripts of genes for coding lipid droplet-associated proteins (CideC, Plin1, and Bscl2), TG synthesis (DGAT2) and do novo lipogenesis (FAS, ACC) after 3 days' adipogenic stimulation (Figure 2-2B), as compared to shCTRL cells. Adipogenesis is predominantly regulated by turning on or off a cascade of transcriptional regulators [165]. Accordingly, the key transcriptional factors that promote adipogenesis, PPARγ [166], C/EBPα [167], KLF15 [168], Ebf1 [169], SREBP1 [170], were less responsive to the adipogenic cocktail in shSOAT1 preadipocytes than shCTRL preadipocytes. In contrast, the genes that negatively regulating adipogenesis, such as KLF2 [171] and SIRT2 [172], were either upregulated or failed to be downregulated during adipogenesis in shSOAT1 preadipocytes, as compared to shCTRL ones (Figure S2-3C). Collectively, SOAT1 deficiency suppressed the inducement of adipogenic transcriptional cascade up on adipogenic stimulation at the early stage of adipogenesis *in vitro*.

LD size expansion is one of the key contributor to fat mass expansion. As the mRNA levels of SOAT1 was positively associated with fat mass (Figure 2-1B), we examined the contribution of SOAT1 to adipocyte size expansion. In the mature adipocytes that differentiated from SVF in ingWAT of $SOAT1^{fl/fl}$ mice, we knocked out SOAT1 with cre-expressing adenovirus, and the corresponding control group was treated with

control adenovirus (Figure S2-2I). Surprisingly, the LD size distribution was not significantly different between the CTRL and SOAT1-KO adipocytes (Figures S2-2 J-K). Collectively, these results demonstrated that SOAT1 is not required for lipid droplet expansion in mature adipocytes in the *in vitro* system.

2.4.3 SOAT1 regulated intracellular cholesterol homeostasis, including cholesterol quantity and distribution

During adipogenesis, the content of free cholesterol (FC) increases as triglyceride (TG) accumulation occurs [173]. Simultaneously, the PM cholesterol content decreased in hypertrophied cells [137]. Considering that more than 95% of cholesterol in adipocytes are in the form of FC [174], maintaining equilibrium in cholesterol homeostasis may play a crucial role in adipocyte function. SOATs are the only enzymes so far found to convert FC to CE intracellularly to adjust FC availability [143], and SOAT1 is the predominant isoform in murine and human adipocytes during adipogenesis. Thus, we further investigated the role of SOAT1 in regulating FC pool during adipogenesis.

For total cholesterol quantity, KD SOAT1 attenuated the increment of total cholesterol that induced by adipogenic cocktail during adipogenesis (figure 2-3B), while this attenuation can be rescued by overexpressing SOAT1. As for cholesterol sub-segments, FC could be categorized into plasma-membrane FC and intracellular FC based on the location. After five day's adipogenic stimulation, we found that shSOAT1 adipocytes exhibited lower cholesterol level in the plasma membrane but higher cholesterol level intracellularly with the help of oxidation-based assay, as compared to shCTRL adipocytes (Figure 2-3C). To further confirm the results, we transfected 293T cells with a recombinant RFP-tagged version of domain 4 (D4) expressing plasmid and to visualize the free cholesterol in the cytosolic leaflets of membranes. D4 is a domain of Perfringolysin O and could bind to the cholesterol without cytotoxicity [175]. Consistently, there were less D4-RFP signals distributed in the PM but more in intracellular compartment in shSOAT1 cells comared to shCTRL cells (Figure 2-3D). Therefore, SOAT1 deficiency altered cholesterol distribution between PM and

intracellularly. These data demonstrated that SOAT1 is an important player to regulate cholesterol homeostasis during adipogenesis, including cholesterol quantity and distribution.

Cholesterol homeostasis is determined by uptake, trafficking, efflux, do novo synthesis, utilization, and storage (or esterification). Consistent to the reduced total cholesterol level in shSOAT1 cells as compared to shCTRL cells (Figure 2-3B), knocking down SOAT1 inhibited the upregulation of mRNA levels of several genes that induced by adipogenic cocktail, and these genes are mainly involved in cholesterol uptake (LDLR, CD36), de novo cholesterol synthesis (SREBP1a, SREBP2), and cholesterol trafficking (NPC1, NPC2) (Figure 2-3 E-F). Therefore, that SOAT1 deficiency attenuated cholesterol increment during adipogenesis may be attributed to the inhibition in cholesterol uptake and synthesis. Complementarily, the dominant cholesterol efflux associated gene-ABCA1 was also suppressed by SOAT1-KD during adipogenesis (Figure 2-3F).

Here in this study, higher intracellular cholesterol level and lower PM cholesterol were observed in SOAT1-KD cells than shCTRL cells (figure 2-3C), suggesting a role of SOAT1 in regulating cholesterol trafficking. Moreover, the cholesterol transporter gene NPC1 and NPC2 mRNA levels were higher in shSOAT1 group compared with shCTRL in differentiated adipocytes. (Figure 2-3F). These findings suggest that the knockdown of SOAT1 disrupts the cholesterol trafficking process within adipocytes.

The main gene responsible for cholesterol trafficking have been depicted (Table 2-3). For cholesterol trafficking between ER and endosome, the transcriptional level of related genes, STARD3 and OSBPL1a, were not significantly affected by the deficiency of SOAT1.

OSBPL1a and OSBPL5 serve as cholesterol sensors, facilitating the movement of LDL-derived cholesterol from the late endosome to ER [176, 177]. In our study, the OSBPL5 mRNA was decreased during adipogenesis process, and KD SOAT1 slowed down the rate of decrease, which may imply enhanced cholesterol movement from lysosomes to the ER in SOAT1-deficiency adipocytes.

In addition to ER, lysosomal cholesterol can move to PM and Golgi via OSBPL2 and

STARD5, respectively. OSBPL2 aids in the transport of cholesterol from the lysosome to the PM [178]. Previous research has found that STARD5 is involved in the transfer of cholesterol and other lipids between cellular membranes, such as from lysosomes to the Golgi apparatus [179]. In our study, we observed a decrease in STARD5 mRNA during the adipogenesis process, which was subsequently followed by a gradual increase. Notably, KD SOAT1 resulted in a significant increase in STARD5 mRNA levels.

OSBPL8 located on the ER, promote cholesterol exchange between the ER and PM [180, 181]. In our result, there were no difference on OSBPL8 mRNA level.

Except for lysosome, PM cholesterol could also transfer to ER by GRAMD1s. GRAMD1 proteins facilitate the movement of accessible PM cholesterol, transporting it to the ER [182]. In our study, the Gramd1b mRNA was increased during adipogenesis process, and KD SOAT1 slowed down the rate of increase, which may imply decreased cholesterol movement from lysosomes to the ER in SOAT1-deficiency adipocytes.

PLTP not only transfer phospholipids but also FC from adipose tissue to plasma [183]. It is also known that PLTP can bind directly to ABCA1, contribute to the cholesterol efflux process [184]. In our results, we found a significant increase in PLTP mRNA after SOAT1 KD, suggesting an enhancement of apoA-I-mediated cholesterol efflux in SOAT1-deficiency adipocytes.

The STARD4 gene encodes a protein involved in the regulation of lipid metabolism, particularly the transport of cholesterol and phospholipids between different cellular membranes. A previous study in HEPG2 cells found that KD of STARD4 increased PM cholesterol, decreased ER cholesterol, and reduced CE levels [185]. SREBP2 promotes STARD4 transcription, increasing mitochondrial cholesterol levels in HCC cells [186]. In our study, STARD4 mRNA levels decreased markedly after SOAT1 KD, suggesting a disruption in the dynamic equilibrium of cholesterol distribution.

Those above data suggested that SOAT1 plays a role in regulating cholesterol trafficking, however, the detailed cholesterol trafficking between the intracellular organelles requires further investigation.

2.4.4 SOAT1 deficiency upregulated intracellular FC level and suppressed SREBP2 activation

SOAT1 deficiency led to higher intracellular cholesterol level (Figure 2-3C), but the intracellular location of the increased cholesterol is unknown. There are several cholesterol/sterol sensors in the cells, including INSIGs, SCAP and SREBPs [142].The activation of SREBPs requires the translocation of SREBP2 from ER to the Golgi apparatus for the subsequent cleavage, resulting the active N-terminal fragment of SREBP2, which enters the nucleus and mediates the transcription of the downstream genes [187]. While this translocation is negatively regulated by the ER localized cholesterol level [142]. Our RNA-seq data revealed lower transcripts of both SREBP1 and 2, as well as their downstream targeted genes (Figure S2-3 F-G) in shSOAT1 adipocytes than those in shCTRL ones (day 3 after adipogenic stimulation). Thus, we hypothesized that knocking down SOAT1 increased ER-localized cholesterol, which in turn attenuated the SREBP2 translocation and consequently downregulated the target genes. To test the hypothesis, we examined the pre-SREBP2 and n-SREBP2 protein level in shCTRL and shSOAT1 cells after four days' of adipogenic stimulation. The processed SREBP2 (i.e. nuclear SREBP2, n-SREBP2) to pre-SREBP2 ratio was significantly lower in shSOAT1 adipocytes under cholesterol depletion condition, as compared with shCTRL (Figures 2-3 H-K). Consistently, our confocal microscopy results further validated that knocking down SOAT1 could inhibit SREBP2 maturation (Figures S2-3 H-K). Furthermore, since the reduced level of n-SREBP2 does not necessary lead to the reduced transcriptional activity of SREBP2, we transfected adipocytes with SRE-luciferase plasmid, which contained four copies of SRE, the sequence that SREBP bind to for turning on the downstream gene expression. As expected, SRE luciferase activity was significantly decreased in shSOAT1 cells compared with shCTRL (Figure 2-3G). Consistently, SREBP2's downstream genes (LDLR, CD36) were lower in the transcriptional level in shSOAT1 adipocytes compared with shCTRL (Figure 2-3F). In addition, the KD of SOAT1 increased ERLIN1's transcription level during the early stage of adipogenesis (Figure S2-3E),

while ERLIN1 is one of the major proteins that tightly bind SREBP-SCAP complex in ER as to response to high cholesterol in ER [188].These above data suggested that the knocking down SOAT1 may upregulate the FC pool in ER in adipocytes.

2.4.5 The inhibition of adipogenesis in preadipocytes lacking SOAT1 is mediated through the transcriptional regulation of PPARγ and SREBP1

Previously, we observed a significant reduction in PPARγ mRNA levels upon SOAT1 deficiency (figure 2-2B), and OE-SOAT1 increased PPARγ mRNA level (Figure 2-2E). Considering that PPARγ is a "master" transcription factor for adipogenesis, we hypothesized if SOAT1 regulates adipogenesis via regulating PPARγ transcriptionally. To test it, we loaded PPARγ agonist, rosiglitazone, during the first two days of adipogenesis and found that LD (figure 2-4 A-B) and PPARγ, SCD1 and SREBP2 genes (figure 2-4C) could be fully rescued in shSOAT1 adipocytes. Thus, SOAT1-deficiency suppressed adipogenesis via, at least partially, inhibiting PPARγ.

Besides the well-known role of PPARγ in controlling adipogenesis, there are also PPARγ-independent pathways that can contribute to adipogenesis [189]. Early study have found that SREBP1 in 3T3-L1 cells induce PPARγ mRNA level [190]. Previously, we found that knocking down SOAT1 downregulated SREBP1 targeted genes, including SCD1 and FASN (Figure 2B, S3G), OE-SOAT1 resuce SCD1 mRNA level (Figure 2-4E). Therefore, we employed an LXR agonist-T0901317 to stimulate SREBP1 transcription. Interestingly, the LXR agonist rescued adipogenesis in SOAT1-deficient preadipocytes without increasing the mRNA level of PPARγ (Figure 2-4 D-F). Thus, SOAT1-deficiency suppressed adipogenesis via, at least partially, reducing SREBP1 transcription.

KLF2 (Krüppel-like factor 2), a transcription factor known to inhibit adipogenesis by suppressing the PPARγ promoter [191], was found to have significantly upregulated mRNA levels in shSOAT1 cells during day 3 of adipocyte differentiation in our study (Figure S2-4A). To investigate the role of KLF2 in SOAT1-mediated adipogenesis, we employed siRNA targeting mouse KLF2 to knock down its expression. The siRNA

sequence designed for mouse KLF2 effectively reduced KLF2 expression (Figure S2-4B). However, upon performing Oil red-O staining, it was observed that KLF2 siRNA failed to effectively rescue the lipid droplet (LD) accumulation in SOAT1-deficient adipocytes compared to the control group.

Collectively, we have demonstrated that adipogenesis in SOAT1 deficient preadipocytes can be rescued either PPARγ activation or SREBP1 expression.

2.4.6 Nutritional factors could rescue adipogenesis in SOAT1 deficient pre-adipocytes

Although we found that KD of SOAT1 in vitro suppressed adipocyte differentiation (Figure 2-2), previous studies have shown that mice lacking SOAT1 [127] or SOAT2 [192] can still develop similar amount of fat mass, without the compensatory effect from the other SOAT isoform (unpublished data). Given that upregulation of PPARr and SREBP1 could rescue adipogenesis in SOAT1 deficient preadipocytes (Figure 2-4), we hypothesize that nutritional factors in the microenvironment of WAT might rescue the adipogenesis in WAT in vivo via activating PPARr or SREBP1.

Here in our study, Oleic acid (OA), a PPARr enhancer, also serves as the substrate for TG synthesis. Supplementing culture medium with OA successfully induced lipid accumulation in both shCTRL and shSOAT1 groups (Figure 2-5 C-D), with the increment of associated genes (PPARγ, SCD1, and FAS (Figure 2-5E). Meanwhile, the transcription level of SREBP1c were also significantly rescued by OA treatment in the shSOAT1 preadipocytes upon adipogenic stimulation.

In our study, loading cholesterol via methyl-beta-cyclodextrin (MβCD) (Figure 2-5A) successfully rescued adipogenesis, as indicated by the mRNA levels of genes involved in adipogenesis and cholesterol uptake, which were suppressed by SOAT1-KD (Figure 2-5B).

Collectively, these results demonstrated that adipogenic ability of SOAT1 deficient preadipocytes could be restored to the levels as shCTRL preadipocytes under high cholesterol or oleic acid conditions.

2.5 Discussion

WAT is the primary storage depot for TG and it contains the most prominent free cholesterol pools in our body, which is crucial for energy metabolism [193]. Several studies have reported that disrupting cholesterol homeostasis impairs adipocytes function [139]. However, it is still unclear the role of SOAT1, as one of the regulators for cholesterol homeostasis, in regulating such large pool of FC in normal adipocytes during WAT expansion. Our previous study demonstrated that either SOAT1 or SOAT2 deficiency resulted in suppressed lipogenesis and FC level during adipogenesis in murine 3T3-L1 cells [150]. Additionally, global SOAT1 knockout mice fed a chow diet did not show a difference in fat mass compared to controls. However, when fed a HFD, the SOAT1 knockout mice exhibited a significant reduction in fat mass [127]. Therefore, our scientific question is how SOAT1 regulates the cholesterol pool during the adipogenesis process. In this study, we manipulated SOAT1 expression in adipocytes through overexpression or knockdown and demonstrated that SOAT1 is necessary for fat accumulation in both human and murine subjects under obese conditions. SOAT1 deficiency impairs key adipogenesis transcriptional factor transcription and glucose uptake, blocking SREBP2 maturation process by decreased PM cholesterol level and relatively increased intracellular part in adipocytes.

For the tissue distribution of SOAT1, SOAT1 is widely expressed in various tissues of adult mice [194], while in human samples, it is primarily expressed in the adrenal glands [195]. Here, we found that the mRNA level of SOAT1 in either mice or human was higher in obesity than that in lean ones (Figure 1A-B). In contrast, the mRNA level of SOAT2 in human WAT is extremely low, while that in mouse EpiWAT was positively associated with adiposity level (Figure S1C). Interestingly, the mRNA level and protein level of SOAT1 are consistently associated with adiposity in mice (Figure 1B-C), while the protein level of SOAT2 was undetectable in WAT from mice (Figure S1E). This absence of SOAT2 in WB may be due to its property of being easily degradable with fewer transmembrane structures than SOAT1 [144, 196]. Considering the mRNA of SOAT2 is extremely low in WAT of human, we postulate that SOAT1 is the dominant

isoform regulating CE in human WAT. Thus, we focused on SOAT1 in the later investigations. Notably, in murine samples, knockdown either SOAT1 or SOAT2 could suppress adipogenesis [154], suggesting the non-negligible roles of either isoform of SOATs. Although it is not clear whether SOAT1 and SOAT2 in adipocytes overlaps significantly, we may need to be careful about the compensatory effect between SOAT1 and SOAT2 when study the role of SOATs in adipocytes using murine samples. Additionally, the difference in expression pattern in WAT between human and mice should be considered as well.

Our results demonstrated that SOAT1 regulates cholesterol quantity and distribution during adipogenesis in vitro. We found that KD of SOAT1 decreased PM cholesterol levels while upregulating intracellular part. Consistently, a previous study found inhibiting SOAT1 decreased PM cholesterol levels in T cells, leading to modulation of cholesterol metabolism and promotion of an antitumor response [121]. Agpat2 deficient adipocytes did not alter PM cholesterol content, but decreased caveolae number and impaired adipogenesis, suggesting the cholesterol distribution in PM, besides PM cholesterol quantity, is also critical [197]. The PM cholesterol content exert crucial role in adipocyte function. Previous study found sterol depletion in 3T3-L1 adipocytes lead to glucose oxidation inhibition, inflammation and GLUT4 mRNA level decreased [141]. Ortegren et al, founded that membrane cholesterol decreased would result in insulin mediated glucose uptake signal pathway impaired [198]. The other cholesterol metabolism regulator genes such as ABCA1 and ABCG1 also associated with changes in energy metabolism and function of adipocytes. Previous study found that ABCG1 stable KD in 3T3-L1 preadipocytes reduces TG storage and diminishes lipid droplet size through inhibition of PPARγ protein level [199].

Lipogenesis is active and important in adipocytes. Previously, we found either SOAT1 or SOAT2 deficiency inhibit adipogenesis in 3T3-L1 adipocytes [154]. Here, we found that deficiency of SOAT1 in pre-adipocytes blocks adipocyte differentiation in both human and murine cells. Consistently, a few studies have explored the link of SOAT1 and lipogenesis in non-adipocytes and also found that target SOAT1 block LD synthesis. SOAT1 expression is highly induced in various aggressive cancer cells,

including adrenocortical cancer [200], glioma cancer [201], renal cancer [202] and liver cancer [119]. Inhibiting SOAT1 could suppress the proliferation of several types of cancer cells [203] and extend survival rate in xenograft models [117]. One of the popular underlying mechanism was that SOAT1 inhibited SREBP1 maturation and subsequently reduced the transcriptional expression of its downstream lipogenic genes [117]. SOAT1 also promotes the expression of SREBP1 and SREBP2, resulting in elevated levels of VEGFC, thereby facilitating the invasion of gastric cancer [118]. Additionally, KD of SOAT1 inhibits cell proliferation and slows down lipid synthesis by reducing the desaturase activity of SCD1, which is upregulated in prostate cancer [203]. The regulation of palmitoylation by fatty acids directly influences axonal amyloid-beta peptide (Aβ) generation in Alzheimer's disease [204]. Inhibition of ACAT, an enzyme involved in the transfer of fatty acyl groups, leads to a substantial reduction in the levels of both palmitoylated APP and Aβ [205].

For the role of SOAT1 in adipocyte hypertrophy, in our SVF differentiated mature adipocyte model, we did not observe a significant role of SOAT1 in altering LD size. However, in the JBC paper using 3T3-L1 cell model, overexpressing SOAT1 in mature adipocytes with 1500 fold reduced LD size and impaired insulin signalling [151]. This suggested that too high level of SOAT1 expression may disturb the reservoir of FC, and subsequently disturb the FC associated process, including LD expansion and caveolae associated signalling pathways. Notably, about four decades ago, Krause and Hartman's teams found that the cholesterol storage in subcutaneous adipocytes increased, without changing adipocyte size, with the increment of plasma cholesterol level [134]. Thus, the size of adipocytes is not always positively correlated with the level of cholesterol storage.

In summary, our results suggested that SOAT1's role in adipocytes may be delivered via SREBP2-dependent pathway. SOAT1 deficiency resulted in suppression of lipogenesis and the re-distribution of cholesterol pool. Therefore, it is worth to explore SOAT1 inhibition effect on anti-obesity treatment.

2.6 Acknowledgement

We would like to thank Prof. Martin Wabitsch for providing us with the SGBS cells and detailed cell culture guidance; Prof. Ta-Yuan Chang for providing us with the SOAT1 $^{flox/flox}$ mice; Dr. DENG Yongqiang for providing us with the D4 plasmid; Dr. ZHONG Jin for providing us with the SREBP2 plasmid; Dr. CHENG King Yip and Dr. LONG Kekao for their insightful comments, and Dr. Michael Yuen for his technical support in confocal microscopy. We would also like to thank the University Research Facility in Life Sciences (ULS) for providing equipment and technical support.

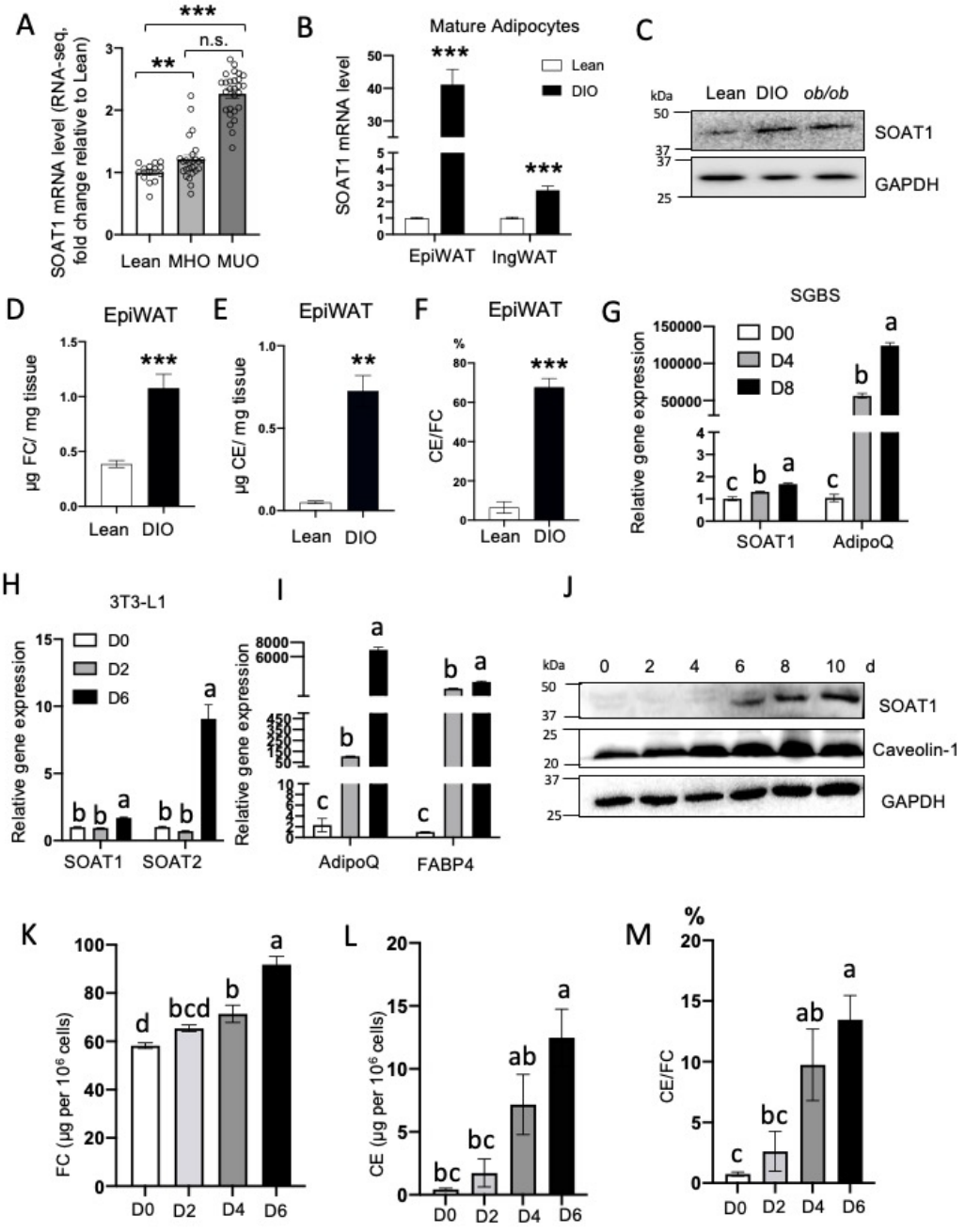
A
SOAT1 mRNA level (RNA-seq, fold change relative to Lean)
***
n.s.
**
Lean MHO MUO
B
Mature Adipocytes
SOAT1 mRNA level
***
Lean
DIO
***
EpiWAT IngWAT
C
kDa
Lean DIO ob/ob
50
37
37
25
SOAT1
GAPDH
D
EpiWAT
µg FC/ mg tissue
***
Lean DIO
E
EpiWAT
µg CE/ mg tissue
**
Lean DIO
F
EpiWAT
%
CE/FC
***
Lean DIO
G
SGBS
Relative gene expression
D0
D4
D8
c b a
c b a
SOAT1 AdipoQ
H
3T3-L1
Relative gene expression
D0
D2
D6
b b a
b b a
SOAT1 SOAT2
I
Relative gene expression
c b a
c b a
AdipoQ FABP4
J
kDa
0 2 4 6 8 10 d
50
37
25
20
37
25
SOAT1
Caveolin-1
GAPDH
K
FC (µg per 10^6 cells)
d bcd b a
D0 D2 D4 D6
L
CE (µg per 10^6 cells)
bc bc ab a
D0 D2 D4 D6
M
%
CE/FC
c bc ab a
D0 D2 D4 D6

Figure 2-1 The expression of SOAT1 in adipocytes was associated with WAT expansion.

(A) SOAT1 expression in subcutaneous abdominal adipose tissue in the Lean-normal (Lean-NL; n=14), Obese-normal (Ob-MHO; n=25) and obese-unhealth (Ob-MUO; n=27). Data are means ± SEM *p<0.05, ***p<0.001. CPM=counts per million. (B) SOAT1 mRNA level in mature adipocytes from lean and DIO mice (HFD for 14 weeks) white adipose tissue. (C) SOAT1 protein level in epididymal adipose tissue of corresponding mice. (D) Free cholesterol level in eWAT of lean and obese mice. (E) Cholesterol ester level in eWAT of lean and obese mice. (F) The proportion of eesterified cholesterol over free cholesterol. SGBS and 3T3-L1 were differentiated and collected during the adipogenic time course for qPCR (G-I) and WB (J) analysis. Free cholesterol (K) and cholesterol ester (L) were extracted at different differentiation time in 3T3-L1 cells. (M) The proportion of esterified cholesterol over free cholesterol been calculated at indicated time. Data is presented as Mean ± SEM and analysed by independent t-test or two-way ANOVA followed by Turkey's test. Difference at values of p<0.05 were considered to be significant.

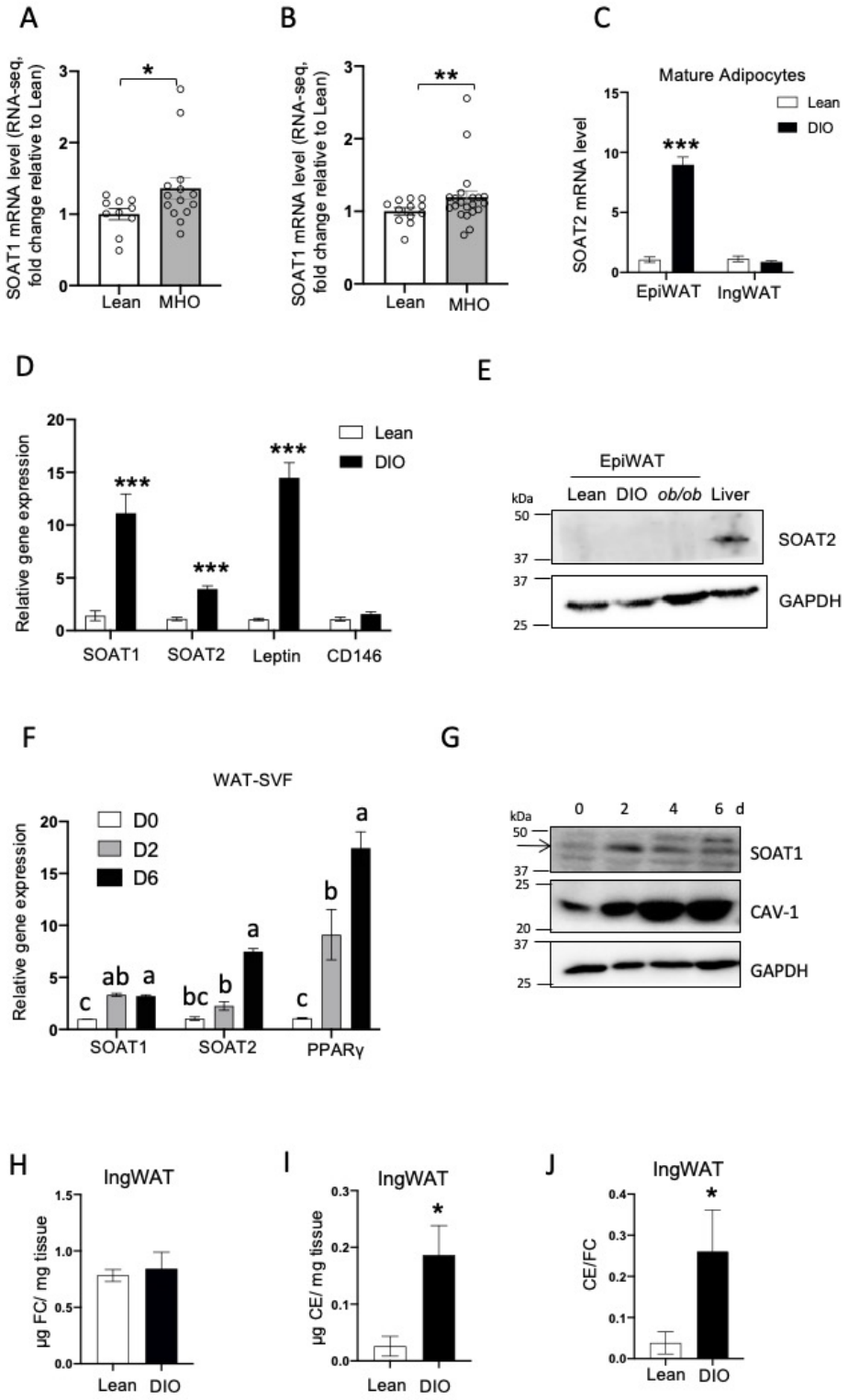
A
SOAT1 mRNA level (RNA-seq, fold change relative to Lean)
Lean
MHO
B
SOAT1 mRNA level (RNA-seq, fold change relative to Lean)
Lean
MHO
C
Mature Adipocytes
Lean
DIO
SOAT2 mRNA level
EpiWAT
IngWAT
D
Relative gene expression
Lean
DIO
SOAT1
SOAT2
Leptin
CD146
E
EpiWAT
Lean DIO ob/ob Liver
kDa
SOAT2
GAPDH
F
WAT-SVF
D0
D2
D6
Relative gene expression
SOAT1
SOAT2
PPARγ
G
0 2 4 6 d
kDa
SOAT1
CAV-1
GAPDH
H
IngWAT
μg FC/ mg tissue
Lean DIO
I
IngWAT
μg CE/ mg tissue
Lean DIO
J
IngWAT
CE/FC
Lean DIO

Figure S2-1 SOAT1 expression upregulated during obesity progress

(A) SOAT1 expression in subcutaneous abdominal adipose tissue in the Lean-normal (Lean-NL; n=10), Obese-normal (Ob-NL; n=14). Data are means ± SEM *p<0.05, ***p<0.001. CPM=counts per million.(B) SOAT1 expression in subcutaneous abdominal adipose tissue in the Lean-normal (Lean-NL; n=12), Obese-normal (Ob-NL; n=21). (C) SOAT2 mRNA level in mature adipocytes of lean and DIO mice in white adipose tissue. (D) Epididymal Adipose tissue was harvested from HFD (60% fat) feed 8 weeks old mice by Trizol reagent for RT-PCR analysis. (E) SOAT2 protein level in epididymal adipose tissue of corresponding mice. SVF were differentiated and collected during the adipogenic time course for qPCR (F) and WB (G) analysis. (H) Free cholesterol level in iWAT of lean and obese mice. (I) Cholesterol ester level in iWAT of lean and obese mice. (J) The proportion of eesterified cholesterol over free cholesterol. Data is presented as Mean ± SEM and analysed by independent t-test or two-way ANOVA followed by Turkey's test. Difference at values of p<0.05 were considered to be significant.

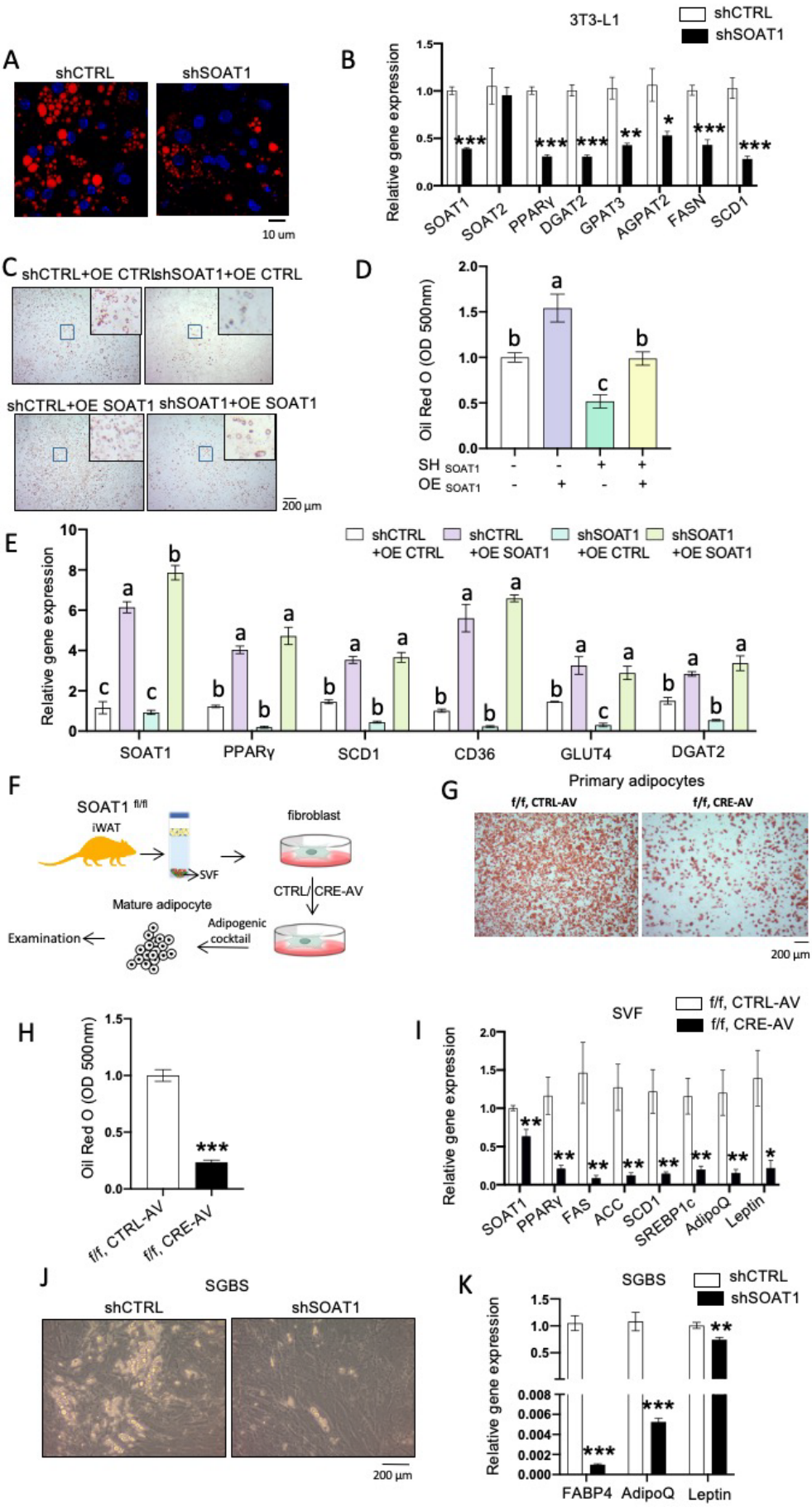
A
shCTRL
shSOAT1
10 um
B
3T3-L1
shCTRL
shSOAT1
Relative gene expression
SOAT1
SOAT2
PPARγ
DGAT2
GPAT3
AGPAT2
FASN
SCD1
C
shCTRL+OE CTRL
shSOAT1+OE CTRL
shCTRL+OE SOAT1
shSOAT1+OE SOAT1
200 μm
D
Oil Red O (OD 500nm)
SH SOAT1
OE SOAT1
E
shCTRL +OE CTRL
shCTRL +OE SOAT1
shSOAT1 +OE CTRL
shSOAT1 +OE SOAT1
Relative gene expression
SOAT1
PPARγ
SCD1
CD36
GLUT4
DGAT2
F
SOAT1 fl/fl
iWAT
SVF
fibroblast
CTRL/ CRE-AV
Mature adipocyte
Adipogenic cocktail
Examination
G
Primary adipocytes
f/f, CTRL-AV
f/f, CRE-AV
200 μm
H
Oil Red O (OD 500nm)
f/f, CTRL-AV
f/f, CRE-AV
I
SVF
f/f, CTRL-AV
f/f, CRE-AV
Relative gene expression
SOAT1
PPARγ
FAS
ACC
SCD1
SREBP1c
AdipoQ
Leptin
J
SGBS
shCTRL
shSOAT1
200 μm
K
SGBS
shCTRL
shSOAT1
Relative gene expression
FABP4
AdipoQ
Leptin

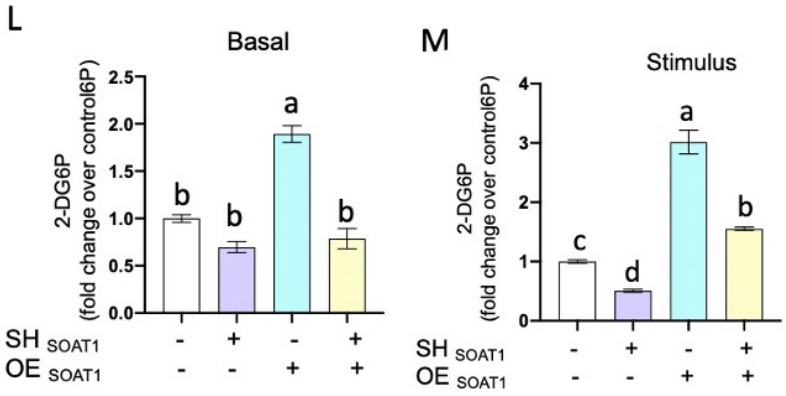

Figure 2-2 SOAT1 was important for adipogenesis, but not necessary for adipocyte hypertrophy in vitro

(A) Nile red staining of LDs in 3T3-L1 mature adipocytes. (B) mRNA levels of genes involved in adipogenic transcription program and TG synthesis in 3T3-L1 mature adipocytes. (C) ORO staining of 3T3-L1 mature adipocytes under different treatment. (D) LD accumulation of ORO of figure C. (E) mRNA levels of genes involved in adipogenic transcription program and TG synthesis in 3T3-L1 mature adipocytes. (F) schematic of SVF cell culture. (G) ORO staining of primary adipocytes and (H) the intensity of the TG spots in ORO was quantified by absorbance at 500nm. (I) mRNA level of genes involved in adipogenic transcription program and TG synthesis in SVF differentiated adipocytes. (J) Lipid droplets were observed under microscopy after 12 days of differentiation. (K) Adipogenesis related gene expression of SGBS cell. (L-M) Glucose uptake ability were measured in 3T3-L1 of fours days differentiation. Data is presented as Mean ± SEM and analysed by independent t-test or two-way ANOVA followed by Turkey's test. Difference at values of $p<0.05$ were considered to be significant.

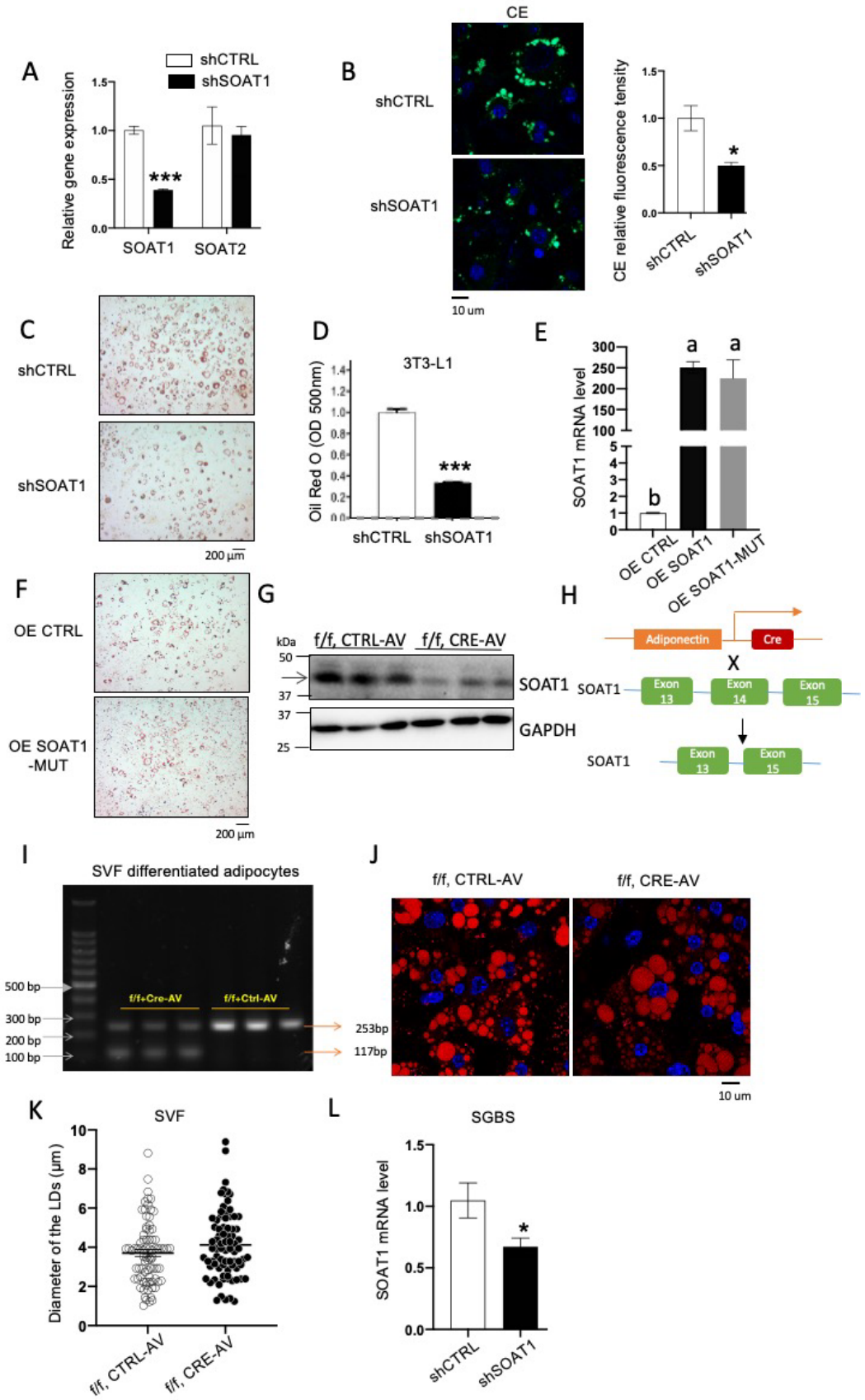
A
shCTRL
shSOAT1
Relative gene expression
1.5
1.0
0.5
0.0
***
SOAT1
SOAT2
B
CE
shCTRL
shSOAT1
10 um
CE relative fluorescence tensity
1.5
1.0
0.5
0.0
*
shCTRL
shSOAT1
C
shCTRL
shSOAT1
200 μm
D
3T3-L1
Oil Red O (OD 500nm)
1.4
1.2
1.0
0.8
0.6
0.4
0.2
0.0
***
shCTRL
shSOAT1
E
SOAT1 mRNA level
300
250
200
150
100
5
4
3
2
1
0
a
a
b
OE CTRL
OE SOAT1
OE SOAT1-MUT
F
OE CTRL
OE SOAT1
-MUT
200 μm
G
kDa
f/f, CTRL-AV
f/f, CRE-AV
50
37
37
25
SOAT1
GAPDH
H
Adiponectin
Cre
X
SOAT1
Exon
13
Exon
14
Exon
15
SOAT1
Exon
13
Exon
15
I
SVF differentiated adipocytes
500 bp
300 bp
200 bp
100 bp
f/f+Cre-AV
f/f+Ctrl-AV
253bp
117bp
J
f/f, CTRL-AV
f/f, CRE-AV
10 um
K
SVF
Diameter of the LDs (μm)
10
8
6
4
2
0
f/f, CTRL-AV
f/f, CRE-AV
L
SGBS
SOAT1 mRNA level
1.5
1.0
0.5
0.0
*
shCTRL
shSOAT1

Figure S2-2 SOAT1 was important for adipogenesis, but not necessary for adipocyte hypertrophy in vitro

(A) mRNA level in pre-adipocyte of 3T3-L1 cells. (B) 0.5μg/ml 22-NBD were loaded in mature adipocyte of each group for 6h. (C) ORO staining of shCTRL and shSOAT1 group. (D) ORO quantification of (C). (E) SOAT1 mRNA level in pre-adipocyte of each group. (F) ORO staining of control and mutant group. (G) SOAT1 protein level in SVF cells with or without cre Ad-virus. (H) Schematic of Cre- loxp system. (I) Depletion of SOAT1 was confirmed by PCR analysis of cDNA to detect the loxp/loxp, excised genes for each of the SOAT1 subunits in primary adipocytes. (J) Cre were added at Differentiation day 4 and Nile red staining of LDs in primary adipocytes. (K) Quantification of the LDs size in I. n=70. (L) SOAT1 mRNA level in SGBS pre-adipocytes. Data is presented as Mean ± SEM and analysed by independent t-test or two-way ANOVA followed by Turkey's test. Difference at values of $p<0.05$ were considered to be significant.

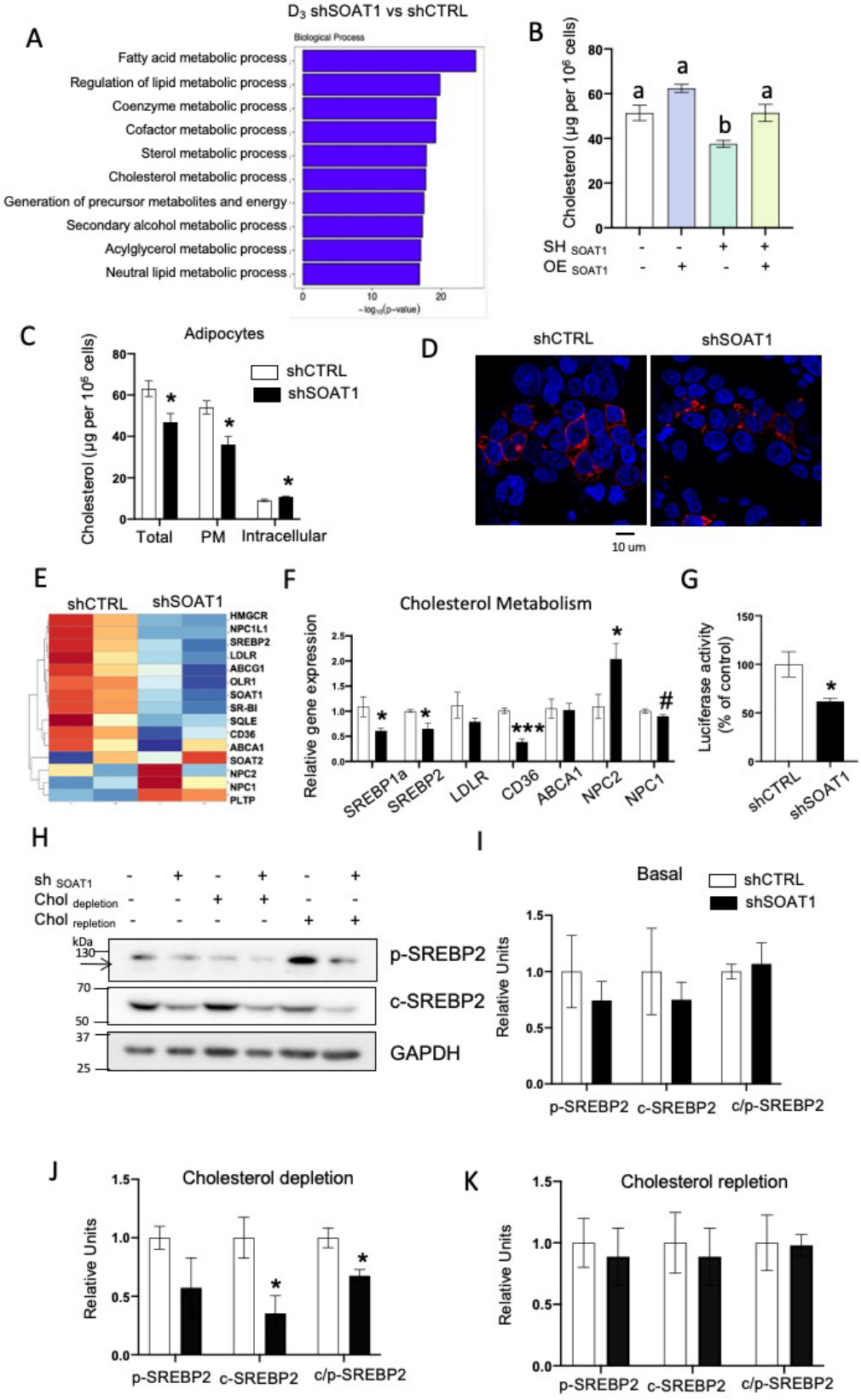
A
D3 shSOAT1 vs shCTRL
Biological Process
Fatty acid metabolic process
Regulation of lipid metabolic process
Coenzyme metabolic process
Cofactor metabolic process
Sterol metabolic process
Cholesterol metabolic process
Generation of precursor metabolites and energy
Secondary alcohol metabolic process
Acylglycerol metabolic process
Neutral lipid metabolic process
B
Cholesterol (µg per 10^6 cells)
SH SOAT1
OE SOAT1
C
Adipocytes
shCTRL
shSOAT1
Cholesterol (µg per 10^6 cells)
Total
PM
Intracellular
D
shCTRL
shSOAT1
10 um
E
shCTRL
shSOAT1
HMGCR
NPC1L1
SREBP2
LDLR
ABCG1
OLR1
SOAT1
SR-BI
SQLE
CD36
ABCA1
SOAT2
NPC2
NPC1
PLTP
F
Cholesterol Metabolism
Relative gene expression
SREBP1a
SREBP2
LDLR
CD36
ABCA1
NPC2
NPC1
G
Luciferase activity (% of control)
shCTRL
shSOAT1
H
sh SOAT1
Chol depletion
Chol repletion
kDa
p-SREBP2
c-SREBP2
GAPDH
I
Basal
shCTRL
shSOAT1
Relative Units
p-SREBP2
c-SREBP2
c/p-SREBP2
J
Cholesterol depletion
Relative Units
p-SREBP2
c-SREBP2
c/p-SREBP2
K
Cholesterol repletion
Relative Units
p-SREBP2
c-SREBP2
c/p-SREBP2

Figure 2-3 SOAT1 regulated intracellular cholesterol homeostasis, including cholesterol quantity and distribution

(A)Top 10 downregulated signalling pathway analysed by biological process in shSOAT1 vs shCTRL cells in D3. (B) Cholesterol level were measured after fully differentiation under different groups of 3T3-L1 cells. (C) Cholesterol quantification of total, plasma membrane and intracellular part in 3T3-L1 mature adipocytes. (D) D4 plasmid transfect in shCTRL and shSOAT1 of 293T cells at D0, image were taken by D1. (E) Heat map depicting the fold change of representative genes in cholesterol metabolism pathway of D3. (F) mRNA levels of genes involved cholesterol metabolism in differentiated D3 of 3T3-L1 adipocytes. (G) Luciferase activity of SRE reporter constructs in shCTRL and shSOAT1 pre-adipocytes. (H) 3T3-L1 cells were harvested at day 4 and subject to immunoblotting under different treatment. (I-K) Quantification of SREBP2 protein levels. Data is presented as Mean ± SEM and analysed by independent t-test or two-way ANOVA followed by Turkey's test. Difference at values of $p<0.05$ were considered to be significant.

Supplementary 3

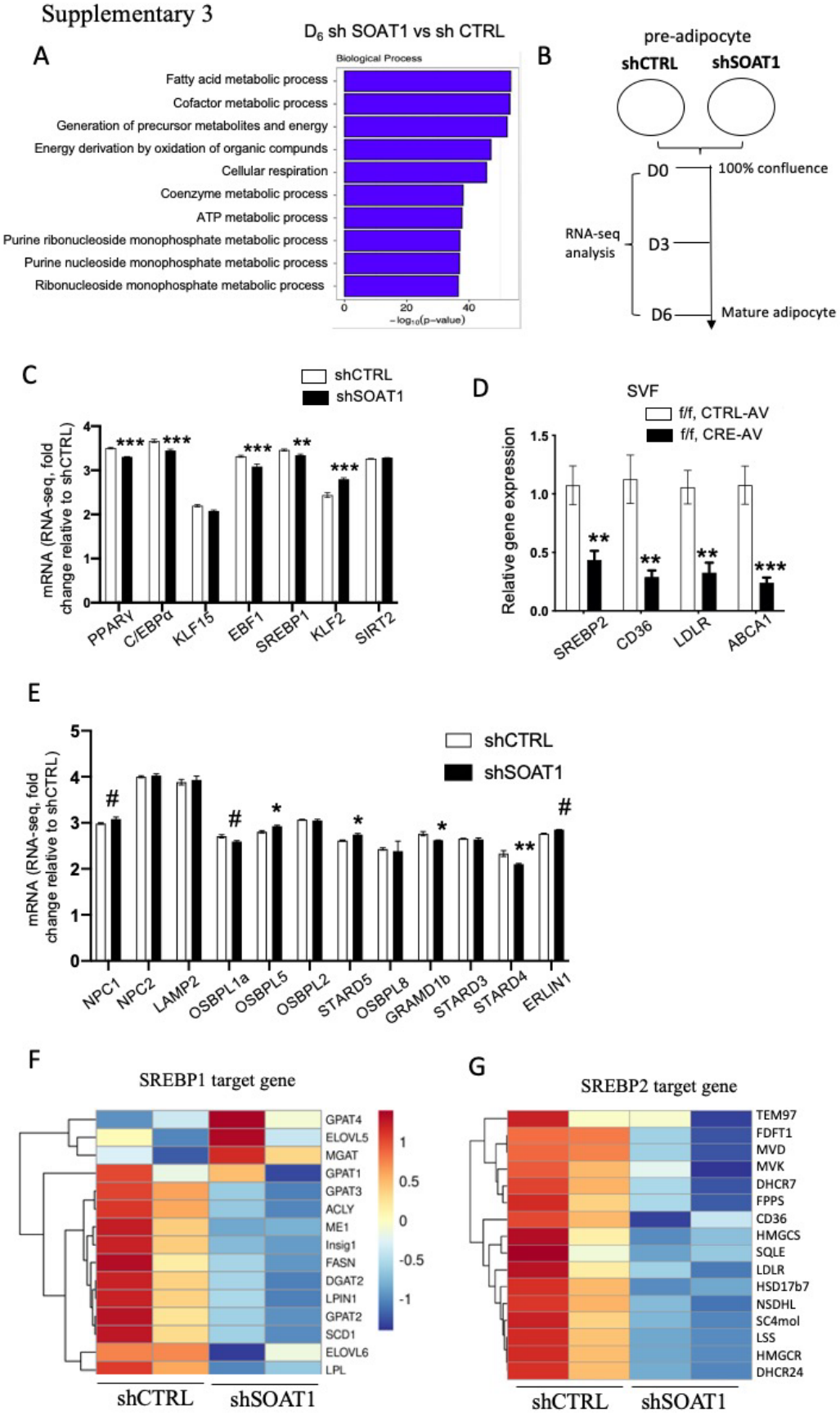

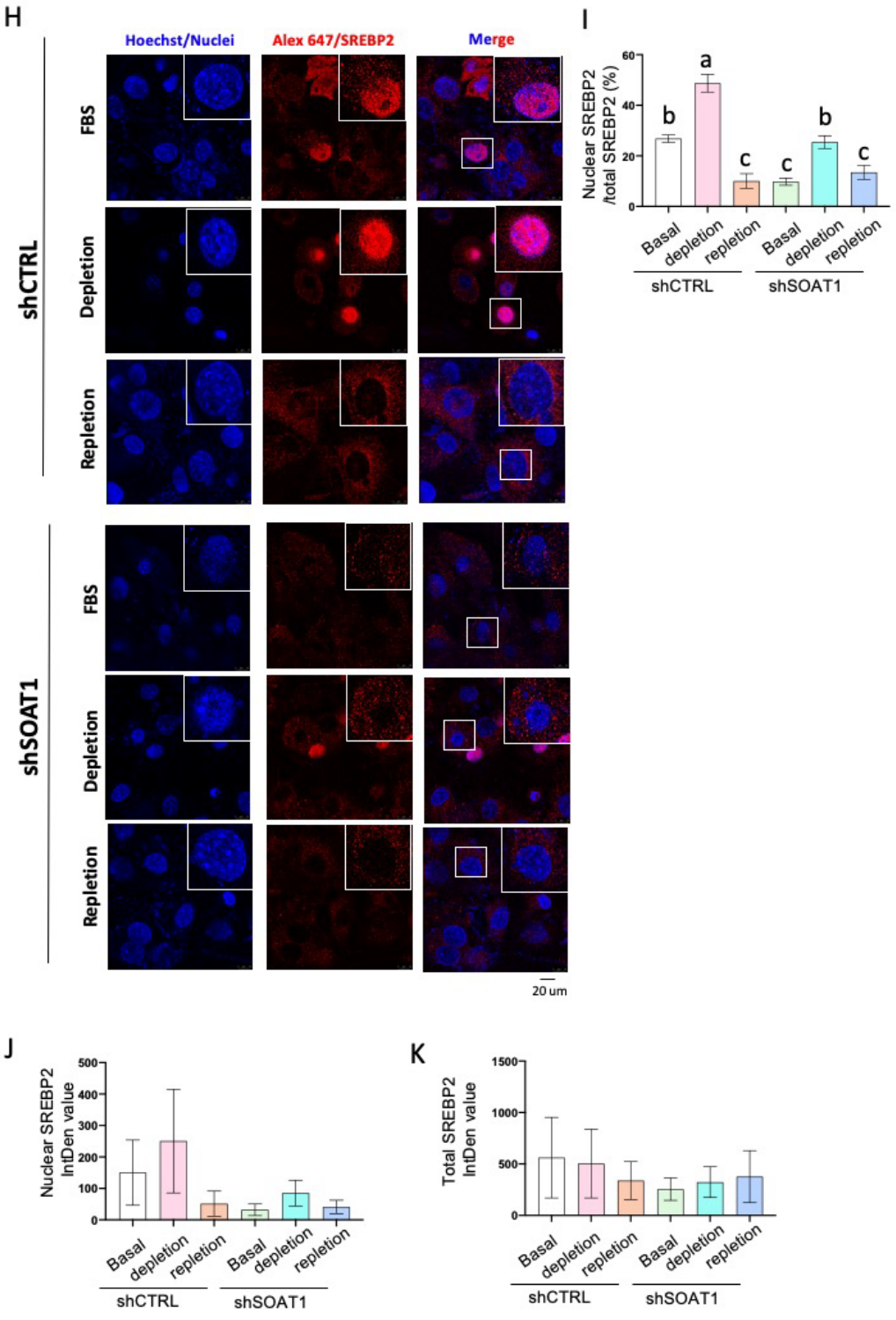
H
Hoechst/Nuclei
Alex 647/SREBP2
Merge
shCTRL
shSOAT1
FBS
Depletion
Repletion
20 um
I
Nuclear SREBP2 /total SREBP2 (%)
a
b
c
c
b
c
Basal
depletion
repletion
Basal
depletion
repletion
shCTRL
shSOAT1
J
Nuclear SREBP2 IntDen value
Basal
depletion
repletion
Basal
depletion
repletion
shCTRL
shSOAT1
K
Total SREBP2 IntDen value
Basal
depletion
repletion
Basal
depletion
repletion
shCTRL
shSOAT1

Figure S2-3 SOAT1 regulated intracellular cholesterol homeostasis, including cholesterol quantity and distribution

(A)Top 10 downregulated signalling pathway analysed by biological process in shSOAT1 vs shCTRL cells in D6. (B) Schematic of RNA-seq sample collection. (C) mRNA expression in D3 differentiated adipocyte (n=3). Data are means ± SEM *p<0.05, ***p<0.001. CPM=counts per million. (D) mRNA levels of genes involved in cholesterol metabolism in SVF differentiated mature adipocytes. (E) mRNA expression in D3 differentiated adipocyte (n=3). Data are means ± SEM *p<0.05, ***p<0.001. CPM=counts per million. (F-G) The heat map analysis of SREBP1 and SREBP2 target genes was performed based on D3 shSOAT1 vs shCTRL. (H) SREBP2 immunofluorescence staining under different treatment. (I) Percentages of SREBP2 intensity in the nuclei normalized to the total SREBP2 intensity in (H), (J) Nuclear SREBP2 intensity in (H), (K) total SREBP2 intensity in (H). 10 cells/trail, 3 independent trails. Data is presented as Mean ± SEM and analysed by independent t-test or two-way ANOVA followed by Turkey's test. Difference at values of $p<0.05$ were considered to be significant.

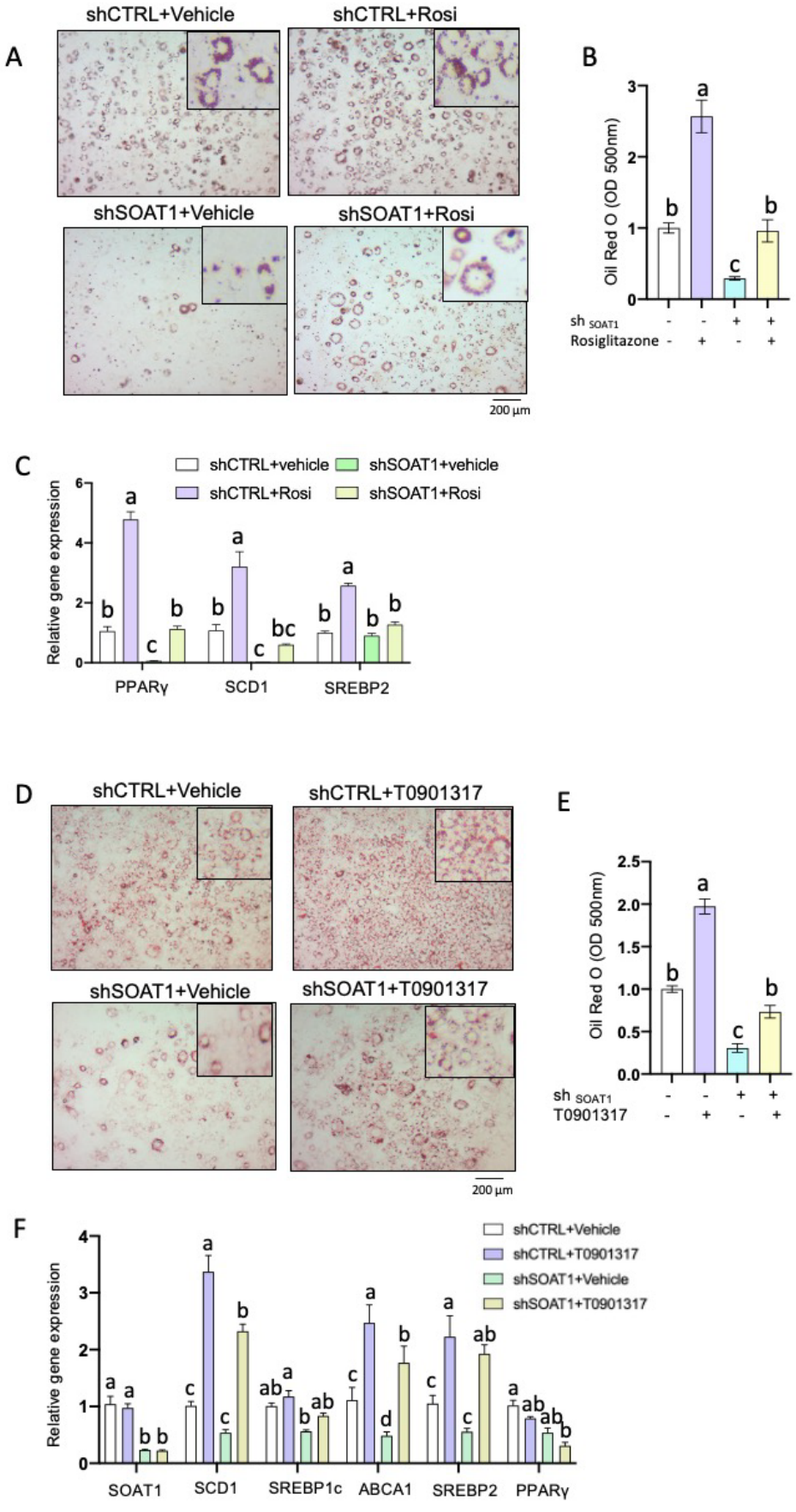
A
shCTRL+Vehicle
shCTRL+Rosi
shSOAT1+Vehicle
shSOAT1+Rosi
200 μm
B
Oil Red O (OD 500nm)
sh SOAT1
Rosiglitazone
C
shCTRL+vehicle
shSOAT1+vehicle
shCTRL+Rosi
shSOAT1+Rosi
Relative gene expression
PPARγ
SCD1
SREBP2
D
shCTRL+Vehicle
shCTRL+T0901317
shSOAT1+Vehicle
shSOAT1+T0901317
200 μm
E
Oil Red O (OD 500nm)
sh SOAT1
T0901317
F
shCTRL+Vehicle
shCTRL+T0901317
shSOAT1+Vehicle
shSOAT1+T0901317
Relative gene expression
SOAT1
SCD1
SREBP1c
ABCA1
SREBP2
PPARγ

Figure 2-4 The inhibition of adipogenesis in preadipocytes lacking SOAT1 is mediated through the transcriptional regulation of PPARγ and SREBP1

(A) ORO staining of LDs in 3T3-L1 mature adipocytes. (B) Quantification of ORO staining in (A). (C) mRNA levels of genes involved in adipogenic in 3T3-L1 mature adipocytes. (D) ORO staining of LDs in 3T3-L1 mature adipocytes. (E) Quantification of ORO staining in (D). (F) mRNA levels of genes involved in adipogenic in 3T3-L1 mature adipocytes. Data is presented as Mean ± SEM and analysed by independent t-test or two-way ANOVA followed by Turkey's test. Difference at values of $p<0.05$ were considered to be significant.

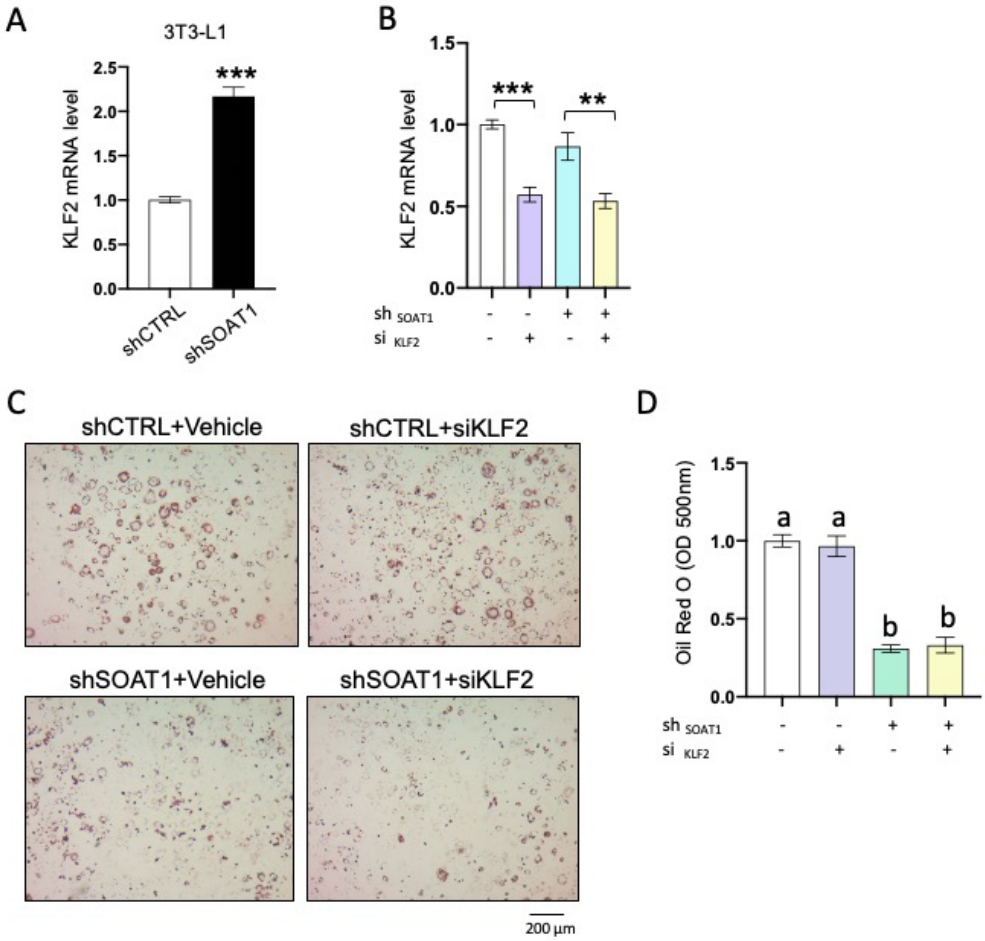

Figure S2-4 siKLF2 not promote LD accumulation in 3T3-L1 cells

(A) KLF2 mRNA level in differentiated D3 of 3T3-L1 adipocytes. (B) KLF2 mRNA level in both shCTRL and shSOAT1 pre-adipocytes. (C) ORO staining of LDs in 3T3-L1 mature adipocytes. (D) Quantification of ORO staining in (C). Data is presented as Mean ± SEM and analysed by independent t-test or two-way ANOVA followed by Turkey's test. Difference at values of $p<0.05$ were considered to be significant.

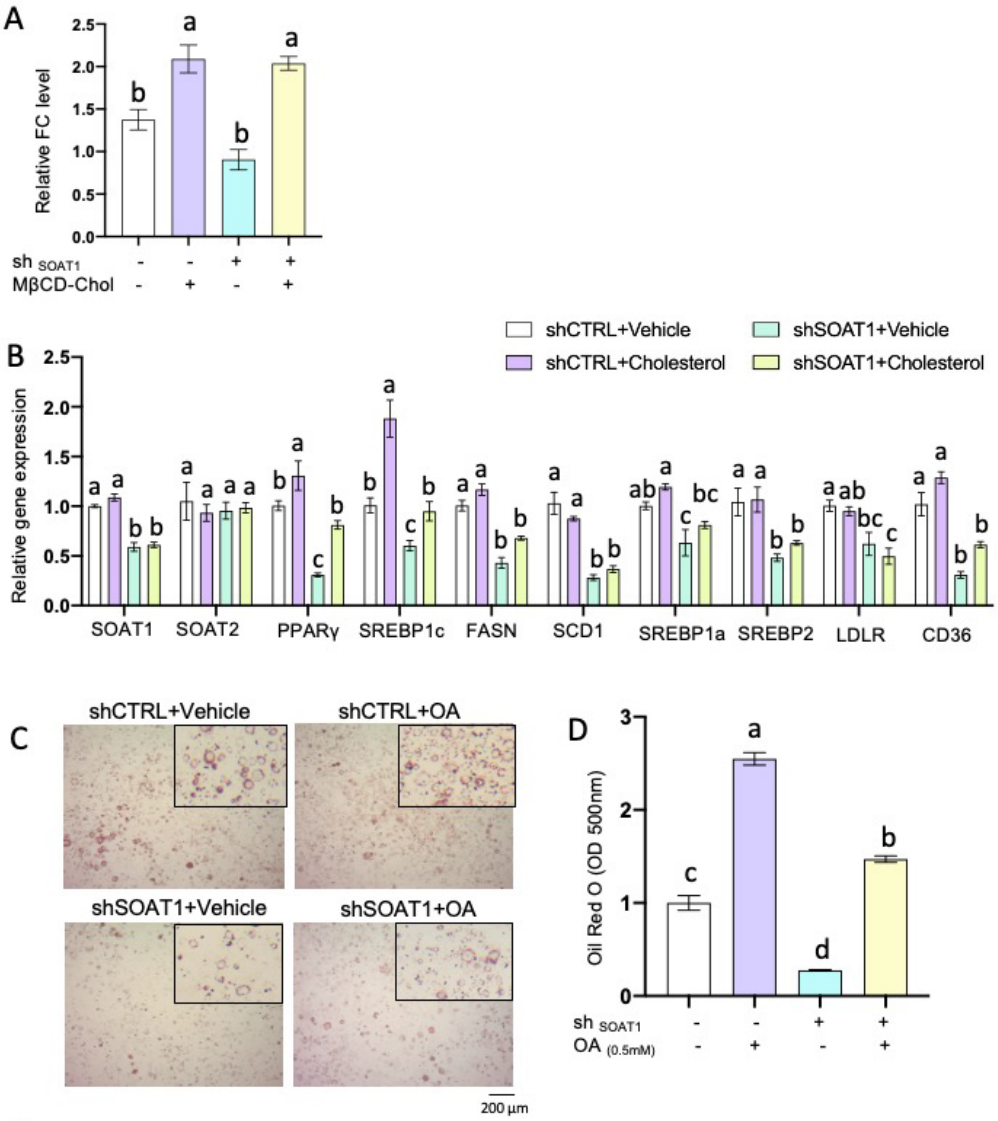
A
Relative FC level
sh SOAT1
MβCD-Chol
B
shCTRL+Vehicle
shCTRL+Cholesterol
shSOAT1+Vehicle
shSOAT1+Cholesterol
Relative gene expression
SOAT1
SOAT2
PPARγ
SREBP1c
FASN
SCD1
SREBP1a
SREBP2
LDLR
CD36
C
shCTRL+Vehicle
shCTRL+OA
shSOAT1+Vehicle
shSOAT1+OA
200 μm
D
Oil Red O (OD 500nm)
sh SOAT1
OA (0.5mM)
E
shCTRL+Vehicle
shCTRL+OA
shSOAT1+Vehicle
shSOAT1+OA
Relative gene expression
SOAT1
PPARγ
FASN
SREBP1c
SCD1
LPL
SREBP2

Figure 2-5 Nutritional factors could rescue adipogenesis in SOAT1 deficient pre-adipocytes

(A) Cholesterol level measured in 3T3-L1 mature adipocytes with or without MβCD-coated cholesterol. (B) mRNA levels of genes involved in cholesterol metabolism and adipogenesis in 3T3-L1 mature adipocytes. . (C) ORO staining of 3T3-L1 adipocytes and (D) the intensity of the TG spots in ORO was quantified by absorbance at 500nm. (E) mRNA levels of genes involved in fatty acid metabolism and adipogenesis in 3T3-L1 mature adipocytes. Data is presented as Mean ± SEM and analysed by independent t-test or two-way ANOVA followed by Turkey's test. Difference at values of $p<0.05$ were considered to be significant.

Table 2-1 Primer sequence

Primer	Sequence
D4-RFP	GGTGGAGGCGGTTCAAAGGGAAAAATAAACTTAGATCATAGTGGAGCCTATGT TGCACAGTTTGAAGTAGCATGGGATGAAGTTTCAGCgcTGACAAAGAAGGAAAT GAAGTTTTAACTCATAAAACATGGGATGGAAATTATCAATGGtggAAAACAGCTC ACTATTCAACAGTAATACCTCTTGAAGCCAATGCAAGAAATATAAGAATAAAG GCAAGAGAGTGTACAGGTCTTTGGtggTGGGAATGGTGGAGAGATGTTATAAGT GAATATGATGTTCCATTAACAAATAATATAAATGTTTCAATATGGGGAACTACT TTATACCCTGGATCTAGTATTACTTACAATTAA

Table 2-2 qRT-PCR primers

Gene name	Forward primer	Revere primer
Gapdh	AAGAAGGTGGTGAAGCAGGCATC	CGAAGGTGGAAGAGTGGGAGTTG
β-actin	AGATGACCCAGATCATGTTTGAGA	CACAGCCTGGATGGCTACGT
CD146	CGAGGCAGAAAGTAACCAGGAC	GTCTCACGTTGTTTAGCTGGAGG
F4/80	CTTTGGCTATGGGCTTCCAGTC	GCAAGGAGGACAGAGTTTATCGTG
GPAT3	AGTGAGCTGGTGCATCTGACCT	GATTGGCGACACAGATACCTCC
SOAT1	TCGCACTCCTCATCCTATTCG	GTACCAGCCTTCCTTCATCGAT
SOAT2	AGACTTGGTGCAATGGACTCGAC	CATAGGGCCCGATCCAACAG
AGPAT2	TTTGAGGTCAGCGGACAGAA	AGGATGCTCTGGTGATTAGAGATGA
SCD1	GGTGATGTTCCAGAGGAGGTACTAC	AGCGTGGGCAGGATGAAG
CD36	GTTCTTCCAGCCAATGCCTTT	ATGTCTAGCACACCATAAGATGTACAGT
Ppar-γ	ACCTCTGCTGGGGATCTGAA	TGGCATTGTGAGACATCCCC
AdipoQ	GGAACTTGTGCAGGTTGGAT	GCTTCTCCAGGCTCTCCTTT
Glut4	GGCTTTGTGGCCTTCTTTGAG	GACCCATAGCATCCGCAACAT
Fas	ATGCACACTCTGCGATGAAG	CAGTGTTCACAGCCAGGAGA
Srepb1c	GGCCCGGGAAGTCACTGT	CATCTTTAAAGCAGCGGGTG
ACC	GTCCCCAGGGATGAACCAATA	GCCATGCTCAACCAAAGTAGC
LDLR	AGGCTGTGGGCTCCATAGG	TGCGGTCCAGGGTCATCT
Dgat2	GCCGTGTGGCGCTACTTC	GTGGTCAGCAGGTTGTGTGTCT
Leptin	CACACACGCAGTCGGTATCC	AGCCCAGGAATGAAGTCCAA
ABCA1	AGTTTCGGTATGGCGGGTTT	AGCATGCCAGCCCTTGTTAT
LPL	GCGTAGCAGGAAGTCTGACCAA	AGCGTCATCAGGAGAAAGGCGA
hSOAT1	GAAGTTGGCAGTCACTTTGATGA	GAGCGCACCCACCATTATCTA
hAdipoQ	GGTGAGAAGGGTGAGAAAGGA	TTTCACCGATGTCTCCCTTAG

Table 2-3 Summary of cholesterol trafficking gene

Cholesterol Trafficking direction	Related gene name	mRNA Changes during day 0-3	mRNA Changes during day 3-6	Effect of SOAT1 deficiency during day 0-3	Effect of SOAT1 deficiency during day 3-6	references
Lysosome to intracellular part	NPC1	Significantly decreased	Significantly increased	Significantly decreased	Significantly increased	[206]
Lysosome to intracellular part	NPC2	Significantly decreased	Significantly increased	Trend to decrease	Significantly increased	[206]
cholesterol export out of lysosome	LAMP2	Significantly decreased	Significantly increased	Significantly decreased	Significantly increased	[207]
Lysosome to ER	OSBPL1a	No difference	Significantly decreased	No difference	No difference	[176]
Lysosome to ER	OSBPL5	Significantly decreased	No difference	Significantly decreased	Trend to increase	[177]
Lysosome to PM	OSBPL2	No difference	Significantly increased	No difference	No difference	[178]
Lysosome to Golgi	STARD5	No difference	Significantly increased	No difference	No difference	[179]
Between ER and PM	OSBPL8	No difference	Significantly increased	No difference	Trend to increase	[180, 181]

PM to ER	GRAMD1b	Significantly increased	No difference	Significantly increased	No difference	[182]
ER to lysosome	STARD3	No difference	No difference	No difference	No difference	[208]

Chapter 3 ADIPOCYTE SOAT1 DEFICIENCY PROMOTE IWAT BEIGE AND ENHANCE ADIPOSE TISSUE LIPOLYSIS IN HIGH CHOLESTEROL FED MICE

3.1 Abstract

Adipose tissue (AT) thermogenesis stimulated by cold exposure or sympathetic innervation is regarded as a potential therapeutic strategy against obesity. Maintaining cholesterol homeostasis is crucial for AT function. However, the physiological effects of cholesterol esterification on adipocyte function remain unclear. Sterol-O-acyltransferase-1 (SOAT1), is the key enzyme responsible for catalyzing free cholesterol (FC) into cholesteryl ester (CE). Here, we used adipocyte-specific SOAT1-knockout (AKO) mice and SOAT1 $^{flox/flox}$ (CTRL) mice and fed them a high-cholesterol diet (HCD) for 21 weeks. Compared to CTRL mice, the AKO mice increased energy expenditure (EE) and inguinal white adipose tissue (iWAT) browning at room temperature without any external stimulus, despite similar fat mass, food intake and glucose tolerance. Mechanistically, RNA-seq analysis of iWAT revealed a significant upregulation of UCP1 mRNA levels, along with beige-related marker genes (Dio2, COX7a1). This was further supported by UCP1 IHC staining, which showed a significant upregulation in the iWAT tissue of AKO mice compared to CTRL. Additionally, the protein level of ATGL was significantly enhanced in iWAT, suggesting that the knockout of SOAT1 induced WAT lipolysis may contribute to the beige adipocyte formation process. To further confirm the effect of SOAT1 knockout in adipocytes, we utilized an in vitro model by knocking out SOAT1 in mature adipocytes derived from the stromal vascular fraction (SVF). This in vitro model also resulted in a significant upregulation of UCP1 and beige marker gene (PGC1α, PRDM16) mRNA levels, as well as an increase in ATGL protein level and glycerol release from the cell culture medium in the KO group. We conclude that blocking SOAT1 in adipocytes promotes browning of iWAT and enhances lipolysis under HCD feeding. Our work reveals a potential mechanism for the regulation of thermogenic adipocytes and

cholesterol esterification. Blocking SOAT1 could serve as a potential target to treat obesity

3.2 Introduction

White adipose tissue (WAT), traditionally recognized for its primary role in energy storage, has been gaining increasing attentions due to its dynamic functionality and plasticity. The ability of WAT to 'beige' or 'brown', forming cells that possess biochemical and functional characteristics of brown adipose tissue (BAT), is of particular interest [209]. Compared to regular white adipocytes, beige adipocytes exhibit thermogenic capabilities and are distinguished by their expression of uncoupling protein 1 (UCP1). UCP1, a protein localizes in the mitochondrial, uncouples electron transfer from ATP production in the electron transfer chain and subsequently resulted in heat dissipation. The conversion of WAT into a thermogenic phenotype promises as a potential therapeutic approach for addressing obesity and associated metabolic disorders [210].

During the process of adipocyte hypertrophy, the cholesterol content also increases, with almost half of the cholesterol being stored in AT during obesity [133]. Therefore, maintaining cholesterol homeostasis is critical for AT function. However, there is limited research focusing on AT cholesterol homeostasis. There are three studies have investigated the physiological role of key enzymes involved in cholesterol efflux (ABCA1, ABCG1) and synthesis (HMGCR) in adipocytes, as well as their effects on metabolic health. Parks et al. conducted a study using adipocyte-specific knockout ABCA1 mice and fed them a high-fat, high-cholesterol (HFHC) diet for 16 weeks. The knockout mice exhibited significantly decreased body weight, fat mass, and adipocyte size compared to control mice [139]. Frisdal et al. used lentivirus intraperitoneal injection to knock down ABCG1 in epididymal white adipose tissue (eWAT) for 4 weeks, along with high-fat diet feeding. The knockdown group showed decreased body weight and adiposity compared to the control group [199]. Yeh et al. created adipocyte-specific knockout HMGCR mice, and these mice developed lipodystrophy [211]. These

studies collectively suggest that adipocyte cholesterol homeostasis plays a key role in maintaining metabolic health. However, the role of cholesterol esterification in regulating metabolic health remains unclear.

Adipose tissue lipolysis involves the breakdown of triglycerides stored within adipocytes, releasing glycerol and free fatty acids to meet the body's energy demands. This process is initiated by the activation of lipolytic enzymes such as hormone-sensitive lipase (HSL) and adipose triglyceride lipase (ATGL), which are the main enzymes responsible for hydrolyzing triglycerides [212]. ATGL deficiency impairs lipolysis process and promote TG accumulation in WAT. Multiple proteins could faciliteta the ATGL from ER translocate to LDs to activate the lipolysis process [213]. Most of the adipocyte-free cholesterol is located on the surface of LDs rather than the plasma membrane [136, 214]. Disruption of the cholesterol esterification process may lead to an increase in free cholesterol levels on the LD surface, promoting the translocation of phosphorylated HSL. Adipose tissue lipolysis can be induced by various factors such as cold exposure, hormonal signals (glucagon, GH), and catecholamines, which can also induce the browning of WAT [215]. Previous studies have found that lipolysis-derived linoleic acid from WAT can promote the proliferation of beige fat progenitor cells [216]. lipolysis-induced release of FFAs activates signaling pathways that promote the browning of WAT by stimulating the expression and activation of key regulatory proteins, such as PGC-1α and PRDM16 [217].

SOAT1 is the enzyme mainly responsible for transferring free cholesterol into cholesterol esters in adipocytes. It is a nine-transmembrane domain protein located in the endoplasmic reticulum (ER). Recent research has identified its enrichment in the ER-mitochondrial contact site called the mitochondria-associated membrane (MAM) [148]. The MAM region is rich in cholesterol and sphingolipids [218]. Previous studies have shown that inhibiting SOAT1 can increase the ER-mitochondrial contact site and enhance its activity [219]. This suggests that an increased pool of free cholesterol may facilitate the transfer of calcium ions from the ER to mitochondria. Mitochondria are cellular organelles responsible for generating ATP through oxidative phosphorylation, which involves the coupling of electron transport and ATP synthesis. In the presence of

uncoupling protein 1 (UCP1), the energy derived from electron transport can be uncoupled from ATP synthesis and dissipated as heat [220]. Whether SOAT1 regulates mitochondrial function is still not fully understood.

In this study, we constructed adipocyte-specific knockout mice lacking SOAT1 to investigate its function. Remarkably, when these KO mice were fed a HCD diet, we observed the formation of beige adipocytes in iWAT and an enhancement in EE. In addition, we found that SOAT1 deficiency promoted lipolysis in iWAT both in vivo and in vitro. However, the KO of SOAT1 also result in inflammation in iWAT and lipid accumulation in liver. Overall, our findings provide valuable insights into the molecular mechanisms through which SOAT1 regulates iWAT browning under HCD conditions.

3.3 Methods and materials

3.3.1 Animal model and treatment

All animal experiments were conducted at The Hong Kong Polytechnic University and were approved by the Centralized Animal Facilities (CAF). The mice used in this study were of C57BL/6J background and were housed at room temperature with a 12-hour light/dark cycle. They were fed with HCD (1.25% cholesterol with 0.5% sodium cholate) (Shuyishuer Bio. China) and given sterile water ad libitum. $SOAT1^{flox/flox}$ mice were generated by inserting two Loxp sites covering SOAT1 exon 14 (provided by Dr. Ta-Yuan Chang [126]. Adipocyte-specific SOAT1 knockout mice (Adipoq-SOAT1) were generated by crossing $SOAT1^{flox/flox}$ mice with adiponectin-Cre (Adipoq-Cre, provided by Dr. CHENG, King Yip [152]). Male $SOAT1^{flox/flox}$ mice aged 4-6 weeks were used in this study for stromal vascular fraction isolation.

3.3.2 Mice genotyping

Genotyping was carried out using PCR with genomic DNA extracted from tail biopsies and follow the procedure as previously stated [21]. The PCR primers for SOAT1 Loxp site were as follows: forward, 5'-TATGCCCTCGCCATCTGCCT-3'; reverse, 5'-

CCAGCAGTAGGCTCTCATATGC-3’.

3.3.3 Glucose and insulin tolerance tests

For the glucose tolerance test, mice were fasted overnight followed by i.p. injection with glucose (2g/kg). For insulin tolerance test, mice were day fasting 6h and i.p. inject with human insulin (0.75 IU/kg). Glucose level were measured from tail blood at indicated time point by using glucose meter (Roche, Switzerland).

HOMA-IR was calculated based on the following equation: HOMA-IR=fasting serum insulin (mU/L) * fasting serum glucose (mg/dl)/405.

3.3.4 Metabolic cage studies

Mice were housed individually and acclimated for 2 days to the metabolic chambers (Promethion System, Sable system international, United States) with ad libitum access to food and water at CAF. Data collected as indicated were used to calculate food intake, RER, energy expenditure and physical activity as previously described [221].

3.3.5 Histological staining

Hematoxylin and eosin (H&E) staining was performed as previous described [222]. Briefly, tissue were fixed in 10% formalin and subjected to paraffin embedding, and sectioned with 5 μm thickness. Adipocyte sizes were quantified by AdipoCount software [223].The F4/80 and UCP1 immunohistochemistry (IHC) were performed by Servicebio (China) company. Images were taken using a Nikon TS100 microscope (Japan) and were quantified by ImageJ software (Version 2.0).

3.3.6 Fecal calorie measurement

Fecal samples were collected after 21 weeks of treatment. One gram of dried stool was used to prepare pellets, and the calorie content was determined using a bomb calorimeter 6200 instrument with a 1108 oxygen-bomb model (Parr Instrument Co., Moline, Illinois) [224]. Benzoic acid was utilized as the calibration standard.

3.3.7 Mature adipocyte isolation

After euthanizing the mice, their adipose tissue was collected immediately. This tissue was then dissected, cut into small pieces, and digested in a solution of PBS with 1 mg/ml Collagenase IV (17101015, Thermo) and 2.4 IU/ml Dispase II (D4693, Sigma-Aldrich) for about 50 minutes at 37°C. This digestion was performed in a shaker water bath operating at 100rpm. Following digestion, the cells were strained through a 100 μm cell strainer (352360, Falcon) into a fresh tube and then centrifuged at 600g for 5 minutes at 4°C. The adipocytes that floated to the top were transferred to another 15ml conical tube with DMEM/F12 (11995065, Thermo) medium. A second centrifugation was performed under the same conditions, and the adipocytes were then transferred to a 1.5ml tube for future experiments.

3.3.8 Blood collection, TG, FFA, glycerol, cholesterol and hormone measurement of mouse serum

Blood samples were collected from overnight or day fasting mice. The blood was stand in RT for 30min, then centrifuge at 2,000 g for 30 min to get the supernatant. Serum levels of TG were determined by TG kit (A110-1-1, nanjingjiancheng). TC, FC and CE were determined by Amplex Amplex Red cholesterol assay kit (A12216, Thermo). Adiponectin were measured by Elisa kit (Cat. 32010, IMD). All experimental procedures were conducted in accordance with the guidelines provided by the manufacturer.

3.3.9 Statistical analysis

The data are presented as means ± S.D. or means ± S.E.M., as specified in the figure legends. Statistical significance for comparisons between control and treatment groups was assessed using GraphPad Prism software (version 9.0) with a two-tailed student's t-test or one-way ANOVA. Statistical significance is reported for comparisons with a p-value < 0.05, as indicated in the figure legends.

3.4 Results

3.4.1 SOAT1 is selectively deleted by adipocytes

To investigate the function of SOAT1 in adipocytes in vivo, we generated mice lacking SOAT1 in adipose tissue (AKO) by crossing adiponectin-Cre mice to SOAT1 floxed mice (Figure 3-1 A). As WAT is composed of various types of cells and SOAT1 is highly expressed in macrophages. we employed multiple methods to evaluate the efficacy of knockout: 1) tail genotyping (Figure 3-1 B); 2) examine SOAT1 mRNA level by PCR and electrophoresis on WAT samples, with primers targeting on exon 13 and 15, respectively (exon 14 is flanked by loxP sites) (Figure 3-1 C); 3) examine SOAT1 protein and mRNA level in mature adipocytes (MA) isolated from iWAT and eWAT, stromal vascular fraction (SVF) serving as a positive control. Notably, F4/80 mRNA level were significantly reduced in MA (Figure 3-1 D), while the AdipoQ mRNA level markable elevated in MA compared to SVF (Figure 3-1 E), indicating the purity of the isolated adipocytes. The mRNA (Figure 3-1 F) and protein (Figure 3-1 I) level of SOAT1 were significantly diminished in both iWAT and eWAT of AKO mice compared to CTRL mice, with no alteration observed in SOAT1 content in SVF (Figure 3-1 G) or other tissues (Figure 3-1 H-I). It is important to note that our mouse model did not exhibit SOAT1 knockout in brown adipose tissue (BAT). 4) To assess the CE content, we observed a prominent decrease in CE levels in WAT of AKO mice compared to CTRL mice, as well as a decrease in the CE to FC ratio, but no significant changes were observed in liver tissue (Figure 3-1 J-K). 5) using a fluorescent reporter mouse to cross with adipoQ-cre mouse for checking the cre-recombination activity. The AKO mice exhibited a strong fluorescence signal compared with CTRL in sWAT but not in liver (Figure 3-1 L), validating higher cre-recombination activity in sWAT of AKO mice. Overall, these findings confirm the successful and specific knockout of SOAT1 in WAT of AKO mice.

3.4.2 Adipocyte-specific SOAT1 deletion enhance energy expenditure in room temperature despite similar body mass

SOAT1 is an enzyme involved in cholesterol esterification, which plays a crucial role in the storage and transport of cholesterol within cells. To understand the functional relevance of SOAT1-mediated adipocytes in obesity and its associated metabolic disorders, we challenged the CTRL and AKO mice with the HCD diet for 21 weeks (Figure 3-2 A). Under HCD for 21 weeks, there was no significant difference in body weight or % fat mass between the CTRL and AKO groups, but a slightly increased heart mass in the AKO group compared to CTRL (Figure 3-2 B-E). The serum adiponectin showed no difference between the CTRL and AKO groups (Figure 3-2 F). Next, we examined the effect of SOAT1 on energy balance by measuring the accumulated food intake during the 21-week treatment period, as well as the individual food intake in the metabolic cage. We found no difference in energy intake between CTRL and AKO mice (Figure 3-2 G-H). Fecal energy excretion was significantly upregulated in AKO mice compared to CTRL (Figure 3-2 I). Interestingly, the results of the metabolic cage study showed that EE of AKO mice in both the dark and light cycles was significantly upregulated compared to CTRL, although respiratory exchange ratio (RER) and physical activity showed no difference (Figure 3-2 J-M). Collectively, these results indicate that the loss of SOAT1 in adipocytes has a minimal effect on body weight and adipose tissue mass but significantly upregulates EE.

3.4.3 Adipocyte-specific SOAT1 deletion promotes iWAT beiging

As whole body thermogenesis is equivalent to total EE [225], we hypothesized that the deficiency of SOAT1 promotes WAT browning or enhances BAT thermogenic ability, leading to increased heat production. Upon sacrificing the mice, we observed a distinct darkening of the iWAT in AKO mice compared to CTRL, while no such change was observed in eWAT (Figure 3-3 A). Consistently, hematoxylin and eosin (H&E) staining revealed the presence of multilocular lipids, indicative of beige fat biogenesis, in iWAT of AKO mice compared to CTRL, but not in eWAT (Figure 3-3 B).

Uncoupling protein 1 (UCP1) is a mitochondrial protein predominantly found in BAT, responsible for dissipating energy as heat by uncoupling oxidative phosphorylation from ATP synthesis [226]. To confirm the browning effect in iWAT of the AKO group, UCP1 staining was performed, revealing higher UCP1 expression in AKO mice compared to CTRL (Figure 3-3 C-D). Additionally, RNA-seq analysis of iWAT in both CTRL and AKO mice was conducted to explore the underlying mechanism. Among the top 500 expressed genes based on fold change, UCP1 mRNA level exhibited the most significant upregulation in AKO mice compared to CTRL (Figure 3-3 E). Heatmap analysis further supported these findings, showing upregulation of beige markers and downregulation of adipogenic markers in AKO mice compared to CTRL (Figure 3-3 F). The conversion of inactive thyroxine (T4) to its active form, triiodothyronine (T3), is crucial for thermogenesis and energy metabolism, with Dio2 playing a key role [227]. Cytochrome c oxidase subunit 7A1 (COX7a1) and Cytochrome c oxidase subunit 8B (COX8b) are genes involved in mitochondrial function and thermogenesis [228]. To validate the RNA-seq results, qPCR analysis was performed, confirming the upregulation of beige markers in AKO mice compared to CTRL (Figure 3-3 G). However, UCP1 mRNA was not induced in BAT or eWAT (Figure 3-3 H), and adipocyte morphology remained unchanged in BAT (Figure 3-3 I). Overall, these results suggest that the deficiency of SOAT1 in adipocytes promotes increased energy expenditure, as well as the formation of beige adipocytes in iWAT under HCD challenges.

3.4.4 Adipocyte-specific SOAT1 deletion promote adipocyte lipolysis.

We further evaluated UCP1 protein level and found it significantly upregulated in iWAT of AKO mice (Fugure 3-4 A). The lipolysis releases free fatty acids (FFAs), which could activate the beige adipocyte differentiation process. Therefore, we tested the levels of lipolysis-related proteins, ATGL and pHSL [217]. The ATGL protein level were significantly enhanced in the AKO group compared to CTRL (Figure 3-4 A-D).

Additionally, the serum TG levels were notably higher in the AKO group compared to the CTRL group, while no difference was observed in non-esterified fatty acids (NEFA) levels (Figure 3-4 E-F). To confirm the in vivo results, stromal vascular fraction (SVF) was isolated from iWAT of SOAT1$^{fl/fl}$ mice and induced adipogenesis in vitro. SOAT1 was knocked out using cre-expressing adenovirus at the mature adipocyte stage, and the knockout efficiency was confirmed by PCR (Figure 3-4 G-H). Interestingly, UCP1 mRNA levels were found to be upregulated in the SOAT1 KO group compared to CTRL under basal or CL-216,243 stimulus conditions (Figure 3-4 I). Treatment of mature adipocytes with the SOAT1 inhibitor Avasimibe (AVA) resulted in upregulated UCP1 mRNA levels under basal conditions (Figure 3-4 J). Consistent with the in vivo results, the other beige marker gene expression (PGC1α, PRDM16, Dio2) and genes involved in mitochondrial function and thermogenesis (COX7a1 and COX8b) were markably upregulated in SOAT1-KO group compared with CTRL (Figure 3-4 K). The ATGL and UCP1 protein level increased in SOAT1-deficient adipocytes compared to CTRL (Figure 3-4 L-N). Moreover, glycerol levels, indicative of lipolysis activity, were significantly higher in the SOAT1-KO group compared to CTRL when measuring the cell differentiation medium collected from mature adipocytes (Figure 3-4 O). In order to test if SOAT1 KO promotes lipolysis and further enhances UCP1 mRNA levels through ATGL, we loaded the ATGL inhibitor, Atglistatin, in both CTRL and SOAT1 KO adipocytes. As expected, the UCP1 mRNA levels and glycerol (Figure 3-4 P-Q) from the cell culture medium in the KO group were successfully rescued. In summary, these findings demonstrate that adipocyte-specific depletion of SOAT1 promote UPC1 mRNA and protein expression and upregulates adipocyte lipolysis both in vivo and in vitro.

3.4.5 Adipocyte-specific SOAT1 deletion induce inflammation and macrophage infiltration in adipose tissue

After performing digital gene expression (DGE) analysis, functional enrichments were conducted on the differentially expressed genes (DEGs) using Kyoto Encyclopedia of

Genes and Genomes (KEGG) analysis. The significantly upregulated pathways were identified in ascending order of the p-value, revealing that inflammation-related pathways were the most enriched (Fig 3-5 A). Heatmap analysis revealed the upregulation of pro-inflammatory cytokines, such as TNF-α and interleukin-1 beta (IL-1β), in AKO mice compared to CTRL (Figure 3-5 B). Consistent with our study, previous studies have shown that browning of WAT involves significant remodeling of the adipose tissue microenvironment, leading to inflammatory responses characterized by changes in extracellular matrix composition and immune cell interactions [229]. Furthermore, we performed F4/80 staining of iWAT and observed higher macrophage infiltration in AKO mice compared to CTRL (Figure 3-5 C-D), suggesting a more pro-inflammatory state in the iWAT of AKO mice. Additionally, the expression of proinflammation-related genes (INOS, IL-6) in SOAT1 KO adipocytes was significantly upregulated, while anti-inflammation-related genes (CD206, MGL2) were downregulated compared to the CTRL (Figure 3-5 E). To test if pro-inflammatory cytokines were released from adipocytes, we collected the conditioned medium from SVF-differentiated mature adipocytes and co-cultured it with macrophages. Compared to the CTRL group, the inflammatory gene expression in macrophages co-cultured with SOAT1-KO medium was enhanced (Figure 3-5 F). Taken together, these results suggest that the deletion of SOAT1 in adipocytes induce inflammation and reduces macrophage infiltration in adipose tissue.

3.4.6 Adipocyte-specific SOAT1 deletion promotes ectopic lipid deposition in liver

The liver assumes a pivotal role in the metabolism of lipids throughout the body and contributes significantly to overall metabolic health. Therefore, we investigated whether liver function is affected by the KO of SOAT1 in adipocytes. We observed no abnormal morphology in hepatocytes after SOAT1 KO, but there was a slight increase in TG levels in the AKO group compared to the CTRL group (Figure 3-6 A-B). Consistently, the mRNA levels of TG synthesis genes, such as SCD1 and DGAT2, were significantly higher in the AKO group than in the CTRL group (Figure 3-6 C). However,

there were no differences in free cholesterol and total cholesterol levels between the CTRL and AKO mice (Figure 3-6 D). These findings suggest that adipocyte-specific deletion of SOAT1 may promote TG synthesis in the liver.

3.4.7 Adipocyte-specific SOAT1 deletion has little effect on serum and WAT cholesterol levels

In the absence of functional SOAT1, there would be a disruption in the normal process of cholesterol ester formation. Therefore, we measured cholesterol levels in adipose tissue, liver, and serum. The free cholesterol level in adipocytes was not altered by SOAT1 deficiency (Figure 3-7 A). Heatmap analysis also demonstrated no difference in the expression of genes involved in cholesterol synthesis, uptake, and efflux between the CTRL and AKO groups (Figure 3-7 B). While there was a trend towards decreased levels of free cholesterol and high-density lipoprotein cholesterol (HDL-C) in the AKO group compared with CTRL, there were no differences in CE and low-density lipoprotein cholesterol (LDL-c) (Figure 3-7 C-E). Collectively, these results indicate that the overall cholesterol levels in adipose tissue and serum were not influenced by SOAT1 depletion in adipocytes.

3.4.8 Adipocyte-specific SOAT1 deletion has little effect on glucose tolerance and insulin sensitivity

Glucose homeostasis are important markers of metabolic health. Efficient glucose regulation, characterized by healthy glucose tolerance and high insulin sensitivity, is linked to a decreased risk of metabolic disorders. Conversely, impaired glucose tolerance and reduced insulin sensitivity indicate an elevated risk of metabolic dysregulation and associated health conditions [230]. Our aim was to investigate the role of adipocyte SOAT1 in glucose tolerance and insulin sensitivity. After 21 weeks of HCD treatment, there were no differences in glucose tolerance as assessed by glucose tolerance test (GTT), insulin sensitivity as assessed by insulin tolerance test (ITT), and pyruvate tolerance as assessed by pyruvate tolerance test (PTT) between the CTRL and

AKO groups (Figure 3-8 A-C). Consistently, fasting insulin levels, serum glucose levels, and the homeostatic model assessment of insulin resistance (HOMA-IR) showed no differences between the CTRL and AKO groups (Figure 3-8 D-F). Overall, these data suggest that SOAT1 deficiency in adipocytes has minimal effect on glucose tolerance and insulin sensitivity.

3.5 Discussion

Activation of WAT browning is accompanied by improved systemic health under obese status [231, 232]. The beige adipocytes are generally considered to be more transient or short-lived. They can be induced to differentiate from precursor cells under specific stimuli but can also revert back to a white adipocyte phenotype if the stimulating factors are removed. This plasticity allows them to dynamically respond to meet metabolic demands [233, 234]. In this study, we found that SOAT1 deficiency in adipocytes promotes iWAT browning and enhances lipolysis without any external stimulus. However, body mass, fat mass and glucose homeostasis were not influenced by adipocyte specific SOAT1 KO. Our findings uncover a novel role of SOAT1 in beige fat biology, highlighting the potential of SOAT1 inhibitors as beneficial agents for promoting the browning of WAT. Thus, it presents itself as a prospective target for addressing obesity and its associated metabolic diseases.

Beige cells are a type of mitochondrial-rich adipocytes. Mitochondria regulate the formation of beige adipocytes through multiple ways, including increased mitochondrial biogenesis and enhanced oxidative capacity [235]. Additionally, mitochondria in beige adipocytes contain a higher density of UCP1. A previous study found that adipocyte-specific knockout of IFI27 in mice exhibited decreased EE and inhibited adipocyte thermogenic ability, mainly due to decreased mitochondrial cristae disrupting mitochondrial function [236]. Due to the limited availability of cholesterol in the inner mitochondrial membrane (IMM), cholesterol homeostasis may play a critical role in regulating mitochondrial metabolism [237]. The ER is physiologically connected to the outer membrane of mitochondria [238]. The MAM region exert key

role in supporting Ca^{2+} directly from the MAM to mitochondrial [239, 240]. The MAM area contains high levels of neutral lipids, ceramides, and cholesterol [241]. The synthesis of phosphatidylethanolamine in mitochondria occurs via MAM to transport the precursor phosphatidylserine through intermembrane lipid transport [242]. However, the mechanism of cholesterol transportation in the MAM is unclear. Previous studies have reported that inhibition of SOAT1 strengthens the connection between ER and mitochondria, as well as increases cholesterol content in the MAM [219]. Therefore, it is possible that adipocyte SOAT1 deficiency mediated cholesterol transportation improves mitochondrial function and promotes adipocyte beige capacity.

BAT activity is markedly related to cold exposure, which are actually beige adipocytes [243]. WAT contains fewer mitochondria than BAT and shows lower expression of FA oxidation-related enzymes [244]. In our study, we observed beige adipocytes in iWAT, while eWAT and BAT showed no difference in morphology or UCP1 gene expression. The possible reason for this discrepancy may be that SOAT1 is not depleted in BAT, as the mRNA and protein levels of SOAT1 in the BAT of the AKO group were not reduced compared to the control group (Figure 3-1 H-I). In a previous study, Cdkn2a ^{UCP1} KO mice exhibited increased EE under HFHS diet, but BAT morphology, as well as the thermogenic gene profile, remained unaltered. Thus, beige adipocyte formation may not always be accompanied by altered BAT activity.

It is interesting to note that lipolysis is enhanced in SOAT1-deficient adipocytes. TGs within WAT undergo lipolysis, resulting in the release of FFAs into the bloodstream. A larger proportion of FFAs are taken up by hepatocytes, where they are further esterified into TGs, CE, or phospholipids [245]. A previous study demonstrated that UCP1-dependent heat production in activated beige adipocytes is induced by FAs generated through lipolysis [220]. FFAs can activate the cyclic adenosine monophosphate (cAMP) pathway, leading to the activation of protein kinase A (PKA), which phosphorylates and activates UCP1, resulting in increased thermogenesis. Along with the presence of beige adipocytes in AKO mice, these mice also exhibited ectopic lipid accumulation in the liver in our results. These results are intriguing, as beige adipocyte activity has shown an inverse correlation with BMI, body fat percentage, glucose levels, and age [246-

249]. Recent studies have found that beige adipocytes function as endocrine organs, secreting peptides, proteins, or lipids to influence systemic metabolism. Therefore, our results suggest that the ectopic lipid accumulation in the liver may result from an increased release of FFAs from AKO mice, or beige adipocytes may communicate with the liver to promote lipid deposition.

In summary, we have identified SOAT1 as an important player in beige adipocyte formation under HCD feeding. Our work introduces the concept that beige adipocytes can be formed under room temperature without any external stimuli and could potentially be developed as an alternative therapeutic target for the treatment of obesity.

3.6 Acknowledgement

This work was supported by a start-fund from The Hong Kong Polytechnic University and Research Grants Council (RGC) of Hong Kong. I greatly appreciate Prof. Ta-Yuan Chang for providing us with the SOAT1 $^{flox/flox}$ mice; Dr. CHENG King Yip for providing us with adiponectin-Cre mice; Mr. Xiaohan PAN for RNA-seq data analysis and Dr. Alan Leung for his technical support in metabolic cage. I would also like to thank the University Research Facility in Life Sciences (ULS) for providing equipment and technical support.

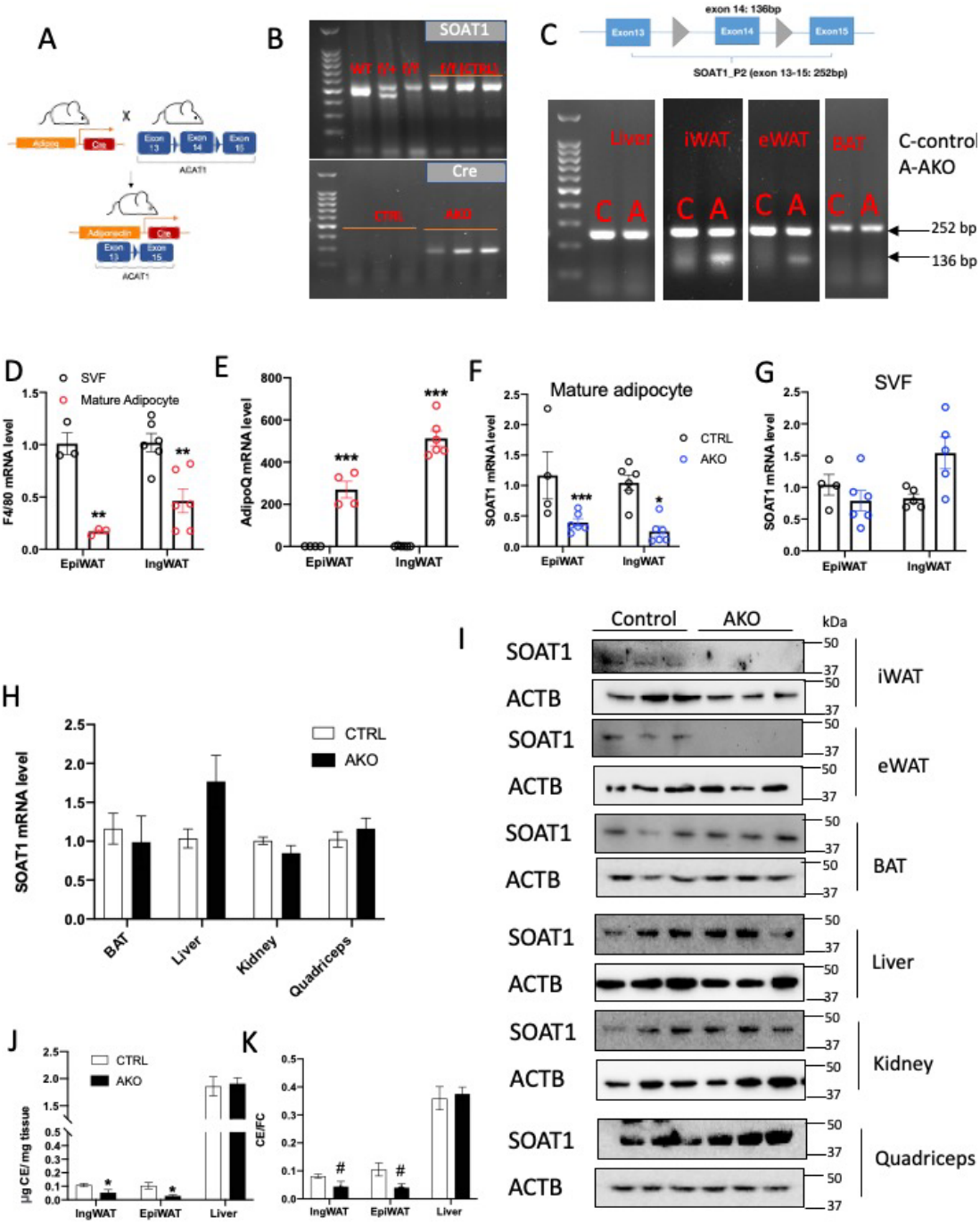
A
B
C
SOAT1
WT
Cre
CTRL
AKO
exon 14: 136bp
Exon13
Exon14
Exon15
SOAT1_P2 (exon 13-15: 252bp)
Liver
iWAT
eWAT
BAT
C-control
A-AKO
252 bp
136 bp
D
SVF
Mature Adipocyte
F4/80 mRNA level
EpiWAT
IngWAT
E
AdipoQ mRNA level
F
Mature adipocyte
CTRL
AKO
SOAT1 mRNA level
G
SVF
H
BAT
Liver
Kidney
Quadriceps
I
Control
AKO
kDa
SOAT1
ACTB
iWAT
eWAT
BAT
Liver
Kidney
Quadriceps
J
μg CE/ mg tissue
K
CE/FC

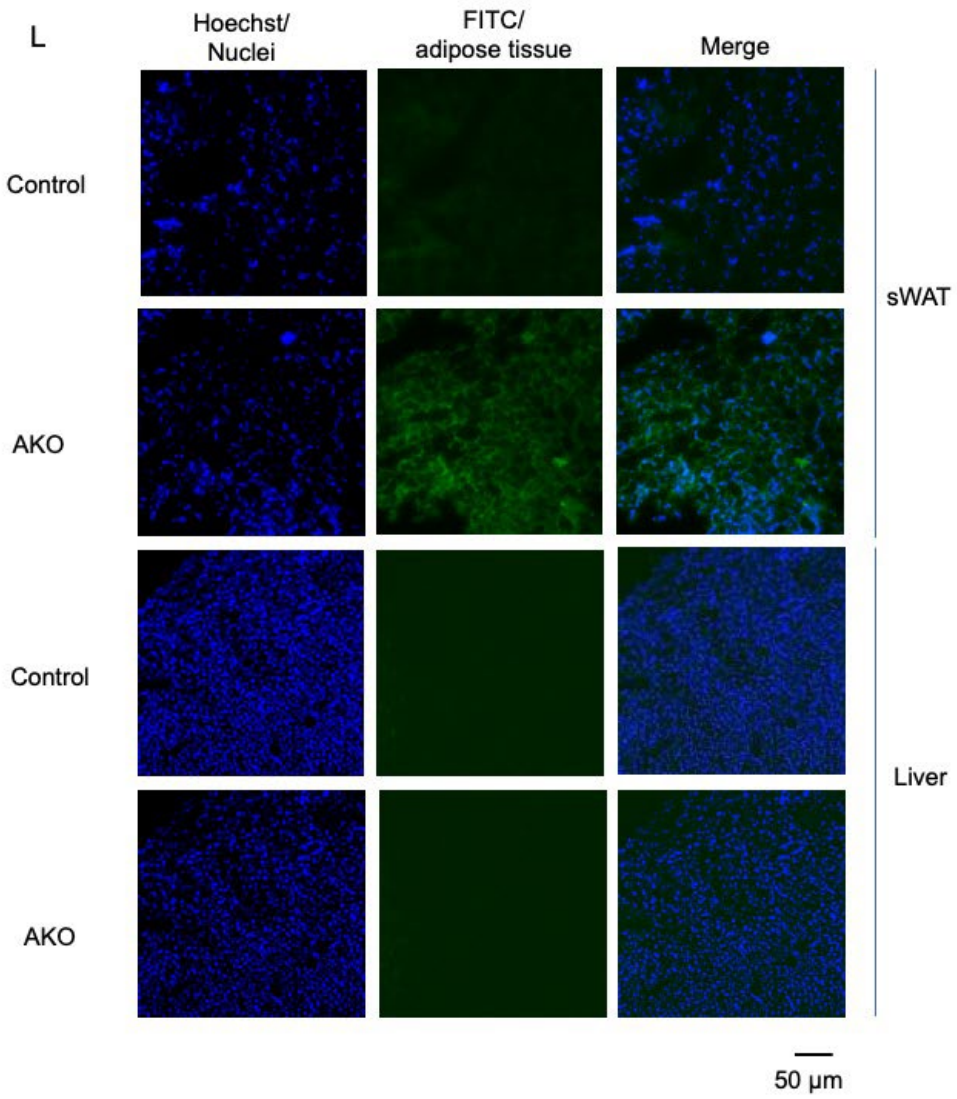
L
Hoechst/
Nuclei
FITC/
adipose tissue
Merge
Control
AKO
sWAT
Control
AKO
Liver
50 µm

Figure 3-1. SOAT1 is selectively ablation in adipocytes.

A, Scheme of SOAT1 KO mice construction. B, Gel analysis of PCR product for mice genotyping. C, PCR analysis genomic DNA to detect loxp/loxp and excised genes and determination of the transcription levels for each of the SOAT1 subunits in tissues. D, F4/80 mRNA level in SVF and mature adipocytes . E, AdipoQ mRNA level in SVF and mature adipocytes. F, SOAT1 mRNA level in mature adipocytes from CTRL and AKO mice. G, SOAT1 mRNA level in SVF from CTRL and AKO mice. H, SOAT1 mRNA level in different tissues from CTRL and AKO mice (n=4-6 per group). I, Western blot analysis of SOAT1 in different tissue from CTRL or AKO mice. J, Cholesterol ester level in different tissues from CTRL or AKO mice (n=4-6 per group). K, The proportion of esterified cholesterol over free cholesterol (n=4-6 per group). L, Adipose tissue and liver were collected and take photos by epi-fluroscence microscopy. Scale bar, 50 μm. Data is presented as Mean ± SEM and analysed by independent t-test, #p<0.1, *p<0.05, **p<0.01, ***p<0.001.

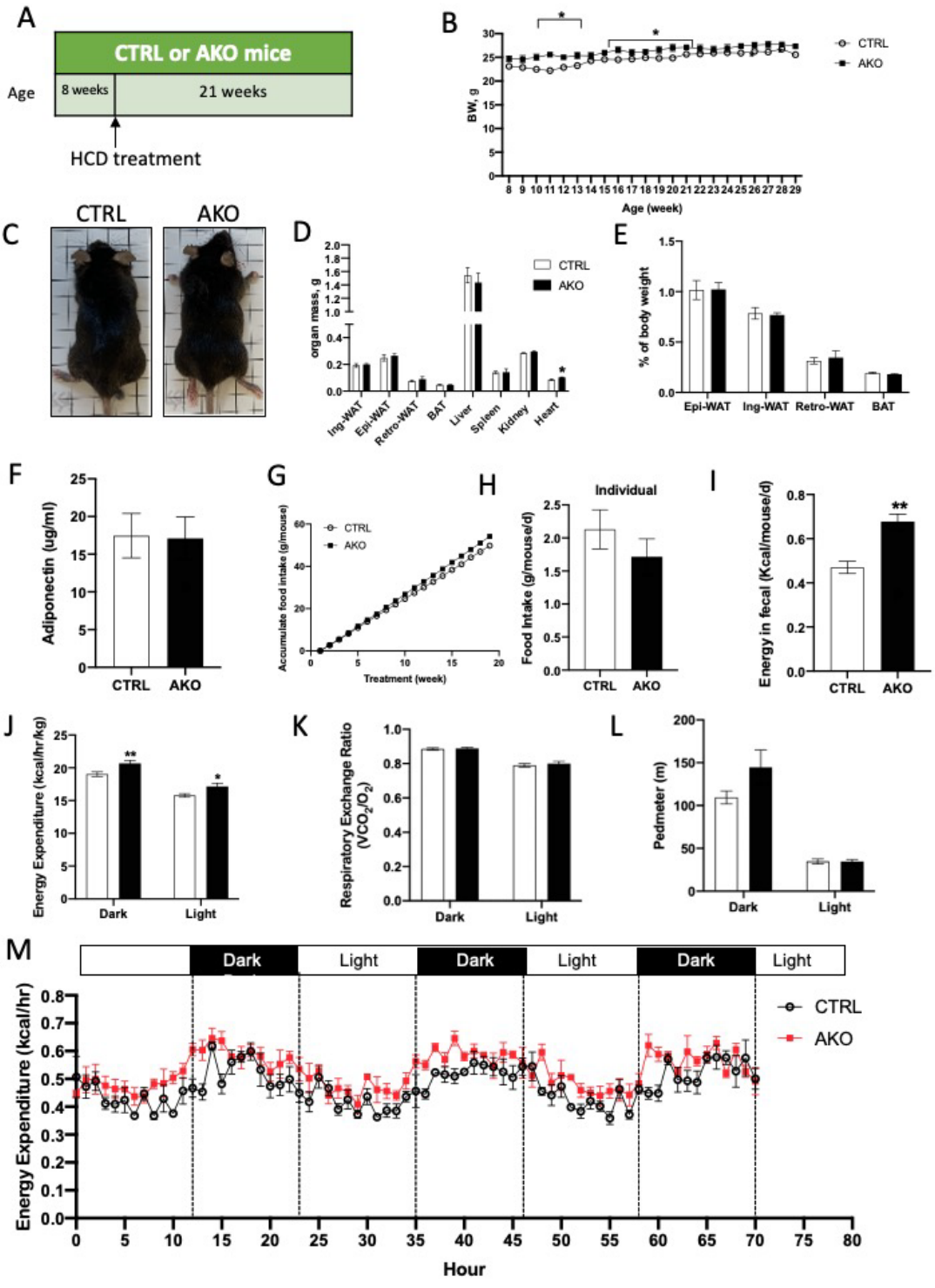
A
CTRL or AKO mice
Age
8 weeks
21 weeks
HCD treatment
B
BW, g
Age (week)
CTRL
AKO
C
CTRL
AKO
D
organ mass, g
Ing-WAT
Epi-WAT
Retro-WAT
BAT
Liver
Spleen
Kidney
Heart
E
% of body weight
Epi-WAT
Ing-WAT
Retro-WAT
BAT
F
Adiponectin (ug/ml)
G
Accumulate food intake (g/mouse)
Treatment (week)
H
Individual
Food Intake (g/mouse/d)
I
Energy in fecal (Kcal/mouse/d)
J
Energy Expenditure (kcal/hr/kg)
Dark
Light
K
Respiratory Exchange Ratio
L
Pedmeter (m)
M
Dark
Light
Energy Expenditure (kcal/hr)
Hour

Figure 3-2. Adipocyte-specific SOAT1 (AKO) mice exhibit enhanced energy expenditure.

A, Experiment procedure. 8-weeks-old CTRL and AKO male mice were feed with HCD diet for 21 weeks in room temperature. B, Body weight of CTRL or AKO mice (n=4-6 per group). C, Representative images of 29-weeks-old CTRL or AKO mice. D, Organ mass of different tissue (n=4-6 per group). E, The adipose tissue weight were relative to body weight of CTRL or AKO mice (n=4-6 per group). F, Serum Adiponectin level from CTRL or AKO mice (n=4-6 per group). G, Accumulate food intake for 21 weeks treatment of CTRL or AKO mice. H, Food intake were measured by individual mice (n=4-6 per group). I, Fecal samples collected from these mice were subjected to bomb calorimetry to measure fecal (n=4-6 per group). The mice were subjected to metabolic cage for 4 days. Metabolic cage detected VO2 and VCO2 every 30 minutes. Average of three dark cycles and three light cycles were used to calculate energy expenditure J and respiratory exchange ratio K. L, Pedmeter value were recorded by metabolic cage. M, Energy expenditure of CTRL and AKO mice fed with HCD. Data is presented as Mean ± SEM and analysed by independent t-test, *$p<0.05$, **$p<0.01$, ***$p<0.001$.

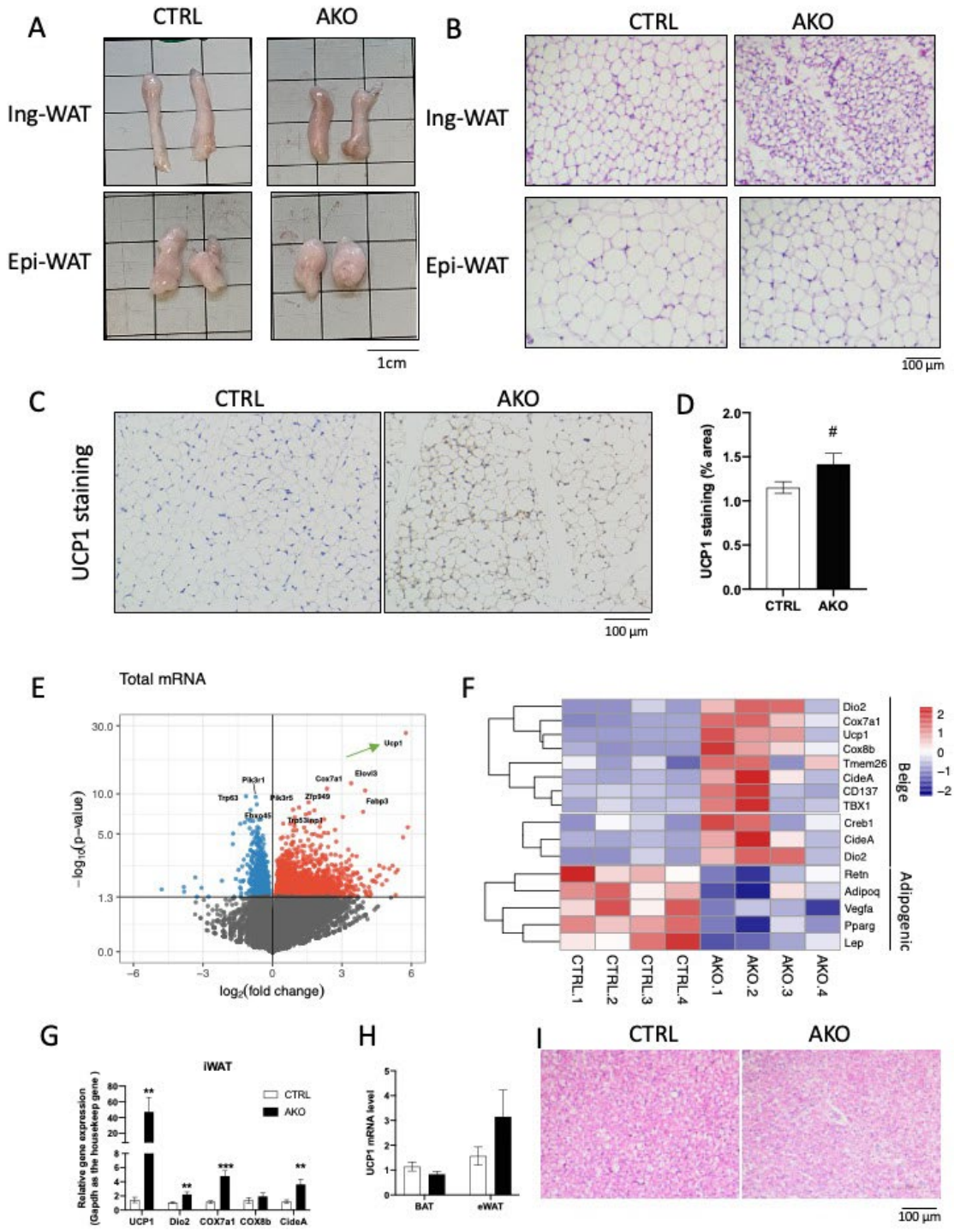
A
CTRL
AKO
Ing-WAT
Epi-WAT
1cm
B
CTRL
AKO
Ing-WAT
Epi-WAT
100 μm
C
CTRL
AKO
UCP1 staining
100 μm
D
UCP1 staining (% area)
2.0
1.5
1.0
0.5
0.0
#
CTRL
AKO
E
Total mRNA
−log10(p−value)
log2(fold change)
Ucp1
Cox7a1
Elovl3
Pik3r1
Pik3r5
Zfp949
Trp63
Fabp3
Ebpl45
Trp53inp1
F
Dio2
Cox7a1
Ucp1
Cox8b
Tmem26
CideA
CD137
TBX1
Creb1
CideA
Dio2
Retn
Adipoq
Vegfa
Pparg
Lep
Beige
Adipogenic
CTRL.1
CTRL.2
CTRL.3
CTRL.4
AKO.1
AKO.2
AKO.3
AKO.4
G
iWAT
CTRL
AKO
Relative gene expression (Gapdh as the housekeep gene)
UCP1
Dio2
COX7a1
COX8b
CideA
H
UCP1 mRNA level
BAT
eWAT
I
CTRL
AKO
100 μm

Figure 3-3. Adipocyte-specific KO SOAT1 mice exhibited iWAT browning.

A, Representative images of iWAT and eWAT from CTRL and AKO mice. B, H&E stained of iWAT and eWAT. C, Adipocyte image of UCP1 staining and quantification data in D. E, Volcano plot representation of differential expression analysis of genes in AKO versus CTRL mice. F, Heat map depicting the fold change of representative genes in beige and adipogenic pathway. G, mRNA level of beige marker in iWAT. H, UCP1 mRNA level of BAT and eWAT. I, H&E stained of BAT from CTRL and AKO mice. Data is presented as Mean ± SEM and analysed by independent t-test, #$p<0.1$, *$p<0.05$, **$p<0.01$, ***$p<0.001$.

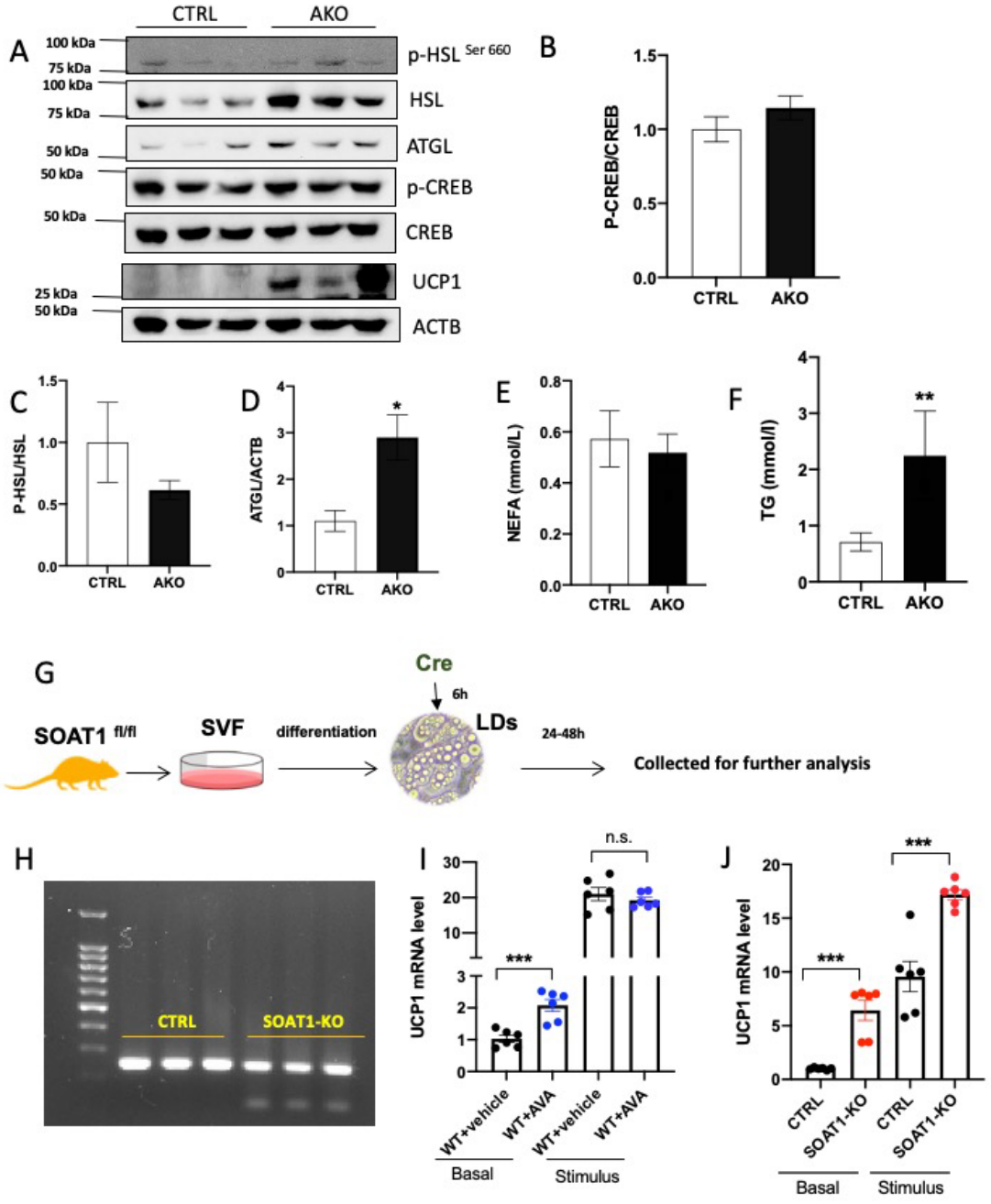
A
CTRL
AKO
100 kDa
75 kDa
p-HSL Ser 660
100 kDa
75 kDa
HSL
50 kDa
ATGL
50 kDa
p-CREB
50 kDa
CREB
25 kDa
50 kDa
UCP1
ACTB
B
P-CREB/CREB
C
P-HSL/HSL
D
ATGL/ACTB
E
NEFA (mmol/L)
F
TG (mmol/l)
G
SOAT1 fl/fl
SVF
differentiation
Cre
6h
LDs
24-48h
Collected for further analysis
H
CTRL
SOAT1-KO
I
UCP1 mRNA level
n.s.
WT+vehicle
WT+AVA
Basal
Stimulus
J
UCP1 mRNA level
CTRL
SOAT1-KO
Basal
Stimulus

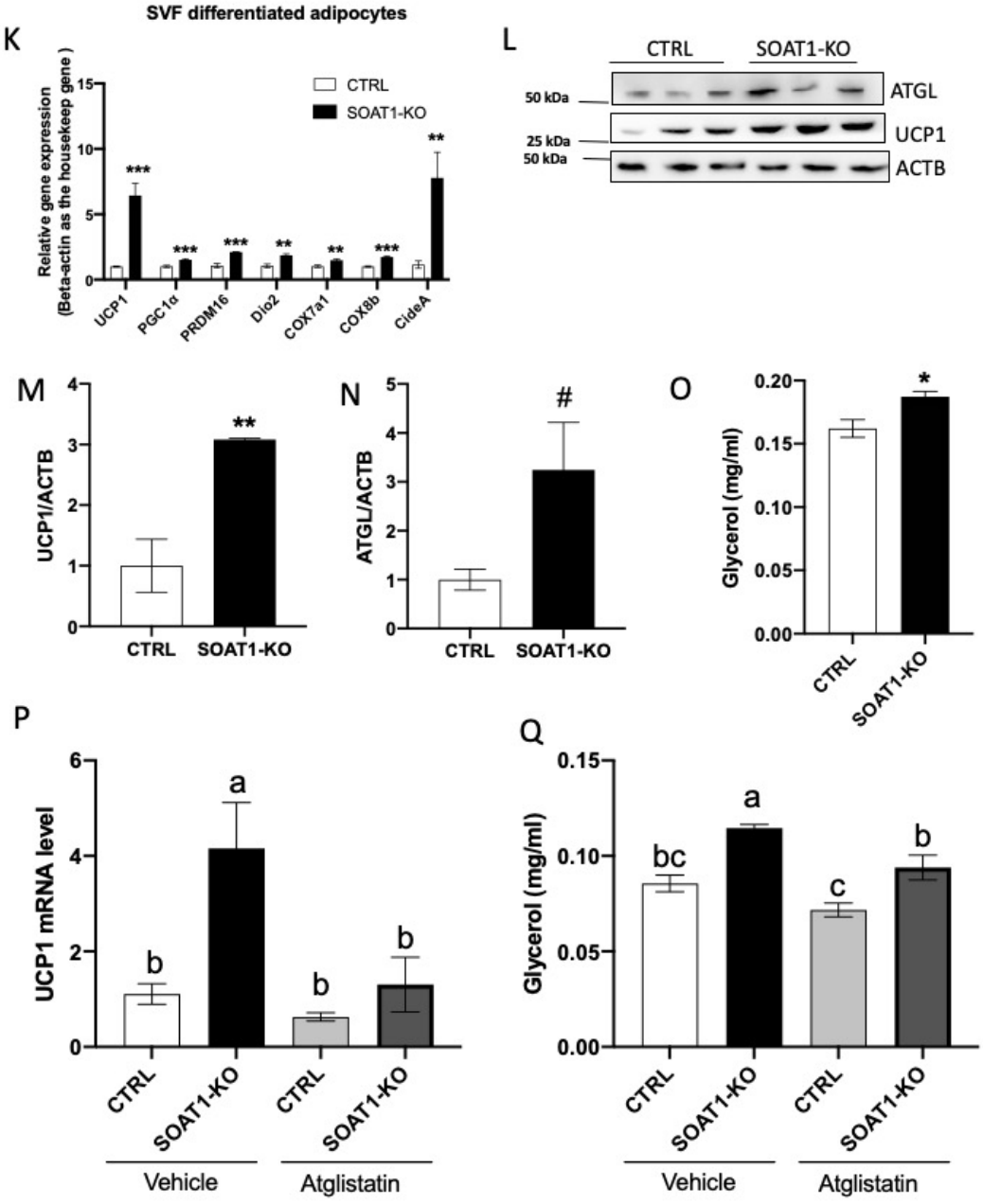
K
SVF differentiated adipocytes
Relative gene expression (Beta-actin as the housekeep gene)
CTRL
SOAT1-KO
UCP1
PGC1α
PRDM16
Dio2
COX7a1
COX8b
CideA
L
CTRL
SOAT1-KO
50 kDa
ATGL
UCP1
25 kDa
50 kDa
ACTB
M
UCP1/ACTB
CTRL
SOAT1-KO
N
ATGL/ACTB
CTRL
SOAT1-KO
O
Glycerol (mg/ml)
CTRL
SOAT1-KO
P
UCP1 mRNA level
CTRL
SOAT1-KO
CTRL
SOAT1-KO
Vehicle
Atglistatin
Q
Glycerol (mg/ml)
CTRL
SOAT1-KO
CTRL
SOAT1-KO
Vehicle
Atglistatin

Figure 3-4. Adipocyte-specific KO SOAT1 mice promote iWAT lipolysis and down-regulate AMPK activity.

A, Western blot analysis of iWAT from CTRL and AKO mice and quantification data in B-D. The mice were under day fasting and serum NEFA in E and TG in F were analyzed. G, Schematic illustration of the cellular system of KO SOAT1 in vitro. H, PCR analysis genomic DNA to detect loxp/loxp and excised genes and determination of the transcription levels. I, UCP1 mRNA level in CTRL or SOAT1 KO mature adipocytes with or without CL-216,243 stimulus. J, UCP1 mRNA level in CTRL or Avasimibe treated mature adipocytes with or without CL-216,243 stimulus. K, mRNA level of beige marker in iWAT from CTRL and SOAT1-KO adipocytes. L, Western blot analysis of mature adipocytes from CTRL and SOAT1-KO adipocytes. M-N: Data quantification of L. O, Glycerol level in cell culture medium from CTRL and SOAT1-KO adipocytes. P, UCP1 mRNA level in CTRL or SOAT1 KO mature adipocytes with or without Atglistatin. Q, Glycerol level in cell culture medium from CTRL and SOAT1-KO adipocytes. Data is presented as Mean ± SEM and analysed by independent t-test or two-way ANOVA followed by Turkey's test. Difference at values of $p<0.05$ were considered to be significant.

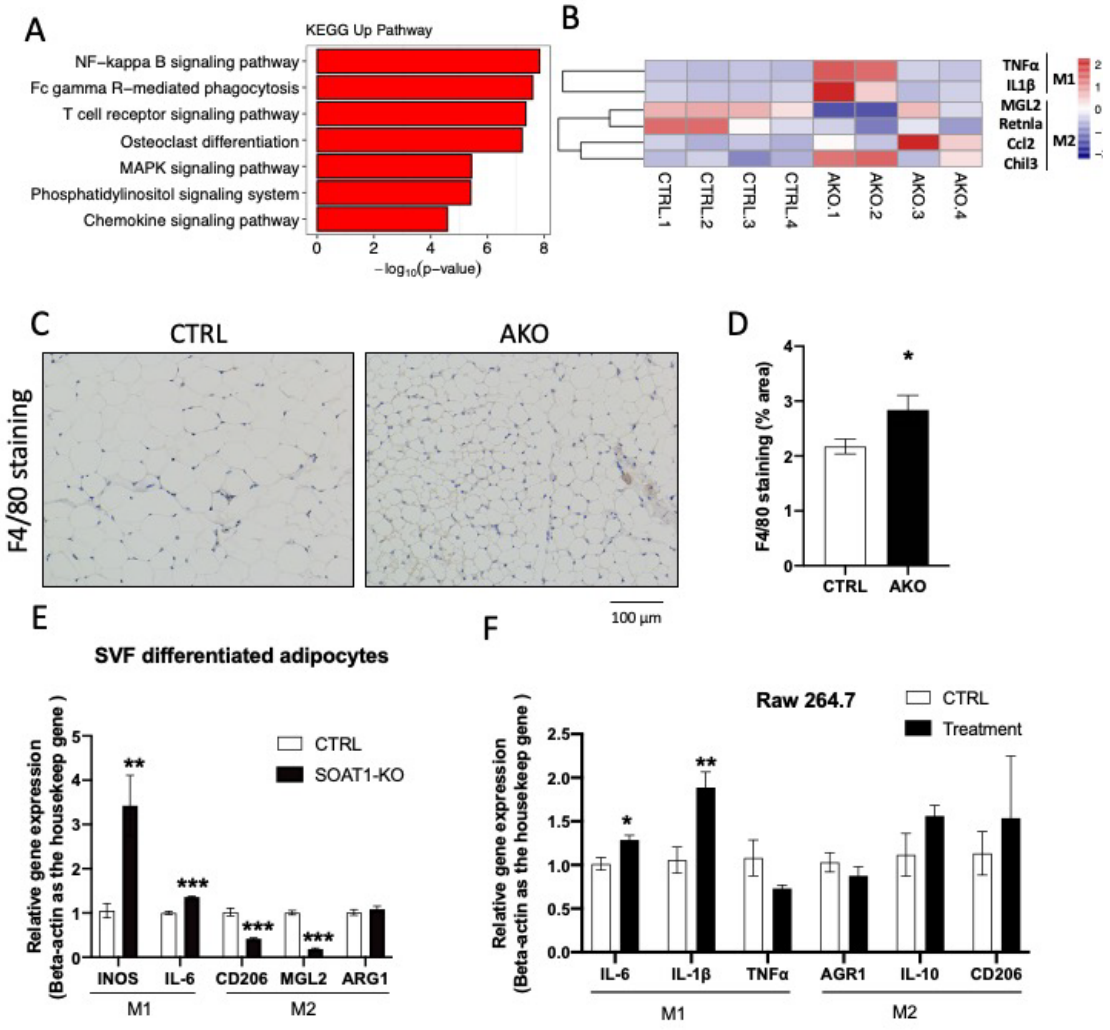

Figure 3-5. Adipocyte-specific KO SOAT1 mice promote iWAT inflammation.

A, Upregulated signalling pathway analysed by KEGG in AKO versus CTRL mice. B, Heat map depicting the fold change of representative genes in inflammation pathway. C, Representative adipocyte image of F4/80 stained of iWAT from CTRL and AKO mice and quantification data in D. E, mRNA level of genes involve in inflammation pathway from CTRL and SOAT1-KO adipocytes. F. mRNA level of genes involve in inflammation pathway, CTRL-macrophage co-culture with CTRL adipocytes differentiated medium, Treatment- macrophage co-culture with SOAT1-KO adipocytes differentiated medium. Data is presented as Mean ± SEM and analysed by independent t-test, *p<0.05, **p<0.01, ***p<0.001.

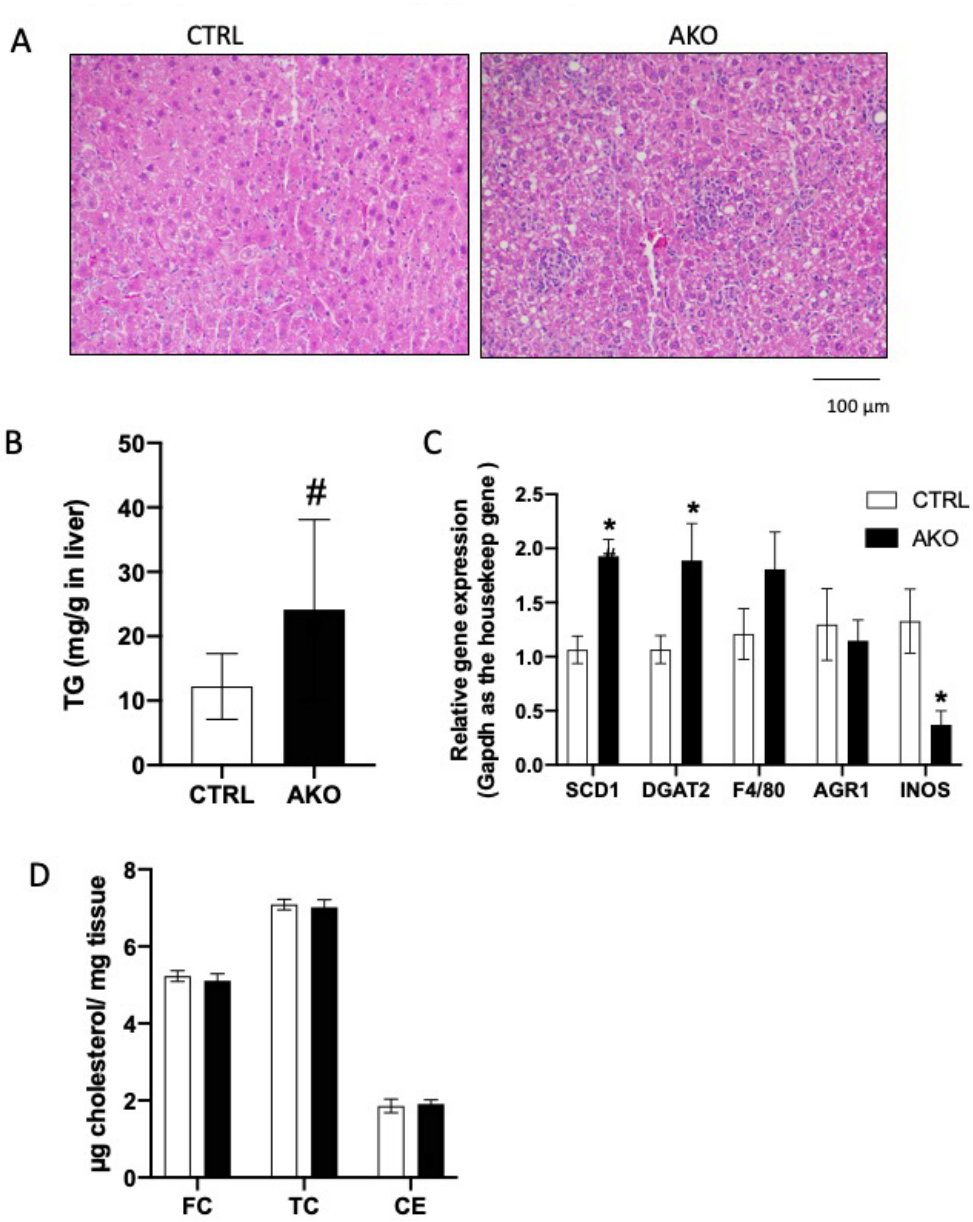

Figure 3-6. Adipocyte-specific KO SOAT1 mice promote TG synthesis in liver.

A, Representative image of H&E stained of liver from CTRL and AKO mice. B, TG quantification of liver tissue from CTRL and AKO mice. C, mRNA level of genes involved in TG synthesis of liver in CTRL and AKO mice. D, Cholesterol quantification of liver tissue from CTRL and AKO mice. Data is presented as Mean ± SEM and analysed by independent t-test, #p<0.1, *p<0.05, **p<0.01, ***p<0.001.

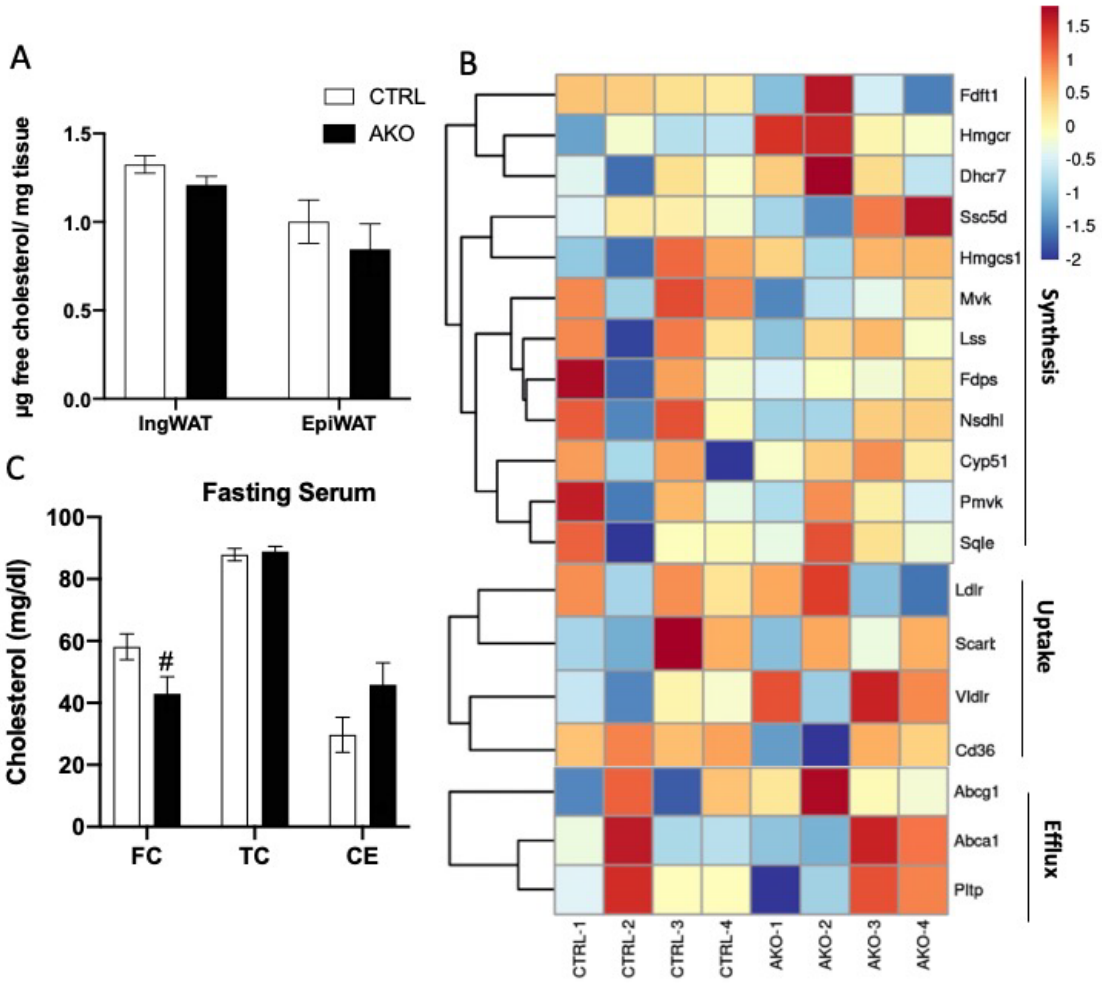
A
CTRL
AKO
µg free cholesterol/ mg tissue
1.5
1.0
0.5
0.0
IngWAT
EpiWAT
B
Fdft1
Hmgcr
Dhcr7
Ssc5d
Hmgcs1
Mvk
Lss
Fdps
Nsdhl
Cyp51
Pmvk
Sqle
Ldlr
Scarb
Vldlr
Cd36
Abcg1
Abca1
Pltp
Synthesis
Uptake
Efflux
CTRL-1
CTRL-2
CTRL-3
CTRL-4
AKO-1
AKO-2
AKO-3
AKO-4
1.5
1
0.5
0
-0.5
-1
-1.5
-2
C
Fasting Serum
Cholesterol (mg/dl)
100
80
60
40
20
0
#
FC
TC
CE
D
HDL-C (mg/dl)
80
60
40
20
0
#
CTRL
AKO
E
LDL-C (mg/dl)
15
10
5
0
CTRL
AKO

Figure 3-7. Adipocyte-specific SOAT1 deletion has little effect on serum and WAT cholesterol levels

A, Cholesterol quantification of adipose tissue from CTRL and AKO mice. B, Heat map depicting the fold change of representative genes in cholesterol metabolism pathway. C, CTRL and AKO mice were fast 6h before sacrifice and serum cholesterol were measured. D, Serum HDL-c level of CTRL and AKO mice. E, Serum LDL-c level of CTRL and AKO mice. Data is presented as Mean ± SEM and analysed by independent t-test, #$p<0.1$, *$p<0.05$, **$p<0.01$, ***$p<0.001$.

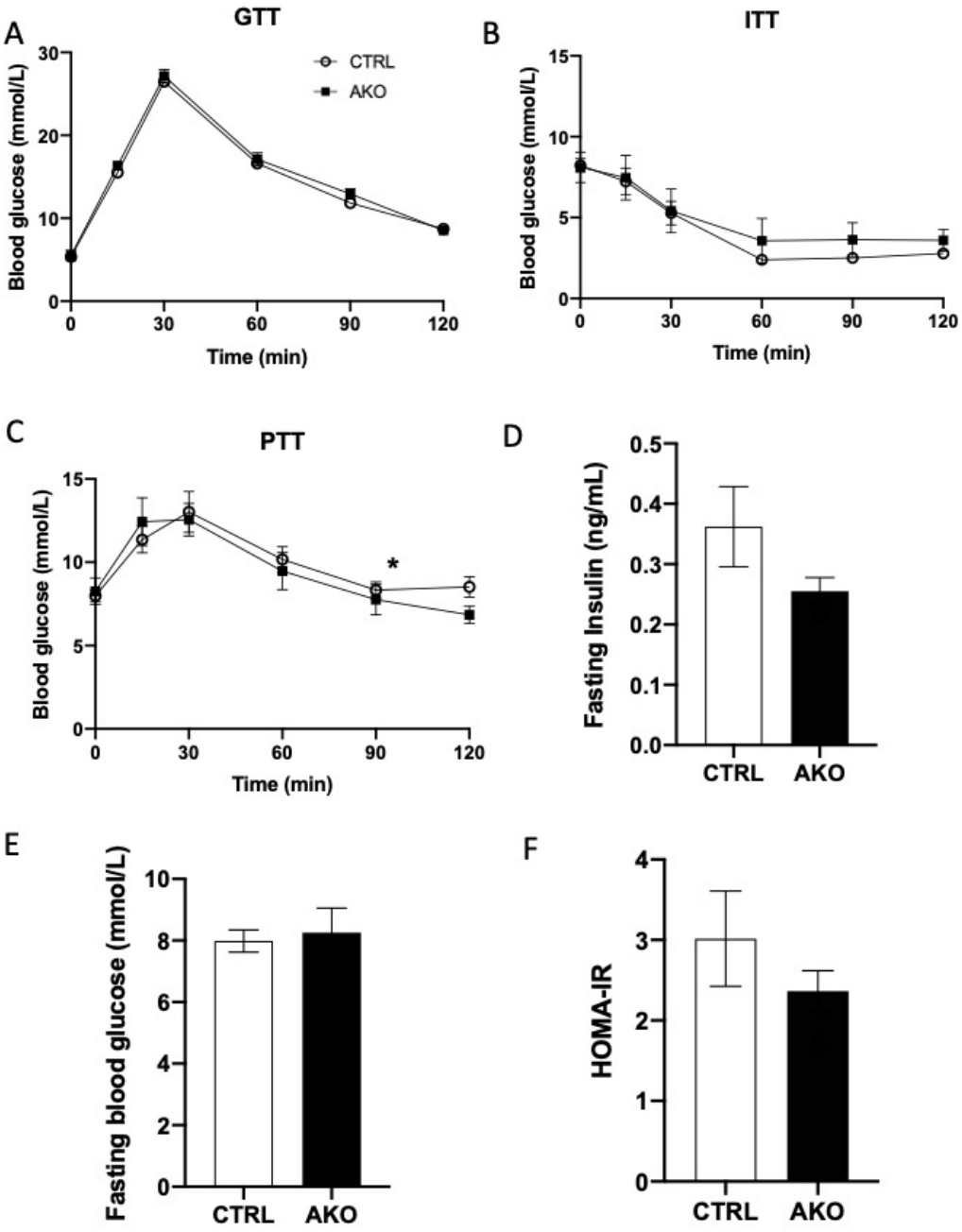
A
GTT
CTRL
AKO
Blood glucose (mmol/L)
Time (min)
B
ITT
Blood glucose (mmol/L)
Time (min)
C
PTT
*
Blood glucose (mmol/L)
Time (min)
D
Fasting Insulin (ng/mL)
CTRL
AKO
E
Fasting blood glucose (mmol/L)
CTRL
AKO
F
HOMA-IR
CTRL
AKO

Figure 3-8. Adipocyte-specific KO SOAT1 mice have minimum effect on glucose metabolism.

A, The blood glucose level of CTRL and AKO mice under HCD after i.p. injection glucose for glucose tolerance tests (GTT). B, The blood glucose level of CTRL and AKO mice under HCD after i.p. injection insulin for insulin tolerance tests (ITT). C, The blood glucose level of CTRL and AKO mice under HCD after i.p. injection pyruvate for pyruvate tolerance tests (GTT). D, Fasting serum insulin level of CTRL and AKO mice. E, Fasting serum blood glucose level of CTRL and AKO mice. F, The HOMA-IR was calculated according to the equation shown in the Materials and Methods section. Data is presented as Mean ± SEM and analysed by independent t-test, *$p<0.05$, **$p<0.01$, ***$p<0.001$.

Table 3-1 qRT-PCR primers

Gene name	Forward primer	Revere primer
UCP1	TCATCATCAATTGTACAGAGCTGGTA	CGTCATCTGCCAGTATTTTGTTG
DIO2	CAGTGTGGTGCACGTCTC	TGAACCAAAGTTGACCACCAG
COX7a1	AGCTGCTGAGGACGCA	GCTTCTGCTTCTCTGCCAC
COX8b	TTCCCAAAGCCCATGTCTCT	GGCTAAGACCCATCCTGCT
CideA	ATACATCCAGCTCGCCCTTT	ACTTACTACCCGGTGTCCAT
PGC1α	CTCTGGAACTGCAGGCCTAA	TGCCTTGGGTACCAGAACA
PRDM16	CAGCACGGTGAAGCCATTC	GCGTGCATCCGCTTGTG
IL-6	TGAACAACGATGATGCACTTG	CTGAAGGACTCTGGCTTTGTC
INOS	CTGCAGCACTTGGATCAGGAACCTG	GGAGTAGCCTGTGTGCACCTGGAA
IL-1β	GCAACTGTTCCTGAACTCAACT	ATCTTTTGGGGTCCGTCAACT
TNF-α	TCTGTCTACTGAACTTCGGGGTG	ACTTGGTGGTTTGCTACGACG
ARG1	CCCCAGTACCAACAGGACTACC	TGAACGTGGCGGAATTTTGT
IL-10	CGGGAAGACAATAACTGCACCC	CGGTTAGCAGTATGTTGTCCAGC
CD206	GGGACTCTGGATTGGACTCA	CCAGGCTCTGATGATGGACT

CHAPTER 4. ADIPOCYTE-SPECIFIC SOAT1 DEFICIENCY DECREASED DIET INDUCED HEPATIC STEATOSIS AND PROMOTED HEART HYPERTROPHY

4.1 Abstract

Although adipocyte cholesterol homeostasis is closely associated with obesity and systemic health, the exact mechanism is still not well-studied. SOAT1 is the key enzyme responsible for synthesizing CE from FC. Previously, we found that knocking down SOAT1 in pre-adipocytes inhibited adipogenesis. However, the physiological function of SOAT1 remains unknown. We employed SOAT1 flox/flox (CTRL) mice and adipocyte-specific SOAT1-knockout (AKO) mice and fed them with HFHC diet for 21 weeks. Compared to CTRL mice, AKO mice exhibited little effects on body weight, adipose tissue mass, adipocyte size. Consistently, no significant differences were observed between CTRL and AKO mice in systemic energy intake, energy expenditure or glucose tolerance. Interestingly, we found that NAFLD activity score decreased in AKO mice, with decreased expression of lipogenic genes (SCD1, CD36) and reduced macrophage infiltration (F4/80 IHC staining), compared to CTRL mice. However, we performed echocardiography and found a significant decrease in % fractional shortening and % ejection fraction, and the heart mass markedly increased by 16.7% in AKO mice compared to CTRL, suggesting that heart function had worsened in the AKO mice.

Collectively, our study demonstrated that SOAT1 deficiency in adipocytes has a minimal influence on adipose tissue mass or body weight in HFHC diet fed mice. However, adipocyte-SOAT1 may engage in the crosstalk between adipose tissue and organs in distance, including the liver and heart.

4.2 Introduction

White adipose tissue (WAT) is an important endocrine and metabolic organ that secretes

a variety of bioactive factors, known as adipokines, that influence systemic metabolism. The adipokine include adiponectin, leptin, resistin, and several pro-inflammatory cytokines such as TNF-α and IL-6 [250]. There is increasing recognition that WAT communicates with other organs, including the heart and liver. This crosstalk allows WAT to regulate energy metabolism in distant organs and conversely, allows other organs to modulate WAT function. Disruption of intercellular communication within adipose tissue has been associated with obesity, insulin resistance, cardiovascular disease, and various other disorders [251].

Adipokines can directly influence liver function and metabolism by binding to specific receptors on hepatocytes (liver cells) or by modulating the expression of genes associated with hepatic lipid and glucose metabolism. Adipose tissue crosstalk also impacts cardiac structure and function [252]. Obesity induces pathological cardiac hypertrophy, which involves enlargement of cardiomyocytes and increased protein synthesis. This is accompanied by inflammation, oxidative stress, and impaired cardiac metabolism. Adiponectin, leptin, and FABP4 among others, are thought to play key roles in initiating and promoting obesity-related cardiomyopathy. Leptin and FABP4 have been shown to directly induce pathological hypertrophy of cardiomyocytes. Dysregulation of lipid metabolism, particularly increased fatty acid uptake and oxidation, also promote the development of cardiac hypertrophy and dysfunction in obesity [253].

SOAT1 is an enzyme involved in the biosynthesis of cholesterol esters. Previous studies have reported that adipocyte-specific knockout (KO) of ABCA1, a key enzyme involved in cholesterol efflux, in mice reduced serum HDL-c levels when fed a HFHC diet [139]. This indicates that maintaining cholesterol homeostasis is involved in the synthesis and release of different lipoproteins, including HDL-c. Elevated levels of HDL-c are typically linked to a decreased risk of cardiovascular diseases, as they facilitate the reverse transport of cholesterol, removing excess cholesterol from the body's tissues, including the heart and liver [254].

In summary, white adipose tissue communicates with the heart, liver, and other organs through the release of adipokines and lipids in a process termed adipose tissue crosstalk.

Further study is needed to fully elucidate the complex interactions between white fat, liver, and heart mediated by SOAT1 and other factors. Understanding adipose tissue crosstalk may reveal new therapeutic strategies to mitigate obesity-related cardiovascular and metabolic disorders that impact public health.

4.3 Methods and materials

4.3.1 Animal model and treatment

All animal experiments were conducted at The Hong Kong Polytechnic University and were approved by the Centralized Animal Facilities (CAF). The mice used in this study were of C57BL/6J background and were housed at room temperature with a 12-hour light/dark cycle. They were fed with HFHC (1.25% cholesterol, 60% kcal% from fat) (Shuyishuer Bio. China) and given sterile water ad libitum. SOAT1$^{flox/flox}$ mice were generated by inserting two Loxp sites covering SOAT1 exon 14 (provided by Dr. Ta-Yuan Chang [126]). Adipocyte-specific SOAT1 knockout mice (Adipoq-SOAT1) were generated by crossing SOAT1$^{flox/flox}$ mice with adiponectin-Cre (Adipoq-Cre, provided by Dr. CHENG, King Yip [152]).

4.3.2 Adipose tissue ex-vivo lipolysis

The adipose tissue was collected from different depots and incubated with KRPH buffer (20 mM Hepes, 5 mM KH2PO4, 1 mM MgSO4, 1 mM CaCl2, 136 mM NaCl, 4.7 mM KCl, pH 7.4) containing 2% fatty acid-free BSA at 37°C for 2 hours. Subsequently, the medium was collected for the measurement of NEFA (Cat. No. A042-1-1, Nanjing Jiancheng, China), glycerol (F6428, Sigma-Aldrich, USA), and TG (Cat. No. A110-1-1, Nanjing Jiancheng, China) levels. All assays were conducted following the instructions provided by the respective manufacturers. Tissue weight was used to normalize glycerol and FFA values.

4.3.3. Real-time RT-PCR analysis

Trizol reagent (TR 118, Millipore) was used to isolate total RNA from different tissue and subsequently reverse to cDNA and perform real-time PCR as described in chapter 2 method part. The mRNA levels were normalized to ACTB and calculated with the comparative CT method.

4.3.4 Glucose tolerance and pyruvate tolerance measurement.

Mice were fasted 16h for GTT and 6h for PTT at 25 weeks of age. Blood samples were obtained from the mice's tail, and glucose levels were assessed using a glucometer as described in chapter 3 method part.

4.3.5 Echocardiography in mice

The mouse heart Echocardiography is performed by Fujifilm VisualSonics (Vevo 3100, Canada) [255]. Briefly, the mouse was gently in the palm of one hand and anesthesia by isoflurane. Pre-warm the echo transmission gel and apply it to the hairless chest of the mouse. The parasternal long-axis view captures a side view of the heart, allowing assessment of its structures and function. The short-axis view at the papillary muscle level provides detailed information about the left ventricle and the integrity of valves. 2-D guided M-mode imaging enables real-time visualization of cardiac motion, facilitating measurements of cardiac dimensions and movement during the cardiac cycle.

4.3.6 Histological analysis

Adipose tissue samples are collected and fixed 10% formalin. Thin sections (usually around 4-6 μm) of the adipose tissue are cut using a microtome. These sections are mounted onto glass slides and dried. Then the slide was performed F4/80 IHC or HE stained following the standard procedure as described in chapter 3 method part.

4.3.7 Statistical analysis

The data are presented as means ± S.D. or means ± S.E.M., as specified in the figure legends. Statistical significance for comparisons between control and treatment groups was assessed using GraphPad Prism software (version 9.0) with a two-tailed student's t-test or one-way ANOVA. Statistical significance is reported for comparisons with a p-value < 0.05, as indicated in the figure legends.

4.4 Results

4.4.1 Adipocyte-specific SOAT1 deletion has little impact on metabolic phenotype when fed with HFHC diet

In order to explore the function of SOAT1 in obesity and metabolic syndrome-related diseases, we introduced a HFHC diet to SOAT1 knockout (KO) mice. The CTRL and AKO mice were treated with HFHC from 8 weeks to 29 weeks old (Figure 4-1 A). There was no difference in body weight between the CTRL and AKO groups during the 21-week treatment period (Figure 4-1 B-C), as well as in organ mass (Figure 4-3 D). Adiponectin levels provide insights into insulin sensitivity and overall metabolic health, while leptin levels indicate adiposity, appetite regulation, and leptin signaling status [256]. We then measure the fasting serum levels of adiponectin and leptin and no difference was observed between the CTRL and AKO groups (Figure 4-1 E-F). Energy balance was assessed by monitoring individual food intake in metabolic cages (Figure 4-1 G), measuring fecal calorie content (Figure 4-1 H), and evaluating EE in metabolic cages (Figure 4-1 I, L), but no significant differences were found between the CTRL and AKO groups. The RER levels, which indicate substrate utilization, were similar between the CTRL and AKO groups and close to 0.7 (Figure 4-1 J), suggesting a preference for fat as an energy source. Additionally, physical activity measured by pedometer showed no significant difference between the CTRL and AKO groups (Figure 4-1 K). These results indicate that SOAT1 deficiency in adipocytes has little effect on the metabolic phenotype in HFHC feeding.

4.4.2 Adipocyte-SOAT1 deficiency has little impact on adipose tissue adipogenesis and inflammation when fed with HFHC diet

Following 21 weeks of treatment, the mice were euthanized, and no significant alterations in fat phenotype or the percentage of fat mass were observed between the CTRL and AKO groups (Figure 4-2 A-B). F4/80 staining was performed on Ing-WAT, Epi-WAT, and Retro-WAT to evaluate inflammation and morphology in different adipose tissue depots, but no differences in macrophage infiltration were observed between the CTRL and AKO groups (Figure 4-2 C, G-I). Adipocyte size distribution in Epi-WAT and Ing-WAT also showed no significant difference (Figure 4-2 D-E), although there was an increased prevalence of small adipocytes and a decreased prevalence of large adipocytes in Retro-WAT (Figure 4-2 F). Genes involved in triglyceride synthesis (DGAT2), fatty acid metabolism (SCD1), adipogenesis regulation (PPARγ), and adipokine encoding (AdipoQ and Resistin) did not show significant differences between the CTRL and AKO groups (Figure 4-2 J-K). Collectively, these results suggest that SOAT1 deficiency in adipocytes has little impact on adipose tissue mass and inflammation in the context of HFHC feeding.

4.4.3 Adipocyte-SOAT1 deficiency has little impact on adipose tissue lipolysis and total cholesterol level

Lipolysis is a crucial metabolic process occurring in adipose tissue, wherein stored triglycerides are enzymatically broken down into fatty acids and glycerol. This process is crucial for regulating energy balance and maintaining overall metabolic health. We examined whether the lipolysis process would be altered by SOAT1 KO. The mice were fasted overnight, and fat mass was collected for ex-vivo lipolysis experiments. However, there were no significant differences in glycerol and NEFA levels in both iWAT and eWAT between the CTRL and AKO mice (Figure 4-3 A-B). The released glycerol from the breakdown of triglycerides in adipose tissue could enter the bloodstream. Therefore, we measured the glycerol, NEFA, and TG levels in the serum and found no significant differences between the CTRL and AKO groups (Figure 4-3 C-E). Next, we determined

if the absence of SOAT1 in adipocytes affects overall cholesterol storage in adipose tissue. We measured total cholesterol and free cholesterol levels in Ing-WAT, Epi-WAT, and Retro-WAT and found no differences between the CTRL and AKO groups (Figure 4-3 F-H). In summary, these data suggest that SOAT1 deficiency in adipocytes has minimal impact on adipose tissue lipolysis and cholesterol levels in the context of HFHC feeding.

4.4.4 Adipocyte-SOAT1 deficiency ameliorates hepatic steatosis when fed with HFHC diet

The liver plays a crucial role in lipid metabolism, undertaking essential processes related to the synthesis, storage, and distribution of lipids. Interestingly, although the lipid homeostasis does not seem to change in WAT of AKO mice, there is a significant reduction in lipid droplet (LD) content in hepatocytes and TG content in the liver compared to CTRL (Figure 4-4 A-B). This reduction is accompanied by decreased expression of TG synthesis genes (Figure 4-4 G). Additionally, macrophage infiltration, as demonstrated by F4/80 staining, is significantly decreased in AKO mice compared to CTRL (Figure 4-4 C-D), suggesting reduced inflammation. No collagen fibers are observed in the livers of both CTRL and AKO mice when fed HFHC (Figure 4-4 E). Total cholesterol and free cholesterol levels show no difference between CTRL and AKO mice, although there is a trend towards decreased expression of cholesterol efflux (ABCG1) and synthesis (HMGCS) genes in AKO mice compared to CTRL (Figure 4-4 F-G). In summary, these results demonstrate that SOAT1 deficiency in adipocytes may ameliorate hepatic steatosis in HFHC feeding.

4.4.5 Adipocyte-SOAT1 deficiency promotes heart hypertrophy when fed with HFHC diet

It is interesting to found that the heart mass of the AKO group is significantly higher than the CTRL group (Figure 4-5 A), as well as the ratio of heart weight to BW (Figure 4-5 B). Heart hypertrophy refers to the enlargement or thickening of the heart muscle,

specifically the myocardium. Obesity is often associated with systemic metabolic abnormalities, such as insulin resistance, dyslipidemia, and chronic low-grade inflammation. These factors can further contribute to the development of heart hypertrophy and cardiovascular complications [257]. To investigate if heart function is damaged in the AKO group, we performed heart echocardiography on mice. As expected, the left ventricular mass (LV mass) was significantly higher in the AKO group compared with the CTRL group (Figure 4-5 C), indicating the presence of cardiac hypertrophy. The thickness of the anterior wall of the left ventricle during systole (LVAW;s), representing the phase of ventricular contraction when the heart pumps blood out to the body, was increased in AKO mice. Similarly, the thickness of the anterior wall of the left ventricle during diastole (LVAW;d), representing the phase of ventricular relaxation and filling when the heart receives blood from the atria, was also increased in AKO mice. Left Ventricular Posterior Wall at Systole (LVPW;s) and Left Ventricular Posterior Wall at Diastole (LVPW;d) were higher in AKO mice compared with CTRL (Figure 4-5 D), indicating hypertrophy of the ventricular walls. Additionally, the diastolic and systolic diameters (Figure 4-5 E) were increased, further suggesting ventricular wall hypertrophy in AKO mice. Increased chamber diameters may indicate chamber dilation, which can occur in conditions such as heart failure or volume overload. Ejection fraction (EF) quantifies the heart's pumping capacity and signifies the percentage of blood expelled from the left ventricle during each contraction. A lower EF suggests impaired systolic function in the AKO group when compared to the CTRL group (Figure 4-5 F). Fractional shortening (FS) is another measure of systolic function and represents the percentage of change in left ventricular diameter during contraction. The decreased FS in the AKO group indicates impaired systolic function compared to the CTRL group (Figure 4-5 G). The MV E/A ratio is a parameter used to assess diastolic function, specifically the filling of the left ventricle during relaxation. The ratio compares the early (E) and late (A) diastolic velocities of blood flow across the mitral valve. An increased MV E/A ratio indicates diastolic impairment in AKO mice compared to the CTRL group (Figure 4-5 H). Global longitudinal strain (GLS) reflects the overall contraction and relaxation ability of the LV myocardium. The decreased

value of GLS in the AKO group suggests impaired diastolic function (Figure 4-5 I). ANP (atrial natriuretic peptide) is a marker of heart hypertrophy. The ANP mRNA level in the hearts of AKO mice is higher than in CTRL mice (Figure 4-5 J), further confirming that heart hypertrophy has occurred in AKO mice. Collectively, these data suggest that SOAT1 deficiency in adipocytes promotes heart hypertrophy in the context of HFHC feeding.

4.4.6 Adipocyte-SOAT1 deficiency reduces serum HDL-C level when fed with HFHC diet

Cholesterol plays a vital role as a fundamental component of lipoproteins, encompassing both LDL and HDL. The TC, FC, CE, and LDL-C levels showed no difference between the CTRL and AKO groups. However, there was a significant reduction in HDL-C levels in AKO mice compared to the CTRL group (Figure 4-6 A-C). Reduced levels of HDL-C are linked to an elevated risk of cardiovascular diseases and impaired reverse cholesterol transport, suggesting that AKO mice may have metabolic abnormalities.

4.4.7 Adipocyte-SOAT1 deficiency has little effect on glucose tolerance but improve insulin sensitivity when fed with HFHC diet

Glucose tolerance and insulin sensitivity are important indices for assessing metabolic health. The pyruvate tolerance test (PTT) primarily reflects the liver's capacity for gluconeogenesis, which involves converting pyruvate into glucose. In our study, we compared the results of GTT, PTT, and fasting blood glucose levels between CTRL and AKO groups (Figure 4-7 A-C). We found no significant differences between the two groups in these measures. However, when we examined serum fasting insulin levels and HOMA-IR, we observed a significant decrease in AKO mice compared to the CTRL group (Figure 4-7 D-E). This finding suggests that AKO mice exhibit improved insulin sensitivity, despite no apparent effects on glucose tolerance or gluconeogenesis ability. In summary, our data suggest that the absence of SOAT1 in adipocytes does not

significantly affect glucose tolerance or gluconeogenesis but does improve insulin sensitivity.

4.5 Discussion

The excessive accumulation of adipose tissue in obesity can disrupt the delicate equilibrium of cholesterol metabolism. Here, we use an adipocyte-specific SOAT1 KO mouse model to evaluate the role of adipocyte SOAT1 in diet-induced obesity. The results show that in mice on an HFHC diet, AKO mice have a minimal effect on body weight, fat mass, and adipocyte morphology, but it may engage in crosstalk with the heart and liver. The hepatic steatosis was ameliorated in AKO mice, along with a decrease in macrophage infiltration. However, heart function was impaired, and hypertrophy was observed in AKO mice. Adipose tissue is an active endocrine organ that secretes adipokines to communicate with other organs, and SOAT1 may serve as a key regulator for metabolic regulation.

Mounting evidence suggests that alterations in cholesterol uptake and efflux are connected to modifications in energy metabolism and the functioning of adipocytes. ABCA1, the key gene in regulating cholesterol efflux, was found to have significantly lower body weight, eWAT weight, and adipocyte size in an ABCA1 KO mice model fed with an HFHC diet [139]. In our previous study, we found that knocking down SOAT1 in pre-adipocytes blocked LD formation [154]. Thus, we hypothesized that KO of SOAT1 in adipocytes could exacerbate obesity. However, we found no significant difference in body weight, adipose tissue mass, and cholesterol levels between CTRL and AKO groups. We will perform lipidomic analysis to examine if the lipid profile has been altered by SOAT1 KO in WAT.

Various studies have found that adipose tissue can crosstalk with the liver through adipokines and hepatokines, AT-derived miRNAs, inflammatory signals, etc. By inhibiting autophagy specifically in white adipose tissue, adipocyte-specific Atg7 knockout (KO) mice demonstrated improvements in liver steatosis and fibrosis, as well as a reduction in serum free fatty acid (FFA) levels, indicating the involvement of

adipose-liver crosstalk in these beneficial effects [258]. In our study, we found decreased ectopic LD accumulation in the liver and reduced macrophage infiltration in AKO mice. Adipose tissue and the heart engage in complex crosstalk through various molecular and cellular mechanisms, contributing to cardiovascular health and disease. For example, adipose tissue releases extracellular vesicles, including exosomes, which contain various bioactive molecules, such as proteins, lipids, and microRNAs (miRNAs). These extracellular vesicles can be taken up by cardiac cells and influence their function [259]. A previous study found adipocyte stress-induced small extracellular vesicles (sEVs) were observed to contain an abundance of oxidatively damaged mitochondria. These sEVs have the potential to trigger a surge of reactive oxygen species (ROS) in cardiac tissue. Moreover, the adipocyte-derived pro-oxidant signal protects the heart through hormesis [260]. Chronic low-grade inflammation originating from adipose tissue can lead to the development of conditions like atherosclerosis and heart failure [261]. In our study, we didn't find AKO mice could induce AT inflammation. However, heart function was damaged, and hypertrophy occurred in AKO mice. We will perform serum metabonomics and lipidomics to identify potential factors that ameliorate liver steatosis and cause heart hypertrophy.

In summary, the results from our mouse model provide new insights into the crosstalk between WAT and the heart and liver. Depletion of SOAT1 in adipocytes ameliorates liver steatosis while promoting heart hypertrophy. Further studies are needed to understand how adipocyte-specific KO of SOAT1 causes this phenotype.

4.6 Acknowledgement

This work was supported by a start-fund from The Hong Kong Polytechnic University and Research Grants Council (RGC) of Hong Kong. I greatly appreciate Prof. Ta-Yuan Chang for providing us with the SOAT1 flox/flox mice; Dr. CHENG King Yip for providing us with adiponectin-Cre mice; Dr. miao Zhang for heart echocardiography and Dr. Alan Leung for his technical support in metabolic cage.

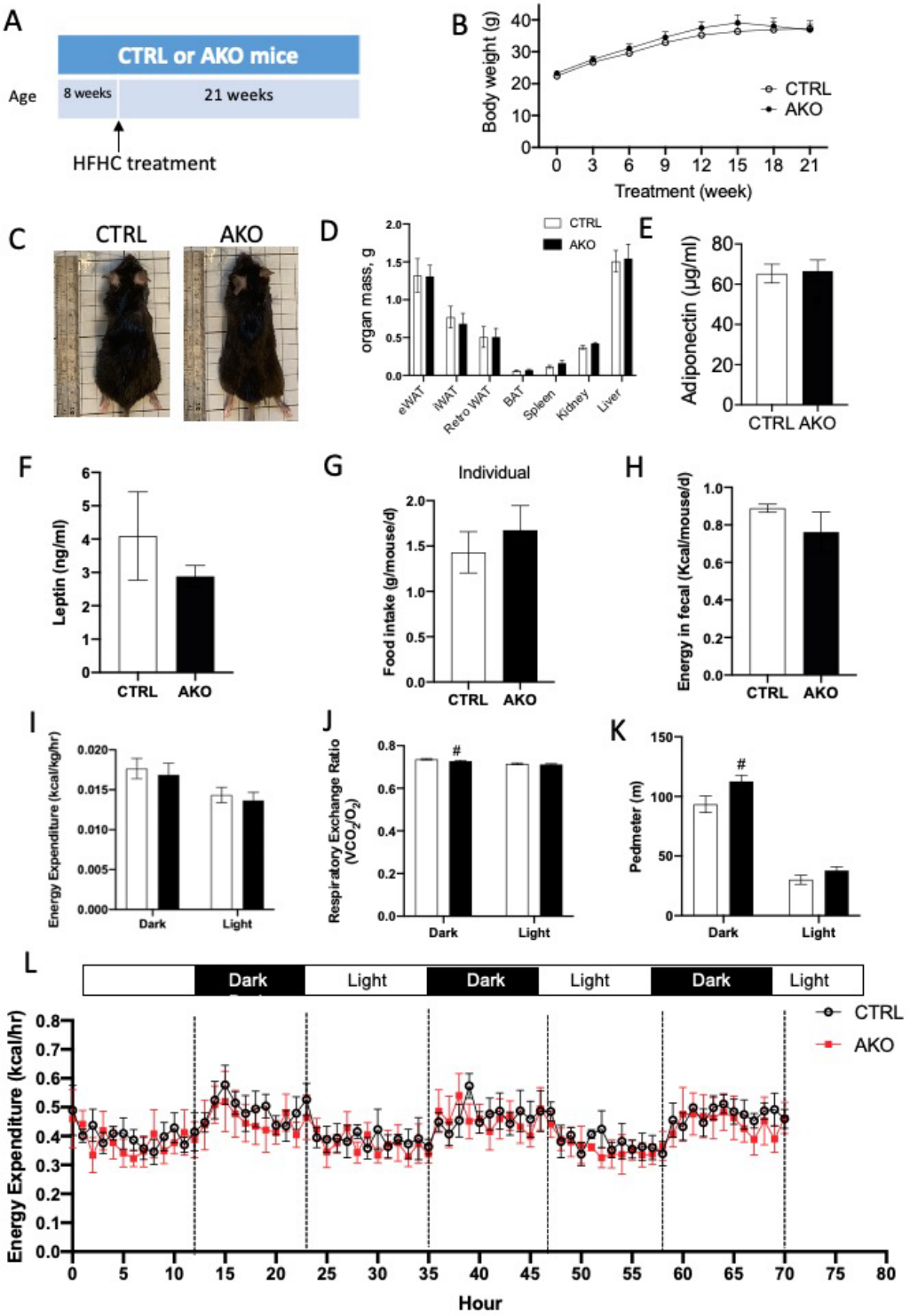
A
CTRL or AKO mice
Age
8 weeks
21 weeks
HFHC treatment
B
Body weight (g)
Treatment (week)
CTRL
AKO
C
CTRL
AKO
D
organ mass, g
eWAT
iWAT
Retro WAT
BAT
Spleen
Kidney
Liver
E
Adiponectin (μg/ml)
F
Leptin (ng/ml)
G
Individual
Food intake (g/mouse/d)
H
Energy in fecal (Kcal/mouse/d)
I
Energy Expenditure (kcal/kg/hr)
Dark
Light
J
Respiratory Exchange Ratio
K
Pedmeter (m)
L
Energy Expenditure (kcal/hr)
Hour

Figure 4-1 Adipocyte-specific SOAT1 (AKO) mice have little effect on metabolic health in HFHC feeding.

A, Experiment procedure. 8-weeks-old CTRL and AKO male mice were feed with HFHC diet for 21 weeks. B, Body weight of CTRL or AKO mice (n=5 per group). C, Representative images of 29-weeks-old CTRL or AKO mice. D, Organ mass of various tissue (n=5 per group). E, Serum Adiponectin level from CTRL or AKO mice (n=5 per group). F, Serum leptin level from CTRL or AKO mice. G, Food intake were measured by individual mice (n=5 per group). H, Fecal samples collected from these mice were subjected to bomb calorimetry to measure fecal (n=5 per group). The mice were subjected to metabolic cage for 4 days. Metabolic cage detected VO2 and VCO2 every 30 minutes. Average of three dark cycles and three light cycles were used to calculate energy expenditure I and respiratory exchange ratio J. K, Pedmeter value were recorded by metabolic cage. L, Energy expenditure of CTRL and AKO mice fed with HFHC. Data is presented as Mean ± SEM and analysed by independent t-test, #$p<0.1$, *$p<0.05$, **$p<0.01$, ***$p<0.001$.

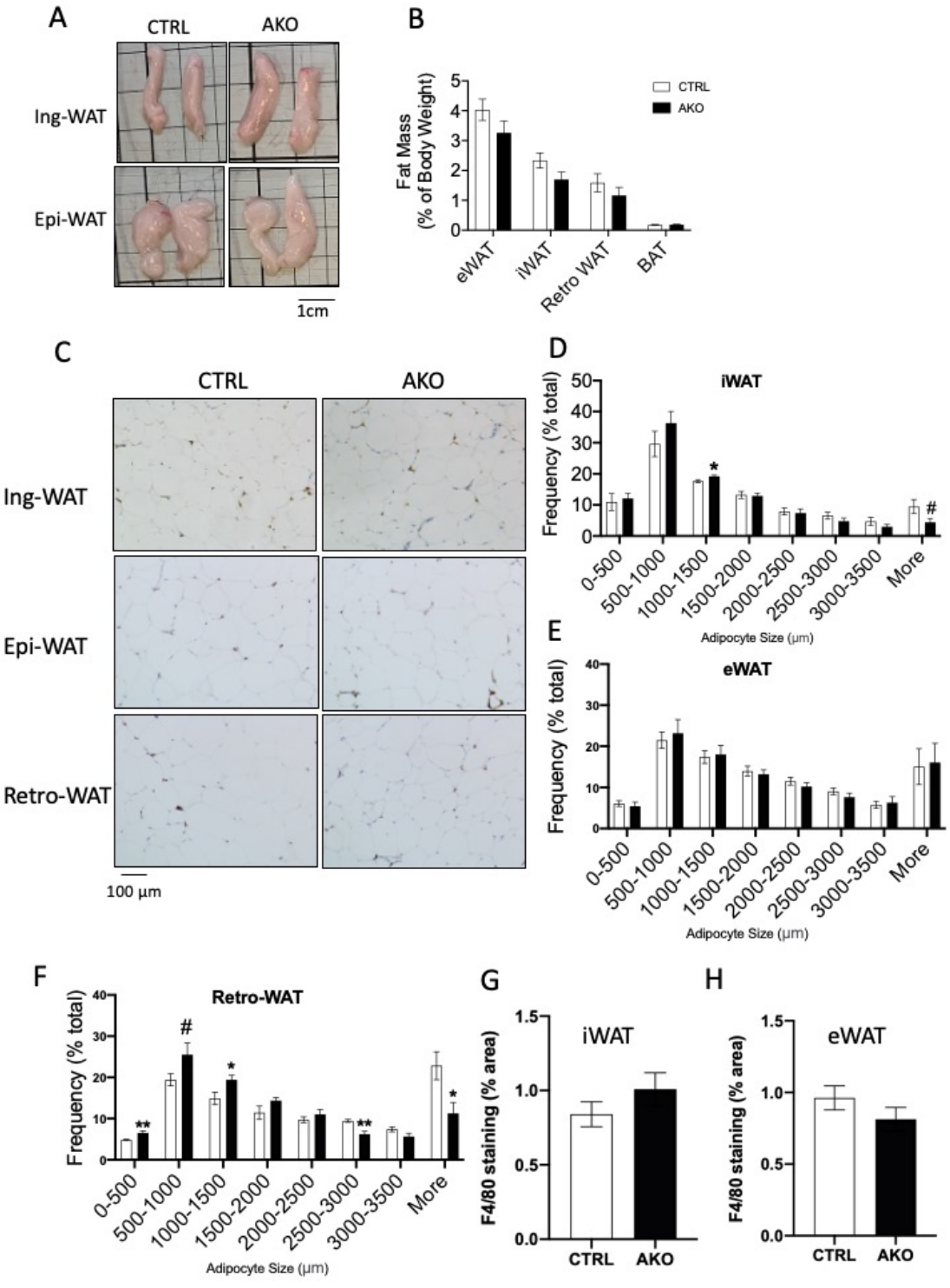
A
CTRL
AKO
Ing-WAT
Epi-WAT
1cm
B
Fat Mass (% of Body Weight)
CTRL
AKO
eWAT
iWAT
Retro WAT
BAT
C
CTRL
AKO
Ing-WAT
Epi-WAT
Retro-WAT
100 μm
D
iWAT
Frequency (% total)
0-500
500-1000
1000-1500
1500-2000
2000-2500
2500-3000
3000-3500
More
Adipocyte Size (μm)
E
eWAT
Frequency (% total)
Adipocyte Size (μm)
F
Retro-WAT
Frequency (% total)
Adipocyte Size (μm)
G
iWAT
F4/80 staining (% area)
CTRL
AKO
H
eWAT
F4/80 staining (% area)
CTRL
AKO

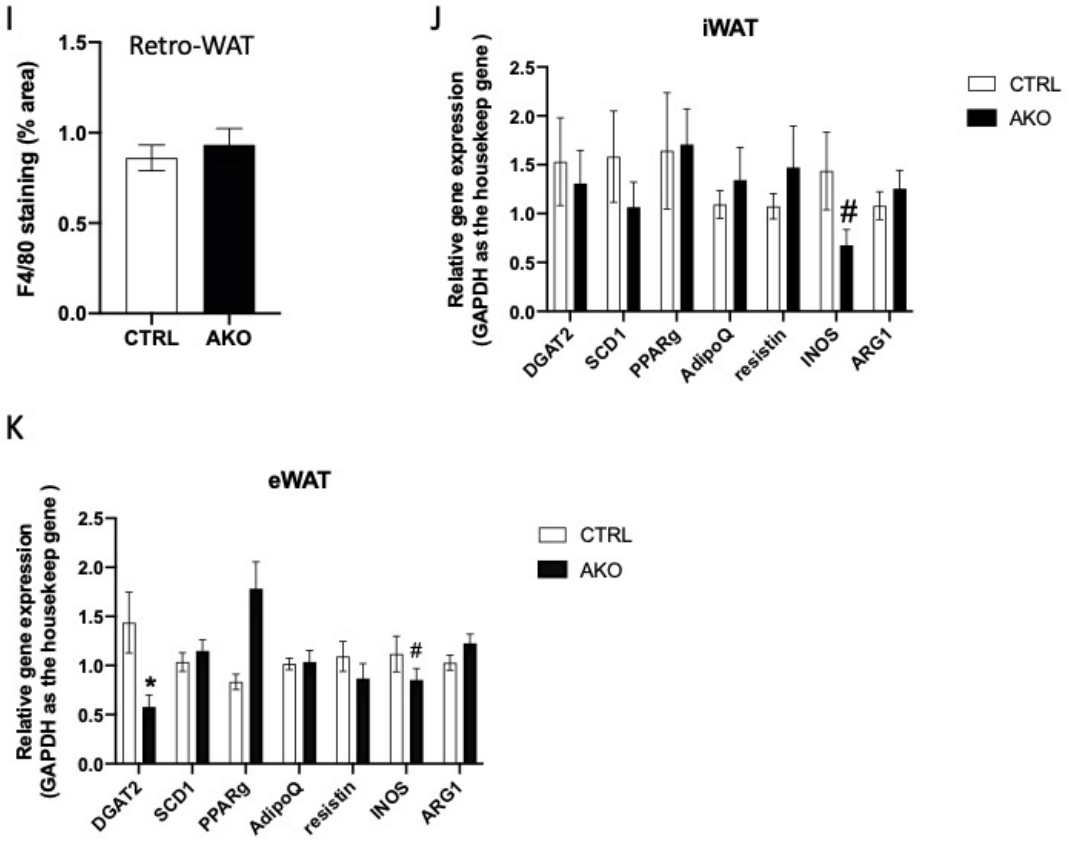

Figure 4-2 Adipocyte-specific SOAT1 knockout (AKO) mice has minimum effect on adipocyte adipogenesis and inflammation.

A, Representative images of iWAT and eWAT from CTRL and AKO mice. B, The adipose tissue weight were relative to body weight of CTRL or AKO mice (n=5 per group). C, Representative adipocyte image of F4/80 stained of iWAT, eWAT and Retro-WAT from CTRL and AKO mice. D-F, Adipocyte size quantification of different depots of AT. G-I, F4/80 quantification of different depots of AT. J-K, mRNA level of genes involved in adipogenesis and inflammation of iWAT and eWAT. Data is presented as Mean ± SEM and analysed by independent t-test, #p<0.1, *p<0.05, **p<0.01, ***p<0.001.

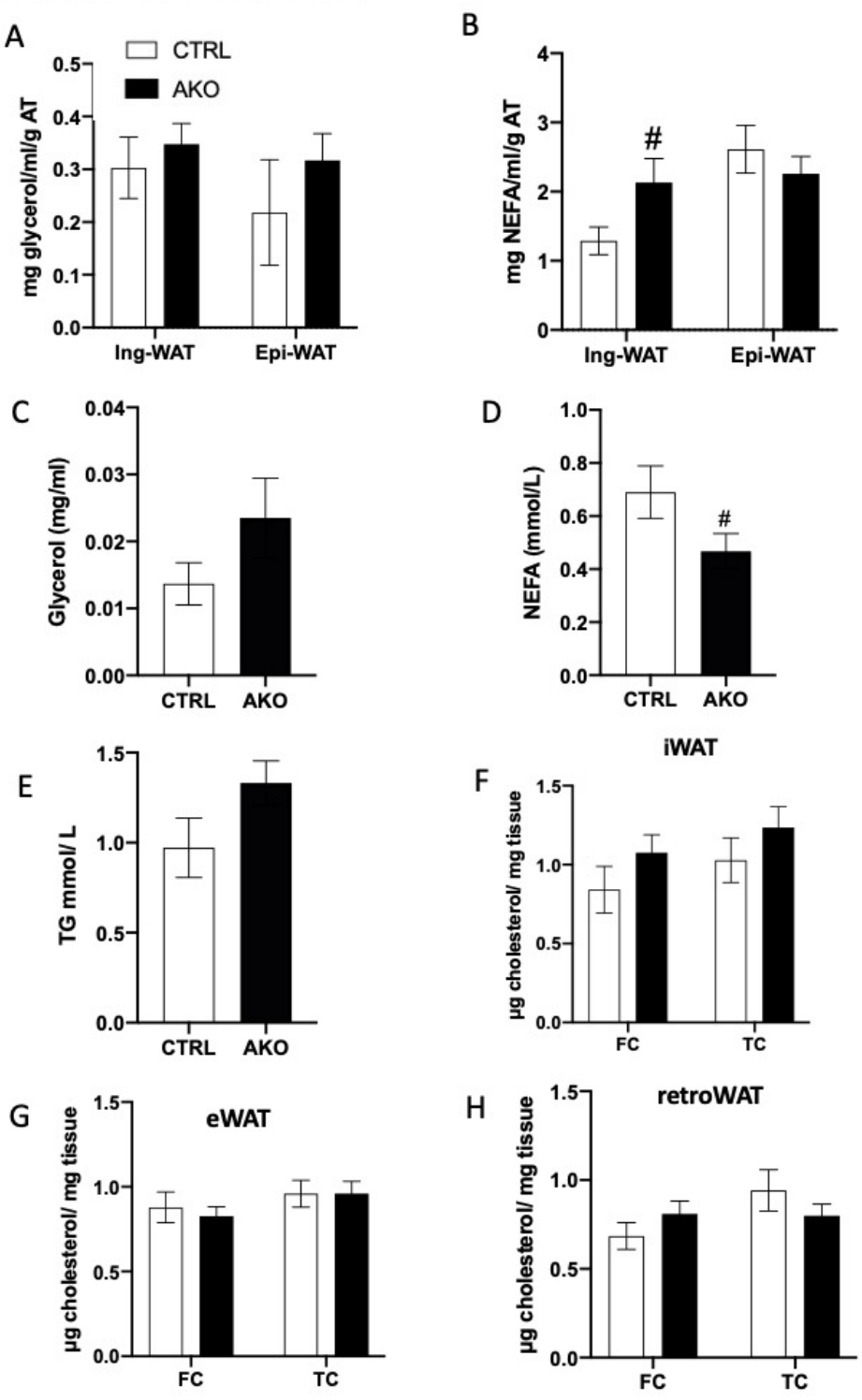
A
CTRL
AKO
mg glycerol/ml/g AT
0.5
0.4
0.3
0.2
0.1
0.0
Ing-WAT
Epi-WAT
B
mg NEFA/ml/g AT
4
3
2
1
0
#
Ing-WAT
Epi-WAT
C
Glycerol (mg/ml)
0.04
0.03
0.02
0.01
0.00
CTRL
AKO
D
NEFA (mmol/L)
1.0
0.8
0.6
0.4
0.2
0.0
#
CTRL
AKO
E
TG mmol/ L
1.5
1.0
0.5
0.0
CTRL
AKO
F
iWAT
µg cholesterol/ mg tissue
1.5
1.0
0.5
0.0
FC
TC
G
eWAT
µg cholesterol/ mg tissue
1.5
1.0
0.5
0.0
FC
TC
H
retroWAT
µg cholesterol/ mg tissue
1.5
1.0
0.5
0.0
FC
TC

Figure 4-3 Adipocyte-specific SOAT1 knockout (AKO) mice has minimum effect on adipocyte lipolysis and cholesterol level.

The mice were sacrificed, WAT ex-vivo lipolysis for 2h and medium is collected to measure glycerol in A and NEFA in B. C, Serum glycerol level. D, Serum NEFA level. E, Serum TG level. Mice WAT were homogenized and applied to Amplex cholesterol kit to measure free cholesterol and total cholesterol level in iWAT (F), eWAT (G) and Retro-WAT (H). Data is presented as Mean ± SEM and analysed by independent t-test, #$p<0.1$, *$p<0.05$, **$p<0.01$, ***$p<0.001$.

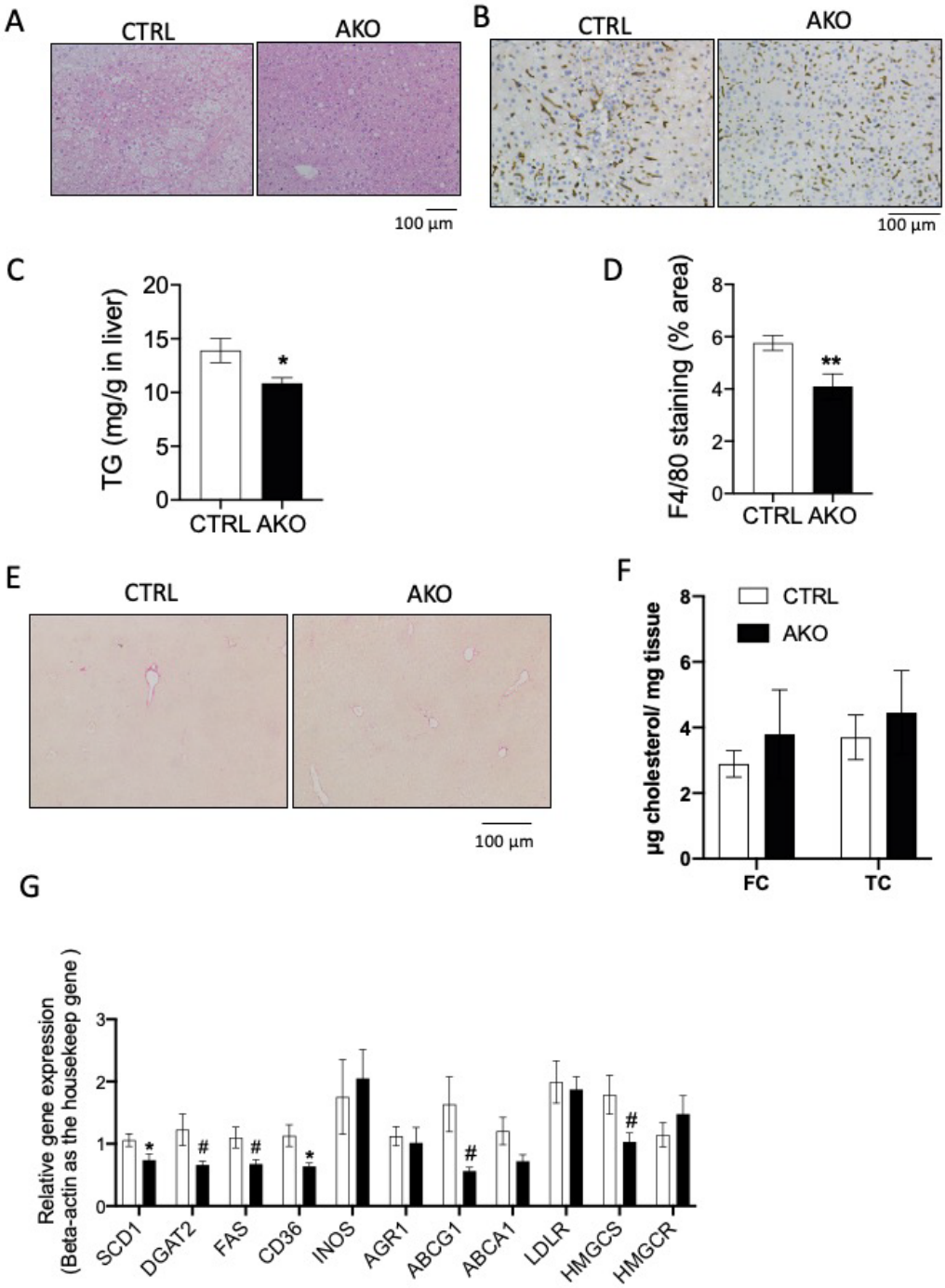
A
CTRL
AKO
100 μm
B
CTRL
AKO
100 μm
C
TG (mg/g in liver)
20
15
10
5
0
*
CTRL AKO
D
F4/80 staining (% area)
8
6
4
2
0
**
CTRL AKO
E
CTRL
AKO
100 μm
F
μg cholesterol/ mg tissue
CTRL
AKO
8
6
4
2
0
FC
TC
G
Relative gene expression
(Beta-actin as the housekeep gene)
3
2
1
0
SCD1
DGAT2
FAS
CD36
INOS
AGR1
ABCG1
ABCA1
LDLR
HMGCS
HMGCR

Figure 4-4 Adipocyte-specific SOAT1 knockout (AKO) mice ameliorates hepatic steatosis.

A, Representative image of H&E stained of liver from CTRL and AKO mice. B, TG quantification of liver tissue from CTRL and AKO mice. C, Representative image of F4/80 stained of liver from CTRL and AKO mice. D, F4/80 quantification of liver tissue from CTRL and AKO mice. E, Representative image of sirus stained of liver from CTRL and AKO mice. F, Free cholesterol and total cholesterol in liver tissue. G, mRNA level of adipogenesis, cholesterol homeostasis related gene in liver tissue. Data is presented as Mean ± SEM and analysed by independent t-test, #$p<0.1$, *$p<0.05$, **$p<0.01$, ***$p<0.001$.

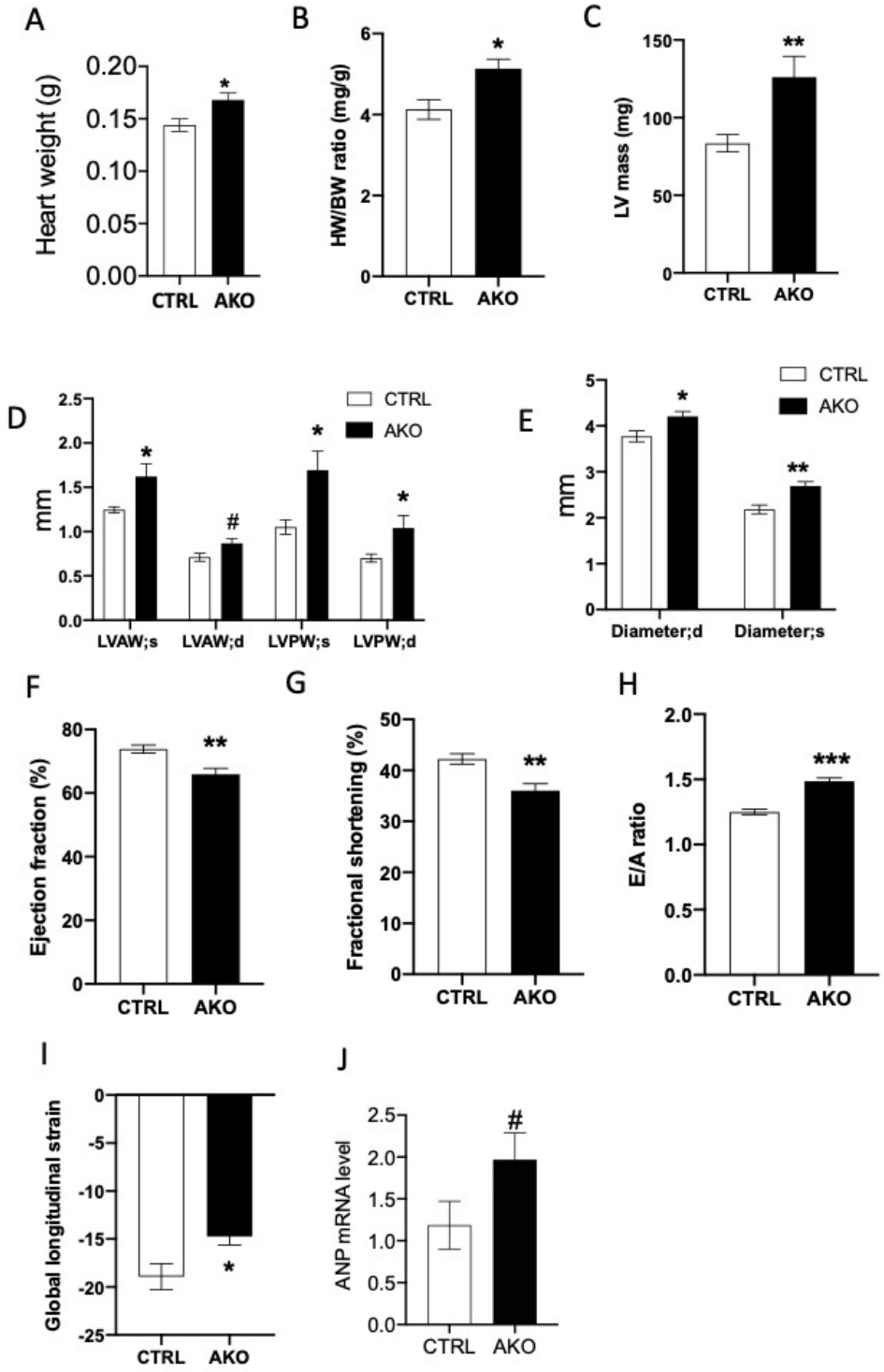
A
Heart weight (g)
0.20
0.15
0.10
0.05
0.00
*
CTRL AKO
B
HW/BW ratio (mg/g)
6
4
2
0
*
CTRL AKO
C
LV mass (mg)
150
100
50
0
**
CTRL AKO
D
mm
2.5
2.0
1.5
1.0
0.5
0.0
CTRL
AKO
*
#
*
*
LVAW;s LVAW;d LVPW;s LVPW;d
E
mm
5
4
3
2
1
0
CTRL
AKO
*
**
Diameter;d Diameter;s
F
Ejection fraction (%)
80
60
40
20
0
**
CTRL AKO
G
Fractional shortening (%)
50
40
30
20
10
0
**
CTRL AKO
H
E/A ratio
2.0
1.5
1.0
0.5
0.0
***
CTRL AKO
I
Global longitudinal strain
0
-5
-10
-15
-20
-25
*
CTRL AKO
J
ANP mRNA level
2.5
2.0
1.5
1.0
0.5
0.0
#
CTRL AKO

Figure 4-5 Adipocyte-specific SOAT1 knockout (AKO) mice promote heart hypertrophy.

A, Heart weight of CTRL and AKO mice in HFHC feed. B, The ratio of heart weight to body weight. C, Left ventricular mass of CTRL and AKO mice. D, LVAW;d, LVAW;d, LVPW;s and LVPW;d measurement of CTRL and AKO mice. E, Diameters;d and diameter;s measurement of CTRL and AKO mice. F-I, EF, FS MV E/A and GLS measurement by heart echocardiography. J, ANP mRNA level of heart tissue. Data is presented as Mean ± SEM and analysed by independent t-test, #p<0.1, *p<0.05, **p<0.01, ***p<0.001.

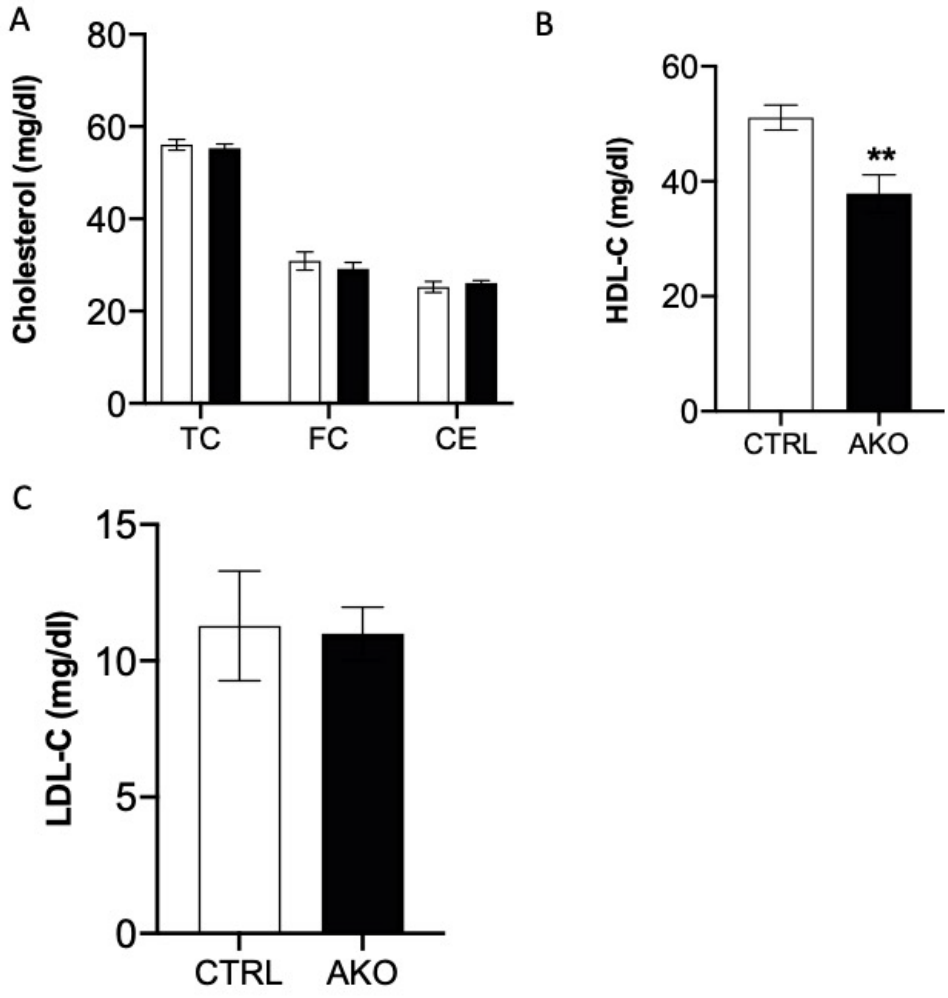

Figure 4-6. Adipocyte-specific SOAT1 knockout (AKO) mice reduced serum HDL-c level.

A, Serum total cholesterol, fee cholesterol and cholesteryl ester measurement. B, Serum HDL-c level. C, Serum LDL-C level. Data is presented as Mean ± SEM and analysed by independent t-test, *p<0.05, **p<0.01, ***p<0.001.

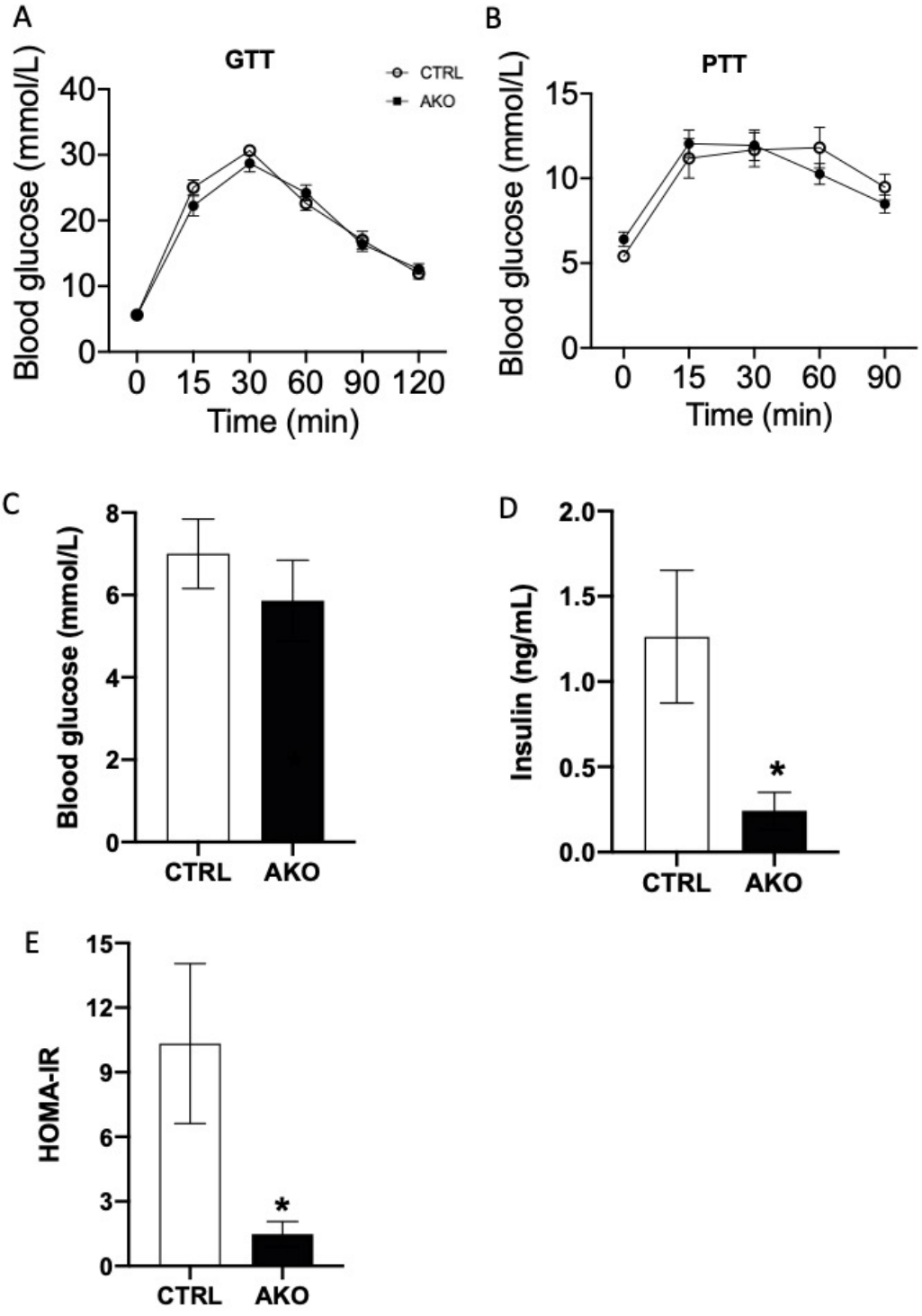
A
GTT
CTRL
AKO
Blood glucose (mmol/L)
40
30
20
10
0
0 15 30 60 90 120
Time (min)
B
PTT
Blood glucose (mmol/L)
15
10
5
0
0 15 30 60 90
Time (min)
C
Blood glucose (mmol/L)
8
6
4
2
0
CTRL AKO
D
Insulin (ng/mL)
2.0
1.5
1.0
0.5
0.0
*
CTRL AKO
E
HOMA-IR
15
12
9
6
3
0
*
CTRL AKO

Figure 4-7 Adipocyte-specific SOAT1 knockout (AKO) mice improves insulin sensitivity.

A, The blood glucose level of CTRL and AKO mice under HFHC after i.p. injection glucose for glucose tolerance tests (GTT). B, The blood glucose level of CTRL and AKO mice under HFHC after i.p. injection pyruvate for pyruvate tolerance tests (PTT). C, Fasting serum blood glucose level of CTRL and AKO mice. D, Fasting serum insulin level of CTRL and AKO mice. E, The HOMA-IR was calculated according to the equation shown in the Materials and Methods section. Data is presented as Mean ± SEM and analysed by independent t-test, *$p<0.05$, **$p<0.01$, ***$p<0.001$.

CHAPTER 5. ADIPOCYTE-SPECIFIC SOAT1 DEFICIENCY PROMOTE FAT MASS AND ADIPOCYTE HYPERTROPHY

5.1 Abstract

Cholesterol homeostasis plays an important role in adipose tissue function; however, its impact on adipocyte expansion remains unclear. SOAT1 is a key enzyme responsible for converting free cholesterol (FC) to cholesteryl ester (CE). In this study, we utilized a mouse model with adipocyte-specific knockout of SOAT1 (AKO) and corresponding control (CTRL) mice fed a normal diet (ND) for 21 weeks. Comparing AKO mice to CTRL mice, little effects were observed on body weight, energy intake, energy expenditure, or glucose tolerance. Surprisingly, AKO mice displayed a significant increase in adipose tissue (AT) mass, accompanied by enlarged adipocyte size. This phenotype was also evident in 8-week-old mice, where AKO mice exhibited higher white adipose tissue (WAT) mass and larger average cell size compared to CTRL mice. These findings suggest that SOAT1 deficiency promotes adipogenesis in early-stage adipose tissue.

In summary, our study demonstrates that SOAT1 deficiency in adipocytes has little impact on body weight or energy balance in mice fed a normal diet. However, specific to adipocytes, SOAT1 may play a role in the process of adipocyte expansion.

5.2 Introduction

Adipose tissue, as a specialized form of connective tissue, serves a vital function in the human body by playing a critical role in energy storage and metabolism. Despite its essential role in multiple bodily functions, excessive accumulation and expansion of adipose tissue are associated with numerous health complications, including conditions such as obesity, diabetes, cardiovascular diseases, and specific forms of cancer. This multifaceted interplay between adipose tissue and human health is underpinned by a complex regulatory process known as adipogenesis [262, 263].

Adipogenesis is the biological process through which precursor cells, or preadipocytes,

differentiate into mature adipocytes. The regulation of this process involves a precise sequence of transcriptional events, which prominently feature essential transcription factors such as peroxisome PPARγ and C/EBPs [264, 265].

Adipose tissue can expand through two primary mechanisms: hypertrophy, which involves an increase in the size of adipocytes, and hyperplasia, which involves an increase in the number of adipocytes. The balance between these two mechanisms is considered critical for maintaining metabolic health. However, uncontrolled adipose tissue expansion, as observed in obesity, can lead to a pathological state termed 'adiposopathy' or 'sick fat', characterized by dysregulated adipokine secretion, inflammation, and insulin resistance. Therefore, understanding the molecular intricacies of adipose tissue adipogenesis and expansion is pivotal for developing therapeutic strategies for metabolic disorders [266, 267].

SOAT1, is an enzyme that plays a critical role in cholesterol homeostasis. It is primarily involved in the esterification of cholesterol, a process that converts FC into CE for storage in the LDs of cells. SOAT1 is particularly enriched in the endoplasmic reticulum of adipocytes, highlighting its importance in adipose tissue biology [268]. Cholesterol homeostasis is a tightly regulated process that balances the levels of cholesterol production, intake, and excretion to maintain cellular and systemic health. Disruption of cholesterol homeostasis can lead to a variety of health issues, including atherosclerosis, cardiovascular disease, and neurodegenerative diseases. Cholesterol homeostasis plays a crucial role in adipose tissue by ensuring the structural integrity and optimal functioning of adipocytes. Recent evidence suggests that cholesterol imbalance can interfere with adipogenesis and adipocyte function, further underscoring the relevance of cholesterol homeostasis in adipose tissue biology [269, 270].

Overall, the intricate relationship between adipose tissue adipogenesis and expansion, the role of SOAT1, and cholesterol homeostasis presents a complex, yet fascinating, area of exploration. Unravelling these complexities might pave the way for novel therapeutic interventions for a range of metabolic disorders associated with adipose tissue dysfunction.

5.3 Methods and materials

5.3.1 Animal model and treatment

All animal experiments were conducted at The Hong Kong Polytechnic University and were approved by the Centralized Animal Facilities (CAF). The mice used in this study were of C57BL/6J background and were housed at room temperature with a 12-hour light/dark cycle. They were fed with HFHC (PicoLab Rodent Diet 20) (Lab supply) and given sterile water ad libitum. SOAT1$^{flox/flox}$ mice were generated by inserting two Loxp sites covering SOAT1 exon 14 (provided by Dr. Ta-Yuan Chang [126]). Adipocyte-specific SOAT1 knockout mice (Adipoq-SOAT1) were generated by crossing SOAT1$^{flox/flox}$ mice with adiponectin-Cre (Adipoq-Cre, provided by Dr. CHENG, King Yip [152]).

5.3.2. Metabolic cage studies

The mice were individually housed in metabolic cages (Promethion System, Sable System International) featuring wire mesh floors and distinct compartments for food and water. These cages were maintained in a temperature-controlled room operating on a 12-hour light/dark cycle. To measure oxygen consumption (VO2) and carbon dioxide production (VCO2), an indirect calorimetry system integrated into the metabolic cages was utilized. The respiratory exchange ratio (RER), which reflects substrate utilization, was calculated as the ratio of VCO2 to VO2. Locomotor activity was monitored using infrared beam breaks, and total activity counts were recorded. Data were collected and analyzed as described in chapter 3 method part.

5.3.3 Glucose and insulin tolerance tests

Glucose tolerance was evaluated following an overnight fast. Mice received an intraperitoneal injection of glucose (2 g/kg body weight), and blood samples were collected from the tail vein at baseline and at specific time intervals post-injection. Insulin tolerance was assessed after a 6-hour fasting period, where mice were

intraperitoneally injected with 0.75 IU/kg insulin, and blood glucose levels were measured using a glucometer (Roche, Switzerland) at designated time points.

5.3.4 Histological staining

Different depots of adipose tissue were collected and fixed in 10% formalin. After fixation, the tissues were dehydrated by gradually passing them through a series of increasing concentrations of alcohol. The dehydrated tissues were then infiltrated with a medium, typically paraffin wax or resin, to provide support and facilitate sectioning. Subsequently, H&E staining was performed as described in chapter 3 method part.

5.3.5 Blood collection, TG, FFA, glycerol, cholesterol and hormone measurement of mouse serum

Blood samples were collected from overnight fasting mice, and experiment reagents and methods were described in chapter 3 method part.

5.3.6 Statistical analysis

The data are presented as means ± S.D. or means ± S.E.M., as specified in the figure legends. Statistical significance for comparisons between control and treatment groups was assessed using GraphPad Prism software with a two-tailed student's t-test or one-way ANOVA. Statistical significance is reported for comparisons with a p-value < 0.05, as indicated in the figure legends.

5.4 Results

5.4.1 Adipocyte-specific SOAT1 deletion has little impact on metabolic phenotype

In order to explore the physiological function of SOAT1 in vivo, we constructed adipocyte-specific SOAT1 knockout (AKO) mice as described in chapter 3 and fed them a ND until 29 weeks old (Figure 5-1 A). After 21 weeks of treatment, there was no significant difference in body weight between the CTRL and AKO mice (Figure 5-1 B). Interestingly, all white adipose tissue (WAT) masses were significantly upregulated in AKO mice compared to CTRL, while other organs showed no difference (Figure 5-1 C). Serum adiponectin levels were significantly downregulated in AKO mice, while leptin levels were upregulated compared to CTRL (Figure 5-1 D-E). Adiponectin levels are generally inversely correlated with adiposity, suggesting reduced adiposity in AKO mice. During the 21 weeks of treatment, the accumulated food intake showed no difference between CTRL and AKO mice (Figure 5-1 F). Subsequently, the mice were placed in metabolic cages to record individual food intake and energy expenditure (EE). There was no significant difference in individual food intake between CTRL and AKO groups (Figure 5-1 G), but fecal energy was significantly upregulated in AKO mice (Figure 5-1 H). EE, RER, and physiological activity showed no significant difference between CTRL and AKO mice (Figure 5-1 I-L). In conclusion, these results demonstrate that adipocyte-specific SOAT1 deficiency has little effects on body weight and energy balance.

5.4.2 Adipocyte-SOAT1 deficiency promote adipose tissue mass and adipocyte size

After the mice were sacrificed, the fat mass increased by approximately 50% in eWAT, iWAT, and Retro-WAT (Figure 5-2 A). We further evaluated adipocyte size and inflammation by conducting F4/80 staining on different depots of WAT (Figure 5-2 B). The AKO group exhibited a greater accumulation of larger adipocytes compared to the CTRL group, particularly in iWAT (Figure 5-2 C-E). This increase in adipocyte size suggests adipocyte hypertrophy in AKO mice. Quantification of F4/80 staining showed no significant difference in macrophage infiltration between WAT of CTRL and AKO

mice (Figure 5-2 F-H), suggesting that macrophage infiltration was not enhanced by SOAT1 knockout in adipocytes. The adipogenesis-related mRNA level were no significantly difference between CTRL and AKO group in both iWAT and eWAT. Overall, these data indicate that adipocyte-SOAT1 deficiency promotes adipocyte hypertrophy but does not enhance macrophage infiltration.

5.4.3 Adipocyte-SOAT1 deficiency promote fat mass at 8 weeks old

Because we observed a significant upregulation of fat mass in 29-week-old AKO mice, we hypothesized that adipocyte hypertrophy occurs in the early stages of adipogenesis. To test this hypothesis, we sacrificed 8-week-old mice and found a significant increase in iWAT fat mass in the AKO group compared to the CTRL group, even though BW showed no difference (Figure 5-3 A-B). To further evaluate adipocyte morphology, we conducted H&E staining (Figure 5-3 C) and observed a similar distribution of adipocyte sizes between CTRL and AKO mice (Figure 5-3 D-E). However, the average adipocyte size was larger in AKO mice compared to CTRL (Figure 5-3 F-G). Taken together, these data suggest that adipocyte-SOAT1 deficiency promotes adipocyte hypertrophy at 8 weeks old.

5.4.4 Adipocyte-SOAT1 deficiency has decrease adipose tissue cholesterol level

Adipose tissue is recognized as the primary site for storing FC in the body. Previous research has provided evidence of a positive association between TG levels and cholesterol levels within adipose tissue [271]. Based on this knowledge, we measured cholesterol levels in both adipose tissue and serum. In our study, we observed a decrease in TC and FC levels specifically in the iWAT of AKO mice compared to the CTRL group. However, there was no significant difference in these cholesterol levels in eWAT (Figure 5-4 A-B). Furthermore, when we examined the cholesterol levels in the serum, we found no significant differences in TC, FC, or CE levels between the AKO and CTRL groups (Figure 5-4 C). However, we did observe a slight decrease in HDL-c

levels in the AKO mice compared to the CTRL group (Figure 5-4 D). Taken together, these findings suggest that adipocyte-SOAT1 deficiency leads to a decrease in cholesterol levels specifically in adipose tissue.

5.4.5 Adipocyte-SOAT1 deficiency has little impact on adipose tissue lipolysis

Next, we assessed the lipolysis ability of adipose tissue. The mice were fasted overnight, and different depots of white adipose tissue (WAT) were cultured ex-vivo for 2 hours. The culture medium was collected to measure levels of NEFA and glycerol, which are indicators of lipolysis. However, we did not observe any significant differences in glycerol and NEFA levels between the CTRL and AKO mice in the lipolysis medium (Figure 5-5 A-B). Furthermore, we measured the levels of glycerol and NEFA in the serum and found no apparent differences between the CTRL and AKO groups. However, the levels of TG in the serum were significantly upregulated in AKO mice compared to CTRL (Figure 5-5 C-E). Taken together, these results indicate that adipocyte-SOAT1 deficiency has little effect on adipose tissue lipolysis.

5.4.6 Adipocyte-SOAT1 deficiency has little effect on glucose homeostasis

Glucose tolerance reflects metabolic health by indicating the body's ability to regulate blood glucose levels, its sensitivity to insulin, the risk of developing type 2 diabetes, and its association with metabolic syndrome. In our study, we performed the glucose tolerance test and insulin tolerance test to assess these parameters and compared the results between the CTRL and AKO mice (Figure 5-6 A-B). Interestingly, we did not observe any significant differences in glucose tolerance between the two groups. The fasting blood glucose levels were also similar in both groups. However, we found that insulin levels were significantly decreased in AKO mice compared to CTRL, suggesting a potential improvement in insulin sensitivity. This observation was further supported by the trend towards decreased HOMA-IR, indicating improved insulin sensitivity in AKO mice (Figure 5-6 C-E). Collectively, these results demonstrate that adipocyte-SOAT1 deficiency has a minimal effect on glucose homeostasis.

5.5 Discussion

Adipocyte hypertrophy refers to the enlargement of individual fat cells within adipose tissue, whereas adipocyte hyperplasia involves an increase in the number of adipocytes present [272]. In our study, we constructed adipocyte-specific SOAT1-deficient mice and treated them with a normal diet (ND) for 29 weeks. We found that this deficiency significantly promoted adipocyte hypertrophy and increased AT mass. Consistently, the WAT mass increased in 8-week-old AKO mice, suggesting that SOAT1 deficiency in adipocytes may cause adipocyte hypertrophy. Our data reveal that SOAT1 itself or other interaction functions are involved in the adipogenesis process.

Adipocyte hypertrophy occurs as a response to prolonged positive energy balance and helps distribute the storage capacity for triglycerides across more adipocytes, potentially offering metabolic benefits compared to excessive hypertrophy [48, 273]. In our study, we did not observe any differences in energy balance, but adipocyte mass was upregulated in AKO mice, suggesting that SOAT1 is important for adipocyte maintenance. Intracellular cholesterol has been implicated in the dysfunction of adipose tissue. Adipocytes derived from individuals with obesity exhibit elevated levels of both triglycerides (TGs) and cholesterol within their cellular stores [173]. However, in our study, we observed larger adipocytes in the AKO group with decreased cholesterol levels, suggesting that the cholesterol level is not always positively related to TG levels in lean mice. It is intriguing that although adipogenesis-related gene expression is similar between the control and AKO group, the fat mass was significantly upregulated. We will perform lipidomics to analyze the changes in lipid profiles caused by SOAT1 knockout and elucidate the underlying mechanisms.

SOAT1 deficiency has no obvious of inter-organ crosstalk effect under ND feeding, while under HFHC feeding, AKO mice show the opposite phenotype with decreased non-alcoholic fatty liver disease. The underlying mechanism may involve adipose tissue functioning as a central mediator in regulating crosstalk among multiple organs and tissues [274]. When the body senses high nutrient levels, detrimental effects such as lipid ectopic deposition in the liver occur under HFHC [275]. SOAT1 KO adipocytes

may release factors like EVs or adipokines that mediate the crosstalk process between adipose tissue and other organs like the liver, thereby further ameliorating hepatic steatosis. Under ND, the SOAT1 activity in adipose tissue is much weaker than in HFHC (unpublished data). Additionally, lipid ectopic deposition would not occur in the liver, and the crosstalk effect may be ignored, resulting in no observable phenotype in the liver.

Regarding adipose tissue, previous study discovered that SOAT1 deficiency caused hair loss and decreased lifespan [109], suggesting that SOAT1 may participate in the development process. Another study found that high-affinity SOAT1 ligands remodel cholesterol metabolism to inhibit tumor growth [268]. SOAT1 KO in adipose tissue may also be involved in cholesterol remodeling, which further inhibits adipose tissue development. However, under HFHC conditions, the effects of lipolysis or other processes are stronger than fat mass accumulation, resulting in no difference in adipose tissue mass and adipocyte size distribution.

In summary, the results from our study on adipocyte-specific SOAT1 knockout in the ND study reveal that SOAT1 plays an important role in the adipose tissue expansion process. Depletion of SOAT1 in adipocytes promotes WAT mass and adipocyte hypertrophy. Further studies are needed to understand how adipocyte SOAT1 affects the adipogenesis process.

5.6 Acknowledgement

This work was supported by a start-fund from The Hong Kong Polytechnic University and Research Grants Council (RGC) of Hong Kong. I greatly appreciate Prof. Ta-Yuan Chang for providing us with the SOAT1 flox/flox mice; Dr. CHENG King Yip for providing us with adiponectin-Cre mice and Dr. Alan Leung for his technical support in metabolic cage. I would also like to thank the University Research Facility in Life Sciences (ULS) for providing equipment and technical support.

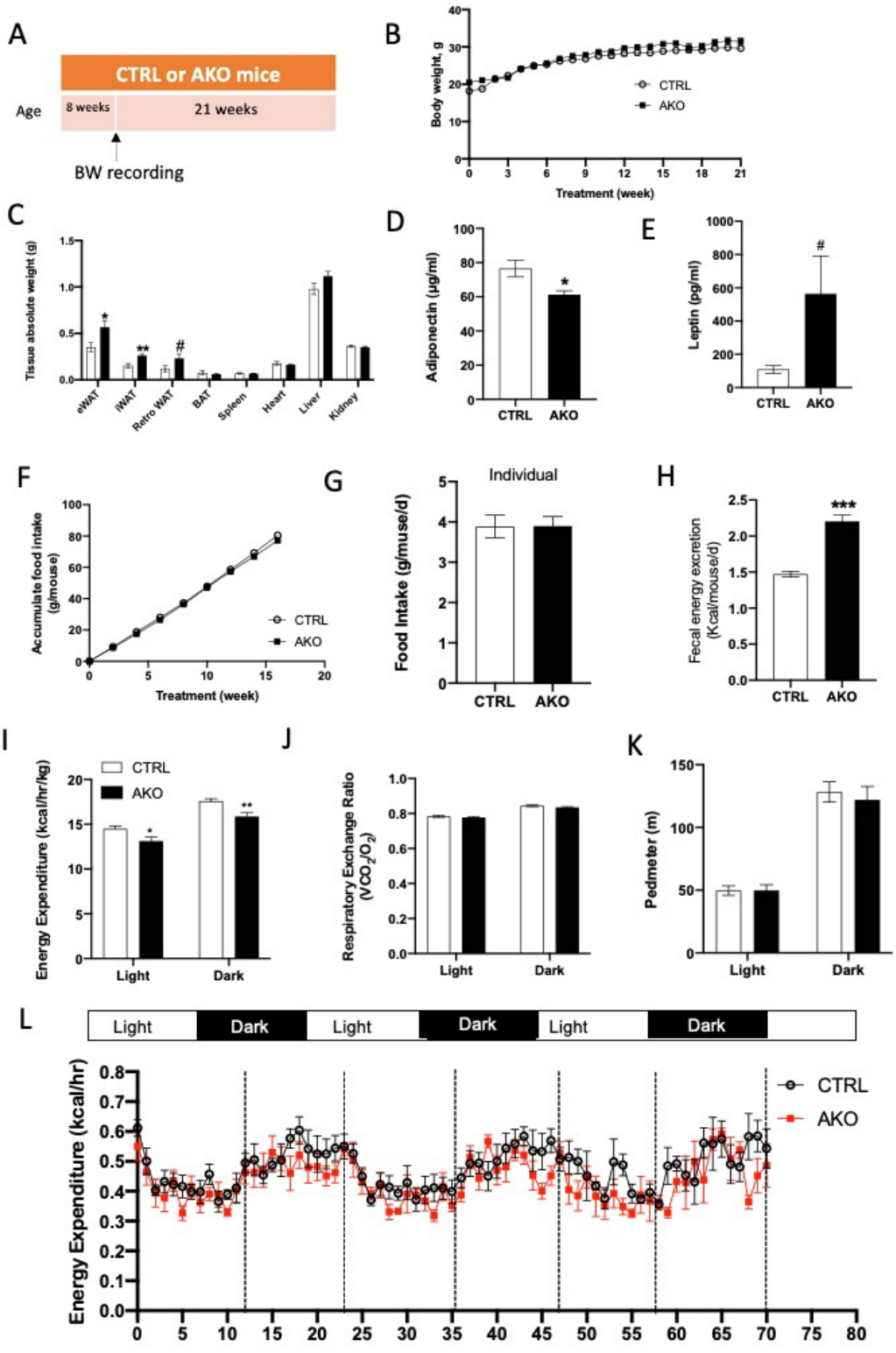
A
CTRL or AKO mice
Age
8 weeks
21 weeks
BW recording
B
Body weight, g
Treatment (week)
CTRL
AKO
C
Tissue absolute weight (g)
eWAT
iWAT
Retro WAT
BAT
Spleen
Heart
Liver
Kidney
D
Adiponectin (μg/ml)
CTRL
AKO
E
Leptin (pg/ml)
CTRL
AKO
F
Accumulate food intake (g/mouse)
Treatment (week)
CTRL
AKO
G
Individual
Food Intake (g/muse/d)
CTRL
AKO
H
Fecal energy excretion (Kcal/mouse/d)
CTRL
AKO
I
Energy Expenditure (kcal/hr/kg)
CTRL
AKO
Light
Dark
J
Respiratory Exchange Ratio (VCO_2/O_2)
Light
Dark
K
Pedmeter (m)
Light
Dark
L
Light
Dark
Light
Dark
Light
Dark
Energy Expenditure (kcal/hr)
CTRL
AKO

Figure 5-1 Adipocyte-specific SOAT1 (AKO) mice have minimum effect on metabolic health.

A, Experiment procedure. 8-weeks-old CTRL and AKO male mice were feed with ND for 21 weeks. B, Body weight of CTRL or AKO mice (n=6 per group). C, Organ mass of various tissue (n=6 per group). D, Serum Adiponectin level from CTRL or AKO mice (n=6 per group). E, Serum leptin level from CTRL or AKO mice. F, Accumulated food intake of CTRL or AKO mice during 21 week treatment time. G, Food intake were measured by individual mice (n=6 per group). H, Fecal samples collected from these mice were subjected to bomb calorimetry to measure fecal (n=6 per group). The mice were subjected to metabolic cage for 4 days. Metabolic cage detected VO2 and VCO2 every 30 minutes. Average of three dark cycles and three light cycles were used to calculate energy expenditure I and respiratory exchange ratio J. K, Pedmeter value were recorded by metabolic cage. L, Energy expenditure of CTRL and AKO mice fed with HFHC. Data is presented as Mean ± SEM and analysed by independent t-test, #$p<0.1$, *$p<0.05$, **$p<0.01$, ***$p<0.001$.

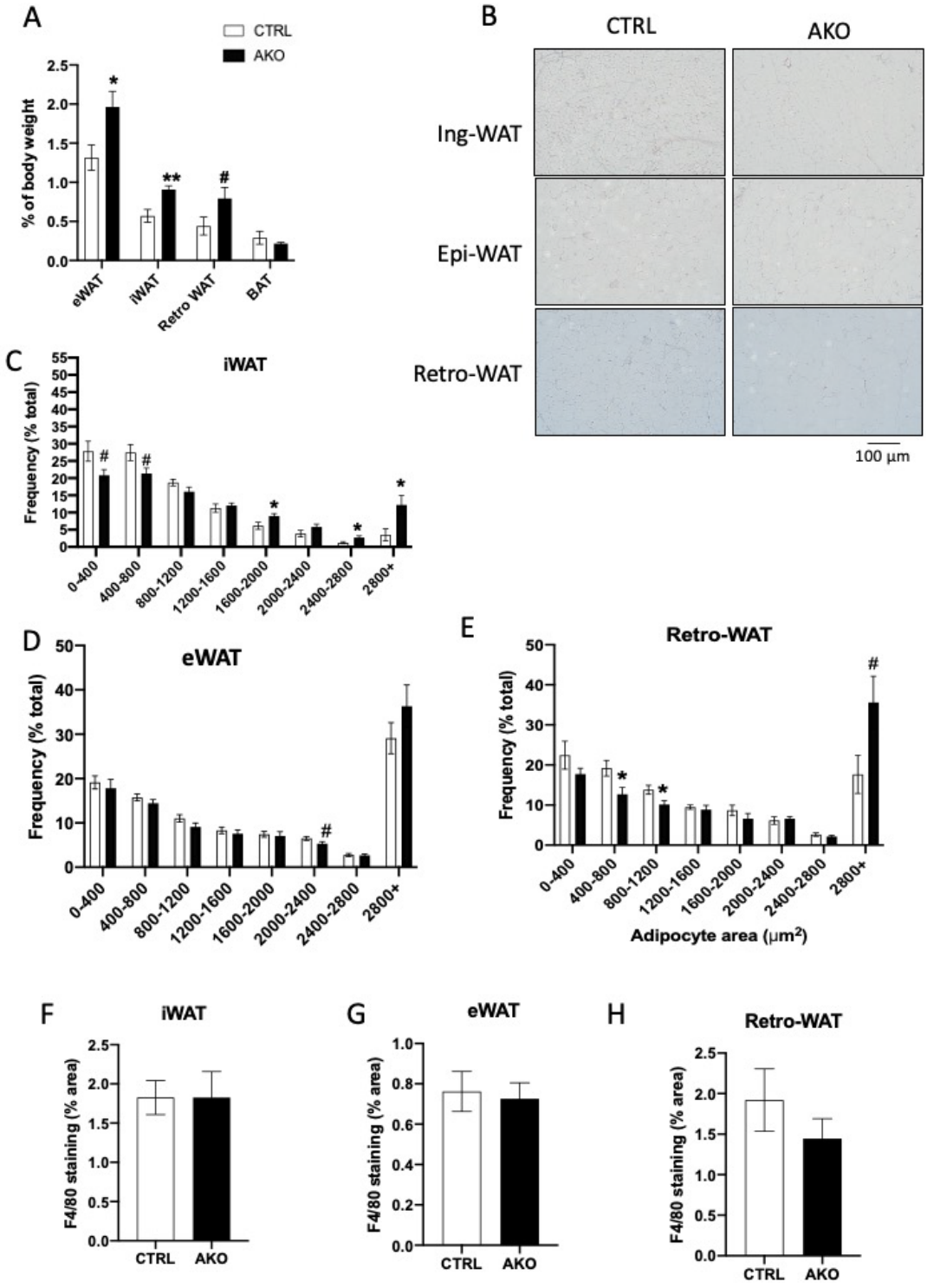
A
CTRL
AKO
% of body weight
eWAT
iWAT
Retro WAT
BAT
B
CTRL
AKO
Ing-WAT
Epi-WAT
Retro-WAT
100 µm
C
iWAT
Frequency (% total)
0-400
400-800
800-1200
1200-1600
1600-2000
2000-2400
2400-2800
2800+
D
eWAT
Frequency (% total)
E
Retro-WAT
Frequency (% total)
Adipocyte area (µm²)
F
iWAT
F4/80 staining (% area)
CTRL
AKO
G
eWAT
H
Retro-WAT

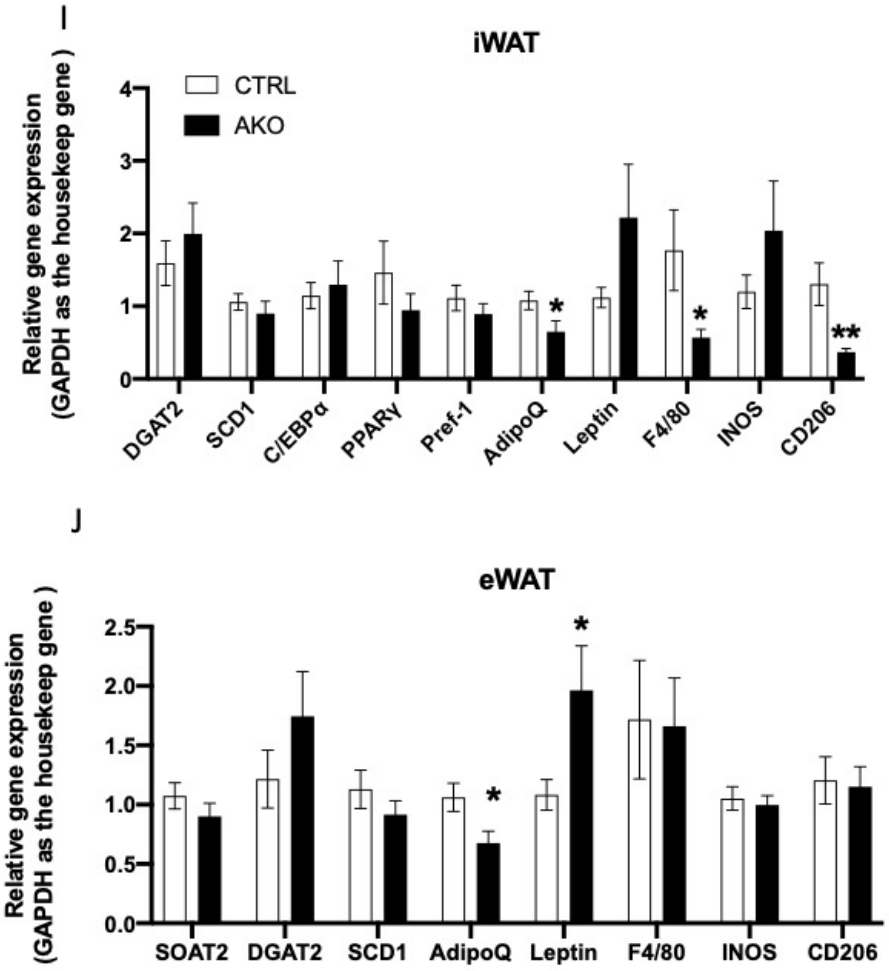

Figure 5-2 Adipocyte-specific SOAT1 knockout (AKO) mice promote adipose tissue mass.

A, The adipose tissue weight were relative to body weight of CTRL or AKO mice (n=6 per group). B, Representative adipocyte image of F4/80 stained of iWAT, eWAT and Retro-WAT from CTRL and AKO mice. C-E, Adipocyte size quantification of different depots of AT. F-H, F4/80 quantification of different depots of AT. I-J, mRNA level of genes involved in adipogenesis of iWAT and eWAT. Data is presented as Mean ± SEM and analysed by independent t-test, #p<0.1, *p<0.05, **p<0.01, ***p<0.001.

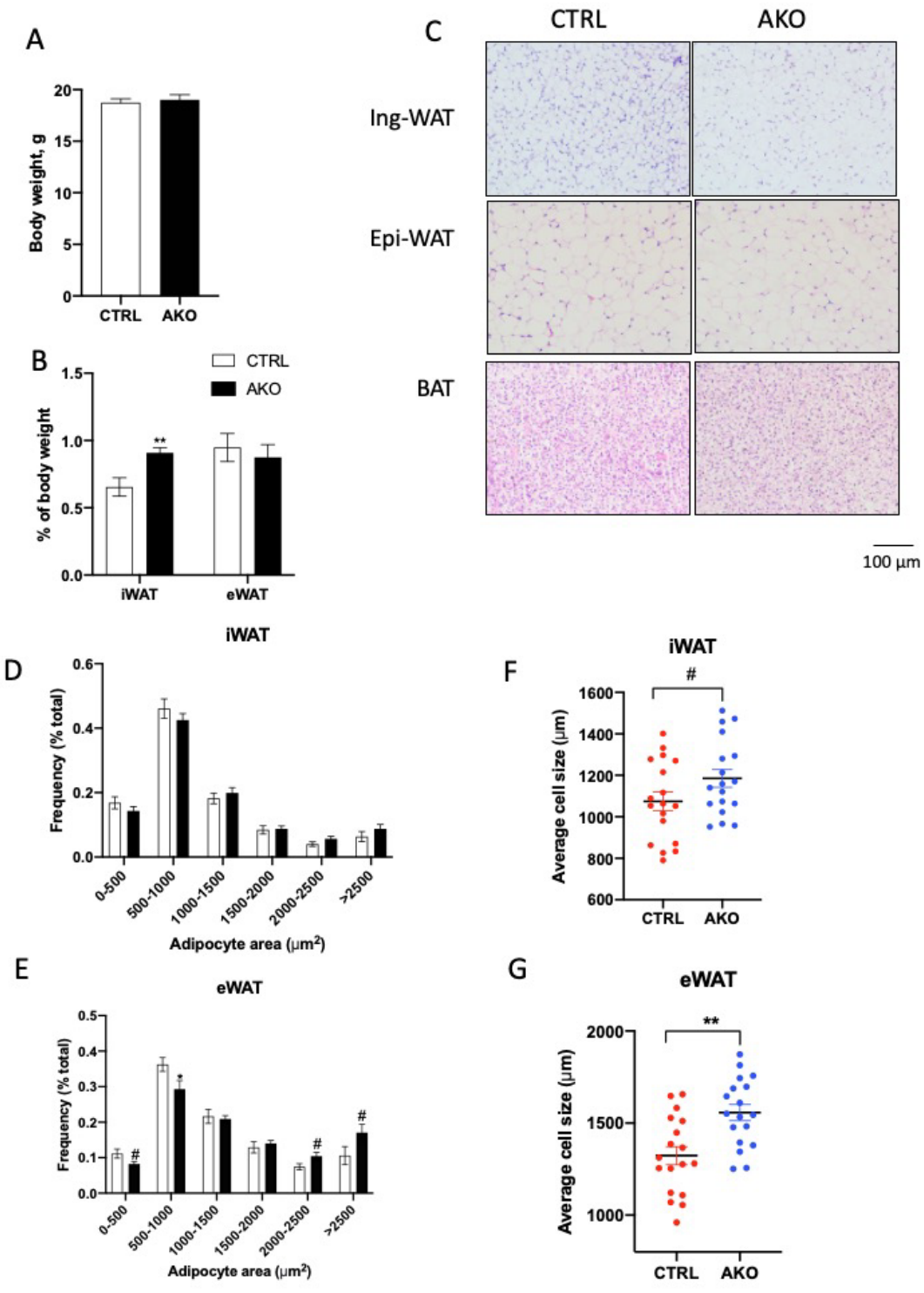
A
Body weight, g
20
15
10
5
0
CTRL
AKO
B
CTRL
AKO
% of body weight
1.5
1.0
0.5
0.0
**
iWAT
eWAT
C
CTRL
AKO
Ing-WAT
Epi-WAT
BAT
100 μm
iWAT
D
Frequency (% total)
0.6
0.4
0.2
0.0
0-500
500-1000
1000-1500
1500-2000
2000-2500
>2500
Adipocyte area (μm²)
F
iWAT
#
Average cell size (μm)
1600
1400
1200
1000
800
600
CTRL
AKO
E
eWAT
Frequency (% total)
0.5
0.4
0.3
0.2
0.1
0.0
*
#
0-500
500-1000
1000-1500
1500-2000
2000-2500
>2500
Adipocyte area (μm²)
G
eWAT
**
Average cell size (μm)
2000
1500
1000
CTRL
AKO

Figure 5-3. Adipocyte-specific SOAT1 knockout (AKO) mice promote adipose tissue hypertrophy at 8 weeks old.

A, Body weight of CTRL and AKO at 8 weeks old (n=6 per group). B, The adipose tissue weight were relative to body weight of CTRL or AKO mice (n=6 per group).C, Representative adipocyte image of H&E stained of iWAT, eWAT and BAT from CTRL and AKO mice. D-E, Adipocyte size quantification of different depots of AT. F-G, Average cell size of iWAT and eWAT. Data is presented as Mean ± SEM and analysed by independent t-test, #$p<0.1$, *$p<0.05$, **$p<0.01$, ***$p<0.001$.

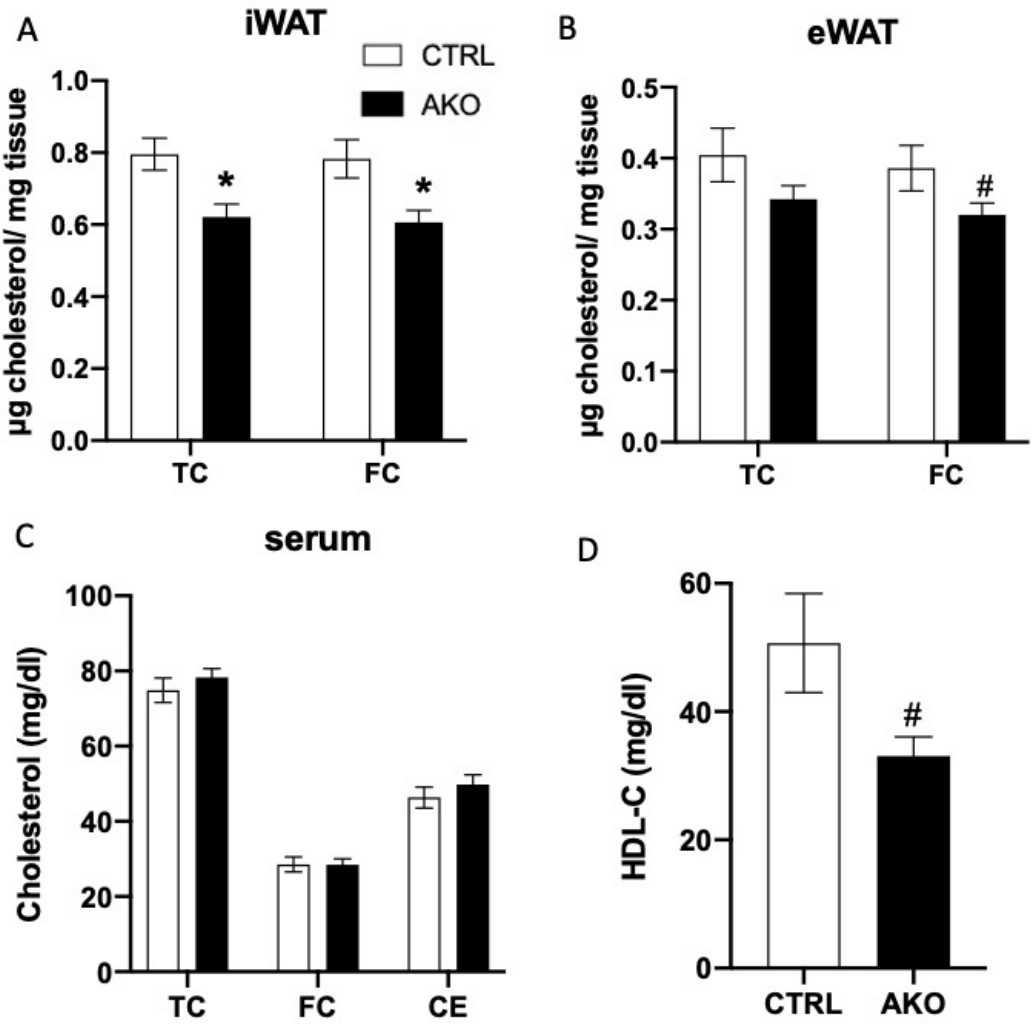

Figure 5-4 Adipocyte-specific SOAT1 knockout (AKO) mice decrease adipose tissue cholesterol level.

A, Total cholesterol and free cholesterol level of CTRL and AKO mice of iWAT. B, Total cholesterol and free cholesterol level of CTRL and AKO mice of eWAT. C, Serum cholesterol level. D, Serum HDL-c level. Data is presented as Mean ± SEM and analysed by independent t-test, #$p<0.1$, *$p<0.05$, **$p<0.01$, ***$p<0.001$.

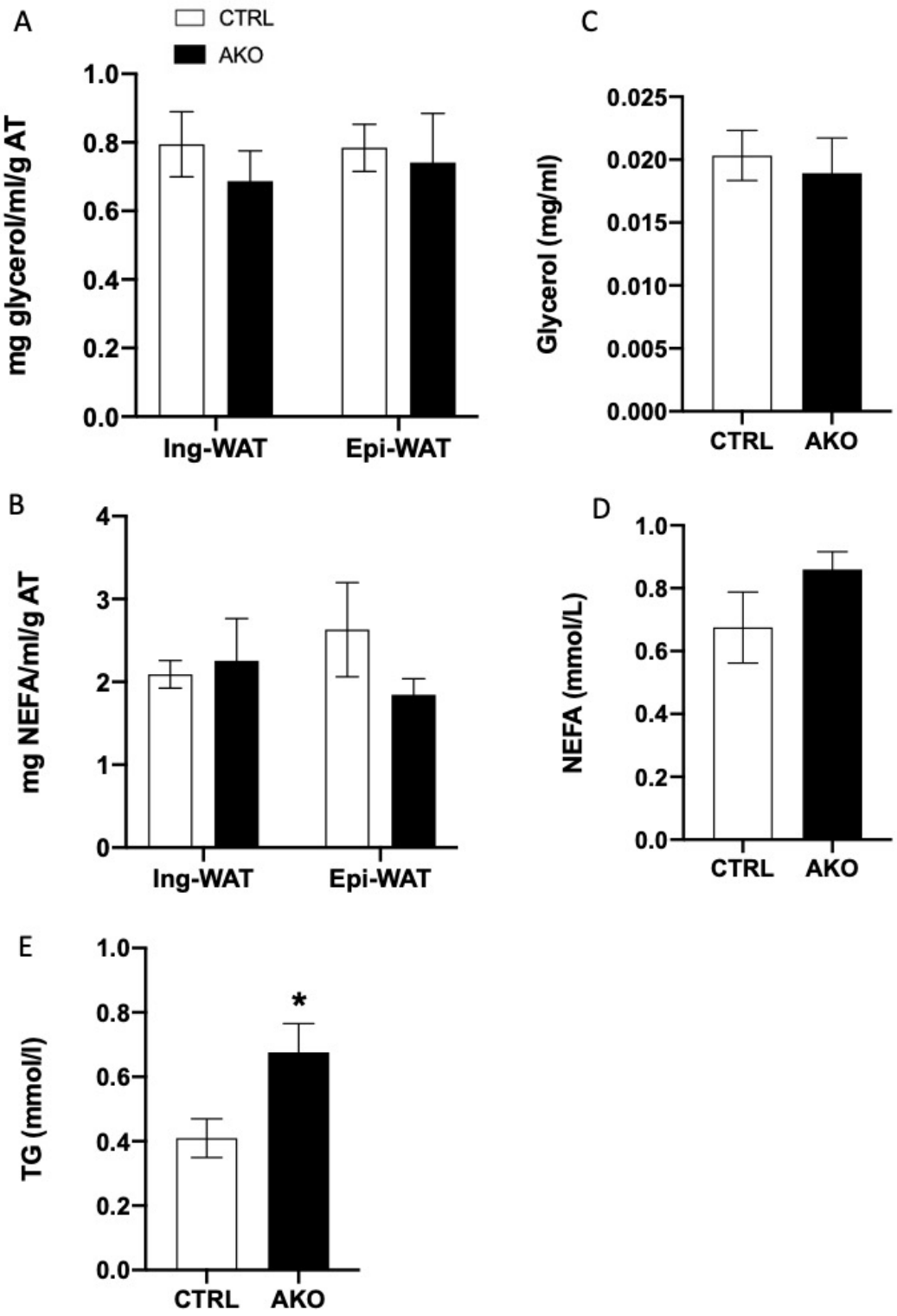

Figure 5-5 Adipocyte-specific SOAT1 knockout (AKO) mice has minimum effect on adipocyte lipolysis.

The mice were sacrificed, WAT ex-vivo lipolysis for 2h and medium is collected to measure glycerol in A and NEFA in B. C, Serum glycerol level. D, Serum NEFA level. E, Serum TG level. Data is presented as Mean ± SEM and analysed by independent t-test, *p<0.05, **p<0.01, ***p<0.001.

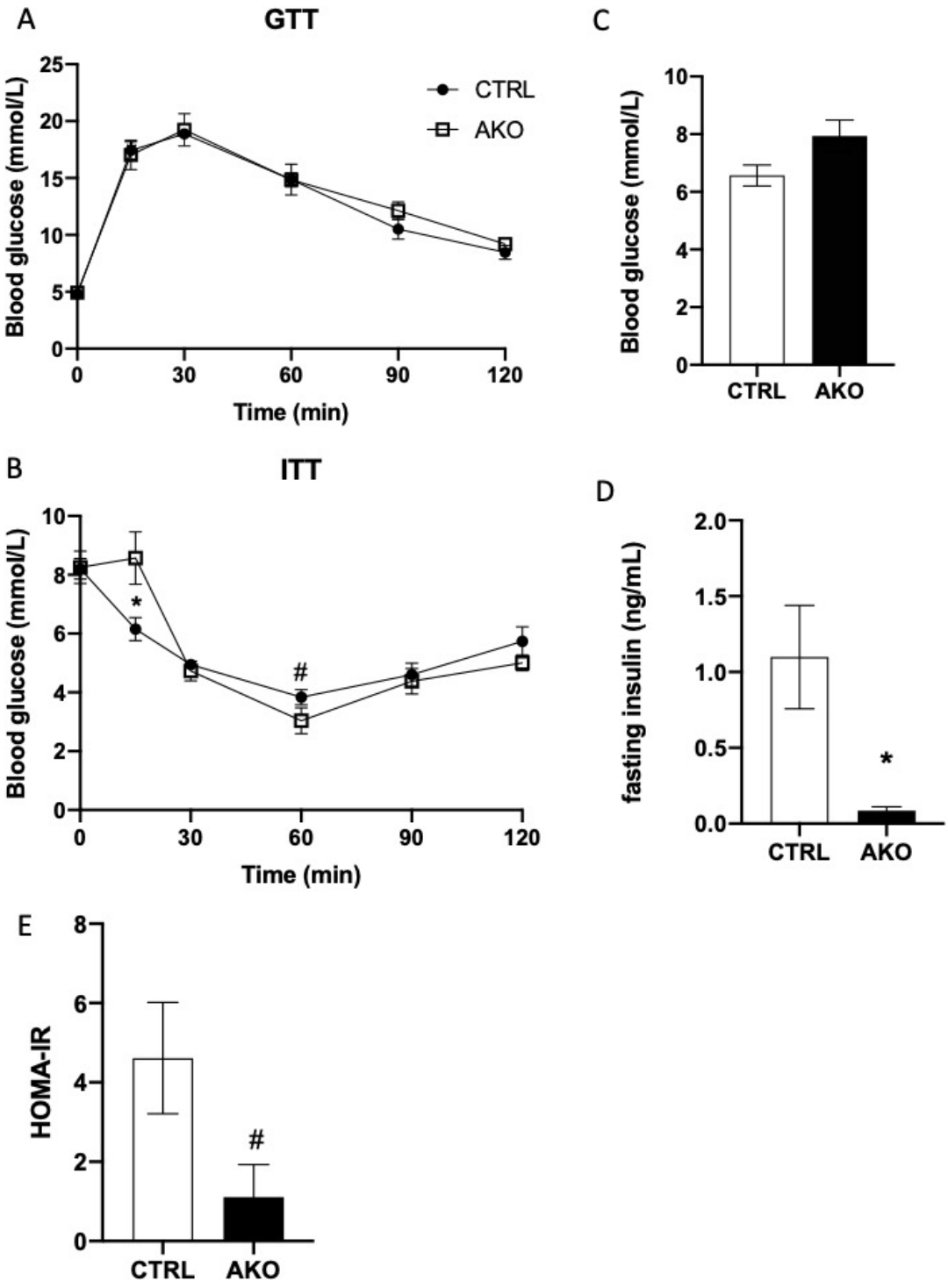
A
GTT
Blood glucose (mmol/L)
Time (min)
CTRL
AKO
B
ITT
Blood glucose (mmol/L)
Time (min)
C
Blood glucose (mmol/L)
CTRL
AKO
D
fasting insulin (ng/mL)
CTRL
AKO
E
HOMA-IR
CTRL
AKO

Figure 5-6 Adipocyte-specific SOAT1 knockout (AKO) mice has minimum effect on glucose homeostasis.

A, The blood glucose level of CTRL and AKO mice after i.p. injection glucose for glucose tolerance tests (GTT). B, The blood glucose level of CTRL and AKO mice after i.p. injection insulin for insulin tolerance tests (ITT). C, Fasting serum blood glucose level of CTRL and AKO mice. D, Fasting serum insulin level of CTRL and AKO mice. E, The HOMA-IR was calculated according to the equation shown in the Materials and Methods section. Data is presented as Mean ± SEM and analysed by independent t-test, #$p<0.1$, *$p<0.05$, **$p<0.01$, ***$p<0.001$.

Chapter 6 FUTURE WORK

6.1 The role of SOAT1 in regulating cholesterol distribution

We found that KD SOAT1 in adipocytes leads to altered cholesterol distribution, suppressing SREBP2 maturation and multiple cholesterol trafficking genes. Similarly, other research groups have observed that SOAT1 KO in NPC1 mutant fibroblasts increases cholesterol content in trans-Golgi-rich membranes and mitochondria, while decreasing cholesterol content in late endosomes or lysosomes [276]. How does SOAT1 KO affect cholesterol content in multiple organelles? It is hypothesized that since SOAT1 is located in the ER and the mitochondrial-associated membrane (MAM) region [148], KO of SOAT1 may redirect the cholesterol storage pool to other organelles through various membrane contacts. Multiple diseases, such as Niemann-Pick disease type C [277], hypolipidemia [278], and Smith-Lemli-Opitz syndrome [279], are associated with cholesterol deficiency in cell membranes. Regarding future directions, one potential therapeutic approach for these diseases is to target SOAT1 in order to influence cholesterol distribution and promote the accumulation of FC in the deficient cholesterol compartments.

6.2 Dietary effect of SOAT1 in adipocyte in vivo

We observed that KO of SOAT1 in adipocytes in vivo promotes energy expenditure and significantly increases UCP1 mRNA levels in iWAT in mice fed a HFD. UCP1 forms a proton channel in the inner mitochondrial membrane (IMM), allowing dissipation of the proton gradient and resulting in heat generation. How does SOAT1 KO influence mitochondrial function, and why does the difference in energy expenditure occur specifically in HCD feeding? Previous studies have indicated that cholesterol overload in late endosomes/lysosomes leads to cholesterol accumulation in the IMM [280]. Another study found that the mitochondria-associated membrane (MAM) region, rich in cholesterol and sphingolipids, facilitates direct supply of calcium ions (Ca^{2+}) from the ER to mitochondria, promoting ATP synthesis [218]. SOAT1 inhibition has been

shown to increase ER-mitochondrial contact sites and strengthen their connectivity [219]. This suggests that the increased FC in the MAM region may enhance their connection and improve mitochondrial function. Further investigation is needed to explore the relationship between SOAT1 KO and mitochondrial function under conditions of cholesterol overload.

We found that SOAT1 KO in adipocytes leads to increased TG levels in the liver under HCD feeding, while decreased TG levels were observed under HFHC feeding (Figure 6-1 A). How does the liver-adipose tissue crosstalk exhibit different responses under varying dietary conditions? Previous studies have shown that rats fed a HCD exhibit increased hepatic TG levels due to suppressed fatty acid beta-oxidation [281]. Fuakda et al. demonstrated that suppression of fatty acid beta-oxidation may contribute to the conversion of fatty acids into TGs and cholesterol esters [282]. One hypothesis is that under HCD conditions, SOAT1 KO induces enhanced fatty acid oxidation in the liver, leading to increased TG levels. Interestingly, we also observed enhanced lipolysis in iWAT of SOAT1 KO mice under HCD feeding conditions. Another hypothesis is that the liver may uptake more free fatty acids (FFAs) from circulation in SOAT1 KO mice, leading to increased TG levels. In contrast, we observed decreased liver TG levels but heart hypertrophy in SOAT1 KO mice under HFHC feeding conditions. The concept that dietary cholesterol levels increase CVD diseases has been discussed since 1968 [283, 284], yet multiple studies have demonstrated no strong relationship between them [285]. It is worth noting that diets rich in both cholesterol and saturated fatty acids (SFA) may increase the risk of CVD due to their SFA content [286]. This raises two possibilities: first, adipose tissue in SOAT1 KO mice may secrete specific lipid species into the bloodstream, inhibiting TG synthesis in the liver while promoting heart hypertrophy. Further lipidomic analysis could shed light on this hypothesis. Second, SOAT1 may play a protective role in pericardial fat and exert its functions in the context of a HFHC (high CVD risk) diet.

6.3 The lipid profile changed in iWAT by SOAT1 KO

We found SOAT1 KO induces browning of iWAT, while fat mass remains unchanged during HCD feeding. Previous studies have shown that cold exposure activates gene programs associated with glycerolipid and glycerophospholipid metabolism, as well as fatty acid elongation in BAT. Cold stimulus leads to an increase in long-chain and odd-numbered acyl chains in TAG [287]. Another recent study demonstrated that the absence of IFI27 in adipocytes promotes thermogenesis and alters the composition of TAG and glycerophospholipid species [236]. How does the composition and distribution of TAG and glycerophospholipid species change in iWAT? Can SOAT1 deficiency in adipocytes induce alterations in the composition of specific lipid classes or remodeling of acyl chain composition? We performed analysis of genes related to fatty acid elongation and glycerophospholipid metabolism, but no significant differences were observed between the CTRL and AKO groups (Figure 6-1 B). For future directions, we can employ mass spectrometry-based lipidomic analysis to investigate if peroxisomal alpha and beta-oxidation of long-chain fatty acids are enhanced in the AKO group, and determine the extent to which this contributes to heat production. We are particularly interested in studying the composition of cardiolipin (CL), a dimeric phospholipid that constitutes approximately 20% of the inner mitochondrial membrane and 3% of the outer mitochondrial membrane. CL composition is closely correlated with thermogenesis and mitochondrial function [288].

6.4 The BAT function in SOAT1 regulation

We observed that only iWAT showed a significant improvement in UCP1 mRNA levels, while there was no significant change in expression observed in eWAT or BAT. Previous studies have indicated that subcutaneous adipose depots, such as iWAT, are more responsive to acquiring BAT characteristics compared to visceral depots like eWAT [289]. BAT is known for its high metabolic activity and role in thermogenesis and heat production. Therefore, it is intriguing to understand why BAT does not respond to SOAT1 knockout (KO). There are two possible explanations. Firstly, it is possible

that the adipocyte-specific KO of SOAT1 in BAT was either not achieved or had minimal impact. Since the expression of adiponectin in WAT is much higher than in BAT, and we utilized adiponectin-Cre mice for the knockout, which may not have efficient KO efficiency in BAT. In future studies, we can employ UCP1-Cre mice to investigate the function of SOAT1 specifically in BAT. Secondly, it is plausible that SOAT1 is knocked out in BAT, but the thermogenic activity observed in the SOAT1 knockout mice under room temperature may be mediated by other factors. Previous research has shown that the upregulation of numerous genes in WAT is primarily attributed to long-term remodeling effects rather than immediate transcriptional events [244]. Beige adipocytes, in particular, are short-lived and easily revert back to normal adipocytes after the removal of external stimuli [290]. In our study, we subjected the mice to long-term HCD treatment for up to 21 weeks without any additional external stimuli. This prolonged treatment may induce remodeling of genes involved in controlling beige cell biogenesis. To understand this remodeling process, we can treat the mice with HCD for different durations, such as 3 days, 1 week, or 12 weeks, to compare the effects with long-term treatment and identify key factors involved.

6.5 The role of SOAT1 and SOAT2 in adipocyte in vivo

We observed that KO of SOAT1 in adipocytes promotes an increase in WAT mass in mice fed a ND, as well as in 8-week-old mice (Figure 5-3B). However, it remains unclear whether SOAT1 deficiency in adipocytes affects the processes of hypertrophy or hyperplasia. For future directions, we can utilize the "Adipochaser" lineage tracing system [291] to investigate this further. It should be noted that global KO of SOAT1 in mice leads to a short lifespan with detrimental consequences [103]. On the other hand, global KO of SOAT2 decreases cholesterol absorption and provides some protection against atherosclerosis [192]. Although SOAT2 is primarily expressed in the intestine and liver, we observed a significant 10-fold increase in its mRNA level in mature adipocytes of DIO mice compared to lean mice (Figure S2-1C). This suggests that SOAT2 might also play a crucial role in obesity. For future investigations, we can

employ SOAT2 KO in adipocytes and study the effects of SOAT1/SOAT2 double KO in adipocytes to further understand the role of cholesterol esterification in regulating adipose tissue expansion.

6.6 The Clinical implication of the observations

In our study, we found that knockdown of SOAT1 in adipocytes led to altered cholesterol distribution and inhibited the SREBP2 maturation process. TY Chang research group had found SOAT1 was localized within the ER and the mitochondrial-associated membrane area [219]. Another group found KO SOAT1 in NPC1 mutant fibroblasts increases cholesterol content in trans-Golgi-rich membranes and mitochondria, while decreasing cholesterol content in late endosomes or lysosomes [276]. It is hypothesis that knockdown of SOAT1 may redirect the cholesterol storage pool to other organelles through various membrane contacts. Multiple diseases, such as Niemann-Pick disease type C [277], hypolipidemia [278], are associated with cholesterol deficiency in cell membranes. Targeting SOAT1 may alter cholesterol distribution within cells and serve as a potential target to treat these diseases.

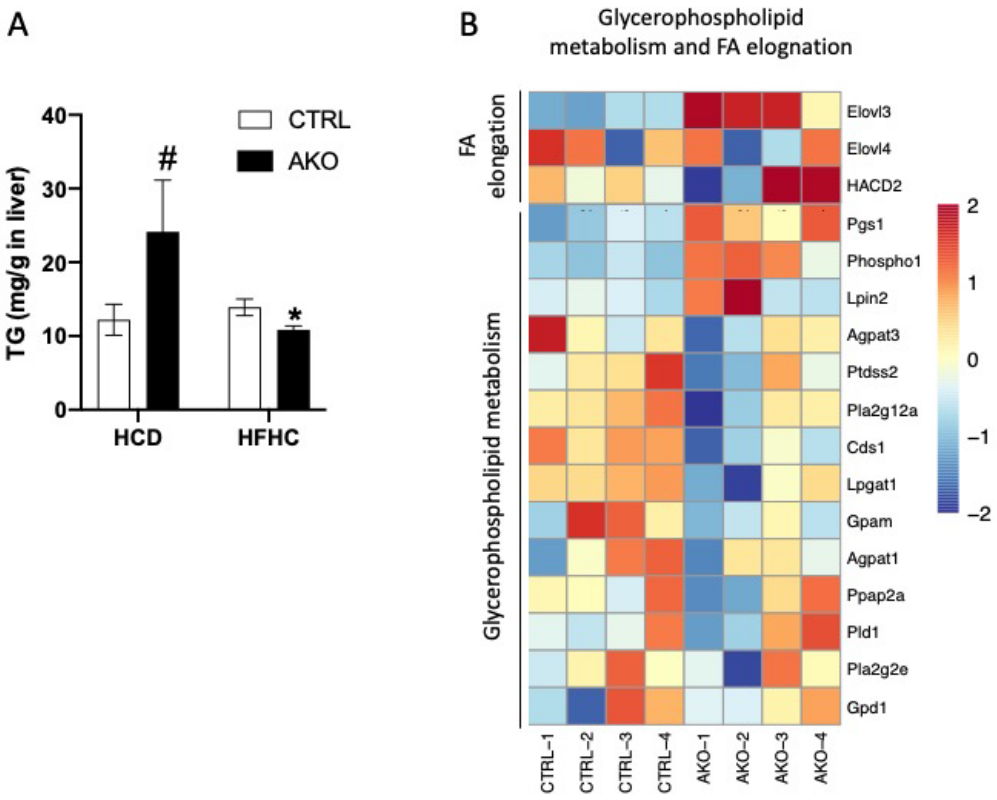

Figure 6-1 For future direction

(A) TG level in liver of HCD and HFHC mice in both CTRL and AKO group. (B) Heatmap analysis of glycerophospholipid metabolism and FA elongation relevant gene in CTRL and AKO group of HCD feeding. Data are shown as mean ± SEM. Data was analyzed by independent t-test, *p<0.05.

Reference

1. Zeng, Q., et al., *Clinical management and treatment of obesity in China.* Lancet Diabetes Endocrinol, 2021. **9**(6): p. 393-405.
2. Zhao, N., et al., *Global obesity research trends during 1999 to 2017: A bibliometric analysis.* Medicine (Baltimore), 2019. **98**(4): p. e14132.
3. Mu, L., et al., *Obesity Prevalence and Risks Among Chinese Adults: Findings From the China PEACE Million Persons Project, 2014-2018.* Circ Cardiovasc Qual Outcomes, 2021. **14**(6): p. e007292.
4. Ma, R.C.W., *Epidemiology of diabetes and diabetic complications in China.* Diabetologia, 2018. **61**(6): p. 1249-1260.
5. Mohammed, M.S., et al., *Systems and WBANs for Controlling Obesity.* J Healthc Eng, 2018. **2018**: p. 1564748.
6. Zhao, X., et al., *The crucial role and mechanism of insulin resistance in metabolic disease.* Front Endocrinol (Lausanne), 2023. **14**: p. 1149239.
7. Bertran, L., et al., *Expression of STING in Women with Morbid Obesity and Nonalcoholic Fatty Liver Disease.* Metabolites, 2023. **13**(4).
8. Lin, H., et al., *Association of genetic variations with NAFLD in lean individuals.* Liver Int, 2022. **42**(1): p. 149-160.
9. Khiyami, A., et al., *IGF-1 is positively associated with BMI in patients with acromegaly.* Pituitary, 2023.
10. Rabijewski, M., *Male-specific consequences of obesity - functional hypogonadism and fertility disorders.* Endokrynol Pol, 2023.
11. Ruban, A., et al., *Current treatments for obesity.* Clin Med (Lond), 2019. **19**(3): p. 205-212.
12. Redondo-Puente, M., et al., *Appetite and Satiety Effects of the Acute and Regular Consumption of Green Coffee Phenols and Green Coffee Phenol/Oat beta-Glucan Nutraceuticals in Subjects with Overweight and Obesity.* Foods, 2021. **10**(11).
13. Lafferty, R.A., P.R. Flatt, and N. Irwin, *GLP-1/GIP analogs: potential impact in the landscape of obesity pharmacotherapy.* Expert Opinion on Pharmacotherapy, 2023. **24**(5): p. 587-597.
14. Wang, J.Y., et al., *GLP-1 receptor agonists for the treatment of obesity: Role as a promising approach.* Front Endocrinol (Lausanne), 2023. **14**: p. 1085799.
15. Tsankof, A., et al., *Which is the optimal antiobesity agent for patients with nonalcoholic fatty liver disease?* Frontiers in Endocrinology, 2022. **13**.
16. Wen, X., et al., *Signaling pathways in obesity: mechanisms and therapeutic interventions.* Signal Transduct Target Ther, 2022. **7**(1): p. 298.
17. Berry, D.C., et al., *The developmental origins of adipose tissue.* Development, 2013. **140**(19): p. 3939-49.
18. Letexier, D., et al., *Comparison of the expression and activity of the lipogenic pathway in human and rat adipose tissue.* J Lipid Res, 2003. **44**(11): p. 2127-34.
19. Vijayakumar, A., et al., *Absence of Carbohydrate Response Element Binding Protein in Adipocytes Causes Systemic Insulin Resistance and Impairs Glucose Transport.* Cell Rep, 2017. **21**(4): p. 1021-1035.
20. Shimano, H., et al., *Elevated levels of SREBP-2 and cholesterol synthesis in livers of mice homozygous for a targeted disruption of the SREBP-1 gene.* J Clin Invest, 1997. **100**(8): p. 2115-24.

21. Danielli, M., et al., *Lipid droplets and polyunsaturated fatty acid trafficking: Balancing life and death.* Frontiers in Cell and Developmental Biology, 2023. **11**.
22. Czaja-Stolc, S., et al., *Pro-Inflammatory Profile of Adipokines in Obesity Contributes to Pathogenesis, Nutritional Disorders, and Cardiovascular Risk in Chronic Kidney Disease.* Nutrients, 2022. **14**(7).
23. Hammarstedt, A., et al., *WISP2 regulates preadipocyte commitment and PPARgamma activation by BMP4.* Proc Natl Acad Sci U S A, 2013. **110**(7): p. 2563-8.
24. Thompson, S.J., et al., *Hepatocytes Are the Principal Source of Circulating RBP4 in Mice.* Diabetes, 2017. **66**(1): p. 58-63.
25. Loskutoff, D.J. and F. Samad, *The adipocyte and hemostatic balance in obesity: studies of PAI-1.* Arterioscler Thromb Vasc Biol, 1998. **18**(1): p. 1-6.
26. Bergmann, K. and G. Sypniewska, *Diabetes as a complication of adipose tissue dysfunction. Is there a role for potential new biomarkers?* Clin Chem Lab Med, 2013. **51**(1): p. 177-85.
27. Galley, J.C., et al., *Adipokines: Deciphering the cardiovascular signature of adipose tissue.* Biochemical Pharmacology, 2022. **206**.
28. ELMeneza, S.A.N., I.M.S. El Bagoury, and K.E. Mohamed, *Role of Serum Apelin in the Diagnosis of Early-Onset Neonatal Sepsis.* Turkish Archives of Pediatrics, 2021. **56**(6): p. 563-568.
29. Sat-Munoz, D., et al., *Adipocytokines and Insulin Resistance: Their Role as Benign Breast Disease and Breast Cancer Risk Factors in a High-Prevalence Overweight-Obesity Group of Women over 40 Years Old.* International Journal of Environmental Research and Public Health, 2022. **19**(10).
30. Gao, J.H., et al., *Visceral adipose tissue-derived serine protease inhibitor accelerates cholesterol efflux by up-regulating ABCA1 expression via the NF-kappaB/miR-33a pathway in THP-1 macropahge-derived foam cells.* Biochem Biophys Res Commun, 2018. **500**(2): p. 318-324.
31. Wang, Y., *Small lipid-binding proteins in regulating endothelial and vascular functions: focusing on adipocyte fatty acid binding protein and lipocalin-2.* Br J Pharmacol, 2012. **165**(3): p. 603-21.
32. Kukla, M., et al., *Potential role of leptin, adiponectin and three novel adipokines--visfatin, chemerin and vaspin--in chronic hepatitis.* Mol Med, 2011. **17**(11-12): p. 1397-410.
33. Song, N.J., et al., *Small Molecule-Induced Complement Factor D (Adipsin) Promotes Lipid Accumulation and Adipocyte Differentiation.* PLoS One, 2016. **11**(9): p. e0162228.
34. Zhang, Y., et al., *Positional cloning of the mouse obese gene and its human homologue.* Nature, 1994. **372**(6505): p. 425-32.
35. Turer, A.T. and P.E. Scherer, *Adiponectin: mechanistic insights and clinical implications.* Diabetologia, 2012. **55**(9): p. 2319-26.
36. Kadowaki, T., et al., *Adiponectin and adiponectin receptors in insulin resistance, diabetes, and the metabolic syndrome.* J Clin Invest, 2006. **116**(7): p. 1784-92.
37. Munitz, A., et al., *Resistin-like molecule alpha decreases glucose tolerance during intestinal inflammation.* J Immunol, 2009. **182**(4): p. 2357-63.
38. Taouis, M. and Y. Benomar, *Is resistin the master link between inflammation and inflammation-related chronic diseases?* Mol Cell Endocrinol, 2021. **533**: p. 111341.

39. Wang, Q.A., et al., *Tracking adipogenesis during white adipose tissue development, expansion and regeneration.* Nat Med, 2013. **19**(10): p. 1338-44.
40. Richard, A.J., et al., *Adipose Tissue: Physiology to Metabolic Dysfunction*, in *Endotext*, K.R. Feingold, et al., Editors. 2000: South Dartmouth (MA).
41. He, W., et al., *Adipose-specific peroxisome proliferator-activated receptor gamma knockout causes insulin resistance in fat and liver but not in muscle.* Proc Natl Acad Sci U S A, 2003. **100**(26): p. 15712-7.
42. Barroso, I., et al., *Dominant negative mutations in human PPARgamma associated with severe insulin resistance, diabetes mellitus and hypertension.* Nature, 1999. **402**(6764): p. 880-3.
43. Cao, Z., R.M. Umek, and S.L. McKnight, *Regulated expression of three C/EBP isoforms during adipose conversion of 3T3-L1 cells.* Genes Dev, 1991. **5**(9): p. 1538-52.
44. Mota de Sa, P., et al., *Transcriptional Regulation of Adipogenesis.* Compr Physiol, 2017. **7**(2): p. 635-674.
45. Christodoulides, C., et al., *Adipogenesis and WNT signalling.* Trends Endocrinol Metab, 2009. **20**(1): p. 16-24.
46. Al-Jaber, H., L. Al-Mansoori, and M.A. Elrayess, *GATA-3 as a Potential Therapeutic Target for Insulin Resistance and Type 2 Diabetes Mellitus.* Curr Diabetes Rev, 2021. **17**(2): p. 169-179.
47. Jiang, N., et al., *Cytokines and inflammation in adipogenesis: an updated review.* Front Med, 2019. **13**(3): p. 314-329.
48. Muir, L.A., et al., *Adipose tissue fibrosis, hypertrophy, and hyperplasia: Correlations with diabetes in human obesity.* Obesity (Silver Spring), 2016. **24**(3): p. 597-605.
49. Chen, T., et al., *MiR-27a promotes insulin resistance and mediates glucose metabolism by targeting PPAR-gamma-mediated PI3K/AKT signaling.* Aging (Albany NY), 2019. **11**(18): p. 7510-7524.
50. Dai, H.B., et al., *Adrenomedullin ameliorates palmitic acid-induced insulin resistance through PI3K/Akt pathway in adipocytes.* Acta Diabetol, 2022. **59**(5): p. 661-673.
51. Hill, J.W., et al., *Acute effects of leptin require PI3K signaling in hypothalamic proopiomelanocortin neurons in mice.* J Clin Invest, 2008. **118**(5): p. 1796-805.
52. Cota, D., et al., *Hypothalamic mTOR signaling regulates food intake.* Science, 2006. **312**(5775): p. 927-30.
53. Yang, S.B., et al., *Rapamycin ameliorates age-dependent obesity associated with increased mTOR signaling in hypothalamic POMC neurons.* Neuron, 2012. **75**(3): p. 425-36.
54. Bost, F., et al., *The role of MAPKs in adipocyte differentiation and obesity.* Biochimie, 2005. **87**(1): p. 51-6.
55. Bost, F., et al., *The extracellular signal-regulated kinase isoform ERK1 is specifically required for in vitro and in vivo adipogenesis.* Diabetes, 2005. **54**(2): p. 402-11.
56. Engelman, J.A., M.P. Lisanti, and P.E. Scherer, *Specific inhibitors of p38 mitogen-activated protein kinase block 3T3-L1 adipogenesis.* J Biol Chem, 1998. **273**(48): p. 32111-20.
57. Aouadi, M., et al., *p38MAP Kinase activity is required for human primary adipocyte differentiation.* FEBS Lett, 2007. **581**(29): p. 5591-6.
58. Solinas, G. and B. Becattini, *JNK at the crossroad of obesity, insulin resistance, and cell stress response.* Mol Metab, 2017. **6**(2): p. 174-184.

59. Lee, S. and M. Lee, *MEK6 Overexpression Exacerbates Fat Accumulation and Inflammatory Cytokines in High-Fat Diet-Induced Obesity.* Int J Mol Sci, 2021. **22**(24).
60. Chung, S. and J.S. Parks, *Dietary cholesterol effects on adipose tissue inflammation.* Curr Opin Lipidol, 2016. **27**(1): p. 19-25.
61. Coelho, M., T. Oliveira, and R. Fernandes, *Biochemistry of adipose tissue: an endocrine organ.* Arch Med Sci, 2013. **9**(2): p. 191-200.
62. Busto, R., J. Sanchez-Wandelmer, and M.A. Lasuncion, *Inhibition of cholesterol biosynthesis prevents adipocyte differentiation.* Atherosclerosis Supplements, 2006. **7**(3): p. 186-187.
63. Prattes, S., et al., *Intracellular distribution and mobilization of unesterified cholesterol in adipocytes.* Molecular Biology of the Cell, 2000. **11**: p. 109a-110a.
64. Tabas, I., *Consequences of cellular cholesterol accumulation: basic concepts and physiological implications.* Journal of Clinical Investigation, 2002. **110**(7): p. 905-911.
65. Yang, L., et al., *Human acyl-coenzyme A:cholesterol acyltransferase 1 (acat1) sequences located in two different chromosomes (7 and 1) are required to produce a novel ACAT1 isoenzyme with additional sequence at the N terminus.* J Biol Chem, 2004. **279**(44): p. 46253-62.
66. Chang, T.Y., et al., *Neuronal Cholesterol Esterification by ACAT1 in Alzheimer's Disease.* Iubmb Life, 2010. **62**(4): p. 261-267.
67. Henriksbo, B.D., et al., *Statins Promote Interleukin-1 beta-Dependent Adipocyte Insulin Resistance Through Lower Prenylation, Not Cholesterol.* Diabetes, 2019. **68**(7): p. 1441-1448.
68. Morton, R.E. and Y. Liu, *The lipid transfer properties of CETP define the concentration and composition of plasma lipoproteins.* J Lipid Res, 2020. **61**(8): p. 1168-1179.
69. Gauthier, A., et al., *Cholesteryl ester transfer protein directly mediates selective uptake of high density lipoprotein cholesteryl esters by the liver.* Arterioscler Thromb Vasc Biol, 2005. **25**(10): p. 2177-84.
70. Casquero, A.C., et al., *Chronic Exercise Reduces CETP and Mesterolone Treatment Counteracts Exercise Benefits on Plasma Lipoproteins Profile: Studies in Transgenic Mice.* Lipids, 2017. **52**(12): p. 981-990.
71. Shimada, A., et al., *Serum CETP status is independently associated with reduction rates in LDL-C in pitavastatin-treated diabetic patients and possible involvement of LXR in its association.* Lipids Health Dis, 2016. **15**: p. 57.
72. Izem, L. and R.E. Morton, *Cholesteryl ester transfer protein biosynthesis and cellular cholesterol homeostasis are tightly interconnected.* Journal of Biological Chemistry, 2001. **276**(28): p. 26534-26541.
73. Marchi, C., et al., *ABCA1- and ABCG1-mediated cholesterol efflux capacity of cerebrospinal fluid is impaired in Alzheimer's disease.* J Lipid Res, 2019. **60**(8): p. 1449-1456.
74. Shi, Y., et al., *Celastrol suppresses lipid accumulation through LXRalpha/ABCA1 signaling pathway and autophagy in vascular smooth muscle cells.* Biochem Biophys Res Commun, 2020. **532**(3): p. 466-474.
75. de Haan, W., et al., *ABCA1 in adipocytes regulates adipose tissue lipid content, glucose tolerance, and insulin sensitivity.* Journal of Lipid Research, 2014. **55**(3): p. 516-523.
76. Karasinska, J.M., et al., *Specific Loss of Brain ABCA1 Increases Brain Cholesterol Uptake and Influences Neuronal Structure and Function.* Journal of Neuroscience, 2009. **29**(11): p. 3579-3589.

77. Chung, S., et al., *Adipose Tissue ATP Binding Cassette Transporter A1 Contributes to High-Density Lipoprotein Biogenesis In Vivo.* Circulation, 2011. **124**(15): p. 1663-U158.
78. Beyea, M.M., et al., *Selective up-regulation of LXR sensitive genes, ABCA1, ABCG1 and APOE, in THP-1 macrophages through partial inhibition of oxidosqualene: Lanosterol cyclase: Implications for attenuation of foam cell formation.* Arteriosclerosis Thrombosis and Vascular Biology, 2005. **25**(5): p. E54-E54.
79. Delvecchio, C.J., et al., *LXR-induced reverse cholesterol transport in human airway smooth muscle is mediated exclusively by ABCA1.* Am J Physiol Lung Cell Mol Physiol, 2008. **295**(5): p. L949-57.
80. Gui, Y.Z., et al., *Betulin attenuates atherosclerosis in apoE(-/-) mice by up-regulating ABCA1 and ABCG1.* Acta Pharmacol Sin, 2016. **37**(10): p. 1337-1348.
81. Ananth, S., et al., *Regulation of the cholesterol efflux transporters ABCA1 and ABCG1 in retina in hemochromatosis and by the endogenous siderophore 2,5-dihydroxybenzoic acid.* Biochim Biophys Acta, 2014. **1842**(4): p. 603-12.
82. Ranalletta, M., et al., *Decreased atherosclerosis in low-density lipoprotein receptor knockout mice transplanted with Abcg1-/- bone marrow.* Arterioscler Thromb Vasc Biol, 2006. **26**(10): p. 2308-15.
83. Murphy, A.J. and L. Yvan-Charvet, *Adipose Modulation of ABCG1 Uncovers an Intimate Link Between Sphingomyelin and Triglyceride Storage.* Diabetes, 2015. **64**(3): p. 689-692.
84. Vazquez, M.M., et al., *Nitro-oleic acid, a ligand of CD36, reduces cholesterol accumulation by modulating oxidized-LDL uptake and cholesterol efflux in RAW264.7 macrophages.* Redox Biol, 2020. **36**: p. 101591.
85. Ehehalt, R., et al., *Uptake of long chain fatty acids is regulated by dynamic interaction of FAT/CD36 with cholesterol/sphingolipid enriched microdomains (lipid rafts).* BMC Cell Biol, 2008. **9**: p. 45.
86. Nassir, F., et al., *CD36 is important for fatty acid and cholesterol uptake by the proximal but not distal intestine.* J Biol Chem, 2007. **282**(27): p. 19493-501.
87. Rubic, T. and R.L. Lorenz, *Downregulated CD36 and oxLDL uptake and stimulated ABCA1/G1 and cholesterol efflux as anti-atherosclerotic mechanisms of interleukin-10.* Cardiovasc Res, 2006. **69**(2): p. 527-35.
88. Fernando, S., et al., *Eukaryotic elongation factor 2 kinase regulates foam cell formation via translation of CD36.* FASEB J, 2022. **36**(2): p. e22154.
89. Zhao, L., et al., *CD36 and lipid metabolism in the evolution of atherosclerosis.* Br Med Bull, 2018. **126**(1): p. 101-112.
90. Cui, Y., et al., *Moxibustion at CV4 alleviates atherosclerotic lesions through activation of the LXRalpha/ABCA1 pathway in apolipoprotein-E-deficient mice.* Acupunct Med, 2019. **37**(4): p. 237-243.
91. Grandl, M., et al., *E-LDL and Ox-LDL differentially regulate ceramide and cholesterol raft microdomains in human Macrophages.* Cytometry A, 2006. **69**(3): p. 189-91.
92. Onat, T., et al., *The Relationship Between Heavy Metal Exposure, Trace Element Level, and Monocyte to HDL Cholesterol Ratio with Gestational Diabetes Mellitus.* Biol Trace Elem Res, 2021. **199**(4): p. 1306-1315.

93. Hunjadi, M., et al., *HDL cholesterol efflux capacity is inversely associated with subclinical cardiovascular risk markers in young adults: The cardiovascular risk in Young Finns study.* Sci Rep, 2020. **10**(1): p. 19223.
94. Yu, B.L., S.P. Zhao, and J.R. Hu, *Cholesterol imbalance in adipocytes: a possible mechanism of adipocytes dysfunction in obesity.* Obes Rev, 2010. **11**(8): p. 560-7.
95. Chung, S., et al., *Dietary cholesterol promotes adipocyte hypertrophy and adipose tissue inflammation in visceral, but not in subcutaneous, fat in monkeys.* Arterioscler Thromb Vasc Biol, 2014. **34**(9): p. 1880-7.
96. Subramanian, S., et al., *Dietary cholesterol worsens adipose tissue macrophage accumulation and atherosclerosis in obese LDL receptor-deficient mice.* Arterioscler Thromb Vasc Biol, 2008. **28**(4): p. 685-91.
97. Ichimura, M., et al., *High-fat and high-cholesterol diet rapidly induces non-alcoholic steatohepatitis with advanced fibrosis in Sprague-Dawley rats.* Hepatol Res, 2015. **45**(4): p. 458-69.
98. Henriksbo, B.D., et al., *Statins Promote Interleukin-1beta-Dependent Adipocyte Insulin Resistance Through Lower Prenylation, Not Cholesterol.* Diabetes, 2019. **68**(7): p. 1441-1448.
99. Le Lay, S., P. Ferre, and I. Dugail, *Adipocyte cholesterol balance in obesity.* Biochem Soc Trans, 2004. **32**(Pt 1): p. 103-6.
100. Xu, Y.Q., et al., *Enhanced acyl-CoA: cholesterol acyltransferase activity increases cholesterol levels on the lipid droplet surface and impairs adipocyte function.* Journal of Biological Chemistry, 2019. **294**(50): p. 19306-19321.
101. Guerre-Millo, M., et al., *Alteration in membrane lipid order and composition in metabolically hyperactive fatty rat adipocytes.* Lipids, 1994. **29**(3): p. 205-209.
102. Chang, C.C., et al., *Molecular cloning and functional expression of human acyl-coenzyme A:cholesterol acyltransferase cDNA in mutant Chinese hamster ovary cells.* J Biol Chem, 1993. **268**(28): p. 20747-55.
103. Meiner, V.L., et al., *Disruption of the acyl-CoA:cholesterol acyltransferase gene in mice: evidence suggesting multiple cholesterol esterification enzymes in mammals.* Proc Natl Acad Sci U S A, 1996. **93**(24): p. 14041-6.
104. Qian, H., et al., *Structural basis for catalysis and substrate specificity of human ACAT1.* Nature, 2020. **581**(7808): p. 333-338.
105. Song, B.L., et al., *Correction: Human acyl-CoA:cholesterol acyltransferase 2 gene expression in intestinal Caco-2 cells and in hepatocellular carcinoma.* Biochem J, 2020. **477**(24): p. 4811.
106. Parini, P., et al., *ACAT2 is localized to hepatocytes and is the major cholesterol-esterifying enzyme in human liver.* Circulation, 2004. **110**(14): p. 2017-23.
107. Buhman, K.K., et al., *Resistance to diet-induced hypercholesterolemia and gallstone formation in ACAT2-deficient mice.* Nature Medicine, 2000. **6**(12): p. 1341-1347.
108. Accad, M., et al., *Massive xanthomatosis and altered composition of atherosclerotic lesions in hyperlipidemic mice lacking acyl CoA:cholesterol acyltransferase 1.* J Clin Invest, 2000. **105**(6): p. 711-9.
109. Yagyu, H., et al., *Absence of ACAT-1 attenuates atherosclerosis but causes dry eye and cutaneous xanthomatosis in mice with congenital hyperlipidemia.* J Biol Chem, 2000. **275**(28): p. 21324-30.

110. Huang, L.H., et al., *Myeloid-specific Acat1 ablation attenuates inflammatory responses in macrophages, improves insulin sensitivity, and suppresses diet-induced obesity.* Am J Physiol Endocrinol Metab, 2018. **315**(3): p. E340-E356.
111. Melton, E.M., et al., *Myeloid Acat1/Soat1 KO attenuates pro-inflammatory responses in macrophages and protects against atherosclerosis in a model of advanced lesions.* J Biol Chem, 2019. **294**(43): p. 15836-15849.
112. Willner, E.L., et al., *Deficiency of acyl CoA : cholesterol acyltransferase 2 prevents atherosclerosis in apolipoprotein E-deficient mice.* Proceedings of the National Academy of Sciences of the United States of America, 2003. **100**(3): p. 1262-1267.
113. Zhang, J., et al., *Tissue-specific knockouts of ACAT2 reveal that intestinal depletion is sufficient to prevent diet-induced cholesterol accumulation in the liver and blood.* J Lipid Res, 2012. **53**(6): p. 1144-52.
114. Ikenoya, M., et al., *A selective ACAT-1 inhibitor, K-604, suppresses fatty streak lesions in fat-fed hamsters without affecting plasma cholesterol levels.* Atherosclerosis, 2007. **191**(2): p. 290-7.
115. Rudel, L.L., et al., *Hepatic origin of cholesteryl oleate in coronary artery atherosclerosis in African green monkeys. Enrichment by dietary monounsaturated fat.* J Clin Invest, 1997. **100**(1): p. 74-83.
116. Li, J., et al., *Abrogating cholesterol esterification suppresses growth and metastasis of pancreatic cancer.* Oncogene, 2016. **35**(50): p. 6378-6388.
117. Geng, F., et al., *Inhibition of SOAT1 Suppresses Glioblastoma Growth via Blocking SREBP-1-Mediated Lipogenesis.* Clin Cancer Res, 2016. **22**(21): p. 5337-5348.
118. Zhu, T., et al., *SOAT1 Promotes Gastric Cancer Lymph Node Metastasis Through Lipid Synthesis.* Front Pharmacol, 2021. **12**: p. 769647.
119. Jiang, Y., et al., *Proteomics identifies new therapeutic targets of early-stage hepatocellular carcinoma.* Nature, 2019. **567**(7747): p. 257-261.
120. Zhong, N., et al., *piRNA-6426 increases DNMT3B-mediated SOAT1 methylation and improves heart failure.* Aging (Albany NY), 2022. **14**(6): p. 2678-2694.
121. Yang, W., et al., *Potentiating the antitumour response of CD8(+) T cells by modulating cholesterol metabolism.* Nature, 2016. **531**(7596): p. 651-+.
122. Liu, X., et al., *Sterol-O-acyltransferase-1 has a role in kidney disease associated with diabetes and Alport syndrome.* Kidney Int, 2020. **98**(5): p. 1275-1285.
123. Tian, Y., et al., *ACAT2 Is a Novel Negative Regulator of Pig Intramuscular Preadipocytes Differentiation.* Biomolecules, 2022. **12**(2).
124. Ding, Y., et al., *Honokiol Alleviates High-Fat Diet-Induced Obesity of Mice by Inhibiting Adipogenesis and Promoting White Adipose Tissue Browning.* Animals (Basel), 2021. **11**(6).
125. Zhu, Y., et al., *Pharmacological inhibition of acyl-coenzyme A:cholesterol acyltransferase alleviates obesity and insulin resistance in diet-induced obese mice by regulating food intake.* Metabolism, 2021. **123**: p. 154861.
126. Huang, L.H., et al., *Myeloid Acyl-CoA:Cholesterol Acyltransferase 1 Deficiency Reduces Lesion Macrophage Content and Suppresses Atherosclerosis Progression.* Journal of Biological Chemistry, 2016. **291**(12): p. 6232-6244.
127. Xu, N., et al., *Sterol O-acyltransferase 1 deficiency improves defective insulin signaling in the brains of mice fed a high-fat diet.* Biochem Biophys Res Commun, 2018. **499**(2): p. 105-111.

128. Bezin, J., et al., *GLP-1 Receptor Agonists and the Risk of Thyroid Cancer.* Diabetes Care, 2023. **46**(2): p. 384-390.
129. Kwon, Y.J., et al., *The Effect of Orlistat on Sterol Metabolism in Obese Patients.* Front Endocrinol (Lausanne), 2022. **13**: p. 824269.
130. Chait, A. and L.J. den Hartigh, *Adipose Tissue Distribution, Inflammation and Its Metabolic Consequences, Including Diabetes and Cardiovascular Disease.* Front Cardiovasc Med, 2020. **7**: p. 22.
131. Saad, B., *A Review of the Anti-Obesity Effects of Wild Edible Plants in the Mediterranean Diet and Their Active Compounds: From Traditional Uses to Action Mechanisms and Therapeutic Targets.* Int J Mol Sci, 2023. **24**(16).
132. Arner, P. and K.L. Spalding, *Fat cell turnover in humans.* Biochem Biophys Res Commun, 2010. **396**(1): p. 101-4.
133. Kovanen, P.T., E.A. Nikkila, and T.A. Miettinen, *Regulation of cholesterol synthesis and storage in fat cells.* J Lipid Res, 1975. **16**(3): p. 211-23.
134. Krause, B.R. and A.D. Hartman, *Relationship between cell size, plasma cholesterol and rat adipocyte cholesterol storage.* Biochim Biophys Acta, 1976. **450**(2): p. 197-205.
135. Luo, J., H. Yang, and B.L. Song, *Mechanisms and regulation of cholesterol homeostasis.* Nat Rev Mol Cell Biol, 2020. **21**(4): p. 225-245.
136. Prattes, S., et al., *Intracellular distribution and mobilization of unesterified cholesterol in adipocytes: triglyceride droplets are surrounded by cholesterol-rich ER-like surface layer structures.* J Cell Sci, 2000. **113 (Pt 17)**: p. 2977-89.
137. Guerre-Millo, M., et al., *Alteration in membrane lipid order and composition in metabolically hyperactive fatty rat adipocytes.* Lipids, 1994. **29**(3): p. 205-9.
138. Zhang, Y., et al., *Adipocyte modulation of high-density lipoprotein cholesterol.* Circulation, 2010. **121**(11): p. 1347-55.
139. Cuffe, H., et al., *Targeted Deletion of Adipocyte Abca1 (ATP-Binding Cassette Transporter A1) Impairs Diet-Induced Obesity.* Arterioscler Thromb Vasc Biol, 2018. **38**(4): p. 733-743.
140. Curley, S., et al., *Metabolic Inflammation in Obesity-At the Crossroads between Fatty Acid and Cholesterol Metabolism.* Mol Nutr Food Res, 2021. **65**(1): p. e1900482.
141. Pohl, J., et al., *Long-chain fatty acid uptake into adipocytes depends on lipid raft function.* Biochemistry, 2004. **43**(14): p. 4179-87.
142. Luo, J., H.Y. Yang, and B.L. Song, *Mechanisms and regulation of cholesterol homeostasis.* Nature Reviews Molecular Cell Biology, 2020. **21**(4): p. 225-245.
143. Chang, T.Y., et al., *Acyl-coenzyme A:cholesterol acyltransferases.* Am J Physiol Endocrinol Metab, 2009. **297**(1): p. E1-9.
144. Shibuya, Y., C.C. Chang, and T.Y. Chang, *ACAT1/SOAT1 as a therapeutic target for Alzheimer's disease.* Future Med Chem, 2015. **7**(18): p. 2451-67.
145. Guan, C.C., et al., *Structural insights into the inhibition mechanism of human sterol O-acyltransferase 1 by a competitive inhibitor.* Nature Communications, 2020. **11**(1).
146. Cheng, D., et al., *Activation of acyl-coenzyme A:cholesterol acyltransferase by cholesterol or by oxysterol in a cell-free system.* J Biol Chem, 1995. **270**(2): p. 685-95.
147. Guo, Z.Y., et al., *The active site His-460 of human acyl-coenzyme A:cholesterol acyltransferase 1 resides in a hitherto undisclosed transmembrane domain.* J Biol Chem, 2005. **280**(45): p. 37814-26.

148. Area-Gomez, E., et al., *Upregulated function of mitochondria-associated ER membranes in Alzheimer disease.* EMBO J, 2012. **31**(21): p. 4106-23.
149. Oni, T.E., et al., *SOAT1 promotes mevalonate pathway dependency in pancreatic cancer.* J Exp Med, 2020. **217**(9).
150. Zhu, Y.Y., et al., *In vitro exploration of ACAT contributions to lipid droplet formation during adipogenesis.* Journal of Lipid Research, 2018. **59**(5): p. 820-829.
151. Xu, Y., et al., *Enhanced acyl-CoA:cholesterol acyltransferase activity increases cholesterol levels on the lipid droplet surface and impairs adipocyte function.* J Biol Chem, 2019. **294**(50): p. 19306-19321.
152. Liu, Z.H., et al., *The Dysfunctional MDM2-p53 Axis in Adipocytes Contributes to Aging-Related Metabolic Complications by Induction of Lipodystrophy.* Diabetes, 2018. **67**(11): p. 2397-2409.
153. Wabitsch, M., et al., *Characterization of a human preadipocyte cell strain with high capacity for adipose differentiation.* International Journal of Obesity, 2001. **25**(1): p. 8-15.
154. Zhu, Y., et al., *In vitro exploration of ACAT contributions to lipid droplet formation during adipogenesis.* J Lipid Res, 2018. **59**(5): p. 820-829.
155. Bertolio, R., et al., *Sterol regulatory element binding protein 1 couples mechanical cues and lipid metabolism.* Nature Communications, 2019. **10**.
156. Guerrero-Juarez, C.F., et al., *Single-cell analysis reveals fibroblast heterogeneity and myeloid-derived adipocyte progenitors in murine skin wounds.* Nat Commun, 2019. **10**(1): p. 650.
157. Brovkovych, V., et al., *Removal of Serum Lipids and Lipid-Derived Metabolites to Investigate Breast Cancer Cell Biology.* Proteomics, 2019. **19**(18).
158. Fuchs, A., et al., *Associations Among Adipose Tissue Immunology, Inflammation, Exosomes and Insulin Sensitivity in People With Obesity and Nonalcoholic Fatty Liver Disease.* Gastroenterology, 2021. **161**(3): p. 968-+.
159. Cifarelli, V., et al., *Decreased adipose tissue oxygenation associates with insulin resistance in individuals with obesity.* Journal of Clinical Investigation, 2020. **130**(12): p. 6688-6699.
160. Beals, J.W., et al., *Increased Adipose Tissue Fibrogenesis, Not Impaired Expandability, Is Associated With Nonalcoholic Fatty Liver Disease.* Hepatology, 2021. **74**(3): p. 1287-1299.
161. Shapiro, H., et al., *Adipose Tissue Foam Cells Are Present in Human Obesity.* Journal of Clinical Endocrinology & Metabolism, 2013. **98**(3): p. 1173-1181.
162. Luo, Y.T., et al., *Macrophagic CD146 promotes foam cell formation and retention during atherosclerosis.* Cell Research, 2017. **27**(3): p. 352-372.
163. Zhi, X.H., et al., *AdipoCount: A New Software for Automatic Adipocyte Counting.* Frontiers in Physiology, 2018. **9**.
164. Jin, E.S., A.D. Sherry, and C.R. Malloy, *Metabolism of glycerol, glucose, and lactate in the citric acid cycle prior to incorporation into hepatic acylglycerols.* J Biol Chem, 2013. **288**(20): p. 14488-14496.
165. Lee, J.E., et al., *Transcriptional and Epigenomic Regulation of Adipogenesis.* Molecular and Cellular Biology, 2019. **39**(11).
166. Tontonoz, P. and B.M. Spiegelman, *Fat and beyond: the diverse biology of PPARgamma.* Annu Rev Biochem, 2008. **77**: p. 289-312.
167. Rosen, E.D., *The transcriptional basis of adipocyte development.* Prostaglandins Leukot Essent Fatty Acids, 2005. **73**(1): p. 31-4.

168. Mori, T., et al., *Role of Kruppel-like factor 15 (KLF15) in transcriptional regulation of adipogenesis.* J Biol Chem, 2005. **280**(13): p. 12867-75.
169. Akerblad, P., et al., *Gene expression analysis suggests that EBF-1 and PPARgamma2 induce adipogenesis of NIH-3T3 cells with similar efficiency and kinetics.* Physiol Genomics, 2005. **23**(2): p. 206-16.
170. Tontonoz, P., et al., *ADD1: a novel helix-loop-helix transcription factor associated with adipocyte determination and differentiation.* Mol Cell Biol, 1993. **13**(8): p. 4753-9.
171. Banerjee, S.S., et al., *The Kruppel-like factor KLF2 inhibits peroxisome proliferator-activated receptor-gamma expression and adipogenesis.* J Biol Chem, 2003. **278**(4): p. 2581-4.
172. Jing, E., S. Gesta, and C.R. Kahn, *SIRT2 regulates adipocyte differentiation through FoxO1 acetylation/deacetylation.* Cell Metab, 2007. **6**(2): p. 105-14.
173. Krause, B.R. and A.D. Hartman, *Adipose-Tissue and Cholesterol-Metabolism.* Journal of Lipid Research, 1984. **25**(2): p. 97-110.
174. Little, M.T. and P. Hahn, *Ontogeny of acyl-CoA: cholesterol acyltransferase in rat liver, intestine, and adipose tissue.* Am J Physiol, 1992. **262**(4 Pt 1): p. G599-602.
175. Maekawa, M. and G.D. Fairn, *Complementary probes reveal that phosphatidylserine is required for the proper transbilayer distribution of cholesterol.* Journal of Cell Science, 2015. **128**(7): p. 1422-1433.
176. Zhao, K. and N.D. Ridgway, *Oxysterol-Binding Protein-Related Protein 1L Regulates Cholesterol Egress from the Endo-Lysosomal System.* Cell Rep, 2017. **19**(9): p. 1807-1818.
177. Du, X., et al., *A role for oxysterol-binding protein-related protein 5 in endosomal cholesterol trafficking.* J Cell Biol, 2011. **192**(1): p. 121-35.
178. Olkkonen, V.M. and E. Ikonen, *Cholesterol transport in the late endocytic pathway: Roles of ORP family proteins.* J Steroid Biochem Mol Biol, 2022. **216**: p. 106040.
179. Rodriguez-Agudo, D., et al., *StarD5: an ER stress protein regulates plasma membrane and intracellular cholesterol homeostasis.* J Lipid Res, 2019. **60**(6): p. 1087-1098.
180. Chung, J., et al., *INTRACELLULAR TRANSPORT. PI4P/phosphatidylserine countertransport at ORP5- and ORP8-mediated ER-plasma membrane contacts.* Science, 2015. **349**(6246): p. 428-32.
181. Kennelly, J.P. and P. Tontonoz, *Cholesterol Transport to the Endoplasmic Reticulum.* Cold Spring Harb Perspect Biol, 2023. **15**(2).
182. Naito, T., et al., *Movement of accessible plasma membrane cholesterol by the GRAMD1 lipid transfer protein complex.* Elife, 2019. **8**.
183. Jiang, X.C., et al., *Targeted mutation of plasma phospholipid transfer protein gene markedly reduces high-density lipoprotein levels.* J Clin Invest, 1999. **103**(6): p. 907-14.
184. Oram, J.F., et al., *Phospholipid transfer protein interacts with and stabilizes ATP-binding cassette transporter A1 and enhances cholesterol efflux from cells.* J Biol Chem, 2003. **278**(52): p. 52379-85.
185. Garbarino, J., et al., *STARD4 knockdown in HepG2 cells disrupts cholesterol trafficking associated with the plasma membrane, ER, and ERC.* J Lipid Res, 2012. **53**(12): p. 2716-25.
186. Yue, X., et al., *SREBF2-STARD4 axis confers sorafenib resistance in hepatocellular carcinoma by regulating mitochondrial cholesterol homeostasis.* Cancer Sci, 2023. **114**(2): p. 477-489.
187. Madison, B.B., *Srebp2: A master regulator of sterol and fatty acid synthesis.* J Lipid Res, 2016. **57**(3): p. 333-5.

188. Huber, M.D., et al., *Erlins restrict SREBP activation in the ER and regulate cellular cholesterol homeostasis.* J Cell Biol, 2013. **203**(3): p. 427-36.
189. Chakraborty, S., et al., *CD10 marks non-canonical PPARgamma-independent adipocyte maturation and browning potential of adipose-derived stem cells.* Stem Cell Res Ther, 2021. **12**(1): p. 109.
190. Fajas, L., et al., *Regulation of peroxisome proliferator-activated receptor gamma expression by adipocyte differentiation and determination factor 1/sterol regulatory element binding protein 1: implications for adipocyte differentiation and metabolism.* Mol Cell Biol, 1999. **19**(8): p. 5495-503.
191. Cui, T., et al., *KLF2 Inhibits Chicken Preadipocyte Differentiation at Least in Part via Directly Repressing PPARgamma Transcript Variant 1 Expression.* Front Cell Dev Biol, 2021. **9**: p. 627102.
192. Buhman, K.K., et al., *Resistance to diet-induced hypercholesterolemia and gallstone formation in ACAT2-deficient mice.* Nat Med, 2000. **6**(12): p. 1341-7.
193. Henry, S.L., et al., *White adipocytes: More than just fat depots.* International Journal of Biochemistry & Cell Biology, 2012. **44**(3): p. 435-440.
194. Yue, F., et al., *A comparative encyclopedia of DNA elements in the mouse genome.* Nature, 2014. **515**(7527): p. 355-64.
195. Fagerberg, L., et al., *Analysis of the human tissue-specific expression by genome-wide integration of transcriptomics and antibody-based proteomics.* Mol Cell Proteomics, 2014. **13**(2): p. 397-406.
196. Wang, Y.J., et al., *Cholesterol and fatty acids regulate cysteine ubiquitylation of ACAT2 through competitive oxidation.* Nat Cell Biol, 2017. **19**(7): p. 808-819.
197. Gonzalez-Hodar, L., et al., *Decreased caveolae in AGPAT2 lacking adipocytes is independent of changes in cholesterol or sphingolipid levels: A whole cell and plasma membrane lipidomic analysis of adipogenesis.* Biochim Biophys Acta Mol Basis Dis, 2021. **1867**(9): p. 166167.
198. Ortegren, U., et al., *A new role for caveolae as metabolic platforms.* Trends in Endocrinology and Metabolism, 2007. **18**(9): p. 344-349.
199. Frisdal, E., et al., *Adipocyte ATP-binding cassette G1 promotes triglyceride storage, fat mass growth, and human obesity.* Diabetes, 2015. **64**(3): p. 840-55.
200. Lacombe, A.M.F., et al., *Sterol O-Acyl Transferase 1 as a Prognostic Marker of Adrenocortical Carcinoma.* Cancers (Basel), 2020. **12**(1).
201. Lohr, M., et al., *SOAT1: A Suitable Target for Therapy in High-Grade Astrocytic Glioma?* Int J Mol Sci, 2022. **23**(7).
202. Matsumoto, K., et al., *Expression of two isozymes of acyl-coenzyme A: cholesterol acyltransferase-1 and -2 in clear cell type renal cell carcinoma.* Int J Urol, 2008. **15**(2): p. 166-70.
203. Liu, Y., et al., *Knockdown of sterol O-acyltransferase 1 (SOAT1) suppresses SCD1-mediated lipogenesis and cancer procession in prostate cancer.* Prostaglandins Other Lipid Mediat, 2021. **153**: p. 106537.
204. Bhattacharyya, R., et al., *Axonal generation of amyloid-beta from palmitoylated APP in mitochondria-associated endoplasmic reticulum membranes.* Cell Rep, 2021. **35**(7): p. 109134.

205. Bhattacharyya, R., C. Barren, and D.M. Kovacs, *Palmitoylation of amyloid precursor protein regulates amyloidogenic processing in lipid rafts.* J Neurosci, 2013. **33**(27): p. 11169-83.
206. Storch, J. and Z. Xu, *Niemann-Pick C2 (NPC2) and intracellular cholesterol trafficking.* Biochim Biophys Acta, 2009. **1791**(7): p. 671-8.
207. Xiong, Q. and Y. Rikihisa, *Subversion of NPC1 pathway of cholesterol transport by Anaplasma phagocytophilum.* Cell Microbiol, 2012. **14**(4): p. 560-76.
208. Wilhelm, L.P., et al., *STARD3 mediates endoplasmic reticulum-to-endosome cholesterol transport at membrane contact sites.* EMBO J, 2017. **36**(10): p. 1412-1433.
209. Ziqubu, K., et al., *An insight into brown/beige adipose tissue whitening, a metabolic complication of obesity with the multifactorial origin.* Front Endocrinol (Lausanne), 2023. **14**: p. 1114767.
210. Keipert, S. and M. Jastroch, *Brite/beige fat and UCP1 - is it thermogenesis?* Biochim Biophys Acta, 2014. **1837**(7): p. 1075-82.
211. Yeh, Y.S., et al., *The Mevalonate Pathway Is Indispensable for Adipocyte Survival.* iScience, 2018. **9**: p. 175-191.
212. Langin, D., *Adipose tissue lipolysis as a metabolic pathway to define pharmacological strategies against obesity and the metabolic syndrome.* Pharmacol Res, 2006. **53**(6): p. 482-91.
213. Cerk, I.K., L. Wechselberger, and M. Oberer, *Adipose Triglyceride Lipase Regulation: An Overview.* Curr Protein Pept Sci, 2018. **19**(2): p. 221-233.
214. Schreibman, P.H. and R.B. Dell, *Human adipocyte cholesterol. Concentration, localization, synthesis, and turnover.* J Clin Invest, 1975. **55**(5): p. 986-93.
215. Harms, M. and P. Seale, *Brown and beige fat: development, function and therapeutic potential.* Nat Med, 2013. **19**(10): p. 1252-63.
216. Abe, I., et al., *Lipolysis-derived linoleic acid drives beige fat progenitor cell proliferation.* Dev Cell, 2022. **57**(23): p. 2623-2637 e8.
217. Jiang, N., et al., *PRDM16 Regulating Adipocyte Transformation and Thermogenesis: A Promising Therapeutic Target for Obesity and Diabetes.* Front Pharmacol, 2022. **13**: p. 870250.
218. Gomez-Suaga, P., et al., *The ER-Mitochondria Tethering Complex VAPB-PTPIP51 Regulates Autophagy.* Curr Biol, 2017. **27**(3): p. 371-385.
219. Harned, T.C., et al., *Acute ACAT1/SOAT1 Blockade Increases MAM Cholesterol and Strengthens ER-Mitochondria Connectivity.* Int J Mol Sci, 2023. **24**(6).
220. Fedorenko, A., P.V. Lishko, and Y. Kirichok, *Mechanism of fatty-acid-dependent UCP1 uncoupling in brown fat mitochondria.* Cell, 2012. **151**(2): p. 400-13.
221. Henagan, T.M., et al., *Dietary quercetin supplementation in mice increases skeletal muscle PGC1alpha expression, improves mitochondrial function and attenuates insulin resistance in a time-specific manner.* PLoS One, 2014. **9**(2): p. e89365.
222. Liu, H., et al., *Evaluation of Decalcification Techniques for Rat Femurs Using HE and Immunohistochemical Staining.* Biomed Res Int, 2017. **2017**: p. 9050754.
223. Zhi, X., et al., *AdipoCount: A New Software for Automatic Adipocyte Counting.* Front Physiol, 2018. **9**: p. 85.
224. Basolo, A., et al., *Procedures for Measuring Excreted and Ingested Calories to Assess Nutrient Absorption Using Bomb Calorimetry.* Obesity (Silver Spring), 2020. **28**(12): p. 2315-2322.

225. Chen, K.Y., et al., *Opportunities and challenges in the therapeutic activation of human energy expenditure and thermogenesis to manage obesity.* J Biol Chem, 2020. **295**(7): p. 1926-1942.
226. Roesler, A. and L. Kazak, *UCP1-independent thermogenesis.* Biochem J, 2020. **477**(3): p. 709-725.
227. Wiersinga, W.M., *T4 + T3 combination therapy: any progress?* Endocrine, 2019. **66**(1): p. 70-78.
228. Asano, H., et al., *Diet-induced changes in Ucp1 expression in bovine adipose tissues.* Gen Comp Endocrinol, 2013. **184**: p. 87-92.
229. Tamucci, K.A., et al., *The dark side of browning.* Protein Cell, 2018. **9**(2): p. 152-163.
230. Yan, Y., et al., *Chlorogenic acid improves glucose tolerance, lipid metabolism, inflammation and microbiota composition in diabetic db/db mice.* Front Endocrinol (Lausanne), 2022. **13**: p. 1042044.
231. Chen, S., et al., *The phytochemical hyperforin triggers thermogenesis in adipose tissue via a Dlat-AMPK signaling axis to curb obesity.* Cell Metab, 2021. **33**(3): p. 565-580 e7.
232. Jiang, J., et al., *Thermogenic adipocyte-derived zinc promotes sympathetic innervation in male mice.* Nat Metab, 2023. **5**(3): p. 481-494.
233. Rosenwald, M., et al., *Bi-directional interconversion of brite and white adipocytes.* Nat Cell Biol, 2013. **15**(6): p. 659-67.
234. Roh, H.C., et al., *Warming Induces Significant Reprogramming of Beige, but Not Brown, Adipocyte Cellular Identity.* Cell Metab, 2018. **27**(5): p. 1121-1137 e5.
235. Lu, X., *Maintaining mitochondria in beige adipose tissue.* Adipocyte, 2019. **8**(1): p. 77-82.
236. Cui, X., et al., *IFI27 Integrates Succinate and Fatty Acid Oxidation to Promote Adipocyte Thermogenic Adaption.* Adv Sci (Weinh), 2023: p. e2301855.
237. Goicoechea, L., et al., *Mitochondrial cholesterol: Metabolism and impact on redox biology and disease.* Redox Biol, 2023. **61**: p. 102643.
238. Rusinol, A.E., et al., *A unique mitochondria-associated membrane fraction from rat liver has a high capacity for lipid synthesis and contains pre-Golgi secretory proteins including nascent lipoproteins.* J Biol Chem, 1994. **269**(44): p. 27494-502.
239. Rizzuto, R., et al., *Mitochondria as biosensors of calcium microdomains.* Cell Calcium, 1999. **26**(5): p. 193-9.
240. Hajnoczky, G. and J.B. Hoek, *Cell signaling. Mitochondrial longevity pathways.* Science, 2007. **315**(5812): p. 607-9.
241. Vance, J.E., *Phospholipid synthesis in a membrane fraction associated with mitochondria.* J Biol Chem, 1990. **265**(13): p. 7248-56.
242. Voelker, D.R., *Interorganelle transport of aminoglycerophospholipids.* Biochim Biophys Acta, 2000. **1486**(1): p. 97-107.
243. van Marken Lichtenbelt, W.D., et al., *Cold-activated brown adipose tissue in healthy men.* N Engl J Med, 2009. **360**(15): p. 1500-8.
244. Rosell, M., et al., *Brown and white adipose tissues: intrinsic differences in gene expression and response to cold exposure in mice.* Am J Physiol Endocrinol Metab, 2014. **306**(8): p. E945-64.
245. Scheja, L. and J. Heeren, *Metabolic interplay between white, beige, brown adipocytes and the liver.* J Hepatol, 2016. **64**(5): p. 1176-1186.

246. Jacene, H.A., et al., *The relationship between patients' serum glucose levels and metabolically active brown adipose tissue detected by PET/CT.* Mol Imaging Biol, 2011. **13**(6): p. 1278-83.
247. Vijgen, G.H., et al., *Brown adipose tissue in morbidly obese subjects.* PLoS One, 2011. **6**(2): p. e17247.
248. Ouellet, V., et al., *Outdoor temperature, age, sex, body mass index, and diabetic status determine the prevalence, mass, and glucose-uptake activity of 18F-FDG-detected BAT in humans.* J Clin Endocrinol Metab, 2011. **96**(1): p. 192-9.
249. Pfannenberg, C., et al., *Impact of age on the relationships of brown adipose tissue with sex and adiposity in humans.* Diabetes, 2010. **59**(7): p. 1789-93.
250. Kirichenko, T.V., et al., *The Role of Adipokines in Inflammatory Mechanisms of Obesity.* Int J Mol Sci, 2022. **23**(23).
251. Romero, A. and J. Eckel, *Organ Crosstalk and the Modulation of Insulin Signaling.* Cells, 2021. **10**(8).
252. Perez, L.M., et al., *Adipokines disrupt cardiac differentiation and cardiomyocyte survival.* Int J Obes (Lond), 2020. **44**(4): p. 908-919.
253. Hall, M.E., R. Harmancey, and D.E. Stec, *Lean heart: Role of leptin in cardiac hypertrophy and metabolism.* World J Cardiol, 2015. **7**(9): p. 511-24.
254. Yu, S., et al., *Lower or higher HDL-C levels are associated with cardiovascular events in the general population in rural China.* Lipids Health Dis, 2020. **19**(1): p. 152.
255. Gao, S., et al., *Echocardiography in Mice.* Curr Protoc Mouse Biol, 2011. **1**: p. 71-83.
256. Zhao, S., C.M. Kusminski, and P.E. Scherer, *Adiponectin, Leptin and Cardiovascular Disorders.* Circ Res, 2021. **128**(1): p. 136-149.
257. daSilva-deAbreu, A., et al., *Interactions of hypertension, obesity, left ventricular hypertrophy, and heart failure.* Curr Opin Cardiol, 2021. **36**(4): p. 453-460.
258. Sakane, S., et al., *White Adipose Tissue Autophagy and Adipose-Liver Crosstalk Exacerbate Nonalcoholic Fatty Liver Disease in Mice.* Cell Mol Gastroenterol Hepatol, 2021. **12**(5): p. 1683-1699.
259. Fu, S., et al., *Extracellular vesicles in cardiovascular diseases.* Cell Death Discov, 2020. **6**: p. 68.
260. Crewe, C., et al., *Extracellular vesicle-based interorgan transport of mitochondria from energetically stressed adipocytes.* Cell Metab, 2021. **33**(9): p. 1853-1868 e11.
261. Khanna, D., et al., *Obesity: A Chronic Low-Grade Inflammation and Its Markers.* Cureus, 2022. **14**(2): p. e22711.
262. Hasegawa, Y., *New perspectives on obesity-induced adipose tissue fibrosis and related clinical manifestations.* Endocr J, 2022. **69**(7): p. 739-748.
263. Bunnell, B.A., et al., *The effect of obesity on adipose-derived stromal cells and adipose tissue and their impact on cancer.* Cancer Metastasis Rev, 2022. **41**(3): p. 549-573.
264. Kirschner, K.M., et al., *Wt1 haploinsufficiency induces browning of epididymal fat and alleviates metabolic dysfunction in mice on high-fat diet.* Diabetologia, 2022. **65**(3): p. 528-540.
265. Koenen, M., et al., *Obesity, Adipose Tissue and Vascular Dysfunction.* Circ Res, 2021. **128**(7): p. 951-968.
266. Zwick, R.K., et al., *Anatomical, Physiological, and Functional Diversity of Adipose Tissue.* Cell Metab, 2018. **27**(1): p. 68-83.

267. Longo, M., et al., *Adipose Tissue Dysfunction as Determinant of Obesity-Associated Metabolic Complications.* Int J Mol Sci, 2019. **20**(9).
268. Wang, Z., et al., *High-affinity SOAT1 ligands remodeled cholesterol metabolism program to inhibit tumor growth.* BMC Med, 2022. **20**(1): p. 292.
269. Mullur, R., Y.Y. Liu, and G.A. Brent, *Thyroid hormone regulation of metabolism.* Physiol Rev, 2014. **94**(2): p. 355-82.
270. Wculek, S.K., et al., *Oxidative phosphorylation selectively orchestrates tissue macrophage homeostasis.* Immunity, 2023. **56**(3): p. 516-530 e9.
271. Kolovou, G.D., et al., *Fasting serum triglyceride and high-density lipoprotein cholesterol levels in patients intended to be treated for dyslipidemia.* Vasc Health Risk Manag, 2005. **1**(2): p. 155-61.
272. Felmerer, G., et al., *Adipose Tissue Hypertrophy, An Aberrant Biochemical Profile and Distinct Gene Expression in Lipedema.* J Surg Res, 2020. **253**: p. 294-303.
273. Anthony, S.R., et al., *Mechanisms linking adipose tissue inflammation to cardiac hypertrophy and fibrosis.* Clin Sci (Lond), 2019. **133**(22): p. 2329-2344.
274. Romacho, T., et al., *Adipose tissue and its role in organ crosstalk.* Acta Physiol (Oxf), 2014. **210**(4): p. 733-53.
275. Radhakrishnan, S., et al., *Considerations When Choosing High-Fat, High-Fructose, and High-Cholesterol Diets to Induce Experimental Nonalcoholic Fatty Liver Disease in Laboratory Animal Models.* Curr Dev Nutr, 2021. **5**(12): p. nzab138.
276. Rogers, M.A., et al., *Acat1/Soat1 knockout extends the mutant Npc1 mouse lifespan and ameliorates functional deficiencies in multiple organelles of mutant cells.* Proc Natl Acad Sci U S A, 2022. **119**(18): p. e2201646119.
277. Las Heras, M., et al., *Understanding the phenotypic variability in Niemann-Pick disease type C (NPC): a need for precision medicine.* NPJ Genom Med, 2023. **8**(1): p. 21.
278. Elmehdawi, R., *Hypolipidemia: a word of caution.* Libyan J Med, 2008. **3**(2): p. 84-90.
279. Svoboda, M.D., et al., *Treatment of Smith-Lemli-Opitz syndrome and other sterol disorders.* Am J Med Genet C Semin Med Genet, 2012. **160C**(4): p. 285-94.
280. Yu, W., et al., *Altered cholesterol metabolism in Niemann-Pick type C1 mouse brains affects mitochondrial function.* J Biol Chem, 2005. **280**(12): p. 11731-9.
281. Wang, Y.M., et al., *The mechanism of dietary cholesterol effects on lipids metabolism in rats.* Lipids Health Dis, 2010. **9**: p. 4.
282. Fukuda, N. and J.A. Ontko, *Interactions between fatty acid synthesis, oxidation, and esterification in the production of triglyceride-rich lipoproteins by the liver.* J Lipid Res, 1984. **25**(8): p. 831-42.
283. Dietschy, J.M. and M.D. Siperstein, *Effect of cholesterol feeding and fasting on sterol synthesis in seventeen tissues of the rat.* J Lipid Res, 1967. **8**(2): p. 97-104.
284. Wilson, J.D., C.A. Lindsey, and J.M. Dietschy, *Influence of dietary cholesterol on cholesterol metabolism.* Ann N Y Acad Sci, 1968. **149**(2): p. 808-21.
285. Soliman, G.A., *Dietary Cholesterol and the Lack of Evidence in Cardiovascular Disease.* Nutrients, 2018. **10**(6).
286. Hu, F.B., J.E. Manson, and W.C. Willett, *Types of dietary fat and risk of coronary heart disease: a critical review.* J Am Coll Nutr, 2001. **20**(1): p. 5-19.

287. Marcher, A.B., et al., *RNA-Seq and Mass-Spectrometry-Based Lipidomics Reveal Extensive Changes of Glycerolipid Pathways in Brown Adipose Tissue in Response to Cold.* Cell Rep, 2015. **13**(9): p. 2000-13.
288. Liang, X., et al., *Rnf20 deficiency in adipocyte impairs adipose tissue development and thermogenesis.* Protein Cell, 2021. **12**(6): p. 475-492.
289. Ibrahim, M.M., *Subcutaneous and visceral adipose tissue: structural and functional differences.* Obes Rev, 2010. **11**(1): p. 11-8.
290. Dufau, J., et al., *In vitro and ex vivo models of adipocytes.* Am J Physiol Cell Physiol, 2021. **320**(5): p. C822-C841.
291. Shao, M., et al., *De novo adipocyte differentiation from Pdgfrbeta(+) preadipocytes protects against pathologic visceral adipose expansion in obesity.* Nat Commun, 2018. **9**(1): p. 890.